MOLECULAR BASIS OF COOPERATIVITY IN PH-TRIGGERED

SUPRAMOLECULAR SELF-ASSEMBLY

APPROVED BY SUPERVISORY COMMITTEE

Daniel Siegwart, Ph.D. (Chair)

Jinming Gao, Ph.D.

Baran Sumer, M.D.

Xuewu Zhang, Ph.D.

MOLECULAR BASIS OF COOPERATIVITY IN PH-TRIGGERED

SUPRAMOLECULAR SELF-ASSEMBLY

by

YANG LI

DISSERTATION

Presented to the Faculty of the Graduate School of Biomedical Sciences

The University of Texas Southwestern Medical Center at Dallas

In Partial Fulfillment of the Requirements

For the Degree of

DOCTOR OF PHILOSOPHY

The University of Texas Southwestern Medical Center at Dallas

Dallas, Texas

August, 2017

the experiment design; Dr. Tian Zhao for close collaboration on related projects; Drs. Xinpeng Ma, Qi Wei, Kejin Zhou, Houliang Tang for their help with the chemical and polymeric synthesis.

I would like to thank UT Southwestern and Simmons Comprehensive Cancer Center for offering a broad set of resources and state of art facilities. I would also like to thank Kelly Tsai, Paula Ribeiro, Mark Thompson and Kathy Holloway for the administrative support and equipment maintenance.

Last but not least, I would like to thank all my family members. Without their unconditional love and continuous support, I would never be able to complete my Ph.D. degree abroad. I am extremely grateful to my parents who raised me with a love of science and supported me in all my pursuits. I am particularly grateful to my grandfather who passed away during my fourth year of Ph.D. study. My grandfather has inspired me throughout my life and would have been very proud of what I have accomplished.

MOLECULAR BASIS OF COOPERATIVITY IN PH-TRIGGERED SUPRAMOLECULAR SELF-ASSEMBLY

Yang Li

The University of Texas Southwestern Medical Center at Dallas, 2017

Jinming Gao, Ph.D.

Responsive nanomaterials have become an attractive biosensing platform because of their versatility in varying the size, composition, shape and other physicochemical properties to address the deficiency of conventional sensors such as low sensitivity and specificity. Compared to small molecular sensors, nanoparticle sensors often deploy a multitude of non-covalent interactions (hydrogen bonding, hydrophobic and electrostatic interactions) and the resulting system frequently displays cooperative behaviors.

pH is an important physiological parameter that plays a critical role in cellular and tissue homeostasis. Dysregulated pH has been recognized as a universal hallmark of cancer. pH-sensitive nanoparticles have been widely used for tumor imaging, study of endosome/lysosome biology and cancer-targeted drug delivery. Recently, we have established a library of ultra-pH sensitive (UPS) nanoprobes with sharp pH transitions that are finely tunable in a broad range of physiological pH (4-8). The UPS nanoprobes

showed significantly improved sensitivity and biological precision over commonly used small molecular and polymeric pH sensors.

Here, we performed the mechanistic study of sharp pH response and binary on/off switch, which are absent in common small molecular and polymeric pH sensors or buffers, in pH-triggered supramolecular self-assembly process. Hydrophobic nanophase separation drove cooperative deprotonation of protonated unimers into neutral copolymers inside micelles. This divergent proton distribution characteristic of a representative PDPA copolymers was not observed in commonly used small molecular and polymeric bases (e.g., PEI). The cooperative deprotonation dynamics can explain the significantly decreased pKa and sharpened pH response. Combination of theoretical modeling and experimental validation allowed identification of key structural parameters on impacting pKa and sharpness in pH transition. Inspired by the impact of counter-ions on the self-assembly of UPS block copolymers, we reported a novel specific anion-induced micellization process. In vitro and in vivo experiments suggested an "capture and integration" mechanism underlying the binary tumor margin delineation performance of UPS nanoparticles.

Results from this study offer molecular insights to help establish the general principles in nanophase transition and supramolecular self-assembly for the development of new nanomaterials-based sensors with binary on/off switch in chemical and biological sensing.

TABLE OF CONTENTS

CHAPTER ONE -- Self-Assembled Nanostructures in Biomedical

CHAPTER THREE-pH-Triggered PEO-b-PR Block Copolymers Supramolecular

CHAPTER FIVE-Supramolecular Self-Assembly of UPS Block Copolymers

Resulting in Strong pH Cooperativity …………………………………..……..176

PRIOR PUBLICATIONS

1. **Li, Y.**; Wang Y.; Huang G.; Gao, J., "Cooperativity in the Development of Self-Assembled nanomedicine", ***Chem. Rev.***, 2017, in preparation (invited review).

2. **Li, Y.**; Zhao, T.; Wang, C.; Huang, G.; Lin, Z.; Sumer, B.; Gao, J. "Molecular Basis of Cooperativity in pH-Triggered Supramolecular Self-Assembly", ***Nat. Commun.***, 2016, 7, 13214

3. **Li, Y.**; Wang, Z.; Wei, Q.; Huang, G.; Gao, J. "Non-Covalent Interactions in Controlling the pH-Responsive Behavior of Self-assembled Nanosystems", ***Polym. Chem.***, 2016, 7, 5949 - 5956.

4. **Li, Y.**; Wang, Y.; Huang, G.; Ma, X.; Zhou, K.; Gao, J. "Chaotropic-Anion-Induced Supramolecular Self-Assembly of Ionic Polymeric Micelles", ***Angew. Chem. Int. Ed.***, 2014, 53, 8074-8078.

5. Zhao, T.; Huang, G.; **Li, Y.**; Ramezani S.; Yang, S.; Lin, Z.; Wang Y.; Ma X.; Zeng, Z.; Xie, X.; Thibodeaux J.; Sun X., Sumer, B.; Gao, J., "pH Transistor Nanoprobes Advance Cancer Detection and Surgery", ***Nature Biomedical Engineering***, 2017, 1, DOI:10.1038/s41551-016-0006.

6. Luo, M.; Wang, H.; Wang Z.; Lu, G.; **Li, Y.**; Chen, X.; Huang, G.; Lea, J.; Frankel, A.; Chen, Z.; Gao, J., "STING-Activating Minimalist Nanovaccine for T Cell Therapy of Cancer", ***Nat. Nanotech.***, 2017, 12, DOI:10.1038/nnano.2017.52

7. Wang, Y.; Wang, C.; **Li, Y.**; Huang, G.; Zhao, T.; Sumer, B.; Gao, J. "Digitization of Endocytic pH by Hybrid Ultra-pH Sensitive Nanoprobes at Single Organelle Resolution", ***Adv. Mater.***, 2017, 29, 1603794.

8. Wang, Z.; Luo, M.; Mao, C.; Wei, Q.; Zhao, T.; Li, Y.; Huang, G.; Gao, J. A Redox-Activatable Fluorescent Sensor for the High-Throughput Quantification of Cytosolic Delivery of Macromolecules. ***Angew. Chem. Int. Ed.***, 2016, 129, 1339-1343.

9. Wang, C.; Zhao, T.; Li, Y.; Huang, G.; White M.; Gao, J., "Investigation of Endosome and Lysosome Biology by Ultra pH-Sensitive Nanoprobes", ***Adv. Drug Deliv. Rev.***, 2016, 104, DOI: 10.1016/j.addr.2016.08.014.

10. Wang, C.; Wang, Y.; Li, Y.; Bodemann, B.; Zhao, T.; Huang, G.; DeBerardinis, R.J.; White, M.A.; Gao, J. "A nanobuffer reporter library for fine-scale imaging and perturbation of endocytic organelles", ***Nat. Commun.***, 2015, 6, 8524.

11. Ma, X.; Wang, Y.; Zhao, T; Li, Y.; Su, L.; Wang, Z.; Huang, G.; Sumer, B.D.; Gao, J. "Ultra-pH-Sensitive Nanoprobe Library with Broad pH Tunability and Fluorescence Emissions", ***J. Am. Chem. Soc.***, 2014, 136, 11085-11092.

12. Huang, X.; Huang, G.; Zhang, S.; Sagiyama, K.; Togao, O.; Ma, X.; Wang, Y.; Li, Y.; Sumer, B. D.; Takahashi, M.; Sherry, A. D.; Gao, J. "Multi-Chromatic pH-Activatable 19F-MRI Nanoprobes with Binary ON/OFF pH Transitions and Chemical-Shift Barcodes", ***Angew. Chem. Int. Ed.***, 2013, 52, 8074-8078.

LIST OF FIGURES

xxv

LIST OF DEFINITIONS

ATRP - atom transfer radical polymerization

AMA-MA- aminoethyl methacrylate

BODIPY - boron-dipyrromethene

CMC - critical micelle concentration

CMPD – critical micelle protonation degree

Cy5 - Cyanine5

DDS – drug delivery system

NDDS – nanoparticle-based drug delivery system

DLS - dynamic light scattering

DMF – dimethylformamide

ELPs -   elastic like polypeptides

EPR - enhanced permeability and retention effect

FRET - fluorescence resonance energy transfer

ICG- indocyanine green

ITC - isothermal titration calorimetry

IV – intravenous

LCST - lower critical solution temperature

LogP - partition coefficient of a molecule between an aqueous and lipophilic phases

NHS - N-hydroxysuccinimide

NIR - near infrared

PBS - phosphate-buffered saline

PC7A - PEO-*b*-poly[2-(hexamethyleneimino)ethyl methacrylate]

PD5A - PEO-*b*-poly[2-(dipentylamino)ethyl methacrylate]

PDBA - PEO-*b*-poly[2-(dipropylamino)ethyl methacrylate]

PDEA - PEO-*b*-poly[2-(diethylamino)ethyl methacrylate]

PDMA - PEO-*b*-poly[2-(dimethylamino)ethyl methacrylate]

PDPA - PEO-*b*-poly[2-(dibutylamino)ethyl methacrylate]

PEG - poly(ethylene glycol)

PEG-PLA - poly(ethylene glycol)–polylactic acid

PEPA - PEO-*b*-poly(ethylpropylaminoethyl methacrylate)

PeT - photo induced electron transfer

PET - positron emission tomography

pH_e - extracellular pH

pH_i - intracellular pH

pHLIP - pH (low) insertion peptide

pH_t -   pH transition

PNIPAM - Poly(N-isopropylacrylamide)

PINS - pH-sensitive ICG-encoded nanoprobes

PMBA – poly (methylbenzylamino) ethyl methacrylate

PMDETA - N,N,N′,N″,N″-pentamethyldiethylenetriamine

SNA – spherical nucleic acid

SOPV - S-chiral oligo(p-phenylenevinylene)

TEM - transmission electron micrographs

THF- tetrahydrofuran

TMR - tetramethyl rhodamine

UCST - upper critical solution temperature

UPS - ultra-pH sensitive

CHAPTER ONE-Self-Assembled Nanostructures in Biomedical Applications

1.1-Introduction

Many diseases originate from abnormal biological processes at nanoscale or molecular level, such as gene mutation, protein misfolding and cell malfunctions as a result of infections[1]. Lots of these molecules and infectious agents are at nanoscale and probably located in nanoscale or macroscale functionalized subcellular organelles or vesicles. Advances in genomics, proteomics and regenerative medicine have inspired development of numerous therapies and technologies for the treatment of various diseases. Similar in scale to biologic molecules, nanomaterials have been extensive investigated for biomedical applications over past several decades[2]. The nanomaterials have very small size ranging from 1 to 100 nanometers with correspondingly large surface-to-volume ratio. A multitude of targeting moieties can be incorporated to the surface of nanostructures via extensively investigated engineering procedures. The physiochemical properties such as composition, size and shape can be sophisticatedly tailored for disease diagnosis, treatment and prevention[3]. Different physiochemical properties like optical, electrical and magnetic responsiveness have been introduced to nanostructures to facilitate biological diagnostics. A recent report revealed that over 250 nanomaterial-based technologies or therapies have been approved by the Food and Drug Administration (FDA) or are currently in different stage of clinical trials[4]. Their intended targets range from the regeneration of hearts to the treatment of diabetes.

With over 10 million new cases every year globally, caner remains a difficult disease to treat and one of the leading causes of death[5]. There has been explosive development of numerous nanotechnologies to diagnose and treat cancer[6]. Nanomaterials

can be engineered to promote the transport of diagnostic or therapeutic agents through biological barrier[7]. For example, poly(ethylene glycol) (PEG) have been introduced on the surface of nanoparticles to achieve a prolonged residence in circulation and decreased degradation by metabolic enzymes[8]. This FDA approved polymers is non-toxic, non-immunogenic and have been playing a crucial role in enhancing the pharmaceutical potential of peptides and proteins as therapeutic agents. Drug delivery systems can also be designed to target abnormal biological signals like pH, reactive oxygen species and overexpressed proteins or enzymes[9]. Molecular imaging platforms are used to locate tumor and facilitate image-guided surgery[10]. The tumor heterogeneity also leads to the growing emphasis on personalized nanomedicine[11]. One extraordinary property of nanomaterials is that they are generally multi-component systems. Different components or subunits of the nanostructures can be sophisticated engineered to address the same specific challenge in medicine, resulting in strong cooperative effect that is absent in monomolecular therapeutics[12].

1.2-Self-assembled nanostructures in medicine

1.2.1-Multivalency and targeted drug delivery

      A fundamental challenge in nanomedicine is to deliver the therapeutic cargos into the targeted cells. Solid tumors usually show anatomical and pathophysiological properties different form normal tissues. The angiogenesis of tumor leads to high vascular density and large gaps between endothelial cells in tumor blood vessels. And tumor tissues also display increased tendency of extravasation and retention of macromolecular therapeutics like nanoparticles, which results in a unique phenomenon of

solid tumors called enhanced permeability and retention (EPR) effect[13]. The EPR effect served as a basis for the development of nanomaterial-based therapies for cancer diagnosis and treatment.

Many anti-cancer drugs like siRNA and chemotherapeutics require intracellular release. Although drug-loaded nanoparticles with optimized size and surface chemistry can be designed to utilize the passive EPR effect to accumulate in tumor sites, the tumor tissues develop a mechanism to resist the anticancer therapeutics – the multidrug resistance (MDR)[14]. Various factors, including over-expressed efflux transporters, defective apoptotic machineries, and higher interstitial fluid pressure, contribute to such MDR effect[15]. Multidrug resistance is also known to be responsible for the failures for many chemotherapy drugs[16]. To overcome the MDR effect, active targeting strategies have been developed to target surface receptors on tumor cells and to enter cancer cells via endocytosis[17]. Ligands can be incorporated onto the surface of nanoparticles by a variety of conjugation chemistries. These ligands-conjugated nanoparticles can specifically bind to the receptors on the surfaces of target tumor cells after extravasation. Then the bound nanocarriers can be internalized via endocytosis, enabling the intracellular release of drugs. Such active targeting methods can overcome the efflux-pump mediated drug resistance and allows improved intracellular drug concentration[18].

The internalization of drug-loaded nanoparticles resides in the receptor-ligand binding and ensuing cellular uptake. Both the binding events and subsequent cellular internalization can be enhanced by multivalent binding between ligand-receptor pairs. The multivalent binding process may display positive cooperativity, where binding of one

ligand on the nanoparticles will localize neighboring ligands closer to unoccupied receptors and facilitate further binding events (**Figure 1.2.1**)[19,20]. The multivalent binding affinity depends on both the monovalent binding affinity and the number of ligand-receptor binding pairs. Cooperative binding can dramatically increase the overall binding affinity compared to monovalent binding pairs. By using multiple folate receptor binding proteins, the nanoparticle-cell association is enhanced by more than 2500 fold[21]. Multivalent antiviral and anti-inflammation therapeutics also showed significantly improved potencies than corresponding monovalent counterparts[22].The overall binding affinity of ligand-modified nanoparticles to targeted cells generally increases with an increasing ligand density. However, there may be a maximum allowable number of ligands for the optimized target efficacy. High ligand density may result in the decrease of binding affinity due to unfavorable steric crowding, where the ligand may have limited conformational freedom to effective bind to the targets.

Many diseases are marked by overexpressed proteins such as folate receptors in
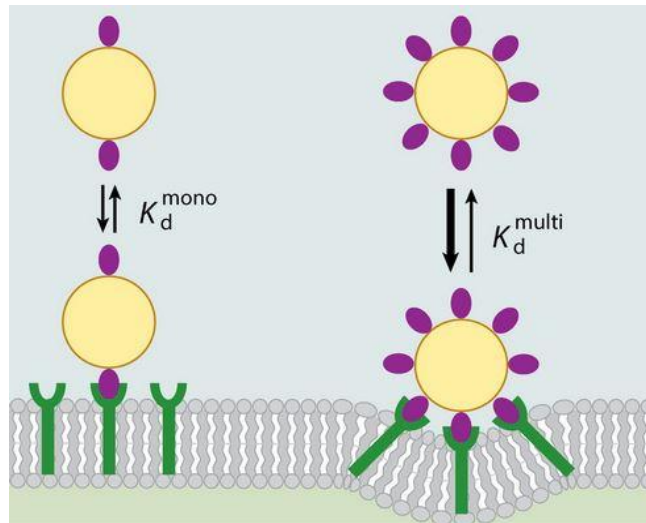
Figure 1.2.1. Cooperative multivalent interactions significantly increases the affinity of ligand-conjugated nanoparticles to cell surface[20].
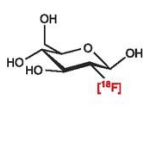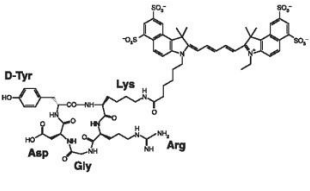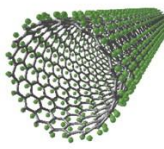
cancer[23]. These biomarkers can be utilized for the design of engineered nanocarriers with active targeting capabilities. Over last two decades, the remarkable improvement in bioorthogonal chemistry has inspired a metabolic labeling strategy for the targeted delivery of chemotherapies and nanomedicines[24]. Metabolic labeling provides a powerful tool to manually introduce chemical receptors onto the cell surfaces and enables a "two-step" targeting strategies. This strategy is especially useful for delivering therapeutics without obvious biomarkers. Kim and co-workers developed a new in vivo active targeting strategy for nanoparticles through copper free bioorthogonal chemistry in the living body[25]. Unnatural sialic acids with azide groups was artificially incorporated on the cell surface of tumors via metabolic glycoengineering, which effectively enhance the accumulation of nanoparticles. In addition, cell surface binding improved the internalization of drug-loaded nanoparticles, showing the feasibility for targeted intracellular drug delivery.

1.2.2-Oligonucleotides-conjugated nanoparticles for selective nucleic acids detections

The sensitive detection of biomolecules is important in a variety of biomedical applications such as disease diagnostics, optical imaging and drug delivery. Abnormal concentration of certain biomolecules like proteins often recognized as hallmarks of various diseases like cancers, neurodegenerative diseases and infectious disease[26]. A biosensor is defined as a detection device that incorporates a living organism or product derived from living systems and a transducer to provide an indication, signal, or other form of recognition of the presence of a specific substance or analyte in the environment[27]. Biosensors usually rely on specific biological recognition elements in

combination with a transducer for signal processing and even amplification. The sensing process operates through either noncovalent approach or covalent binding. The non-covalent approaches rely on the electrostatic interaction, encapsulation in polymers, pi-pi stacking and van der Waals forces between nanomaterials and biological molecules[28]. The non-covalent bindings preserve all properties and functions of both nanomaterials and biological targets. The covalent binding between sensors and target molecules can be achieved via direct chemical reactions like click chemistry. This method shows advantages in minimizing unspecific absorption.

There are different categories of biological sensing modalities including small molecules, peptides, aptamers, antibodies, proteins and different types of nanoparticles (**Figure 1.2.2**)[29]. One significant drawback of conventional bio-sensing technology is that they only allow detection after the target molecules reach critical concentration threshold concentrations, at which the disease is often significantly advanced. Last two decades have witnessed an growing interest in the use of nanomaterials for the development of biosensors in order to address the deficiencies of commonly used biosensors[30]. The

Type	Small molecule	Peptide	Affibody	Aptamer	Antibody	Nanoparticle
Size	<1 nm <0.5 kDa	~1–4 nm ~0.5–2 kDa	~5–10 kDa	~5–15 kDa	~150 kDa	~10–200 nm (no larger than 1,000 nm)
Example	[18F]FDG	RGD-Cy5.5	[68Ga]-DOTA-MUT-DS	Molecular Beacon	ICG-Trastuzumab	RGD-SWNT

Quencher • Donor • Signaling component

Figure 1.2.2. Different categories of optical biosensors[29].

nanomaterials offer several unique advantages in the design of biosensors[31]. First, they have large surface-to-volume ratio as a result of small size. Second, the size, shape and composition of nanomaterials can be easily engineered. Third, targeting ligands can be incorporated on the surface of nanostructures. These unique physical and chemical properties of nanomaterial-based biosensors have enabled the detection of biomolecules with high sensitivity and selectivity.

One such example is spherical nucleic acid (SNAs)-based nano-flares[32]. Such nucleic acid-conjugated gold nanoparticles have been used in the development of various vitro and intracellular molecular sensing and diagnostic platforms for a range of analytes including nucleic acids[33], proteins[34], small molecules[35] and metal-ion-based targets[36]. The combination of inorganic core and polyvalent oligonucleotide shell offers significantly advantages over molecular counterparts. A target analyte such as nucleic acids can be captured by two distinct sets of SNAs, each functionalized with a strand programmed or chemically modified to impart specificity to its target. Then the presence and subsequent capture of target sequences will trigger the reversible aggregation of the SNAs nanoparticles, which is accompanied by a visible color transition due to a red shift in the surface plasmon resonance of the gold nanoparticles. The aggregates formed from a perfectly complementary target nucleic acid sequence exhibits a very narrow melting transition as a result of positive cooperativity as compared to that of duplex DNAs[37]. A single base pair mismatch, insertion or deletion will result in shift of transition temperature and lead to detection of target oligomeric nucleic acids with high specificity[37]. Moreover, the high extinction coefficient of gold nanoparticles allows the

much more sensitive detection of target molecules at lower concentration than conventional molecular dyes.

Recently, the same authors used the nano-flares to develop a new technique for the detection, isolation and culture of live tumor cells from human blood (**Figure 1.3.2**)[38]. Metastasis is the spread of cancer cells to new areas of the body from the primary tumor site[39]. It is believed to progress through a series of steps by which cancer cells originating at a primary tumor intravasate into the blood stream, travel through the blood stream, and extravasate before eventually form secondary tumors at new sites. Early detection of so-called circulating tumor cells (CTCs) may provide unprecedented opportunities for metastatic risk assessment and investigation. The nano-flares were designed to target
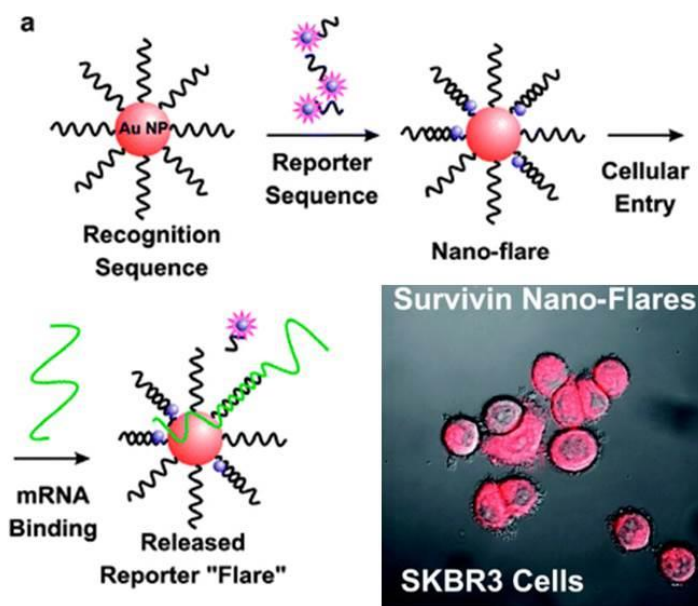
Figure 1.2.3. Design of spherical nucleic acids: nanoparticles functionalized with a recognition sequence are hybridized with a short complementary fluorophore-labeled reporter strand, which can be displaced by the target and emit fluorescence[38].

8

messenger RNA (mRNA) that code for certain proteins known to be biomarkers for breast cancer cells. NanoFlares, in combination with flow cytometry, can be used to fluorescently detect and report the genetic markers of CTCs in blood with less than one percent false positive results. They allowed for the detection of as few as 100 live cancer cells per mL of blood and subsequently culture those cells. This technique also successfully detected CTCs in a murine model of metastatic breast cancer. Such genetic-based approach for detecting, isolating, and characterizing circulating tumor cells from blood may provide new opportunities for cancer diagnosis, prognosis, and personalized therapy.

1.2.3-Thermo-responsive nanomaterials in controlled drug delivery

Specific delivery of therapeutics to the region of disease such as cancer can significantly enhance the therapeutic efficacy and avoid toxicity in healthy tissues as a result of off-target effect[40]. However, temporal and spatial controllable release of therapeutics remains a major challenge in the development of drug delivery systems (DDS)[41]. Variations in physiological parameters are critical hallmarks for different types of diseases, such as cancer, infections, cardiovascular disease and autoimmune diseases. Such pathological abnormalities have inspired the development of stimuli-responsive materials for the targeted delivery of therapeutics to the site of disease[42]. Implementation of such drug delivery systems requires the use of biocompatible materials that can respond to biological stimuli and release the encapsulated or conjugated drug via conformation changes or breakage of linkers. Nanotechnology-based drug delivery

systems have shown promising results in many preclinical animal models and inspired the further investigation and design of next generation precision medications.

Thermo-responsive controllable release is one of the most investigated stimuli-responsive strategies and has been extensively investigated for the treatment of cancers. The temperature-triggered non-linear sharp changes as a result of positive cooperativity can be used for the design of drug release systems following a variation of the temperature in the disease site and surrounding normal tissues. Ideal thermos-responsive drug delivery systems should be stable at body temperature and retain the load in the nanoparticles. Also, they should be able to release the drug upon heating in the region of interest such as tumor. Poly(N-isopropylacrylamide) (PNIPAM) with a solution-gel transition at its low critical solution temperature (LCST) of 32 ℃ is one of the most well-established thermos-responsive polymers and has been explored for biomedical applications since 1980s[43,44]. Extensive efforts have been committed to optimize the LCST closer to the body temperature and accelerate the phase transition process.

Researchers have been working on the development of new nanomaterials to overcome some limitation of conventional thermos-responsive hydrogels such as poor elasticity[45-47] and slow reversible swelling[48-50] upon heating. Xia and co-workers developed a nano-structured smart hydrogels that display rapid and reversible response while maintaining high elasticity[51]. They used thermos-activable nanogels as cross-linkers to construct the constructing nano-scaled architectures. The nano-structured smart hydrogels show very significant improved fast response without compromise in high elasticity. They maintain outstanding elastic properties as proved by sustain high

compressions, resist slicing and withstand high level of deformation. The concurrent rapid and significant stimuli-response and high elasticity may provide enhanced performance in precisely controlled release of encapsulated cargoes.

Other than polymers, several classes of natural or synthetic polypeptides such as elastin-like polypeptides (ELPs) have also attracted considerable attention for the development of stimuli-responsive drug delivery systems. In addition to conventional hydrogels, thermos-responsive polymer micelles and liposome have also been developed for the delivery of different hydrophobic or hydrophilic therapeutics[52]. Kostarelos groups reported lipid-peptide vesicle hybrids for controlled drug release triggered by mild hyperthermia (**Figure 1.2.4, upper panel**)[53]. The hybrid nanoscale vesicles were

Self-associated α-helix bundle (Closed pore)

Disordered conformation (Open pore)

Thermoresponsive Drug Release

Local hyperthermia

$$NH_4HCO_{3(aq)} \xrightarrow{\triangle} NH_{3(aq)} + H_2O_{(l)} + CO_{2(g)}$$

ABC liposomes

Generation of CO_2 bubbles

Creation of permeable defect to trigger drug release
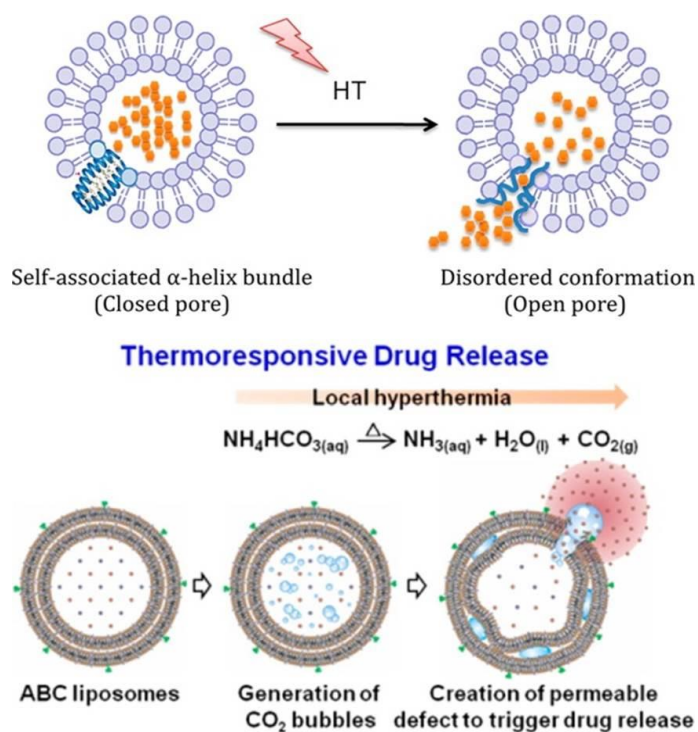
Figure 1.2.4. (Upper panel) Schematic illustration of liposome-peptide hybrids and their response to mild hyperthermia (HT). (Lower panel) Schematic illustration of thermos-responsive, bubble generating liposomes[53].

11

engineered by self-assembled anchoring of the amphiphilic peptide within the lipid bilayer. The rationale in the design of such hybrid vesicles was to combine the advantages of traditional thermo-sensitive liposomes with the dissociative, unfolding properties of a temperature-sensitive peptide to optimize drug release under mild hyperthermia, while improving in vivo drug retention. Doxorubicin was successfully encapsulated in the vesicles at higher than 90% efficiency following the remote loading, pH-gradient methodology. The release of doxorubicin from lipid-peptide hybrids in vitro indicated superior serum stability at physiological temperatures. In vivo results as measured by ^{14}C-doxorubicin suggested significantly increased tumor accumulation 24 hours after intravenous administration, indicating great potential of such materials for further development of clinically relevant mild hyperthermia-triggered therapeutic modalities. Xia and Sung reported another thermos-responsive liposomal system for triggered localized extracellular delivery of therapeutics (**Figure 1.2.4, lower panel**)[54]. The key component of reported liposomal design is the encapsulated ammonium bicarbonate (ABC), which is used to create the transmembrane gradient needed for a highly efficient encapsulation of doxorubicin. With increase of temperature (above 42 ℃), decomposition of ABC generates CO_2 bubbles, creating permeable defects in the lipid bilayer that rapidly release encapsulated cargos. The generated CO^2 bubbles can also serve as ultrasound imaging contrast due to hyper-echogenicity.

1.2.4-pH sensitive nanoparticles in drug delivery and molecular imaging

pH variations have been extensively explored for the development of drug delivery systems to target specific organs such as gastrointestinal tract[55] or intracellular

compartments such as endosomes or lysosomes[56]. Some pathological abnormalities in pH associated with diseases such as cancer[57] or inflammation[58,59] can also be targeted for the design of pH-triggered controllable release systems. Irregular angiogenesis in tumors causes a fast deficit of oxygen and a shift in glycolytic metabolism, leading to acidification of extracellular environment[60]. But the variation between extracellular pH of tumors and normal tissues is very small and an efficient pH-responsive system must have a sharp response and the ability to differentiate such subtle pH difference.

A plethora of pH-responsive nano-platforms have been investigated for the delivery of anticancer therapeutics. Amphiphilic methyl ether poly(ethylene glycol)-b-poly(β-amino ester) copolymers have been synthesized for the pH-triggered release of fluorescent dye and anticancer drug camptothecin (CPT) respectively at acidic environment of tumor tissues[61]. pH-triggered delivery of proteins into ischemic areas was achieved with imidazole and piperidine-engineered PEG-b-poly(β -amino ester) micelles[62]. Some pH-responsive moieties can undergo charge conversion in mildly acidic tumor microenvironment, which may facilitate the internalization of nanocarriers. Hyeon group reported multifunctional pH-sensitive self-assembled nanoparticles for bimodal imaging and treatment of resistant heterogeneous tumors (**Figure 1.2.5**)[63]. These pH-responsive magnetic nanogrenades (PMNs) can targeted tumor via surface-charge switching upon sensing acidic tumor microenvironment and further dissociated into an active state that turns on magnetic resonance, fluorescence and photodynamic therapeutic activity. pH triggered generation of singlet oxygen and photodynamic therapy can selectively kill cancer cells with superior anticancer efficacy in highly heterogeneous drug-resistant tumors. Wang and co-workers developed another pH-sensitive

13
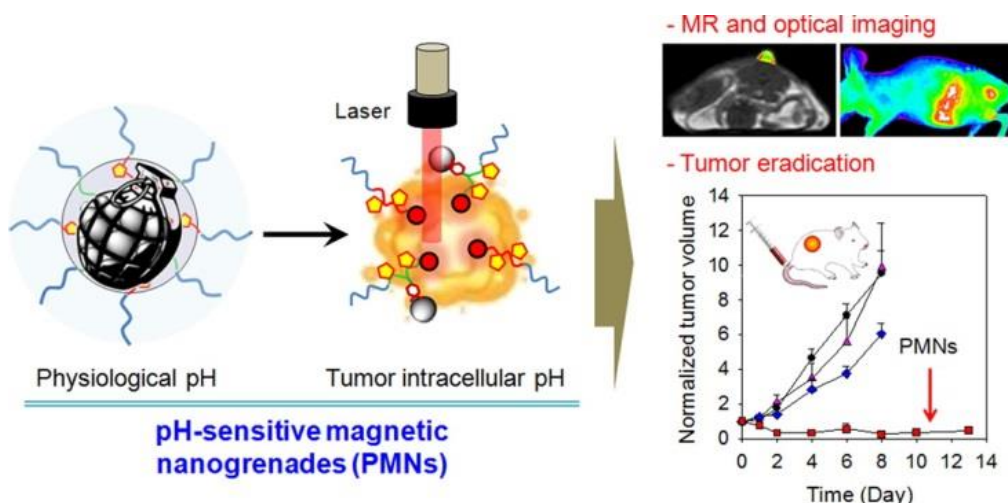
Figure 1.2.5. Schematic illustration of pH-sensitive magnetic nanogrenades (PMNs) design. PMNs are latent in the blood circulation and reverse their surface charge from negative to positive at acidic tumor microenvironment to facilitate tissue permeation and cell internalization. The endocytic pH will caused further dissociation of PMNs with enhanced magnetic resonance contrast and photo-activity[63].

polymer-drug conjugate nanoparticle system to overcome the multi-drug resistance and increase the intracellular drug concentration[64]. The nanoparticle converted its surface charge from negative to positive at tumor extracellular pH (~6.8) to facilitate cell internalization and subsequent intracellular release of anticancer therapeutics.

Organic nanomaterials are predominant in the design of pH-responsive drug delivery systems and molecular imaging probes. However, there is an growing interest in applying inorganic materials for the development of alternative pH-responsive nanomaterials. Lee groups designed a novel mesoporous silica nanoparticles modified with pH controlled, absorbable calcium phosphate (CaP) coatings as pore blockers that allow the facilitated release of encapsulated drugs within acidifying intracellular compartments such as endosomes and lysosomes[65]. Gu and co-workers reported a

transformable liquid-metal nanoparticles for the delivery to anticancer chemotherapeutics[66]. They designed a core–shell nanosphere composed of a liquid-phase eutectic gallium-indium core and a thiolated polymeric shell, through a sonication-mediated method. The nanoparticles loaded with doxorubicin (Dox) showed the capability to fuse and subsequently degrade under a mildly acidic condition with enhanced release of Dox after cellular internalization and improved in vivo tumor inhibition. Kataoka et al reported a novel magnetic resonance imaging (MRI) contrast agents that can amplify MR signals in response to pH[67]. They entrapped Mn^{2+} within pH-responsive calcium phosphate (CaP) nanoparticles with a poly(ethylene glycol) shell. At a low pH, such as in solid tumors, the CaP disintegrates and releases Mn^{2+} ions. And subsequent binding to proteins increases the relaxivity of Mn^{2+} with significantly enhanced contrast. These nanoparticles can rapidly and selectively light up solid tumours and identify hypoxic regions within the tumour matrix.

Cancer is a heterogeneous disease with various inter- and intra-tumor variations from normal tissues[68]. Molecular imaging of cancer specific biomarkers provides great promise for tumor detection and diagnosis. Most common strategies in the development of tumor-targeted optical imaging agents focus on cell surface receptors such as folate receptor[69], chlorotoxin[70], epidermal growth factor receptor[71] and some tumor-associated antigens[72]. Although various preclinical studies have shown the success in tumor diagnosis, the ability to detect a broad range of cancer is often not possible because of genetic or phenotypic heterogeneity among different tumors[73,74]. Tumor acidosis, which is well recognized a hallmark of cancer regardless of genotype and phenotype, can be used as a universal target for the development of pH-sensitive imaging probes. However,

commonly used pH sensors usually display broad pH response (2 pH units) and are not able to differentiate subtle pH variation between tumor tissues and surrounding normal tissues.

Recently, we reported a library of methacrylate-based ultra-pH sensitive (UPS) nanoprobes with sharp pH transitions that are finely tunable in a broad range of physiological pH (4.0-7.4)[75,76]. Besides the introduction of acid labile moieties like acetal groups[77,78], the incorporation of ionizable groups such as amines or carboxylic acids serves as the general strategy in the development of pH sensitive nanomaterials[79-83]. The nanoprobes consist of a block copolymer, PEO-*b*-PR, where PEO is poly(ethylene oxide) and PR is an ionizable tertiary amine block. The UPS nanoprobes achieved over 100 fold fluorescence intensity increase within 0.3 pH units, which is critical for broad tumor imaging and endosome maturation studies (**Figure 1.2.6**)[84,85].
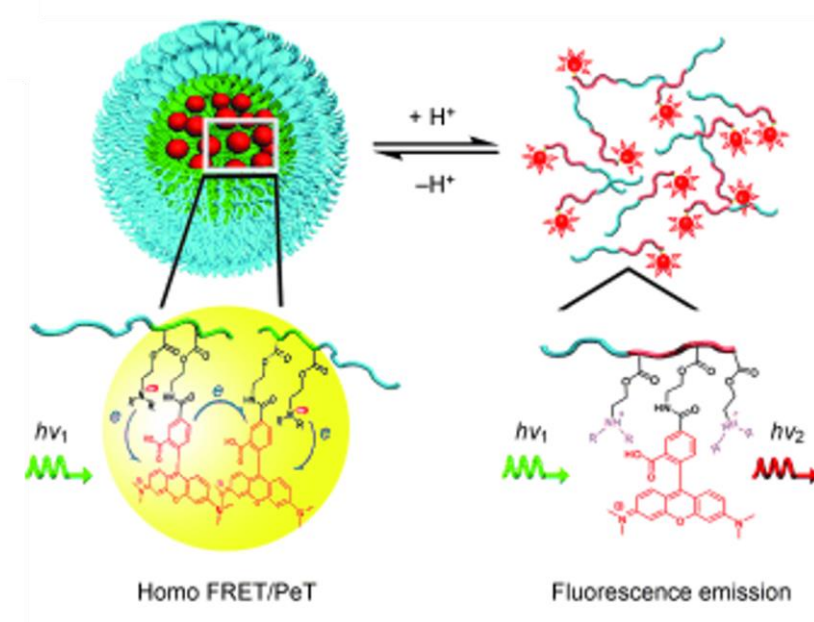
Figure 1.2.6. Schematic illustration of the design of ultra-pH sensitive (UPS) nanoparticles[84].

1.3-Cooperativity in self-assembled nanostructures

Nanomaterials have received considerable attentions that allow for highly selective recognition, catalysis, and transfer operations in a wide range of photonic, electronic and biomedical applications[32,86-91]. In particular, they play an increasingly important role in medicine with numerous nanosystems developed to deliver therapeutic drugs and imaging contrast agents for biochemical sensing, molecular imaging, disease diagnosis and therapeutic treatment[2,40]. Various nanoplatforms have been extensively investigated to address challenges in medicine and deficiencies of conventional small molecular sensors and drugs, resulting in the growing prosperity of nanomedicine.

In contrast to "top-down" methods such as lithography where the final structures are carved from a rigid mold, "bottom up" approach has become a major strategy to prepare functional nanomaterials where the formation of supramolecular architectures are driven by non-covalent interactions and self-assembly of molecular components[92-94].
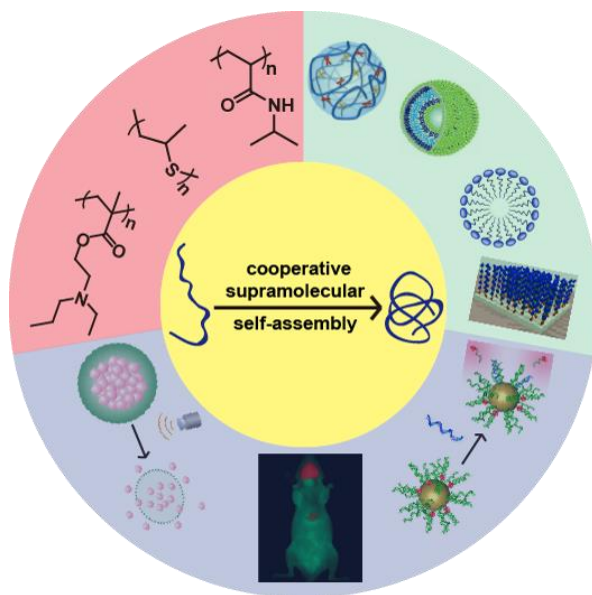
Figure 1.3.1. Cooperative self-assemblies in nanomedicine.

Self-assembly, which bridges the structures of individual building blocks and the function of the obtained nanocomplex, is an essential part of nanotechnology[95]. The underlying supramolecular chemistry principles were first described by Lehn and Whitesides over two decades ago[22,96]. In contrast to covalent chemistry, supramolecular self-assembly engages a multitude of weak and reversible non-covalent interactions to achieve a thermodynamically stable nanostructure. This strategy has the advantage of reaching sizes (10^4-10^{10} Da) that are not easily achievable by covalent chemistry, and the resulting system has faster temporal response to environmental stimuli due to the lower energy barrier in the dissociation of non-covalent complexes than the breaking of covalent bonds.

A hallmark of self-assembled systems is cooperativity[22], which arises from the interplay of two or more non-covalent interactions (**Figure 1.3.1**). As a result, the system as a whole behaves quite differently from the sum of individual parts acting in isolation. Positive cooperativity has been identified to be the mechanism underlying a large number of biological and physiological processes like oxygen binding to hemoglobin[97], which significantly increases the oxygen transport efficiency. Mechanistic investigations on several well established self-assembled nanomedicine platforms also suggest that positive cooperativity contribute to drastically enhanced detection sensitivity and specificity in chemical and biological sensing[32]. Understanding the supramolecular self-assembly process and underlying cooperativity principles may offer a new paradigm for the rational design and development of nanomaterials for medicine.

Despite tremendous advances, there are still major scientific and technological barriers in the development of nanomedicine. There is a lack of mechanistic and

molecular level understanding in the self-assembly process and accompanied cooperativity. Also, the thermodynamic and kinetic principles underlying cooperative responses are still not available, which hinders our capability in the rational design of more potent and sophisticated nanomedicine platforms. Another difficulty is that it is usually impractical to selectively change one parameter without affecting others to pin-point specific contributions from an individual interaction or component. To program, control and predict the performance of nanomaterials for the development of novel tools and therapies to address challenges in medicine, lots of efforts are still needed to unravel the supramolecular chemistry and cooperativity principles underlying the self-assembly processes, which bridge the gap between individual molecular components and integrated functional nanostructures.

1.3.1-Non-covalent interactions and cooperativity

Physics unravels the law of the universe and biology scrutinizes the rules of life. Chemistry builds the bridge between the general laws and specific expression of such

laws like biological systems[95]. Molecular chemistry such as sequential covalent synthesis has create a wide range of natural or unnatural molecules and materials and has provide a very powerful arsenal of techniques for constructing sophisticated molecules from atoms linked by covalent bonds. However, covalent chemistry can only generate well-defined molecules or structures less than 10^4 Dalton. Developing techniques for the facile synthesis of ultra-large molecules remains a major challenge in covalent chemistry. Another synthetic strategy, covalent polymerization, is developed to prepare macromolecules with higher molecular weight. Simple, reactive low molecular weight

monomers can react with each other and generate a polymer with multiple covalently-connected monomers such as polyethylene. Although the synthesis is easy the final molecular weight of obtained polymers can be as high as 10^6 Dalton, the molecular structure is very simple and repetitive. Also, the morphology and three-dimensional structures are less controllable. Neither sequential synthesis nor polymerization is capable of generating well-defined structures with dimension of 1 to 100 nm, the range of numerous biological structures from proteins through virus to subcellular organelles.

Supramolecular chemistry, which connects atoms or molecules via multiple weak, reversible and non-directional non-covalent bonds, has emerged as a powerful strategy to generate well-defined structures at nanoscale. Since most non-covalent bonds are weak and reversible with low energy barrier, the resulted supramolecular structures are usually under thermodynamic control. The distinguish feature of supramolecular structure prepared via such method is self-assembly, where atoms/molecules spontaneously adjust their positions or orientations to reach a thermodynamically minimum. Over the last several decades, supramolecular chemistry has drawn remarkable growing interests and inspired the development of various technologies in physics, chemistry and biology. A

System	Type	Applications/importance
Atomic, ionic, and molecular crystals	S	Materials, optoelectronics
Phase-separated and ionic layered polymers	S	
Self-assembled monolayers (SAMs)	S, T	Microfabrication, sensors, nanoelectronics
Lipid bilayers and black lipid films	S	Biomembranes, emulsions
Liquid crystals	S	Displays
Colloidal crystals	S	Band gap materials, molecular sieves
Bubble rafts	S	Models of crack propagation
Macro- and mesoscopic structures (MESA)	S or D, T	Electronic circuits
Fluidic self-assembly	S, T	Microfabrication
"Light matter"	D, T	
Oscillating and reaction-diffusion reactions	D	Biological oscillations
Bacterial colonies	D, B	
Swarms (ants) and schools (fish)	D, B	New models for computation/optimization
Weather patterns	D	
Solar systems	D	
Galaxies	D	

Figure 1.3.2. Self-assembly at all scales[99].

major goal of supramolecular chemistry is to be able to program, control and predict the outcome of self-assembly process[98]. Moreover, self-assembly exists at all scales throughout the natural and synthetic systems (**Figure 1.3.2**)[99]. Understanding life requires understanding of self-assembly. Also, natural self-assembled structures may inspire the design of sophisticated and functional non-living systems.

Noncovalent interactions play a key role in biological systems. They determine the tertiary structure of DNA, RNA as well as proteins and are responsible for molecular recognition process. Via a multitude of noncovalent interactions, atoms, molecules or groups of molecules self-assemble into organized structures with increasing complexity. The most obvious example is the water. Hydrogen bonding is responsible for why water is a liquid at room temperature instead of a gas, which is one of the prerequisites of life.

When two atoms with unfilled electronic shells come close and start to share electrons, a covalent bond is formed. The electron pairs they share are termed as bonding pairs and the stable balance of attractive and repulsive forces between atoms is known as covalent bonding. The bonding is most efficient when the distance between pairing atoms is less than 0.2 nm. Non-covalent bonds exist at much greater distance than covalent bonds and represents interactions between ions, molecules, and parts of molecules. For example, electrostatic interaction takes place between charges, dipoles and quadrupoles

Species	Strength^a (kJ mol^{-1})	Character
Amphiphilicity	< 50	Nonselective and nondirectional
Strong hydrophobic interactions	5–50	Nonselective and nondirectional
Electrostatic interactions	5–100	Nonselective
Host–guest interactions	10–100	Extremely selective
Hydrogen bonding interactions	5–150	Selective and directional
Stereocomplex interactions	~5	Nonselective and nondirectional
Coordination interactions	50–200	Directional
Covalent interactions	200–1000	Irreversible

^{a} The interaction energy in most cases.

Figure 1.3.3. Noncovalent interactions[100].

instead of electrons. Noncovalent bonds stabilize the self-organized structures from individual molecules but are weak enough to be dynamically broken and re-formed since the bonding strength is usually 10-100 times weaker than that in covalent bonds (**Figure 1.3.3**)[100].

1.3.2-Cooperativity in natural assembled systems

Cells are organized on size scale ranging from angstrom to micrometers. They are considered to be colloidal environment densely packed with and organized from a multitude of macromolecules. Cells' operations are accomplished through a series of biochemical reactions that can be turned sped up and slowed down according to the cells' needs and functions. To avoid the biochemical reactions interfere with each other, cells create different compartments, or organelles with distinct chemical environment. We only have slim knowledge of how proteins and many other molecules come together and self-organize into individual functional compartments. Most of such compartments have a physical boundary that separates them from surrounding environment. In addition, the components like enzymes within them should be able to diffuse freely and enable the occurrence of biochemical reaction. Mitochondria, which contain biochemical environment to make ATP, are separated from cytoplasm by membrane[100]. However, many compartments do not have membranes and are segregated from cytoplasm via phase separation or phase transition[101]. One example is the formation of micrometer-sized droplets, a macroscopic transition between small complexes and large supramolecular polymers[102,103]. Rosen and co-workers reported that the self-assembly of proteins and

RNA as a result of multivalent interactions drove the sharp liquid-liquid phase separation[102], an indication of potential cooperativity.

Self-assembly of macromolecules within the cells also take place at nanometer scale through evolution the intermolecular interfaces, or recruitment of cofactors[104]. For example, ligands can bind to multiple sites on an oligomeric proteins and form macromolecular assemblies. The macromolecular conformational changes are also found in protein folding or nucleic acid helix-coil transitions. Cooperativity is observed in the formation of multicomponent complexes which is considered essential features of cellular biology.

1.3.2.1- Cooperativity in ligand-protein binding

Molecular binding is an interaction between molecules that results in a stable physical association between individual components. For macromolecules having two or more binding sites, cooperativity can be described as the change of the intrinsic equilibrium binding affinity as a result of the reaction progress. For Example, the affinity of a given binding site for a ligand will be altered by the occupancy of other sites by the same or different ligands. Cooperative binding represents one of the most interesting types of molecular interactions observed in nature, though the underlying mechanism is not fully understood. And such cooperativity has been shown to be responsible for a large range of biochemical and physiological processes. Cooperative binding is observed in many biopolymers, including nucleic acids and proteins.

The various cells of our body use oxygen to make ATP, and then provide the energy needed for functions like muscular contraction. Oxygen molecules take a journey

from lungs to individual cells. After the oxygen is breathed in, it diffuses into the blood flowing through our lungs. However, oxygen's solubility in water is low, less than 1 ml of oxygen in 100 ml of blood. That's far from enough to meet the huge metabolic needs of our tissues and cells. Therefore, we need an alternate source for the transportation of oxygen. This alternate source of transportation is hemoglobin, which is a complex protein resides within red blood cells.

Max Perutz first revealed the structure of hemoglobin in various forms[105]. Each hemoglobin molecule consists of two α subunits and two β subunits, functions as a pair of αβ dimers. The α and β subunits have very similar three-dimensional structures. The binding affinity of hemoglobin to oxygen molecules depends on the presence of a bound prosthetic group called heme, which is also responsible for the distinctive red color of blood[106]. Each heme group consists of a central iron atom and an organic component called protoporphyrin. Every iron cores of heme groups can serve as a single binding site and one hemoglobin molecule can bind to four oxygen molecules. Under normal conditions, the iron is in the ferrous (Fe^{2+}) oxidation state with unoccupied coordination site for the binding of oxygen. The binding of the oxygen molecule to the iron ion substantially rearranges the electrons within the iron so that the ion becomes effectively smaller, allowing it to move into the plane of the porphyrin. Such oxygenation-driven conformation change leads to a transition from deoxy T state to oxy R state of quaternary structure of hemoglobin, where one pair of αβ subunits shifts with respect to the other by a rotation of 15 degrees[97,107].

The structural alteration in hemoglobin also significantly changes the oxygen affinity of hemoglobin. Initial oxygen binding to hemoglobin makes it easier for the

second oxygen to bind. Additional oxygen binding further enhances the affinity, resulting in the third and then fourth oxygen molecule binding (**Figure 1.3.4**)[106]. When three sites of the quaternary structure hemoglobin were occupied, the remaining open binding site has an affinity for oxygen more than 20-fold as great as that of fully deoxygenated hemoglobin binding its first oxygen. The cooperative binding significantly improves the oxygen transportation efficiency. The oxygen-hemoglobin saturation curve displays sigmoid shape, a typical curve for a cooperative binding process.
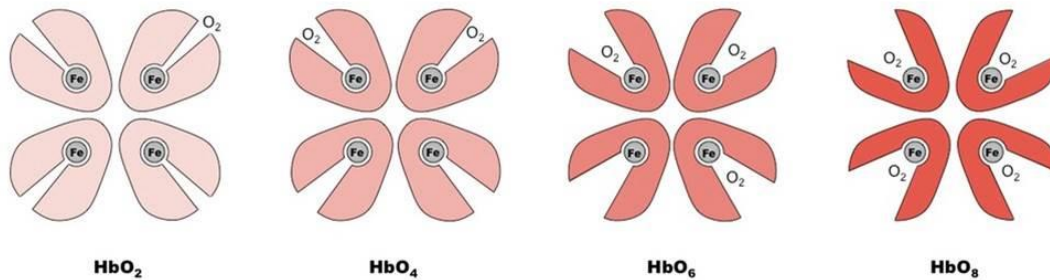
Figure 1.3.4. Cooperative binding of oxygen to hemoglobin. Initial oxygen binding to hemoglobin makes it easier for the second, third and fourth oxygen to bind as a result of conformation changes[106].

1.3.2.2-Cooperativity in cell adhesion

Cell adhesion is the process cells form contacts a surface, substrate or another cell through interactions between molecules of the cell surface. Cell adhesion is critical for many cell functions such as proliferation, migration and apoptosis. Cell adhesion occurs from the action of transmembrane glycoproteins, called cell adhesion molecules. Examples of these proteins include selectins, integrins and syndecans[108]. Although relatively low freedom of motion, these cell surface proteins retain the freedom to diffuse and rotate on the membrane surface, and even partially pre-organizes for ensuing binding events. Constraining these proteins to the membrane surface dramatically reduce the entropy and contribute to an enhancement of binding affinity compared to the same proteins interacting in solution. Cooperativity of molecular adhesion has been proposed
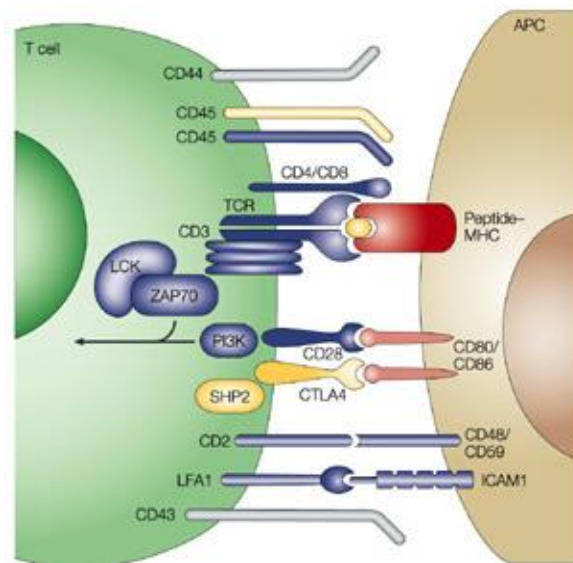
Figure 1.3.5. Key ligand pairs and signaling molecules that are involved in molecular recognition between T cells and antigen-presenting cells (immunological synapse). This process is mediated by a series of cooperative bindings of a complementary array of adhesion and co-stimulatory receptors[113].

as a physiological mechanism for modulating cell adhesion by altering binding affinity of adhesion molecules on the cell surface.

There is evidence that epidermal growth factor receptors (EGFRs) can exist in either ligand-free or pre-dimerized (but inactive) state on the cell surface[109]. A recent research provided evidence for a kinetic intermediate in EGF-mediated receptor activation, where a single EGF molecule is bound to a pre-dimerized receptor through positive cooperativity. The clustered complex greatly facilitates binding of a second EGF molecule and triggers receptor activation[110,111]. Cooperativity due to co-localization on the cell membrane was also observed in the immunological synapse, an organized interaction between closed apposed T cells and antigen-presenting cells (**Figure 1.3.5**)[112,113]. The cooperativity arises from the constraint of the binding partners on the membrane surface at the contact region mediated by a complementary array of adhesion and co-stimulatory receptors on cell surfaces[114].

1.3.2.3. Cooperativity in protein folding

Since first posed about 100 years ago, scientists have been dedicated to decipher the physical code by which an amino acid chain sequence dictates a protein's native structure and the stochastic nature of involved folding process. A "folding funnel" hypothesis is proposed as a specific version of the energy landscape theory of protein folding, which assumes that a protein's native state corresponds to the free energy minimum in living systems[115,116]. The surface 'funnels' a multitude of denatured conformation as well as the unique native structure of proteins. The transition states, the barrier that all molecules must overcome in order to fold into the native state, are

represented by the saddle points on the surface of above landscape. Superimposed on the surface are intermediate states corresponding to different stages of the folding process. The folding funnel theory assumes the existence of many non-native local minima in which partially folded proteins can become trapped.

The folding funnel theory hypothesize hydrophobic collapse as the driving force for protein folding, where sequestration of hydrophobic amino acid side chains stabilizes the intermediate states along the landscape and in the folded domains. The free energy of folded structures can be further lowered by isolation of electrostatically charged side chains on the solvent-accessible protein surface and neutralization of salt bridges within the protein's core. The interplay of involved non-covalent interactions contributes to observed positive cooperativity, a hallmark of protein folding[117].

The dynamic coupling between the interactions which stabilize a packed natural state determines the cooperativity of the folding landscape. In other words, cooperativity implies a favored protein folding pathway to the nature state. Strong coupling between the stabilization forces will lead to a completely cooperative two-state transition in protein folding. Such behavior is observed in small globular proteins consists of one hydrophobic unit[118]. The hydrophobic units that are observed at the interfaces of two-state complexes suggest the cooperative nature of the two-chain protein folding and the impact of the hydrophobic effect[119].

Cooperativity was also observed in the final folding step of proteins when all the side-chains are locked in the natively-packed arrangement and water is squeezed out of the protein core[120,121]. Onuchic group used a minimalist model to explore the interplay between structure-search of the native structure and desolvation in protein folding. Their

results suggested that the majority of the structural formation of the protein is achieved before water is squeezed out of the hydrophobic core, which integrates water expulsion effects into the current funnel energy landscape theory of protein folding. After the folding transition, a near-native intermediate with partially solvated hydrophobic core is formed. This transition is followed by a final step that cooperatively expelled water molecules from the partially hydrated protein core. This principle may readily be extended to describe the assembly of a variety of different proteins, and even other biological macromolecules like nucleic acids.

1.3.3-Cooperativity in synthetic nanomaterials

Polymeric material-based nanoscale assemblies have received considerable attentions in a variety of biomedical applications such as biological sensing, drug delivery, tissue engineering and molecular imaging[122,123]. These efforts have been driven to a large extent by the unmet need to improve the specificity in diagnosis and therapy via precise spatiotemporal control in delivery of therapeutics. Continuous efforts have been dedicated to tailor the three-dimensional architecture of these polymeric assemblies, aiming to augment their function and performance. To achieve these goals, in one way, novel polymeric building blocks are designed to alter the composition, morphology, and surface chemistry. New polymerization and formulation methods have also been developed to control the size, shape and architecture of assembled nanostructures. Capitalizing on the self-organization of polymeric building blocks, many groups including us have been working on the development of assembled nanostructures to address the intrinsic deficiencies of monomolecular materials such as low sensitivity and

selectivity and lack of specific targeting and accumulation in disease area. These nanoscale structures were assembled from individual building block via a multitude of non-covalent interactions, the same as those in the supramolecular assembly of protein and nucleic acids. The packing of preceding building block may more or less affect the assembly of ensuing building blocks that was usually nonexistent in small molecules. Moreover, the subtle interplay of these non-covalent interactions during the self-assembly process also contributes to the cooperativity absent in monomolecular materials. The cooperativity gives rise to unique and superior physical and chemical properties in multiple nanosystems over a broad range of biomedical applications. In this section, we will discuss the cooperativity in several well-established self-assembled nanoplatform and why cooperativity is critical for their performance and biomedical application.

1.3.3.1-Oligonucleotides-Conjugated gold Nanoparticles

Spherical nucleic acids (SNAs) are synthetic polyvalent nucleic acid−nanoparticle conjugates, spherical nanostructures with densely functionalized and highly oriented nucleic acids covalently attached to their surfaces[124]. These structures with spherical geometry were originally made with gold cores and DNA shells as reported by Mirkin Group[125]. The unique orientation of one-dimensional linear nucleic acids within this three-dimensional framework results in fundamentally new chemical, biological, and physical properties, which represent a paradigm shift in the use of nucleic acids for various applications such as materials synthesis, biological sensing, molecular diagnostics, and intracellular gene regulation applications[32].

The linear nucleic acid chains are typically designed with a head group moiety suitable for attachment to the nanoparticle of interest and a tail group that maintains the stability of nano-conjugates in aqueous environment. The first SNA conjugate are prepared by covalent attaching the 3' alkanethiol-terminated, single-stranded oligonucleotides to the surface of spherical gold nanoparticles[125]. A dense nucleic acid loading was achieved through a series of salt additions, where positively charged counterions were used to minimize electrostatic repulsion between adjacent negatively charged DNA strands and thereby enable ensuing DNA packing onto the nanoparticle surface more efficiently. In living systems, the nucleic acids usually exists in hybridized duplex. But the SNAs can be fabricated from both single and double-strand nucleic acid, and their conformation is determined by the sharp of the inorganic cores.

The hybridization of complementary nucleic acid sequence enables the binding interactions between SNA particles and linkers with matched sequence. The hybridization can also occur among different nanoparticles via the recognition region of the DNA sequences on the surface of particles. The assembly of spherical nucleic acid nanoparticles results in the formation of gold-nanoparticle aggregates bridged by the complementary nucleic acid sequence via hydrogen bond between base pairs. The SNA nanoparticle can be release from the aggregates through de-hybridization upon heating because the particles are held together via weak, reversible non-covalent bond and the inorganic cores are not fused. DNA duplexes follow predictable "melting" dehybridization when the temperature is above their melting point (Tm). The same holds true for the SNA nanoparticles.

Ji and co-workers reported a striking sharp melting curve for the dehybridization of spherical nucleic acid nanoparticles (SNA-NPs) aggregates[37]. Typically, the "melting" of double strand oligonucleotides occurs over a quite broad temperature range (∼20 ℃). However, the transition of the duplex-assembled SNA−Au NPs from aggregate state to individual particle state occurs over a much narrower temperature range (∼2−8 °C). In addition, the phase transition takes place at a higher temperature than that of the particle-free DNA duplex. The sharp phase transition were observed in both SNA-NPs and chip-based assay[37,126]. A single oligonucleotide base-pair mismatch is enough to perturb the melting behavior of the aggregates, allowing it to be differentiated from the aggregates made from fully complementary ones. Thus sharp melting transition is critical for diagnostic sensitivity and specificity.

Mechanistic investigation suggest that high surface density of oligonucleotides on SNA-NPs contributes to a greater number of inter-particle connections that are collectively stronger and present at a higher effective concentration compared to free
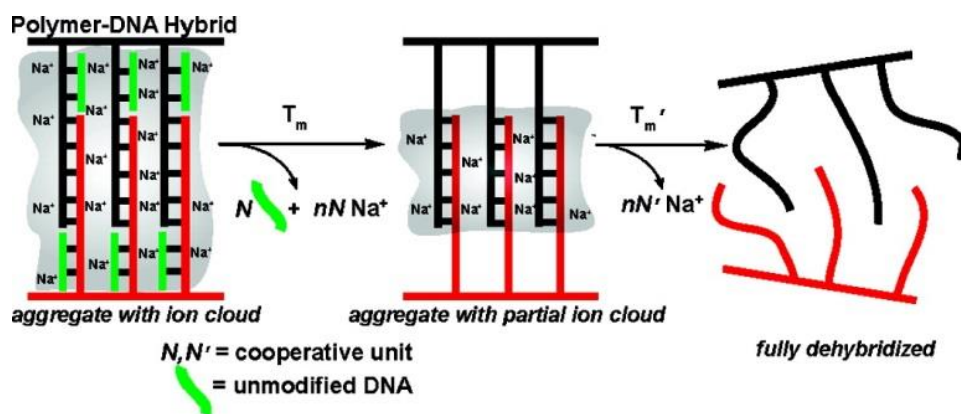
Figure 1.3.6. A Schematic illustration of the cooperative melting of neighboring strands (green) that share a sodium ion cloud with two neighboring duplexes[127].

DNA duplexes in aqueous solution[37]. The structure-property correlation was validated by the observation that decreasing the number of recognition strands on the particle surface results in a broader melting transition at a lower temperature. High local salt concentration is also believed to contribute to the melting cooperativity and resulting sharp phase transition. Later on, Schatz group proposed a "shared ion cloud" theory to describe the cooperative melting transition in SNA-NPs, which is supported by both experimental and theoretical evidence (**Figure 1.3.6**)[127]. Their investigation suggested that the sharp melting curve arises from either a phase transition driven by the macroscopic dissolution of the aggregates or neighboring-duplex interactions in the close-packed environment between adjacent DNA duplexes. The polymer-DNA hybrids, which include both polymer-linked and partially untethered duplexes, were designed to investigate the contribution of neighboring effect.   Upon thermal analysis, both types of duplexes exhibited sharp melting transitions. The sharp melting transition displayed by the partially untethered DNA duplexes offers convincing proof of the neighboring-duplex cooperativity. The established thermodynamic model also enabled the quantitative assessment of the contributions from the neighboring-duplex effect.   Nguyen and co-workers provided additional evidence for this theory based on the observation of cooperative melting in caged dimers with only two DNA duplexes[128]. They designed small molecule-DNA hybrids with only two parallel DNA duplexes which displayed sharper melting curves in comparison to unmodified DNA duplexes. The experiment data fit well to a coarse-grain dynamic stimulation-based analytical model. The oligonucleotides took an orientation that enabled the sharing of ion interactions and resulting cooperative melting behavior.

1.3.3.2. Thermo-responsive Polymers

Stimuli-responsive polymers display a sharp change in physical or chemical properties upon a small or modest change in environmental conditions, which have been used for the design of "smart" nanomaterials for the controlled release of therapeutics[129,130]. Thermo-responsiveness is usually displayed as a nonlinear sharp change in transmittance or solubility of polymeric materials[131,132]. Thermo-responsive nanomaterials are among the most investigated stimuli-responsive systems for their promise in drug delivery and cancer therapy. Such a sharp response can be used for the design of triggered-release of the therapeutics following a variation in the surrounding temperature. For biomedical applications, thermosensitive nanocarriers should retain their load at body temperature (~37 ℃), and rapidly release the cargo within a locally heated disease region (~40–42 ℃). Extensively investigated thermo-responsive systems include liposomes, or polymeric micelles or nanoparticles (usually poly(N-isopropyl acrylamide), PNIPAM) that exhibit a lower critical solution temperature[41].

1.3.3.2.1- Poly(N-isopropylacrylamide) (PNIPAM)

Poly(N-isopropylacrylamide), first synthesized in the 1950s, is the preferred polymer building block for the design of thermosensitive polymeric drug nanocarriers [133,134]. It can be prepared via free radical polymerization from commercially available N-isopropylacrylamide and can be readily functionalized for a variety of applications. When heated in water above 32 ℃, it undergoes a reversible lower critical solution temperature (LCST) phase transition from a swollen hydrated state to a shrunken dehydrated state, losing about 90% of its volume. This LCST temperature is extremely

attractive because of its close proximity to physiological temperatures that can trigger a reversible phase transition of the crosslinked polymers without causing damage to surrounding tissues. Considerable efforts have been dedicated to the design of PNIPAM-based thermo-sensitive nanomaterials as delivery vehicles for controlled drug release[134]. Serres et al.[135] developed P(NIPAM-co-BMAco-AAc) for the intestinal delivery of human calcitonin. Kim et al. investigated the delivery of insulin[136]. Zhang et al. investigated the target efficacy of PNIPAM-based hydrogel for potential delivery of anti-cancer drugs[137].

Thermodynamically, the PNIPAM polymer stays in the most thermodynamically stable state at temperatures below the LCST,, where water molecules form a hydrated cage around the hydrophobic moieties along the polymer chain. When temperatures was raised above the LCST, the hydrogen bonding between the polymer and water molecules become thermodynamically unfavorable compared to polymer–polymer and water–water interactions. Such destabilization results in the desolvation of the hydrophobic groups of polymer chains. The increase in the entropy of the water molecules and hydrophobic interactions drives the collapse of polymer chains. The LCST can be tuned by adjusting the hydrophobicity-hydrophilicity ratio of the polymer chains in which an increase in hydrophilic groups increases the LCST and an increase in hydrophobic groups has the opposite effect[133]. Investigation also suggested that like the phase transition of PNIPAM which is almost independent of the concentration or molecular weight[133,138]. The transition temperature at any given concentration is almost identical to the LCST. It is to be noted that some thermos-responsive systems do display molecular weight or size dependence in cooperative LCST transitions[139,140].

The first detailed study of the temperature-dependent phase transition behavior of PNIPAM in aqueous solution was reported in 1969 by Heskins and Guillet[141]. They observed visually the change in clarity of a solution upon heating and measured that macroscopic phase transition of PNIPAM solutions was 32 °C. Since then, continuous efforts have been dedicated to investigate the phase transition process of PNIPAM and its derivatives, which inspired broad investigation of their potential in biomedical applications. Extensive mechanistic investigation suggests that the driving force for this phase transition is governed by the balance of hydrophilic and hydrophobic moieties[142-144]. PNIPAM chains carry two types of bound water molecules to form water cages around the isopropyl groups. One of them is around the hydrophobic moiety and the other one is bound around the amide group[145]. The phase transition of PNIPAM starts with a rearrangement of bound water molecules around either the hydrophobic moieties only or around both hydrophobic and hydrophilic groups. And the change in the hydration state of the hydrophobic side chains results in hydrophobic association of the hydrophobic groups.

Tanaka and co-worker first reported that the cooperative dehydration of the PNIPAM chains played a crucial role in the temperature-induced phase separation[146]. These authors theoretically studied the phase separation in PNIPAM's aqueous solutions. Based on the calculated phase diagrams, they concluded that the cooperativity dehydration between the neighboring water molecules that were hydrogen-bonded onto the polymer chain leads to sharp phase transition with only little molecular weight dependence. The degree of hydration plotted against the temperature correlated well with experimental data reported by Fujishige et al[147-149]. These authors also built a

"pearl-necklace" model to describe the cooperative dehydration process (**Figure 1.3.7**)[146,150]. When a water molecule succeeds in forming a hydrogen bond with an amide group on a chain, a second water molecule can form a bond more easily because the first molecule causes some displacement of the isopropyl group, which creates more accessible space for the next once. As a result, consecutive sequences of water molecules will be bound to along the chain, which leads to a pearl-necklace type chain conformation. When temperature increases, each sequence will also be dehydrated cooperatively, leading to the collective collapse of the chain and observed sharp melting curve.

Winnik group also investigated the temperature-induced phase transition behavior of cyclic PNIPAM in aqueous solution[151]. They found that the melting curves of cyclic PNIPAM solutions occurred over a much wider temperature range, compared to their linear counterpart, indicating that cyclization may partially inhibited the cooperativity hydration. A recent study by Muller-Buschbaum elucidated the impact of partial
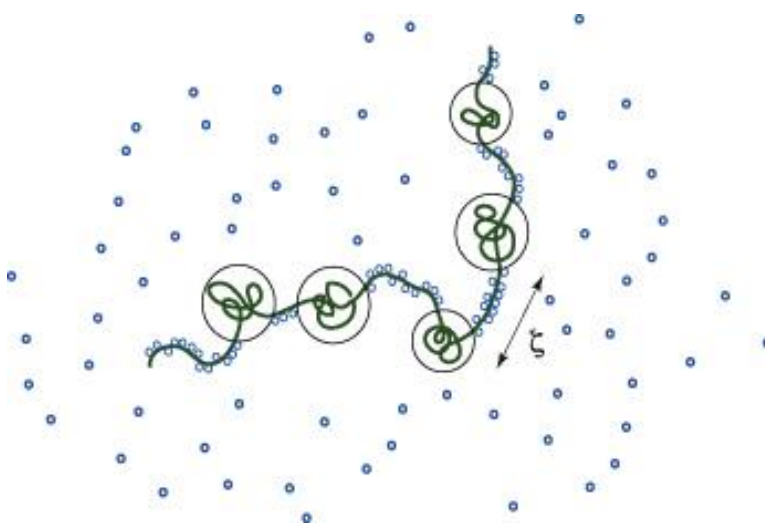
Figure 1.3.7. Pearl-necklace conformation induced by cooperative hydration. Cooperativity originates in the nearest-neighboring bound water molecules[150].

dehydration of PNIPAM on the volume changes related to the phase separation[152]. The impact of the molecular dehydration process on the macroscopic changes in volume was studied over a broad concentration range. The hydration number seems to decrease with the PNIPAM concentration of the solution, which indicates that the entanglement of the macromolecules hinders the full establishment of hydration shells and may affect the cooperative phase transition.

1.3.3.2.2- Elastin Like Polypeptides (ELPs)

Elastin is a highly elastic protein in connective tissue and allows tissues to resume their shape after stretching or contracting[153]. Elastin-like polypeptides (ELPs) are synthetic polypeptides derived from mammalian elastin. They consist of a penta-peptide repeat, VPGXG, where X refers to any natural amino acid except proline[154]. ELPs displayed lower critical solution temperature (LCST) transition similar to that of PNIPAM[154]. They are soluble at temperatures below LCST and aggregates at temperature higher than LCST. The stimuli-responsive phase transition and biocompatibility make them ideal materials for a variety of biomedical applications like drug delivery.

A study in 2010 evaluated a biodegradable drug delivery system for the local cancer radiotherapy consisting of a thermally sensitive elastin-like polypeptide (ELP) conjugated to a therapeutic radionuclide[155]. This injectable and biodegradable depot successfully delayed the tumor progression and showed the potential to control advanced-stage cancers by reducing the bulk of inoperable tumors. The Chilkoti group also reported the first first example of targeting a solid tumor that is externally heated to 42 °C by "heat seeking" drug-loaded polypeptide nanoparticles, which consisted of a

thermally responsive elastin-like polypeptide (ELP) conjugated to multiple copies of a hydrophobic cancer drug[156]. The drug delivery potential of ELP depot was also explored in joint degeneration[157,158], neuro-inflammation[159] and diabetes[160]. ELP-functionalized plasmonic nanoparticles[161], liposomes[162] and dendrimers[163] have also been developed for the controlled drug delivery applications.

Elastin like polypeptides can be genetically encoded and their sequence, stereochemistry and chain length can be precisely designed. Mechanistic investigation of the LCST behavior of ELP may help elucidate the key factors that controlling their phase transition temperature. The ELPs may also serve as a simple model system for the investigation of biophysical behavior of intrinsically disordered proteins (IDPs)[164]. Hinderberger group pioneered the mechanistic investigation of the LCST phase transition behavior of ELP (**Figure 1.3.8**)[165]. They showed that hydrophobic (side chains) and

independent side chain hydration   **coupled hydration layers**
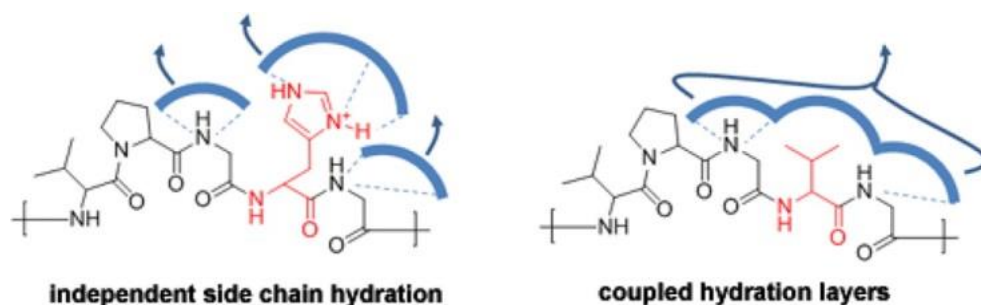
Figure 1.3.8. The hydration layer of the protic guest-residue side chain is individually stabilized by H-bonds and can be decoupled independently from backbone hydration layers (left). The hydration layer of the guest-residue side chain is stabilized via coupling to neighboring backbone hydration layers, and hence dehydration takes place cooperatively[165].

hydrophilic (backbone) hydration layers can exist in a coupled or decoupled state in ELPs. The coupling between these two types of hydration layers significantly influences the LCST transition of ELPs. Strongly coupled hydration state is characterized by a cooperative dehydration of both hydration layers. They also found that the side chain hydrophobicity and backbone length affect the cooperativity of the inverse phase transitions of ELPs. Chilkoti and co-worker established a unified model that predicts the transition temperature of ELPs from composition, chain length, and concentration in phosphate buffered saline[166]. They also provide a molecular description of the LCST behavior of EPLs based on a series of simulations[167]. The increase of temperature will lead to the gradual conformational changes of ELPs, arising from the formation of more ordered secondary structures. Increasing temperature also exposed the hydrophobic valine-side chains to the solvent, contributing to the collapse of polypeptide chains. The cooperative phase separation of ELPs can be attributed to a combination of thermal disruption of the water network that surrounds the polypeptide and increase in its hydrophobicity.

1.3.3.3-pH-(Low) Insertion Peptides (pHLIPs)

Dysregulated pH is emerging as a universal hallmark of cancer as described by Barber and coworkers.[168] Cancer cells display a "reversed" pH gradient with a constitutively increased intracellular pH (pH_i) and decreased extracellular pH (pH_e) compared to normal tissues regardless of their tissue origin and genetic background.[168] The increased increased protects the cancer cells from apoptotic cell deaths, facilitates cell proliferation and is necessary for cell migration. The decreased extracellular

pH[169-172], or tumor acidosis in the microenvironment, promotes extracellular matrix remodeling and stimulates acid-activated proteases for increased cancer local invasion and metastasis. Highly glycolytic tumors are shown to have acidic extracellular pH by Gillies and others[173]. In additional to metabolic abnormality, impaired lymphatic drainage may further contribute to the accumulation of acidic metabolites inside the tumors. Extensive investigations suggest that regardless of the bioenergetic types of tumors, tumor acidosis is a persistent characteristic of solid cancers[174-178].

Therefore, targeting tumor acidity might represent a powerful strategy for the prediction of tumor aggressiveness and delivery of therapeutic agents to tumor microenvironment. A numbers of molecular imaging and drug delivery systems have been designed in which the release of the diagnostic or therapeutic cargos is specifically triggered by the acidic tumor microenvironment[41,132,179-181]. Most of these pH-sensitive polymeric systems display broad pH response over around 2 pH units, similar to small molecular pH sensors. Two responsive polymeric pH sensors with sharp pH response have been developed and extensively investigated. Mechanistic investigation revealed that cooperativity in pH-triggered self-assembly contributed to observed sharp pH transition, which is critical for their biomedical applications. The physiological pH is delicately regulated in both intracellular and extracellular environment. The sharp pH transition enables superior sensitivity and specificity in reading and amplifying subtle pH variations.

Many proteins in living systems have display a unique pH-dependent membrane insertion behavior[182-186]. The membrane insertion some of these proteins needs contributions from the cell such as endocytosis. pHLIPs are a unique class of such

membrane polypeptides, usually consisting of around 36 amino acids, that are capable of undergoing pH-dependent membrane-associated folding. In acidic environment, pHLIPs can fold and insert across the membrane to form a stable transmembrane helix, thus preferentially locating itself in acidic tissues (**Figure 1.3.9**)[187]. Since tumors and other disease tissues like inflammtion are acidic, the pH-dependent insertion has been used for the development of tumor-targeted imaging agents and drug delivery systems[188].

In 2007, Reshetnyak and co-workers developed a fluorescently labeled pHLIP for the precise tumor imaging[189]. The imaging probe located solid tumors with high accuracy and accumulates in them even at a very early stage of tumor development. The fluorescence signal is about five times higher in tumors than in adjacent normal tissues and is stable over more than 4 days. A pHLIP-based delivery system was also reported for the translocation of phalloidin, a cell-impermeable polar toxin, into cytoplasm of cancer cells[190]. The polymeric carrier inserts its C terminus across the cell membrane under acidic conditions upon the formation of helix, which allowed the release of toxin
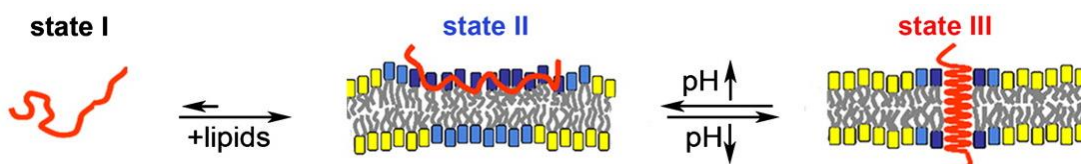
Figure 1.3.9. Schematic illustration of pHLIP 's interaction with a lipid bilayer at neutral and low pH values. State I refers to the peptide in solution at normal and basic pH. Upon addition of vesicles at pH 8, the unstructured peptide is adsorbed on the membrane surface (State II). A drop of pH leads to the protonation of Asp residues, increasing peptide hydrophobicity, and resulting in the insertion and formation of a transmembrane α-helix (State III)[187].

via the cleavage of disulfide bond. The proliferation in cultures of HeLa, JC, and M4A4 cancer cells is significantly inhibited. Nitin and co-workers designed a noninvasive topical delivery of Alexa-647 labeled pHLIP for the imaging of changes in extracellular pH in head and neck squamous cell carcinoma. The fluorescence intensity in clinically abnormal tissues is four to eight-fold higher that of normal tissues, indicating great promise in early detection and diagnosis of head and neck cancer.

Understanding the unique biophysics of pHLIPs and corresponding molecular
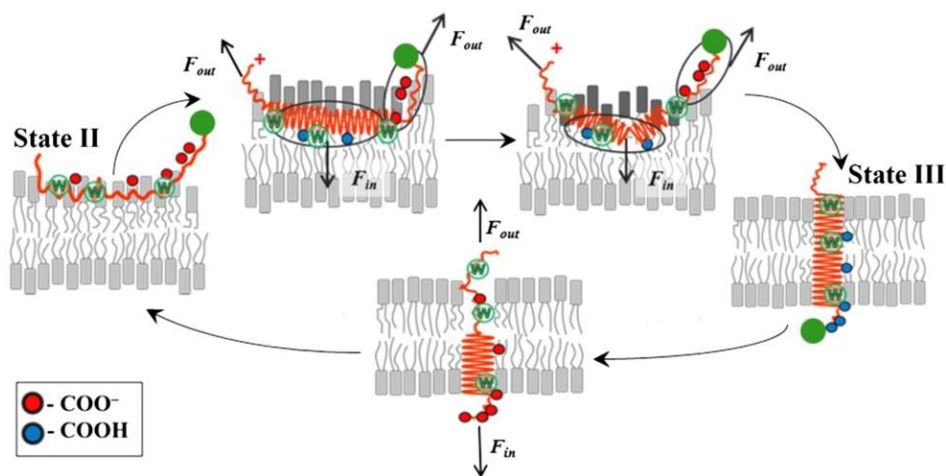
Figure 1.3.10. Molecular description of reversible insertion of pHLIPs. The letter W refers to the approximate positions of Trp residues in the single-Trp pHLIP-4 variants. Small red and blue circles represent the approximate positions of the protonatable carboxyl groups of Asp, Glu, and the C-terminus. The green circle represents polar cargo attached to the inserting end of the peptide. Membrane distortion is shown schematically by lipids with darker head groups. The insertion and folding of peptide chains appears without intermediates as an all-or-none transition, indicating a cooperative self-assembly process[195].

pathway of pH-induced membrane insertion process will further push forward the development of clinical-relevant tools. It is found that pHLIPs can exist in three distinct states: unstructured and soluble in aqueous solution, unstructured and binding to outer leaflet of membrane, and inserting its C-terminus across the membrane upon formation followed by the formation of α helix[191].

The two aspartic acid residues were critical for the observed pH-induced membrane insertion behavior[192]. These residues are negatively charged at neutral or basic environment, posing an energy barrier to prevent their insertion into the hydrophobic interior of phospholipid bilayers. At low pH, the acidic groups are protonated and enable the reduction in polarity enables the conformation change and transmembrane behavior. Previous investigations have suggested that the formation of helix is a cooperative process in many cases[193]. The cooperativity was also found in the pH-triggered assembly of pHLIPs. Engelman and co-workers reported that increasing the number of ionizable residues promote the pH-dependent cooperative membrane insertion process (**Figure 1.3.10**)[194,195]. The insertion generally took place over a wider pH range for peptides with fewer Asp residues. Mechanistic investigation suggested that the protonation of one Asp residue might facilitate the protonation of other ionizable residues and shift their pKa values. The protonation of the first Asp residue probably promote partial insertion of the peptide into the membrane. As a result, the protonation of the neighboring Asp residues would be energetically favored to shield the negative charge and then a positive feedback would be established, triggering complete membrane insertion. The cooperative insertion process was further validated by the report that the physical variable that may affect the membrane attachment and insertion behaviors of pHLIPs[196]. The results suggested that

the proline at position 20, midway through the transmembrane region, is crucial for pH-induced insertion activity. Replacement of proline-20 by glycine resulted in promiscuous insertion over a broader pH range, suggesting much less cooperativity of insertion than wide type pHLIPs.

1.4-References

1   Kim, B., Rutka, J. T. & Chan, W. C. Nanomedicine. *N Engl J Med* **2010**, 2434-2443 (2010).

2   Langer, R. & Tirrell, D. A. Designing materials for biology and medicine. *Nature* **428**, 487-492 (2004).

3   Freitas, R. A. What is nanomedicine? *Nanomedicine: Nanotechnology, Biology and Medicine* **1**, 2-9 (2005).

4   Etheridge, M. L. *et al.* The big picture on nanomedicine: the state of investigational and approved nanomedicine products. *Nanomedicine: nanotechnology, biology and medicine* **9**, 1-14 (2013).

5   Sumer, B. & Gao, J. Theranostic nanomedicine for cancer. *Nanomedicine* **3**, 137-140 (2008).

6   Ferrari, M. Cancer nanotechnology: opportunities and challenges. *Nature Reviews Cancer* **5**, 161-171 (2005).

7   Blanco, E., Shen, H. & Ferrari, M. Principles of nanoparticle design for overcoming biological barriers to drug delivery. *Nature biotechnology* **33**, 941-951 (2015).

8   Veronese, F. M. & Pasut, G. PEGylation, successful approach to drug delivery. *Drug discovery today* **10**, 1451-1458 (2005).

9   Doane, T. L. & Burda, C. The unique role of nanoparticles in nanomedicine: imaging, drug delivery and therapy. *Chemical Society Reviews* **41**, 2885-2911 (2012).

10   Keereweer, S. *et al.* Optical image-guided surgery—where do we stand? *Molecular Imaging and Biology* **13**, 199-207 (2011).

11   Conde, J., Oliva, N. & Artzi, N. Revisiting the 'One Material Fits All'Rule for Cancer Nanotherapy. *Trends in biotechnology* **34**, 618-626 (2016).

12   Zhuang, J., Gordon, M. R., Ventura, J., Li, L. & Thayumanavan, S. Multi-stimuli responsive macromolecules and their assemblies. *Chemical Society Reviews* **42**, 7421-7435 (2013).

13   Fang, J., Nakamura, H. & Maeda, H. The EPR effect: Unique features of tumor blood vessels for drug delivery, factors involved, and limitations and augmentation of the effect. *Advanced Drug Delivery Reviews* **63**, 136-151, doi:http://dx.doi.org/10.1016/j.addr.2010.04.009 (2011).

14   Gottesman, M. M., Fojo, T. & Bates, S. E. Multidrug resistance in cancer: role of ATP–dependent transporters. *Nature Reviews Cancer* **2**, 48-58 (2002).

15   Patel, N. R., Pattni, B. S., Abouzeid, A. H. & Torchilin, V. P. Nanopreparations to overcome multidrug resistance in cancer. *Advanced drug delivery reviews* **65**, 1748-1762 (2013).

16   Persidis, A. Cancer multidrug resistance. *Nature biotechnology* **17**, 94-95 (1999).

17   Peer, D. *et al.* Nanocarriers as an emerging platform for cancer therapy. *Nature nanotechnology* **2**, 751-760 (2007).

18   Schluep, T. *et al.* Preclinical efficacy of the camptothecin-polymer conjugate IT-101 in multiple cancer models. *Clinical Cancer Research* **12**, 1606-1614 (2006).

19   Ho, K., Lapitsky, Y., Shi, M. & Shoichet, M. S. Tunable immunonanoparticle binding to cancer cells: thermodynamic analysis of targeted drug delivery vehicles. *Soft Matter* **5**, 1074-1080 (2009).

20   Lane, L. A., Qian, X., Smith, A. M. & Nie, S. Physical chemistry of nanomedicine: Understanding the complex behaviors of nanoparticles in vivo. *Annual review of physical chemistry* **66**, 521-547 (2015).

21   Hong, S. *et al.* The binding avidity of a nanoparticle-based multivalent targeted drug delivery platform. *Chemistry & biology* **14**, 107-115 (2007).

22   Mammen, M., Choi, S.-K. & Whitesides, G. M. Polyvalent interactions in biological systems: implications for design and use of multivalent ligands and inhibitors. *Angewandte Chemie International Edition* **37**, 2754-2794 (1998).

23   Zwicke, G. L., Ali Mansoori, G. & Jeffery, C. J. Utilizing the folate receptor for active targeting of cancer nanotherapeutics. *Nano reviews* **3**, 18496 (2012).

24   Prescher, J. A. & Bertozzi, C. R. Chemistry in living systems. *Nature chemical biology* **1**, 13-21 (2005).

25   Koo, H. *et al.* Bioorthogonal Copper‐ Free Click Chemistry In Vivo for Tumor-Targeted Delivery of Nanoparticles. *Angewandte Chemie International Edition* **51**, 11836-11840 (2012).

26   Hou, S., Zhang, A. & Su, M.   (Multidisciplinary Digital Publishing Institute, 2016).

27   Luong, J. H., Male, K. B. & Glennon, J. D. Biosensor technology: technology push versus market pull. *Biotechnology advances* **26**, 492-500 (2008).

28   Lei, J. & Ju, H. Signal amplification using functional nanomaterials for biosensing. *Chemical Society Reviews* **41**, 2122-2134 (2012).

29   James, M. L. & Gambhir, S. S. A molecular imaging primer: modalities, imaging agents, and applications. *Physiological reviews* **92**, 897-965 (2012).

30   Holzinger, M., Le Goff, A. & Cosnier, S. Nanomaterials for biosensing applications: a review. *Frontiers in chemistry* **2**, 63 (2014).

31   Davis, M. E. & Shin, D. M. Nanoparticle therapeutics: an emerging treatment modality for cancer. *Nature reviews Drug discovery* **7**, 771-782 (2008).

32   Rosi, N. L. & Mirkin, C. A. Nanostructures in biodiagnostics. *Chemical reviews* **105**, 1547-1562 (2005).

33   Taton, T. A., Mirkin, C. A. & Letsinger, R. L. Scanometric DNA array detection with nanoparticle probes. *Science* **289**, 1757-1760 (2000).

34   Nam, J.-M., Thaxton, C. S. & Mirkin, C. A. Nanoparticle-based bio-bar codes for the ultrasensitive detection of proteins. *science* **301**, 1884-1886 (2003).

35   Han, M. S., Lytton- Jean, A. K., Oh, B. K., Heo, J. & Mirkin, C. A. Colorimetric Screening of DNA- Binding Molecules with Gold Nanoparticle Probes. *Angewandte Chemie International Edition* **45**, 1807-1810 (2006).

36   Liu, C.-W., Hsieh, Y.-T., Huang, C.-C., Lin, Z.-H. & Chang, H.-T. Detection of mercury (II) based on Hg 2+–DNA complexes inducing the aggregation of gold nanoparticles. *Chemical Communications*, 2242-2244 (2008).

37   Jin, R., Wu, G., Li, Z., Mirkin, C. A. & Schatz, G. C. What controls the melting properties of DNA-linked gold nanoparticle assemblies? *Journal of the American Chemical Society* **125**, 1643-1654 (2003).

38   Halo, T. L. *et al.* NanoFlares for the detection, isolation, and culture of live tumor cells from human blood. *Proceedings of the National Academy of Sciences* **111**, 17104-17109 (2014).

39   Chiang, A. C. & Massagué, J. Molecular basis of metastasis. *New England Journal of Medicine* **359**, 2814-2823 (2008).

40   Webber, M. J., Appel, E. A., Meijer, E. W. & Langer, R. Supramolecular biomaterials. *Nat Mater* **15**, 13-26, doi:10.1038/nmat4474 (2016).

41   Mura, S., Nicolas, J. & Couvreur, P. Stimuli-responsive nanocarriers for drug delivery. *Nature materials* **12**, 991-1003 (2013).

42   Lu, Y., Aimetti, A. A., Langer, R. & Gu, Z. Bioresponsive materials. *Nature Reviews Materials* **1**, 16075 (2016).

43   Bae, Y. H., Okano, T., Hsu, R. & Kim, S. W. Thermo- sensitive polymers as on- off switches for drug release. *Die Makromolekulare Chemie, Rapid Communications* **8**, 481-485 (1987).

44   Huffman, A. S., Afrassiabi, A. & Dong, L. C. Thermally reversible hydrogels: II. Delivery and selective removal of substances from aqueous solutions. *Journal of controlled release* **4**, 213-222 (1986).

45   Haraguchi, K., Takehisa, T. & Fan, S. Effects of clay content on the properties of nanocomposite hydrogels composed of poly (N-isopropylacrylamide) and clay. *Macromolecules* **35**, 10162-10171 (2002).

46   Haraguchi, K. & Takehisa, T. Nanocomposite hydrogels: a unique organic-inorganic network structure with extraordinary mechanical, optical, and swelling/de-swelling properties. *Advanced Materials* **14**, 1120 (2002).

47   Sun, J.-Y. *et al.* Highly stretchable and tough hydrogels. *Nature* **489**, 133-136 (2012).

48   Yan, Q. & Hoffman, A. S. Synthesis of macroporous hydrogels with rapid swelling and deswelling properties for delivery of macromolecules. *Polymer* **36**, 887-889 (1995).

49   Yan, H., Fujiwara, H., Sasaki, K. & Tsujii, K. Rapid Swelling/Collapsing Behavior of Thermoresponsive Poly (N- isopropylacrylamide) Gel Containing Poly (2- (methacryloyloxy) decyl phosphate) Surfactant. *Angewandte Chemie International Edition* **44**, 1951-1954 (2005).

50   Yoshida, R., Uchida, K., Kaneko, Y. & Sakai, K. Comb-type grafted hydrogels with rapid de-swelling response to temperature changes. *Nature* **374**, 240 (1995).

51   Xia, L.-W. *et al.* Nano-structured smart hydrogels with rapid response and high elasticity. *Nature communications* **4** (2013).

52   Kono, K. Thermosensitive polymer-modified liposomes. *Advanced drug delivery reviews* **53**, 307-319 (2001).

53   Al-Ahmady, Z. S. *et al.* Lipid–peptide vesicle nanoscale hybrids for triggered drug release by mild hyperthermia in vitro and in vivo. *ACS nano* **6**, 9335-9346 (2012).

54   Chen, K.-J. *et al.* A thermoresponsive bubble-generating liposomal system for triggering localized extracellular drug delivery. *ACS nano* **7**, 438-446 (2012).

55   Zhang, S. *et al.* A pH-responsive supramolecular polymer gel as an enteric elastomer for use in gastric devices. *Nature materials* **14**, 1065-1071 (2015).

56   Convertine, A. J. *et al.* pH-responsive polymeric micelle carriers for siRNA drugs. *Biomacromolecules* **11**, 2904-2911 (2010).

57   Cho, K., Wang, X., Nie, S. & Shin, D. M. Therapeutic nanoparticles for drug delivery in cancer. *Clinical cancer research* **14**, 1310-1316 (2008).

58   Makhlof, A., Tozuka, Y. & Takeuchi, H. pH-Sensitive nanospheres for colon-specific drug delivery in experimentally induced colitis rat model. *European Journal of Pharmaceutics and Biopharmaceutics* **72**, 1-8 (2009).

59   Nugent, S., Kumar, D., Rampton, D. & Evans, D. Intestinal luminal pH in inflammatory bowel disease: possible determinants and implications for therapy with aminosalicylates and other drugs. *Gut* **48**, 571-577 (2001).

60   Švastová, E. *et al.* Hypoxia activates the capacity of tumor- associated carbonic anhydrase IX to acidify extracellular pH. *FEBS letters* **577**, 439-445 (2004).

61   Min, K. H. *et al.* Tumoral acidic pH-responsive MPEG-poly (β-amino ester) polymeric micelles for cancer targeting therapy. *Journal of Controlled Release* **144**, 259-266 (2010).

62   Gao, G. H. *et al.* The use of pH-sensitive positively charged polymeric micelles for protein delivery. *Biomaterials* **33**, 9157-9164 (2012).

63   Ling, D. *et al.* Multifunctional tumor pH-sensitive self-assembled nanoparticles for bimodal imaging and treatment of resistant heterogeneous tumors. *Journal of the American Chemical Society* **136**, 5647-5655 (2014).

64   Du, J.-Z., Du, X.-J., Mao, C.-Q. & Wang, J. Tailor-made dual pH-sensitive polymer–doxorubicin nanoparticles for efficient anticancer drug delivery. *Journal of the American Chemical Society* **133**, 17560-17563 (2011).

65   Rim, H. P., Min, K. H., Lee, H. J., Jeong, S. Y. & Lee, S. C. pH- Tunable Calcium Phosphate Covered Mesoporous Silica Nanocontainers for Intracellular Controlled Release of Guest Drugs. *Angewandte Chemie International Edition* **50**, 8853-8857 (2011).

66   Lu, Y. *et al.* Transformable liquid-metal nanomedicine. *Nature communications* **6** (2015).

67   Mi, P. *et al.* A pH-activatable nanoparticle with signal-amplification capabilities for non-invasive imaging of tumour malignancy. *Nature nanotechnology* (2016).

68   Vogelstein, B. *et al.* Cancer genome landscapes. *science* **339**, 1546-1558 (2013).

69   Van Dam, G. M. *et al.* Intraoperative tumor-specific fluorescence imaging in ovarian cancer by folate receptor-[alpha] targeting: first in-human results. *Nature medicine* **17**, 1315-1319 (2011).

70   Veiseh, M. *et al.* Tumor paint: a chlorotoxin: Cy5. 5 bioconjugate for intraoperative visualization of cancer foci. *Cancer research* **67**, 6882-6888 (2007).

71   Ke, S. *et al.* Near-infrared optical imaging of epidermal growth factor receptor in breast cancer xenografts. *Cancer research* **63**, 7870-7875 (2003).

72   Nakajima, T. *et al.* Targeted, activatable, in vivo fluorescence imaging of prostate-specific membrane antigen (PSMA) positive tumors using the quenched humanized J591 antibody–indocyanine green (ICG) conjugate. *Bioconjugate chemistry* **22**, 1700-1705 (2011).

73   Paik, S. *et al.* HER2 and choice of adjuvant chemotherapy for invasive breast cancer: National Surgical Adjuvant Breast and Bowel Project Protocol B-15. *Journal of the National Cancer Institute* **92**, 1991-1998 (2000).

74   Jacobs, T. W., Gown, A. M., Yaziji, H., Barnes, M. J. & Schnitt, S. J. HER-2/neu protein expression in breast cancer evaluated by immunohistochemistry. *American journal of clinical pathology* **113**, 251-258 (2000).

75   Zhou, K. *et al.* Tunable, Ultrasensitive pH‐ Responsive Nanoparticles Targeting Specific Endocytic Organelles in Living Cells. *Angewandte Chemie International Edition* **50**, 6109-6114 (2011).

76   Ma, X. *et al.* Ultra-pH-sensitive nanoprobe library with broad pH tunability and fluorescence emissions. *Journal of the American Chemical Society* **136**, 11085-11092 (2014).

77   Heller, J., Penhale, D. & Helwing, R. Preparation of polyacetals by the reaction of divinyl ethers and polyols. *Journal of Polymer Science: Polymer Letters Edition* **18**, 293-297 (1980).

78   Gillies, E. R. & Fréchet, J. M. A new approach towards acid sensitive copolymer micelles for drug delivery. *Chemical Communications*, 1640-1641 (2003).

79   Lee, E. S., Shin, H. J., Na, K. & Bae, Y. H. Poly (L-histidine)–PEG block copolymer micelles and pH-induced destabilization. *Journal of Controlled Release* **90**, 363-374 (2003).

80   Roy, K., Mao, H.-Q., Huang, S.-K. & Leong, K. W. Oral gene delivery with chitosan–DNA nanoparticles generates immunologic protection in a murine model of peanut allergy. *Nature medicine* **5**, 387-391 (1999).

81 Choi, Y. H. *et al.* Polyethylene glycol-grafted poly-L-lysine as polymeric gene carrier. *Journal of controlled release* **54**, 39-48 (1998).

82 Boussif, O. *et al.* A versatile vector for gene and oligonucleotide transfer into cells in culture and in vivo: polyethylenimine. *Proceedings of the National Academy of Sciences* **92**, 7297-7301 (1995).

83 Pang, X. *et al.* pH-responsive polymer–drug conjugates: Design and progress. *Journal of Controlled Release* **222**, 116-129 (2016).

84 Wang, Y. *et al.* A nanoparticle-based strategy for the imaging of a broad range of tumours by nonlinear amplification of microenvironment signals. *Nature materials* **13**, 204-212 (2014).

85 Wang, C. *et al.* A nanobuffer reporter library for fine-scale imaging and perturbation of endocytic organelles. *Nature communications* **6** (2015).

86 Liu, X., Yan, C.-H. & Capobianco, J. A. Photon upconversion nanomaterials. *Chemical Society Reviews* **44**, 1299-1301 (2015).

87 Pumera, M. Graphene-based nanomaterials and their electrochemistry. *Chemical Society Reviews* **39**, 4146-4157 (2010).

88 Wang, J. Nanomaterial-based electrochemical biosensors. *Analyst* **130**, 421-426 (2005).

89 Chen, X., Li, C., Grätzel, M., Kostecki, R. & Mao, S. S. Nanomaterials for renewable energy production and storage. *Chemical Society Reviews* **41**, 7909-7937 (2012).

90 Sun, T. *et al.* Engineered nanoparticles for drug delivery in cancer therapy. *Angewandte Chemie International Edition* **53**, 12320-12364 (2014).

91   Hyun, D. C., Levinson, N. S., Jeong, U. & Xia, Y. Emerging Applications of Phase- Change Materials (PCMs): Teaching an Old Dog New Tricks. *Angewandte Chemie International Edition* **53**, 3780-3795 (2014).

92   Stupp, S. I. & Palmer, L. C. Supramolecular chemistry and self-assembly in organic materials design. *Chemistry of Materials* **26**, 507-518 (2013).

93   Lehn, J.-M. Supramolecular chemistry. *Science* **260**, 1762-1764 (1993).

94   Mattia, E. & Otto, S. Supramolecular systems chemistry. *Nature nanotechnology* **10**, 111-119 (2015).

95   Lehn, J. M. Perspectives in chemistry—steps towards complex matter. *Angewandte Chemie International Edition* **52**, 2836-2850 (2013).

96   Lehn, J.-M. Supramolecular chemistry—Scope and perspectives: Molecules—Supermolecules—Molecular devices. *Journal of inclusion phenomena* **6**, 351-396 (1988).

97   Eaton, W. A., Henry, E. R., Hofrichter, J. & Mozzarelli, A. Is cooperative oxygen binding by hemoglobin really understood? *Nature Structural & Molecular Biology* **6**, 351-358 (1999).

98   Lehn, J.-M. Toward complex matter: supramolecular chemistry and self-organization. *Proceedings of the National Academy of Sciences* **99**, 4763-4768 (2002).

99   Whitesides, G. M. & Grzybowski, B. Self-assembly at all scales. *Science* **295**, 2418-2421 (2002).

100   Frieden, E. Non-covalent interactions: key to biological flexibility and specificity. *J. Chem. Educ* **52**, 754 (1975).

101   Hyman, A. A. & Simons, K. Beyond oil and water—phase transitions in cells. *Science* **337**, 1047-1049 (2012).

102   Li, P. *et al.* Phase transitions in the assembly of multivalent signalling proteins. *Nature* **483**, 336-340 (2012).

103   Brangwynne, C. P. Phase transitions and size scaling of membrane-less organelles. *J Cell Biol* **203**, 875-881 (2013).

104   Williamson, J. R. Cooperativity in macromolecular assembly. *Nature chemical biology* **4**, 458-465 (2008).

105   Perutz, M. F. *et al.* Structure of haemoglobin: a three-dimensional Fourier synthesis at 5.5-A. resolution, obtained by X-ray analysis. *Nature* **185**, 416-422 (1960).

106   Perutz, M. F. Mechanisms of cooperativity and allosteric regulation in proteins. *Quarterly reviews of biophysics* **22**, 139-237 (1989).

107   Dickerson, R. E. & Geis, I. *Hemoglobin: structure, function, evolution, and pathology*. Vol. 1983 (Benjamin-Cummings Publishing Company, 1983).

108   Gumbiner, B. M. Cell adhesion: the molecular basis of tissue architecture and morphogenesis. *Cell* **84**, 345-357 (1996).

109   Moriki, T., Maruyama, H. & Maruyama, I. N. Activation of preformed EGF receptor dimers by ligand-induced rotation of the transmembrane domain. *Journal of molecular biology* **311**, 1011-1026 (2001).

110   Teramura, Y. *et al.* Single- molecule analysis of epidermal growth factor binding on the surface of living cells. *The EMBO journal* **25**, 4215-4222 (2006).

111   Yamada, K. M. & Even-Ram, S. Integrin regulation of growth factor receptors. *Nature cell biology* **4**, E75-E76 (2002).

112   Grakoui, A. *et al.* The immunological synapse: a molecular machine controlling T cell activation. *Science* **285**, 221-227 (1999).

113   Huppa, J. B. & Davis, M. M. T-cell-antigen recognition and the immunological synapse. *Nature Reviews Immunology* **3**, 973-983 (2003).

114   Kaizuka, Y., Douglass, A. D., Varma, R., Dustin, M. L. & Vale, R. D. Mechanisms for segregating T cell receptor and adhesion molecules during immunological synapse formation in Jurkat T cells. *Proceedings of the National Academy of Sciences* **104**, 20296-20301 (2007).

115   Dinner, A. R., Šali, A., Smith, L. J., Dobson, C. M. & Karplus, M. Understanding protein folding via free-energy surfaces from theory and experiment. *Trends in biochemical sciences* **25**, 331-339 (2000).

116   Dobson, C. M. Protein folding and misfolding. *Nature* **426**, 884-890 (2003).

117   Keskin, O., Gursoy, A., Ma, B. & Nussinov, R. Principles of protein− protein interactions: What are the preferred ways for proteins to interact? *Chemical reviews* **108**, 1225-1244 (2008).

118   Jackson, S. E. & Fersht, A. R. Folding of chymotrypsin inhibitor 2. 1. Evidence for a two-state transition. *Biochemistry* **30**, 10428-10435 (1991).

119   Tsai, C. J., Lin, S. L., Wolfson, H. J. & Nussinov, R. Studies of protein‐ protein interfaces: A statistical analysis of the hydrophobic effect. *Protein Science* **6**, 53-64 (1997).

120   Levy, Y. & Onuchic, J. N. Water mediation in protein folding and molecular recognition. *Annu. Rev. Biophys. Biomol. Struct.* **35**, 389-415 (2006).

121   Cheung, M. S., Garc á, A. E. & Onuchic, J. N. Protein folding mediated by solvation: water expulsion and formation of the hydrophobic core occur after the structural collapse. *Proceedings of the National Academy of Sciences* **99**, 685-690 (2002).

122   De las Heras Alarc ón, C., Pennadam, S. & Alexander, C. Stimuli responsive polymers for biomedical applications. *Chemical Society Reviews* **34**, 276-285 (2005).

123   Stuart, M. A. C. *et al.* Emerging applications of stimuli-responsive polymer materials. *Nature materials* **9**, 101-113 (2010).

124   Cutler, J. I., Auyeung, E. & Mirkin, C. A. Spherical nucleic acids. *Journal of the American Chemical Society* **134**, 1376-1391 (2012).

125   Mirkin, C. A., Letsinger, R. L., Mucic, R. C. & Storhoff, J. J. A DNA-based method for rationally assembling nanoparticles into macroscopic materials. *Nature* **382**, 607-609 (1996).

126   Taton, T. A., Mucic, R. C., Mirkin, C. A. & Letsinger, R. L. The DNA-mediated formation of supramolecular mono-and multilayered nanoparticle structures. *Journal of the American Chemical Society* **122**, 6305-6306 (2000).

127   Gibbs-Davis, J. M., Schatz, G. C. & Nguyen, S. T. Sharp melting transitions in DNA hybrids without aggregate dissolution: Proof of neighboring-duplex cooperativity. *Journal of the American Chemical Society* **129**, 15535-15540 (2007).

128   Eryazici, I., Prytkova, T. R., Schatz, G. C. & Nguyen, S. T. Cooperative melting in caged dimers with only two DNA duplexes. *Journal of the American Chemical Society* **132**, 17068-17070 (2010).

129   Yoshida, M. & Lahann, J. Smart nanomaterials. *Acs Nano* **2**, 1101-1107 (2008).

130   Dvir, T., Timko, B. P., Kohane, D. S. & Langer, R. Nanotechnological strategies for engineering complex tissues. *Nature nanotechnology* **6**, 13-22 (2011).

131   Dai, S., Ravi, P. & Tam, K. C. Thermo-and photo-responsive polymeric systems. *Soft Matter* **5**, 2513-2533 (2009).

132   Schmaljohann, D. Thermo-and pH-responsive polymers in drug delivery. *Advanced drug delivery reviews* **58**, 1655-1670 (2006).

133   Schild, H. G. Poly (N-isopropylacrylamide): experiment, theory and application. *Progress in polymer science* **17**, 163-249 (1992).

134   Bikram, M. & West, J. L. Thermo-responsive systems for controlled drug delivery. *Expert opinion on drug delivery* **5**, 1077-1091 (2008).

135   Serres, A., Baudyš, M. & Kim, S. W. Temperature and pH-sensitive polymers for human calcitonin delivery. *Pharmaceutical research* **13**, 196-201 (1996).

136   Yong-Hee, K., Bae, Y. H. & Kim, S. W. pH/temperature-sensitive polymers for macromolecular drug loading and release. *Journal of controlled release* **28**, 143-152 (1994).

137   Zhang, J., Chen, H., Xu, L. & Gu, Y. The targeted behavior of thermally responsive nanohydrogel evaluated by NIR system in mouse model. *Journal of controlled release* **131**, 34-40 (2008).

138   Shibayama, M., Norisuye, T. & Nomura, S. Cross-link density dependence of spatial inhomogeneities and dynamic fluctuations of poly (N-isopropylacrylamide) gels. *Macromolecules* **29**, 8746-8750 (1996).

139   Gibson, M. I., Paripovic, D. & Klok, H. A. Size- Dependent LCST Transitions of Polymer- Coated Gold Nanoparticles: Cooperative Aggregation and Surface Assembly. *Advanced Materials* **22**, 4721-4725 (2010).

140   Ieong, N. S. *et al.* Polymers with molecular weight dependent LCSTs are essential for cooperative behaviour. *Polymer Chemistry* **3**, 794-799 (2012).

141   Heskins, M. & Guillet, J. E. Solution properties of poly (N-isopropylacrylamide). *Journal of Macromolecular Science—Chemistry* **2**, 1441-1455 (1968).

142   Tanaka, N., Matsukawa, S., Kurosu, H. & Ando, I. A study on dynamics of water in crosslinked poly (N-isopropylacrylamide) gel by nmr spectroscopy. *Polymer* **39**, 4703-4706 (1998).

143   Sasaki, S., Kawasaki, H. & Maeda, H. Volume phase transition behavior of N-isopropylacrylamide gels as a function of the chemical potential of water molecules. *Macromolecules* **30**, 1847-1848 (1997).

144   Grinberg, N. V. *et al.* Studies of the thermal volume transition of poly (N-isopropylacrylamide) hydrogels by high-sensitivity differential scanning microcalorimetry. 1. Dynamic effects. *Macromolecules* **32**, 1471-1475 (1999).

145   Otake, K., Inomata, H., Konno, M. & Saito, S. Thermal analysis of the volume phase transition with N-isopropylacrylamide gels. *macromolecules* **23**, 283-289 (1990).

146   Okada, Y. & Tanaka, F. Cooperative hydration, chain collapse, and flat LCST behavior in aqueous poly (N-isopropylacrylamide) solutions. *Macromolecules* **38**, 4465-4471 (2005).

147   Tanaka, F., Koga, T. & Winnik, F. M. Temperature-responsive polymers in mixed solvents: competitive hydrogen bonds cause cononsolvency. *Physical review letters* **101**, 028302 (2008).

148   Tanaka, F., Koga, T., Kojima, H. & Winnik, F. M. Temperature-and tension-induced coil− globule transition of Poly (N-isopropylacrylamide) chains in water and mixed solvent of water/methanol. *Macromolecules* **42**, 1321-1330 (2009).

149   Fujishige, S., Kubota, K. & Ando, I. Phase transition of aqueous solutions of poly (N-isopropylacrylamide) and poly (N-isopropylmethacrylamide). *Journal of Physical Chemistry* **93**, 3311-3313 (1989).

150   Tanaka, F., Koga, T., Kaneda, I. & Winnik, F. M. Hydration, phase separation and nonlinear rheology of temperature-sensitive water-soluble polymers. *Journal of Physics: Condensed Matter* **23**, 284105 (2011).

151   Qiu, X.-P., Tanaka, F. & Winnik, F. M. Temperature-induced phase transition of well-defined cyclic poly (N-isopropylacrylamide) s in aqueous solution. *Macromolecules* **40**, 7069-7071 (2007).

152   Philipp, M. *et al.* From molecular dehydration to excess volumes of phase-separating PNIPAM solutions. *The Journal of Physical Chemistry B* **118**, 4253-4260 (2014).

153   Keeley, F. W., Bellingham, C. M. & Woodhouse, K. A. Elastin as a self–organizing biomaterial: use of recombinantly expressed human elastin polypeptides as a model for investigations of structure and self–assembly of elastin. *Philosophical Transactions of the Royal Society of London B: Biological Sciences* **357**, 185-189 (2002).

154   Urry, D. W. Free energy transduction in polypeptides and proteins based on inverse temperature transitions. *Progress in biophysics and molecular biology* **57**, 23-57 (1992).

155   Liu, W. *et al.* Injectable intratumoral depot of thermally responsive polypeptide–radionuclide conjugates delays tumor progression in a mouse model. *Journal of controlled Release* **144**, 2-9 (2010).

156   McDaniel, J. R. *et al.* Rational design of "heat seeking" drug loaded polypeptide nanoparticles that thermally target solid tumors. *Nano letters* **14**, 2890-2895 (2014).

157   Shamji, M. F. *et al.* Development and characterization of a fusion protein between thermally responsive elastin- like polypeptide and interleukin- 1 receptor antagonist: Sustained release of a local antiinflammatory therapeutic. *Arthritis & Rheumatology* **56**, 3650-3661 (2007).

158   Betre, H. *et al.* A thermally responsive biopolymer for intra-articular drug delivery. *Journal of controlled release* **115**, 175-182 (2006).

159   Shamji, M. F. *et al.* Synthesis and characterization of a thermally-responsive tumor necrosis factor antagonist. *Journal of Controlled Release* **129**, 179-186 (2008).

160   Amiram, M., Luginbuhl, K. M., Li, X., Feinglos, M. N. & Chilkoti, A. Injectable protease-operated depots of glucagon-like peptide-1 provide extended and tunable glucose control. *Proceedings of the National Academy of Sciences* **110**, 2792-2797 (2013).

161   Nath, N. & Chilkoti, A. Interfacial phase transition of an environmentally responsive elastin biopolymer adsorbed on functionalized gold nanoparticles studied by colloidal surface plasmon resonance. *Journal of the American Chemical Society* **123**, 8197-8202 (2001).

162   Park, S. M. *et al.* Novel temperature-triggered liposome with high stability: Formulation, in vitro evaluation, and in vivo study combined with high-intensity focused ultrasound (HIFU). *Journal of Controlled Release* **170**, 373-379 (2013).

163   Kojima, C. & Irie, K. Synthesis of temperature- dependent elastin- like peptide- modified dendrimer for drug delivery. *Peptide Science* **100**, 714-721 (2013).

164   Dyson, H. J. & Wright, P. E. Coupling of folding and binding for unstructured proteins. *Current opinion in structural biology* **12**, 54-60 (2002).

165   Kurzbach, D. *et al.* Hydration layer coupling and cooperativity in phase behavior of stimulus responsive peptide polymers. *Journal of the American Chemical Society* **135**, 11299-11308 (2013).

166   McDaniel, J. R., Radford, D. C. & Chilkoti, A. A unified model for de novo design of elastin-like polypeptides with tunable inverse transition temperatures. *Biomacromolecules* **14**, 2866-2872 (2013).

167   Li, N. K., Quiroz, F. G., Hall, C. K., Chilkoti, A. & Yingling, Y. G. Molecular description of the LCST behavior of an elastin-like polypeptide. *Biomacromolecules* **15**, 3522-3530 (2014).

168   Webb, B. A., Chimenti, M., Jacobson, M. P. & Barber, D. L. Dysregulated pH: a perfect storm for cancer progression. *Nat. Rev. Cancer* **11**, 671-677, doi:Doi 10.1038/Nrc3110 (2011).

169   Gillies, R. J., Liu, Z. & Bhujwalla, Z. P-31-Mrs Measurements of Extracellular Ph of Tumors Using 3-Aminopropylphosphonate. *Am. J. Physiol.* **267**, C195-C203 (1994).

170   Gillies, R. J., Raghunand, N., Garcia-Martin, M. L. & Gatenby, R. A. PH imaging. *IEEE Eng. Med. Biol. Mag.* **23**, 57-64, doi:Doi 10.1109/Memb.2004.1360409 (2004).

171   van Sluis, R. *et al.* In vivo imaging of extracellular pH using (1)H MRSI. *Magn. Reson. Med.* **41**, 743-750, doi:Doi 10.1002/(Sici)1522-2594(199904)41:4<743::Aid-Mrm13>3.0.Co;2-Z (1999).

172   Volk, T., Jahde, E., Fortmeyer, H. P., Glusenkamp, K. H. & Rajewsky, M. F. pH in human tumour xenografts: effect of intravenous administration of glucose. *Br. J. Cancer* **68**, 492-500 (1993).

173   Gatenby, R. A. & Gillies, R. J. Why do cancers have high aerobic glycolysis? *Nat. Rev. Cancer* **4**, 891-899, doi:10.1038/nrc1478 (2004).

174   Helmlinger, G., Sckell, A., Dellian, M., Forbes, N. S. & Jain, R. K. Acid production in glycolysis-impaired tumors provides new insights into tumor metabolism. *Clin. Cancer Res.* **8**, 1284-1291 (2002).

175   Newell, K., Franchi, A., Pouyssegur, J. & Tannock, I. Studies with glycolysis-deficient cells suggest that production of lactic acid is not the only cause of tumor acidity. *Proc. Natl. Acad. Sci. U. S. A.* **90**, 1127-1131 (1993).

176   Yamagata, M., Hasuda, K., Stamato, T. & Tannock, I. F. The contribution of lactic acid to acidification of tumours: studies of variant cells lacking lactate dehydrogenase. *Br. J. Cancer* **77**, 1726-1731, doi:Doi 10.1038/Bjc.1998.289 (1998).

177   Neri, D. & Supuran, C. T. Interfering with pH regulation in tumours as a therapeutic strategy. *Nature reviews Drug discovery* **10**, 767-777 (2011).

178   Jose, C., Bellance, N. & Rossignol, R. Choosing between glycolysis and oxidative phosphorylation: a tumor's dilemma? *Biochimica et Biophysica Acta (BBA)-Bioenergetics* **1807**, 552-561 (2011).

179   Blum, A. P. *et al.* Stimuli-Responsive Nanomaterials for Biomedical Applications. *Journal of the American Chemical Society* **137**, 2140-2154 (2015).

180   Wang, C. *et al.* Investigation of endosome and lysosome biology by ultra pH-sensitive nanoprobes. *Advanced Drug Delivery Reviews* (2016).

181   Gao, W., Chan, J. M. & Farokhzad, O. C. pH-responsive nanoparticles for drug delivery. *Molecular pharmaceutics* **7**, 1913-1920 (2010).

182   Vargas-Uribe, M., Rodnin, M. V. & Ladokhin, A. S. Comparison of membrane insertion pathways of the apoptotic regulator Bcl-xL and the diphtheria toxin translocation domain. *Biochemistry* **52**, 7901-7909 (2013).

183   Jakes, K. S. & Cramer, W. A. Border crossings: colicins and transporters. *Annual review of genetics* **46**, 209-231 (2012).

184   Zakharov, S. D., Lindeberg, M. & Cramer, W. A. Kinetic description of structural changes linked to membrane import of the colicin E1 channel protein. *Biochemistry* **38**, 11325-11332 (1999).

185   Zhan, H., Oh, K. J., Shin, Y.-K., Hubbell, W. L. & Collier, R. J. Interaction of the isolated transmembrane domain of diphtheria toxin with membranes. *Biochemistry* **34**, 4856-4863 (1995).

186   Ladokhin, A. S., Legmann, R., Collier, R. J. & White, S. H. Reversible refolding of the diphtheria toxin T-domain on lipid membranes. *Biochemistry* **43**, 7451-7458 (2004).

187   Andreev, O. A. *et al.* pH (low) insertion peptide (pHLIP) inserts across a lipid bilayer as a helix and exits by a different path. *Proceedings of the National Academy of Sciences* **107**, 4081-4086 (2010).

188   Deacon, J. C., Engelman, D. M. & Barrera, F. N. Targeting acidity in diseased tissues: mechanism and applications of the membrane-inserting peptide, pHLIP. *Archives of biochemistry and biophysics* **565**, 40-48 (2015).

189   Andreev, O. A. *et al.* Mechanism and uses of a membrane peptide that targets tumors and other acidic tissues in vivo. *Proceedings of the National Academy of Sciences* **104**, 7893-7898 (2007).

190   An, M., Wijesinghe, D., Andreev, O. A., Reshetnyak, Y. K. & Engelman, D. M. pH-(low)-insertion-peptide (pHLIP) translocation of membrane impermeable phalloidin toxin inhibits cancer cell proliferation. *Proceedings of the National Academy of Sciences* **107**, 20246-20250 (2010).

191   Reshetnyak, Y. K., Andreev, O. A., Segala, M., Markin, V. S. & Engelman, D. M. Energetics of peptide (pHLIP) binding to and folding across a lipid bilayer membrane. *Proceedings of the National Academy of Sciences* **105**, 15340-15345 (2008).

192   Hunt, J. F., Rath, P., Rothschild, K. J. & Engelman, D. M. Spontaneous, pH-dependent membrane insertion of a transbilayer α-helix. *Biochemistry* **36**, 15177-15192 (1997).

193   Scholtz, J. M. & Baldwin, R. L. The mechanism of alpha-helix formation by peptides. *Annual review of biophysics and biomolecular structure* **21**, 95-118 (1992).

194   Barrera, F. N. *et al.* Roles of carboxyl groups in the transmembrane insertion of peptides. *Journal of molecular biology* **413**, 359-371 (2011).

195   Karabadzhak, A. G. *et al.* Modulation of the pHLIP transmembrane helix insertion pathway. *Biophysical journal* **102**, 1846-1855 (2012).

196   Barrera, F. N., Fendos, J. & Engelman, D. M. Membrane physical properties influence transmembrane helix formation. *Proceedings of the National Academy of Sciences* **109**, 14422-14427 (2012).

CHAPTER TWO-pH Responsive Behavior of PEO-b-PR Block Copolymers

2.1-Introduction

2.1.1-pH regulation in biological systems

2.1.1.1-pH homeostasis is critical for cell and tissue functions

Eukaryotic cells are well compartmentalized, segregating specific functions within a multitude of membrane-bounded organelles. Each organelle provides distinct environment and conditions for their individual metabolic pathways. Also, there is the need to store energy as electrochemical gradients across the organelle membrane dielectric. All proteins depend on pH to maintain their structural and functional integrity and the protonation and deprotonation are critical part of many metabolic reactions[3]. Moreover, the proton gradient is the key to generate and convert cellular energy. Thus protons play a crucial role in maintaining cellular homeostasis and intracellular pH is delicately regulated. It is also not surprising that the pH values of different subcellular organelles vary significantly from each other since they have distinct functions and metabolic pathways.

Figure 2.1.1 summarize the pH values of different subcellular organelles[4]. For example, the lysosome has a pH of about 5.0 compared with the rest of the cytoplasm at pH 7.2. Not surprisingly, the enzymes that work within this organelle have a pH optimum at about 5, which makes them distinct from those in the main cellular cytoplasm. Mitochondria is capable of moving protons across their inner membrane during oxidative phosphorylation, resulting in slight alkali matrix pH. The generation of a proton gradient across the inner mitochondrial membrane enables multiple metabolic processes such as
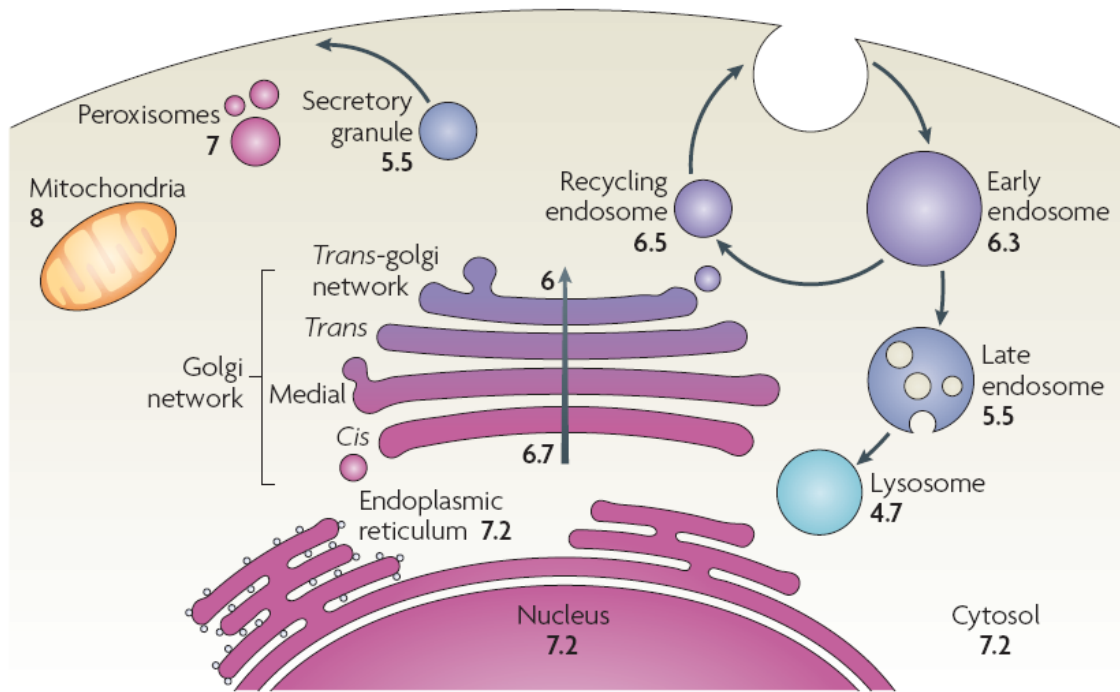
Figure. 2.1.1. pH of different subcellular organelles. The pH of individual cellular compartments in a prototypical mammalian cell[4].

energy conversion, reactive oxygen species production, apoptosis and lipid metabolism. The nuclear envelope has numbers of pores that allow the permeation of molecules with diameter around 4-9 nm, similar to the size of a small protein. Therefore, the nuclear membrane only presents a relatively weak diffusive barrier to protons and the pH value of nucleus is almost identical to that of cytosol.

2.1.1.2-Tumor acidosis is a universal hallmark of cancer

Dysregulated pH is emerging as a universal hallmark of cancer as described by Barber and coworkers[5]. Cancer cells display a "reversed" pH gradient with a constitutively increased intracellular pH (pH_i) and decreased extracellular pH ($pH_{e)}$ compared to normal tissues (**Figure 2.1.2**) regardless of their tissue origin and genetic background[5]. The increased pH_i is sufficient to induce dysplasia[6] and further protects the cancer cells from apoptotic cell deaths[7,8] and is necessary for cell migration[9,10]. The decreased pH_e[11-14], or tumor acidosis in the microenvironment, promotes extracellular
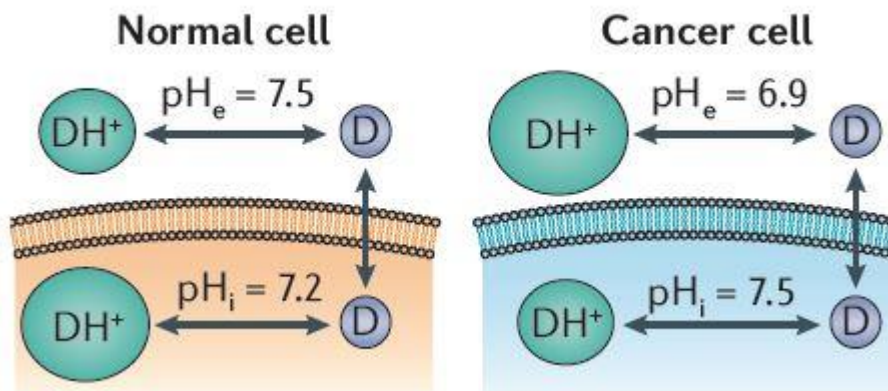
Figure 2.1.2. Dysregulated pH of tumor microenvironment[1].

matrix remodeling and stimulates acid-activated proteases for increased cancer local invasion and metastasis.

Many mechanisms and cell surface protein/pump/exchangers were involved in tumor acidosis (**Figure 2.1.3**)[15]. Highly glycolytic tumors are shown to have acidic extracellular pH by Gillies and others[16]. Conversion of glucose to lactic acids produces two equivalents of protons for each glucose molecule. Cancer cells have elevated expressions of monocarboxylate transporters (e.g., MCT1/4), which efficiently pump lactic acids from cytoplasm to the extracellular environment. Jain and others reported that glycolysis-impaired tumors also have an acidic tumor microenvironment[17-19]. CO_2 from
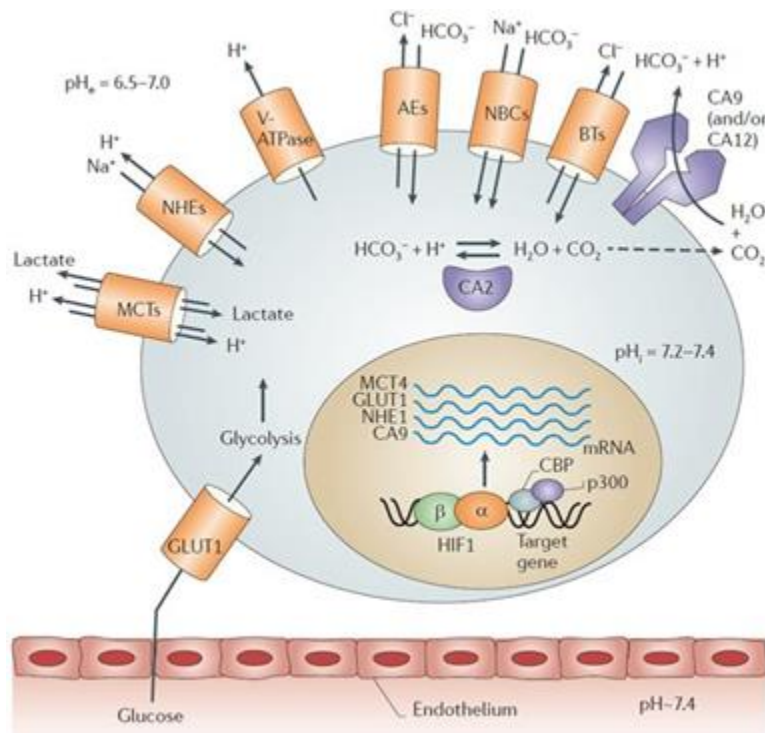
Figure 2.1.3. pH regulatory proteins in a cancer cell. Proton pumping results in tumor acidosis in the microenvironment as well as raising the intracellular pH to promote cell proliferation[2].

elevated mitochondrial metabolism through oxidative phosphorylation (OXPHOS) pathway can also contribute to tumor acidosis as catalyzed by carbonic anhydrase IX (CAIX) on the cancer cell surface[20]. In this process, CO_2 is first converted to carbonic acids that further dissociate into protons and bicarbonates. In addition to MCTs and CAIX, other pH regulatory proteins (e.g., V-ATPase, Na^+/bicarbonate transporter, and anion exchangers) also contribute to acidic pH_e[15]. These findings suggest that regardless of the bioenergetic types of tumors[21], tumor acidosis is a persistent characteristic of solid cancers.

2.1.2-pH responsive probes

Optical sensors are considered to be "eyes and ears capable of seeing and hearing beyond the human perception". The optical sensors employ signal transduction techniques based on reagents that change optical properties upon interactions with targets of interest. In practice, the optical properties such as absorption, fluorescence intensity and decay time are measured in most cases. Nevertheless, the refractive index, light scattering and reflectance may also serve as analytical parameters for optical sensing. **Figure 2.1.4** gives the general principle of the optical pH sensors[22]. In this chapter, we only focus on fluorescence-based sensors for measuring and monitoring pH changes, especially in physiological environment like living cells.

Fluorescence-based pH sensors usually provide higher sensitivity and specificity than absorption-based pH indicators[23]. Compared to pH measurement techniques sucah as NMR, absorbance spectroscopy, the fluorescent spectroscopy also shows better spatial
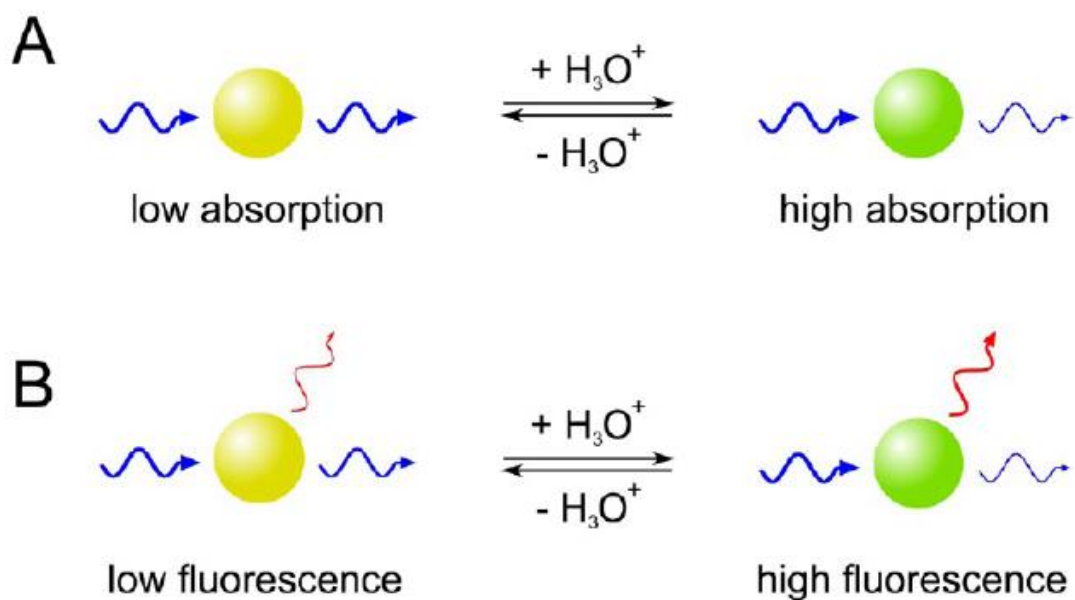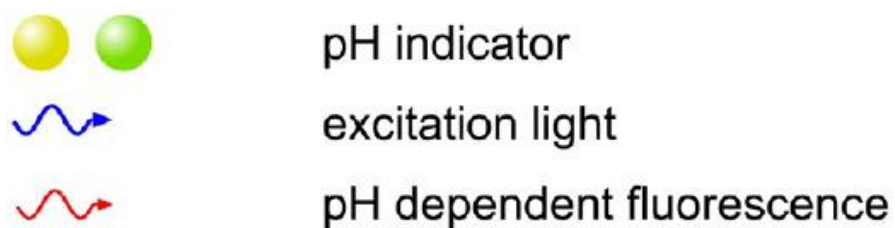
Figure 2.1.4. Schematic representation of the principle of (A) absorption-based and (B) fluorescence-based pH sensing platforms[22].

and temporal resolutions[24]. Moreover, the fluorescence-based pH monitoring is more operation-friendly and non-invasive.

Good fluorescent pH indicators for biomedical applications much have following characteristics: (1) they should respond drastically to a minor change in pH values, which is crucial for dependable measurement; (2) they should have good photo-stability and avoid interference from other cellular species; (3) they should have good selectivity and the ability to work within the appropriate pH ranges like the physiological environment; (4) they should have high fluorescence quantum yield and in turn lower the dose needed for successful imaging; (5) they should minimize the photo damage and the auto-fluorescence; (6) they must be bio-compatible and low-toxic.

2.1.2.1-Commonly used fluorescent pH sensors in biomedical research

Fluoresceins are one of the most commonly used fluorescent reagents with high excitation coefficient, high quantum yield and good bio-compatibility. Their derivatives have been used for the measurement of intracellular pH in single cells[25]. However, the fluorescein dyes do not work well in multicolor applications due to broad fluorescence-emission spectra. The pH measurement is not very accurate in the pH range at 4-6. In addition, the quantification changes in intracellular pH can be difficult since the fluorescein dyes tend to leak out from cells rapidly[26].

Rhodamine dyes are extensively used in cell biology studies as molecular imaging reagents[27,28]. They usually show high extinction coefficient, good photo-stability and relatively high quantum yield. Zhang and his colleagues developed a Rhodamine B based fluorescent probes for the imaging of living cells[27]. By alterating the molecular structures

between spirocyclic (non-fluorescent moeity) and ring-opening (fluorescent moiety) conformation of the rhodamine, the fluorescent intensity of their dyes changes over 100-fold within the pH range 4-6.

The near-infrared (NIR) cyanine dyes have emerged as one of the most popular imaging probes for the various biomedical applications[29,30]. The cyanine dyes also possess high extinction coefficient, good photo-stability and wide response spectrum. Moreover, the emission wavelength can minimize the unwanted photo damage and interference of auto-fluorescence. Tang et al. reported the development of cyanine based-dual NIR pH fluorescent probe for real-time imaging of cellular pH in HepG and HL-7702 cells[31].

Boron-dipyrromethene (BODIPY) can serve as good labeling dyes for proteins in vivo. The BODIPY dyes have sharp fluorescence peaks, high quantum yield and insensitivity to solvent polarity. Boens et al. synthesized a series of BODIPY derivatives with pKa values between 7.5 to 9.3. The absorption and emission of the dyes were 570-580 and 610-620 nm respectively. They have showed promise fluorescent probes for detection of cellular pH. **Figure 2.1.5** highlighted the applications and performances of several representative pH fluorescent probes[27].

2.1.2.2-pH responsive fluorescent nanoprobes

Nanotechnology represents an emerging approach for cancer diagnosis and therapeutics. Stimuli-responsive nanomaterials have been extensively studied for the last several

Probes	Applications	Advantages/Disadvantages
Chlorinated fluoresceins	Real-time pH sensing in living HEK-293T, B16F10 and L929 cells in pH range of 3.5–7.0	High extinction coefficients, excellent fluorescence quantum yield, good water solubility, non-toxicity, fluorescence excitation and emission spectra in visible region/Too broad fluorescence emission spectrum, rapid leakage of the dye from cells and little Stokes shift
Rhodamine dyes 5	Monitoring H$^+$ within living HepG2 cells *in vivo*	High extinction coefficients, good photostability, high fluorescence quantum yield/Weak interactions between probe and targeted biomolecule
Rhodamine dyes 6 and 7	Monitoring lysosome pH in Hela cells *in vivo*	Cell membrane permeability/Short fluorescence lifetime
NIR cyanine 8	pH imaging in HepG2 cells	
NIR cyanine 9	Detecting pH *in situ* in living HepG2 and HL-7702 cells	High extinction coefficients (>200000 L mol^{-1} cm^{-1}), wide response
NIR cyanine 12	Fluorescence-based pH imaging, both intracellular and through photodiffusion in biological tissue within pH ranges of 5.0–9.0	spectrum, good fluorescence function and high photostability/Inferior photostability and thermal stability
Square-650-pH	Studying phagocytic events and monitoring pH changes in cells	Commercial, absorption and emission in the NIR region/NA
BODIPY 13–17	Detecting pH in cells	
BODIPY 18	Working within pH 4.0–6.5 and pH 7.0–8.0, imaging protein-dye conjugates in living COS-7 cells	Uniquely small Stokes shift, high, environment-independent fluorescence quantum yields, and sharp excitation and emission peaks contributing
BODIPY 19–22	Real-time monitoring pH changes in HER2-positive cells *ex vivo* and *in vivo*	to overall brightness/NA

Figure 2.1.5. Highlights of applications and performances of pH fluorescent probes[27].

decades and have shown great promise in addressing the deficiencies of small molecular chemical or biological sensors such as low sensitivity and specificity.

The Engelman groups have been working on the development of pH (low) insertion peptides (pHLIP)[32]. Upon pH changes, the peptides can reversibly folds and inserts into the cellular membranes[33], which enables a unique way to target the acidic tumor microenvironment. They also showed that the tumor targeting efficiency and bio-distribution can be tuned by changing the physiochemical properties of the peptide-lipid bilayer interactions.

The Nie groups reported a strategy in designing pH-sensitive gold nanoparticles based on the use of multi-dentate polymeric ligands[34]. The ligands contain both pH responsive carboxylic acids groups and sterically hindered aliphatic side chains, which enables the pH sensitivity and stabilize the nanoparticles during nucleation and growth. Small pH changes results in sharp transition in water solubility as proved by precipitation of AuNCs. The optical properties changes as a result of aggregation of gold nanoparticles can be applied for imaging applications.

Hyeon and his coworkers also reported a nanoparticle-based integrative pH sensitive platform for the imaging and treatment of tumors[35]. The pH-sensitive magnetic nanogrenades (PMN) consist of pH-responsive ligands and iron-oxide particles. The pH-induced surface-charge transition enables the targeting of acidic tumor microenvironment. The PMN showed superior therapeutic efficacy in highly heterogeneous drug-resistant tumors, indicating potential clinical translation.

2.2-Materials and methods

N-Hydroxysuccinimidal ester of tetramethyl rhodamine (NHS-TMR) was purchased from the Invitrogen Company. Cy5-NHS ester was purchased from the Lumiprobe Corporation. PEO macroinitiator, MeO-PEO114-Br, was prepared from 2-bromo-2-methyl propanoyl bromide and MeO-PEO114-OH according to the procedure in literature. Monomers such as 2-(dimethylamino)ethyl methacrylate (DMA-MA), 2-(diethylamino)ethyl methacrylate (DEA-MA) and 2-aminoethyl methacrylate (AMA) were purchased from Polyscience Company. The 2-(dibutylamino) ethyl methacrylate (DBA-MA) monomer was synthesized following a previous publication[1]. AMA monomer was recrystallized twice with isopropanol and ethyl acetate (3:7) before use. Bromopropane, bromopentane, ethanolamine, methacryloyl chloride and sodium salts were purchased from Sigma-Aldrich. Other solvents and reagents were used as received from Sigma-Aldrich or Fisher Scientific Inc.

2.2.1-Synthesis

2.2.1.1-Syntheses of methacrylate monomers

Methacrylate monomers were synthesized following a published method. Synthesis of 2-(dipropylamino) ethyl methacrylate (DPA-MA) is described here as an example. First, ethanolamine (12.2g, 0.2 mol) and bromopropane (49.2 g, 0.4 mol) were dissolved in 400 mL acetonitrile, and Na_2CO_3 (53.0 g, 0.5 mol) was added to the solution. After overnight reaction, the solution was filtered to remove the precipitated NaBr salt and extra Na_2CO_3. CH_3CN solvent was removed by rotovap. The resulting residue was distilled in vacuo (40~45 ℃ at 0.05 mm Hg) as a colorless liquid to obtain 2-(dipropylamino) ethanol. Then 2-(dipropylamino) ethanol (21.3g, 0.1 mol),

triethylamine (10.1 g, 0.1 mol), and inhibitor hydroquinone (0.11g, 0.001mol) were dissolved in 100 mL CH2Cl2 and methacryloyl chloride (10.4g, 0.1 mol) was added dropwise into a three-neck flask. The solution was refluxed overnight. After reaction, the solution was filtered to remove the precipitated triethylamine-HCl salts, and CH2Cl2 solvent was removed by rotovap. The resulting residue was distilled in vacuo (47-53 ℃ at 0.05 mm Hg) as a colorless liquid. After synthesis, the monomer was characterized by 1H-NMR. All the NMR spectra were obtained in CDCl3 using tetramethylsilane (TMS) as the internal reference on a Varian 500MHz spectrometer.

2.2.1.2-Synthesis of PEO-b-PR block copolymers with different terminal alkyl groups.

PEO-b-PR copolymers were synthesized by atom transfer radical polymerization (ATRP) following similar procedures. The dye free copolymers were used in polymer characterizations. PEO-b-PDPA is used as an example to illustrate the procedure. First, DPA-MA (1.70 g, 8 mmol), PMDETA (21 μL, 0.1 mmol) and MeO-PEO114-Br (0.5 g, 0.1 mmol) were charged into a polymerization tube. Then a mixture of 2-propanol (2 mL) and DMF (2 mL) was added to dissolve the monomer and initiator. After three cycles of freeze-pump-thaw to remove the oxygen, CuBr (14 mg, 0.1 mmol) was added into the polymerization tube under nitrogen atmosphere, and the tube was sealed in vacuo. The polymerization was carried out at 40 ℃ for 8 hours. After polymerization, the reaction mixture was diluted with 10 mL THF, and passed through a neutral Al2O3 column to remove the catalyst. The THF solvent was removed by rotovap. The residue was dialyzed in distilled water and lyophilized to obtain a white powder.

Scheme 2.2.1. Synthesis of PEO-*b*-PR block copolymers.

2.2.2-Characterization

2.2.2.1-TEM and DLS

Samples for TEM and DLS analyses were prepared *in situ* by pH titration. The morphology and size of nanoparticles were characterized by transmission electron microscopy (TEM, FEI Tecnai G2 Spirit Biotwin model). Hydrodynamic diameter (D_h) and scattering count rates were determined by dynamic light scattering (DLS, Malvern Nano-ZS Model, He-Ne Laser, λ=633 nm).

2.2.2.2-Fluorescence

The fluorescence emission spectra were obtained on a Hitachi fluorometer (F-7500 model, Tokyo, Japan). The fluorescent images of PEO-*b*-PDBA-RhoG and Lysosensor Green solutions at different pH values (200 μg/mL for each sample) were obtained using the Maestro imaging system (CRI, Inc., Woburn, MA) with a proper band pass excitation filter and long-pass emission filter according to the instrument manual. All measurements were conducted at room temperature.

2.2.3-pH titration of different pH sensors

2.2.3.1-Preparation of micelle solution

For each copolymer, the stock solution of micelles was prepared following a solvent evaporation method as previously reported[36]. In the example of PEO-*b*-nPDPA micelle solution, 20 mg of the copolymer was first dissolved in 2.0 mL THF and then added into 10 mL deionized water dropwise under sonication. The THF was removed through ultrafiltration with (100 KD) membrane for five times.

Then deionized water was added to adjust the polymer concentration to 5 mg/mL as a stock solution.

2.2.3.2-pH titration of UPS block copolymers

Here we used a representative UPS block copolymer PEO-b-PDPA as an example. PEO-*b*-PDPA copolymer (80 mg) was first dissolved in 5 mL 0.1 M HCl and diluted to 2.0 mg/ml with DI water. NaCl was added to adjust the salt concentration to 150 mM. pH titration was carried out by adding small volumes (1 μL in increments) of 4.0 M NaOH solution under stirring. The pH increase in the range of 2 to 11 was monitored as a function of total added volume of NaOH. The fully protonated state and complete deprotonation states (protonation degree equaled 100% and 0%) were determined by the two extreme value points of pH titration curves' 1st derivation. The pH values were measured using a Mettler Toledo pH meter with a microelectrode. Titration of other pH sensitive polymers followed similar procedures using the same amine molar concentration.

2.2.3.3-Commonly used small molecular and polymeric pH sensors

NH_4Cl (pKa=10.5) and chloroquine (pKa's = 8.3 and 10.8) were commonly used lysosomotropic agents to manipulate the pH of endocytic organelles. We also performed the pH titration of dipropylaminoethanol (DPA, building block of UPS nanoprobe PEO-*b*-PDPA) as a control of UPS block copolymers[37]. In addition, pH titrations of several extensively investigated polybases were also performed. These polymers include polyethylenimine (PEI)[38], poly(L-Lysine) (PLL)[39], chitosan[40] and poly(L-Histidine)

(PLH)[41], which are widely used for nucleic acid delivery. Among these, PEI were extensively studied for gene delivery.

2.2.3.4-UPS block copolymer series

In this part, we compared the pH responsive behaviors a series of PEO-b-PR block copolymers with different terminal aliphatic alkyl groups: PEO-b-PDMA, PEO-b-PDEA, PEO-b-PDPA, PEO-b-PDBA and PEO-b-PD5A.

2.3-Results and discussion

2.3.1-Characterization of monomers and UPS block copolymers

The DMA-MA and DEA-MA monomers were purchased form *Polysceience Inc*. So we only showed the characterization of other monomers which were synthesized as described in previous sections.
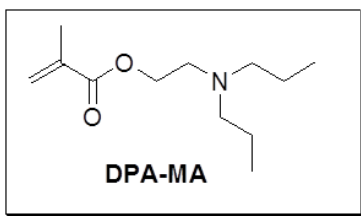
DPA-MA

2-(Dipropylamino) ethyl methacrylate (DPA-MA)
^{1}H NMR (TMS, CDCl$_3$, ppm): 6.10 (br, 1H, C*H*H=C(CH$_3$)-), 5.54 (br, 1H, CH*H*=C(CH$_3$)-), 4.07 (t, 2H, -OC*H$_2$*CH$_2$N-), 3.01 (t, 2H, -OCH$_2$C*H$_2$*N-), 2.68 (t, 4H, -N(C*H$_2$*CH$_2$CH$_3$)$_2$, 1.94 (s, 3H, CH$_2$=C(C*H$_3$*)-), 1.44 (m, 4H, -N(CH$_2$C*H$_2$*CH$_3$)$_2$), 1.01(t, 6H, -N(CH$_2$CH$_2$C*H$_3$*)$_2$)
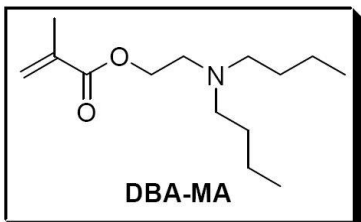
DBA-MA

2-(Dibutylamino)ethyl methacrylate (DBA-MA).
^{1}H NMR (TMS, CDCl3, ppm): 6.09 (br, 1H, C*H*H=C(CH$_3$)-),5.55 (br, 1H, CH*H*=C(CH$_3$)-), 4.19 (t, 2H, -OC*H$_2$*CH2N-), 2.73 (t, 2H, -OCH$_2$C*H$_2$*N-), 2.46 (t, 2H, -N(C*H$_2$*CH$_2$CH$_2$CH$_3$)$_2$), 1.93 (s, 3H, CH$_2$=C(C*H$_3$*)-), 1.41 (m, 4H, -N(CH$_2$C*H$_2$*CH$_2$CH$_3$)$_2$),

1.29 (m, 4H, -N(CH$_2$CH$_2$C*H$_2$*CH$_3$)$_2$), 0.89 (t, 6H, -N(CH2CH2CH2C*H3*)2).
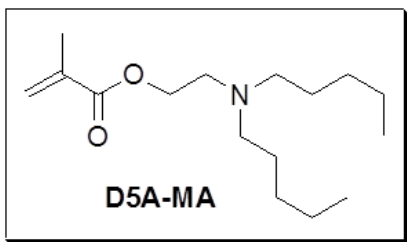
D5A-MA

2-(Dipentylamino) ethyl methacrylate (D5A-MA)
^{1}H NMR (TMS, CDCl$_3$, ppm): 6.10 (br, 1H, C*H*H=C(CH$_3$)-), 5.55 (br, 1H, CH*H*=C(CH$_3$)-), 4.20 (t, 2H, -OC*H$_2$*CH$_2$N-), 2.74 (t, 2H, -OCH$_2$C*H$_2$*N-), 2.45 (t, 4H, -N(C*H$_2$*CH$_2$CH$_2$ CH$_2$CH$_3$)$_2$, 1.94 (s, 3H, CH$_2$=C(C*H$_3$*)-), 1.43 (m, 4H, -N(CH$_2$C*H$_2$*CH$_2$

CH$_2$CH$_3$)$_2$), 1.30 (m, 4H, -N(CH$_2$CH$_2$C*H$_2$* CH$_2$CH$_3$)$_2$), 1.24 (m, 4H, -N(CH$_2$CH$_2$CH$_2$ C*H$_2$*CH$_3$)$_2$), 0.88 (t, 6H, -N(CH$_2$CH$_2$CH$_2$ CH$_2$C*H$_3$*)$_2$),
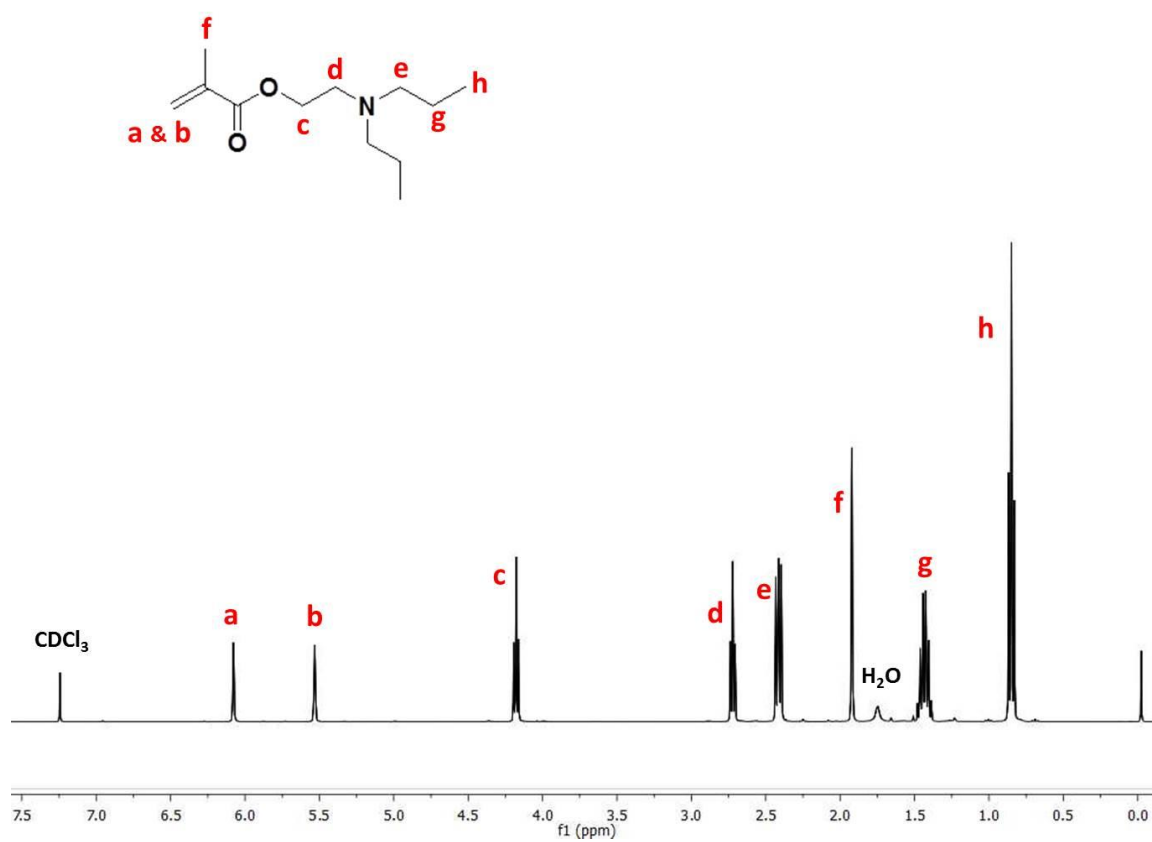
Figure 2.3.1. ^{1}H NMR spectra of a representative monomer DPA-MA in CD$_3$Cl.
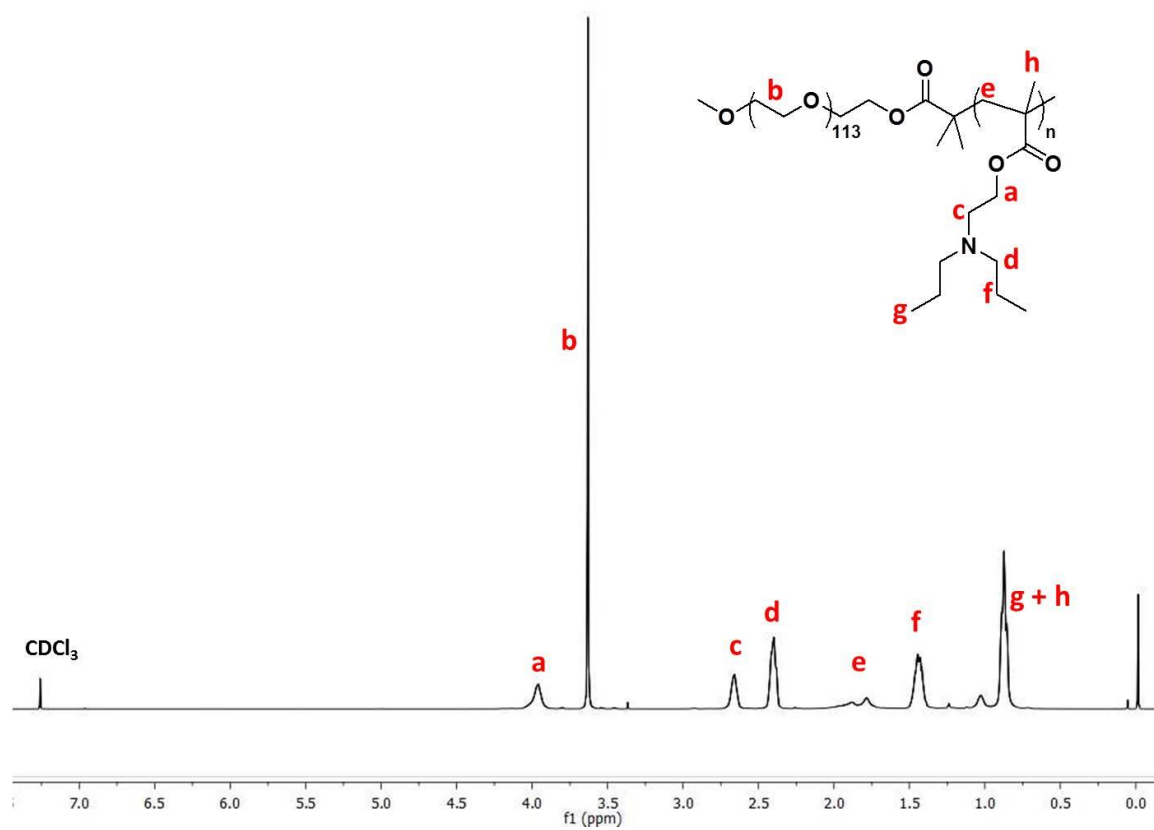
Figure 2.3.2. ^{1}H NMR spectra of a representative copolymers PEO-*b*-nPDPA in CD$_3$Cl.

2.3.2-pH titration curves of different pH sensors

Figure 2.3.3 summarized the structures of pH sensors used in this study. All pH sensors contain one or multiple amines, which is the general strategy in the development of pH sensors. As shown in **Figure 2.3.4**, small molecular pH sensors like NH4Cl and chloroquine both showed broad pH response in the range of pH 7 to 11. pH titration of dipropylaminoethanol (DPA, building block of UPS nanoprobe PEO-*b*-PDPA) also showed similar broad pH response as predicted by the Henderson-Hasselbalch equation[37].

pH titrations of several extensively investigated polybases showed different degrees of broad pH response. These polymeric pH sensors showed different degree of broad pH response similar to small molecular pH sensors. Among these, PEI showed the broadest pH response from pH 3 to 11.

In contrast, pH titration of three UPS nanoprobes (PEO-*b*-PDPA, PEO-*b*-PDBA and PEO-*b*-PD5A) illustrated remarkable pH plateaus within a narrow pH range, indicating strong buffer effect. For further investigation, we compared the titration curves from two other PEO-*b*-PR copolymers with the same methacrylate backbone but less hydrophobic aminoalkyl side chains: methyl and ethyl groups in PEO-*b*-PDMA and PEO-*b*-PDEA copolymers, respectively. PEO-*b*-PDMA displayed a broad pH response from 6.5 to 9.0, similar to small molecular bases. PEO-*b*-PDEA showed hybrid pH response between PEO-*b*-PDMA and PEO-*b*-PDPA.

2.3.3-Buffer capacity

The plateau along the pH titration coordinate indicated the reversible protonation process was accomplished in a relatively narrow pH range, indicating the UPS block
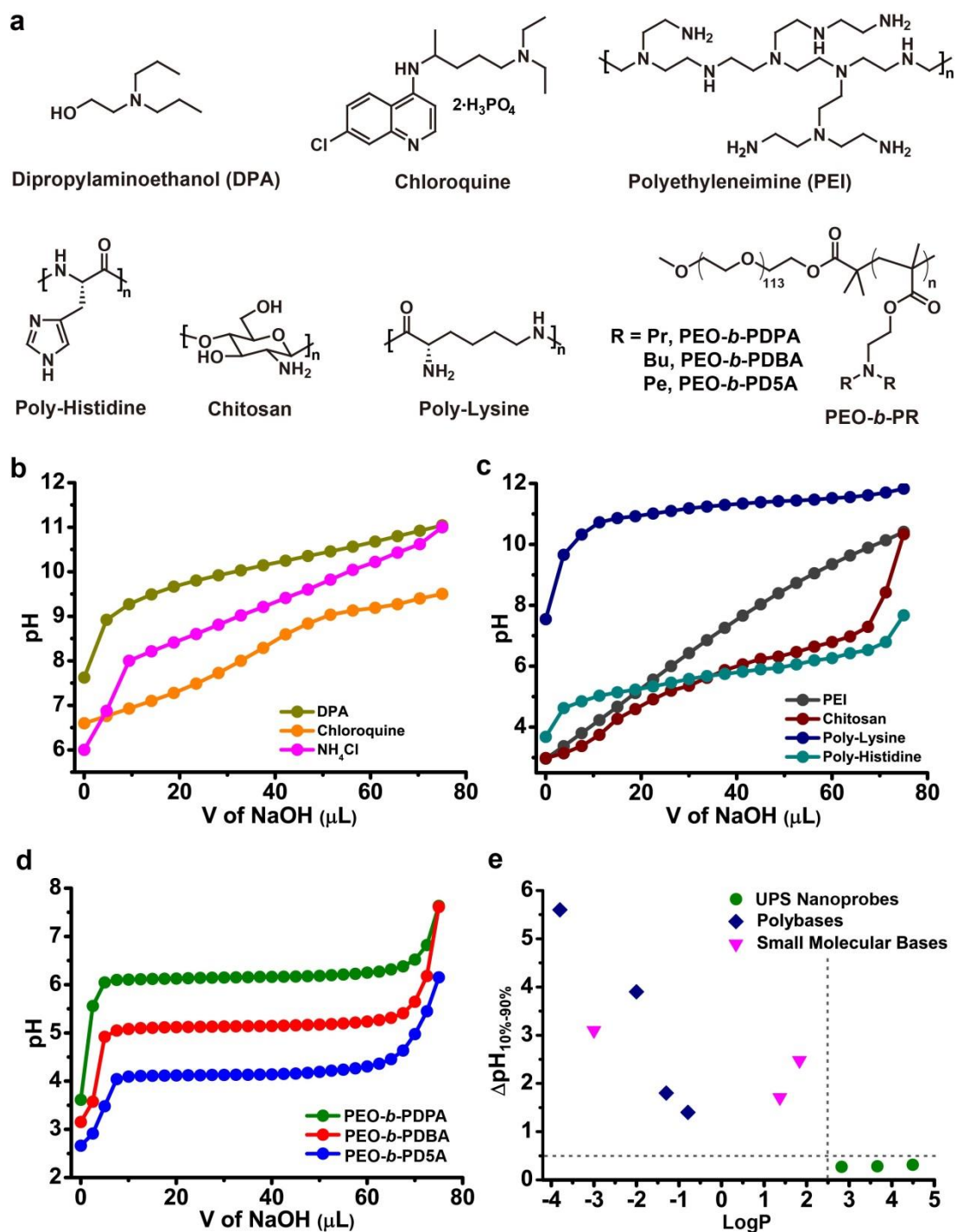
Figure 2.3.3. Structures and pH titration curves of pH sensors used in this study.

copolymers tend to resist the change of environmental pH and showed strong buffer effect. To quantify the strength of resistance, we defined the parameter buffer capacity ($\beta = \Delta B / \Delta pH$). Buffer capacity was expressed as the amount of strong acid or base, in gram-equivalents, that must be added to 1 liter of the solution to change its pH by one unit. In particular, the maximal β values for PEO-b-PD5A, PEO-b-PDBA and PEO-b-PDPA nanoparticles were 1.4, 1.5 and 1.6 mmol HCl per 40 mg of block copolymers, which are 339-, 75- and 30-fold higher than chloroquine at pH 4.4, 5.6 and 6.2, respectively (**Figure 2.3.4**).

In another independent study, we demonstrated that the UPS nanoprobes enable fine-scale imaging and perturbation of endocytic organelles[42] (**Figure 2.3.5**). Endosomes, lysosomes and related catabolic organelles are a dynamic continuum of vacuolar structures that impact a number of cell physiological processes such as protein /lipid metabolism, nutrient sensing and cell survival. Here we develop a library of ultra-pH-sensitive fluorescent nanoparticles with chemical properties that allow fine-scale, multiplexed, spatio-temporal perturbation and quantification of catabolic organelle maturation at single organelle resolution to support quantitative investigation of these processes in living cells. Deployment in cells allows quantification of the proton accumulation rate in endosomes; illumination of previously unrecognized regulatory mechanisms coupling pH transitions to endosomal coat protein exchange; discovery of distinct pH thresholds required for mTORC1 activation by free amino acids versus proteins; broad-scale characterization of the consequence of endosomal pH transitions on cellular metabolomic profiles; and functionalization of a context-specific metabolic vulnerability in lung cancer cells.
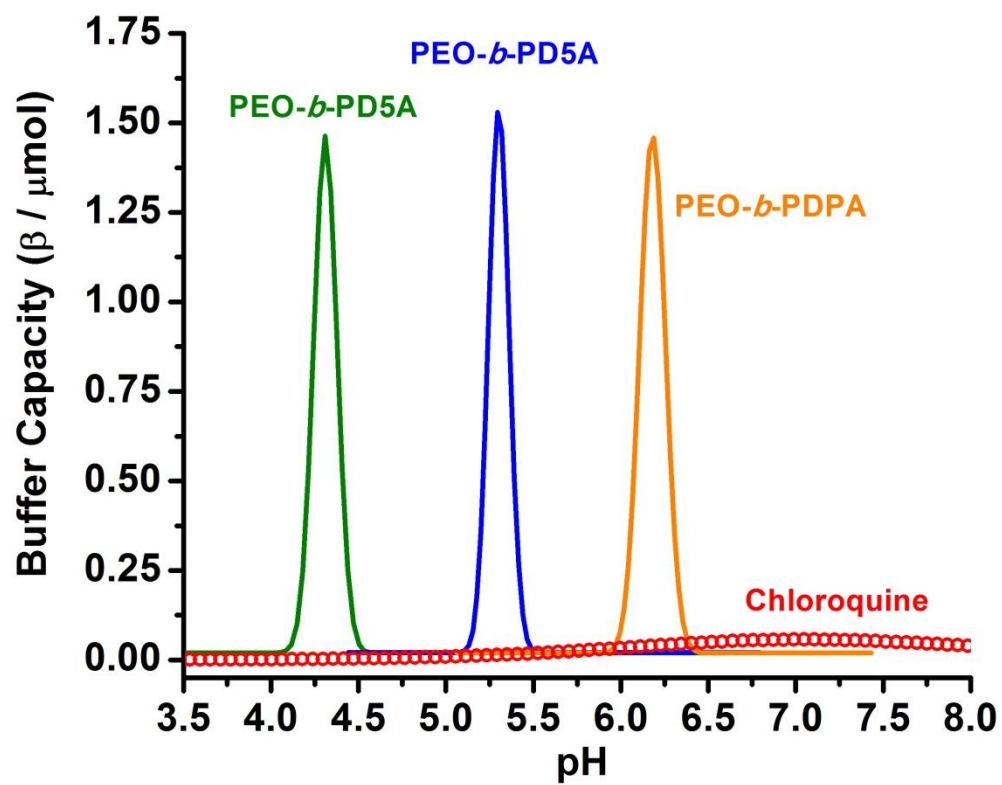
Figure 2.3.4. Buffer capacity comparison of three UPS block copolymers and small molecular pH sensor chloroquine.
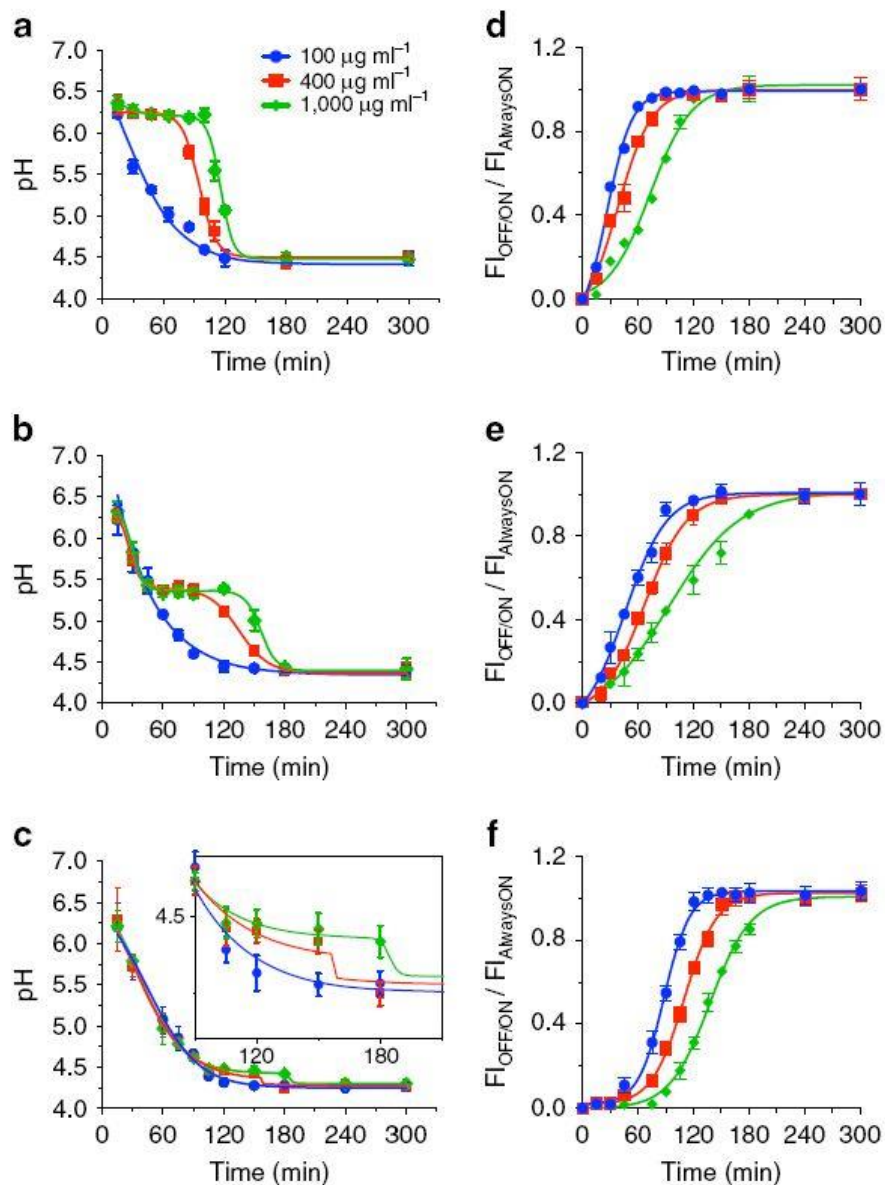
Figure 2.3.5. pH-sensitive buffering of endocytic organelles in HeLa cells. Real-time measurement of endo/lysosomal pH in HeLa cells treated with the indicated doses of PEO-b-PDPA (a), PEO-b-PDBA (b) and UPS4.4 (c). The inset is a zoomed-in view of the curve from pH 4.1 to 4.7 and 90 to 210 min in c. Quantitative analyses of the activation kinetics of always-ON/OFF-ON PEO-b-PDPA (d), PEO-b-PDBA (e) and PEO-b-PD5A (f). The fluorescent intensity of punctae in BODIPY channel (OFF-ON) was normalized to that of Cy3.5 (always-ON). The error bars represent s.d. from 50 organelles at each time point.

2.3.4-Comparison of fluorescence intensity as a function of pH

Conventional small molecular pH sensors exhibit 10-fold change in fluorescence intensity over 2 pH units. In cellular biology, the isothiocyanate derivative of fluorescein is often used to label and track cells in fluorescence microscopy applications (for example, flow cytometry). We prepared a series of fluorescein solutions with the same dye concentration but different pH values. The fluorescent images were captured on a Maestro imaing platform with identical contrast settings. As shown in **Figure 2.3.6**, the fluorescence intensity showed a continuous change within 3 pH units. It is worth to note that the fluorescent reached its maximum values at high pH. Following the same imaging procedures, we also took the images of another small molecular pH sensor Lysosensor Green (**Figure 2.3.7 a**, which have been used to measure the pH of acidic organelles, such as lysosomes. The lysosensor dyes become more fluorescent in acidic environment like UPS naonprobes. However, the continuous change of fluorescence intensity to pH hampers its ability to differentiate small pH variations between pathological pH (e.g., acidic tumor pH, 6.5-6.9[1]) and normal pH (7.4).   In contrast, the

UPS nanoprobes achieve over 100-fold fluorescence intensity changes over 0.2 pH units (see a specific example in **Figure 2.3.7 b**). We also measure the fluorescence intensity of above fluorescent pH sensors in a series of buffers with predesigned pH. We plotted their fluorescence intensity as a function of pH and the results confirmed the sharp pH transition of fluorophore-conjugated UPS nanoprobes (**Figure 2.3.7 c**). The binary on/off transition of UPS nanoprobes was critical to achieve high sensitivity and specificity in molecular imaging such as real-time tumor acidosis imaging. The resultant
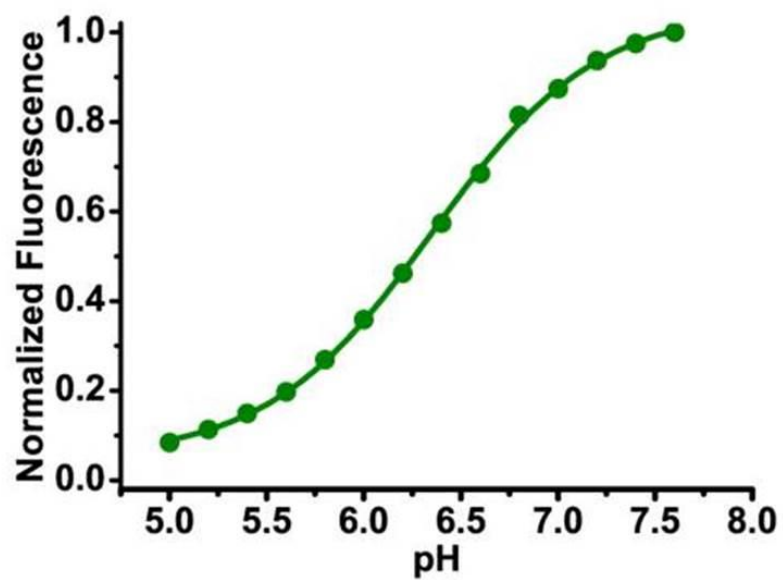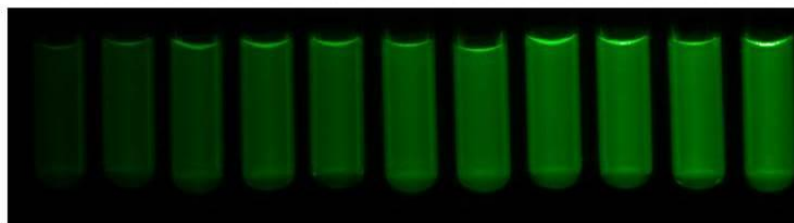
Figure 2.3.6. The fluorescence intensity of fluorescein as a function of pH.
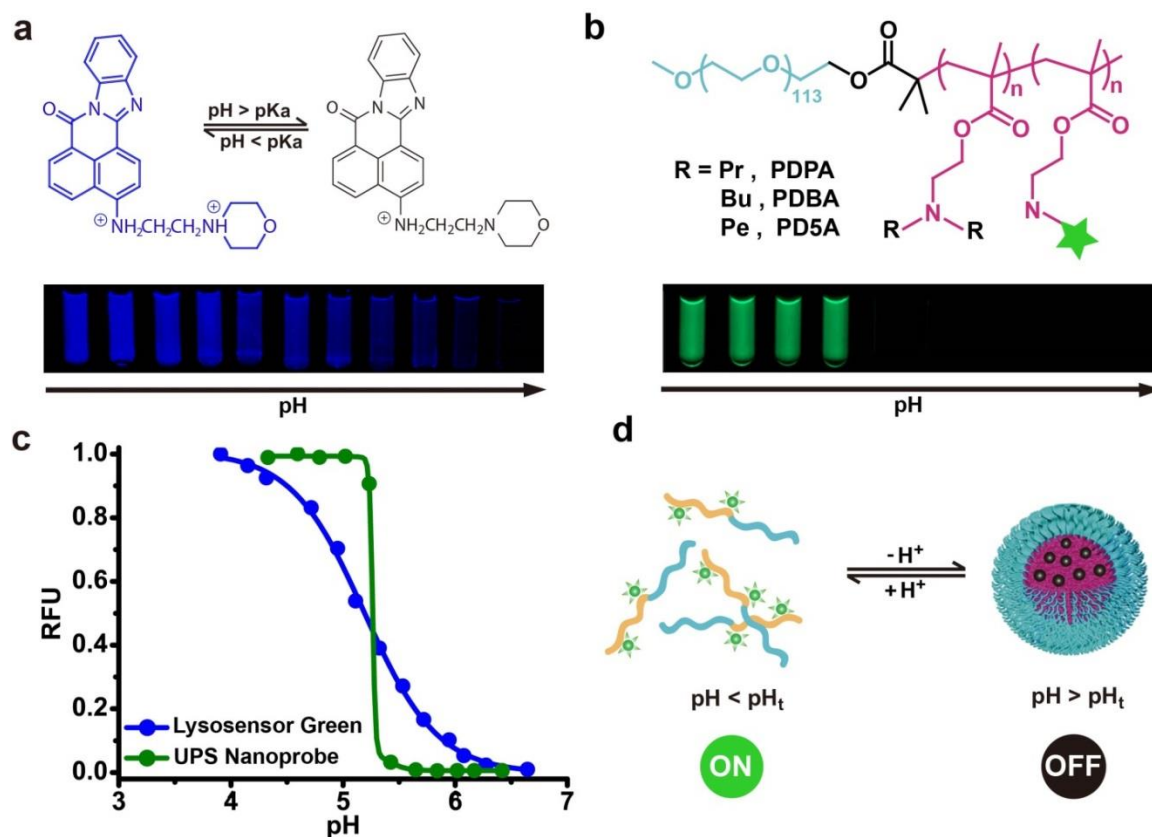
Figure 2.3.7. Sharp fluorescent pH transition of dye-conjugated UPS block copolymers.

a, Structure and fluorescence images of a small molecular pH sensor, Lysosensor Green in aqueous solution at different pH. **b**, Structure and fluorescence images of a UPS nanoprobe, PEO-*b*-PDBA-RhoG in aqueous solution at different pH. **c**, Relative fluorescence intensity as a function of pH for Lysosensor Green and PEO-*b*-PDBA-RhoG nanoprobe.

high resolution imaging can serve as a powerful platform for cancer diagnosis and intra-operative tumor margin delineation for cancer surgery.

2.3.5-Reversibity of pH responsive behaviors of UPS block copolymers

Microscopically, the pH responsive process is the protonation and deprotonation of ionizable tertiary amines. A UPS block copolymer with multiple amines per polymer chain can be treated as a polybase. For small molecular base like NH_3, the protonation and deprotonation is reversible with identical pKa. We want to test whether the protonation of UPS block copolymers was also reversible. We used a series of UPS block copolymers with linear alkyl groups as amines substituents. The pH titrations were performed following the procedures described previously. As shown in **Figure 2.3.8**, all four PEO-b-PR block copolymers showed excellent pH titration reversibility as proved the same pKa values in protonation and deprotonation directions. We further investigated whether the geometry of amine substituents may affect the reversibility of pH response. We performed the pH titration of PEO-b-iPDPA block polymer and used PEO-b-nPDPA as the control. As shown in **Figure 2.3.8**, the pKa value of protonation of neutral PEO-b-iPDPA block copolymers was 0.4 higher than that of deprotonation of charged PEO-b-iPDPA polymers. These data suggested that the geometry of substituents may indeed impact the reversibility of pH response, where the incorporation of branched amines substituents like i-propyl may resulted in slight shift of pKa values of protonation and deprotonation of UPS block copolymers
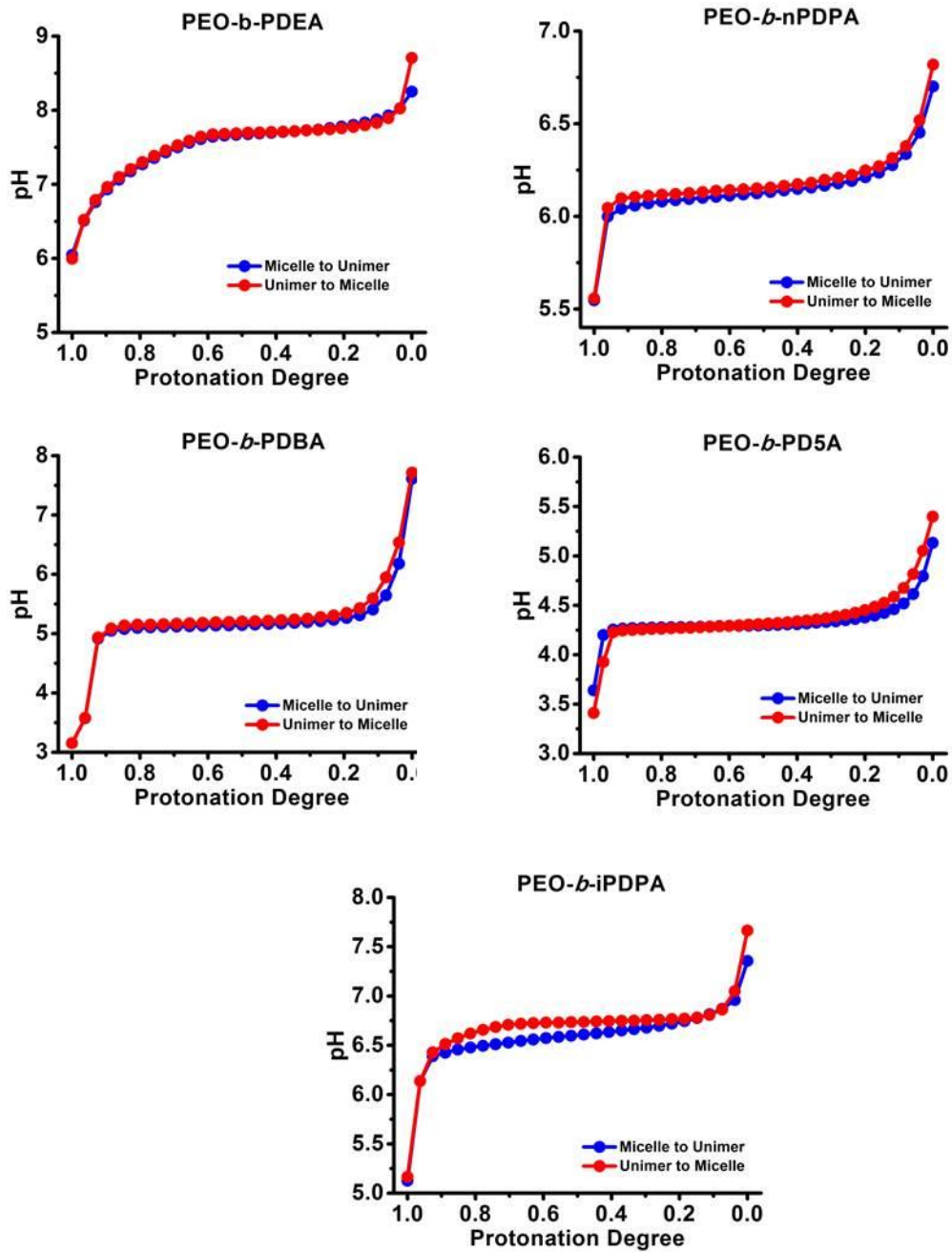
Figure 2.3.8. Reversibility of pH response of PEO-b-PR block copolymers.

2.4-Conclusion

The UPS nanoprobes displayed tunable and ultra-pH sensitive pH response in the physiological pH range (4.0-7.8), distinct from the broad pH response of small molecular and commonly used polymeric pH sensors. Moreover, the dye-conjugated UPS nanoprobes showed binary on/off transition compared to continuous fluorescence intensity changes of extensively used small molecular pH sensors like lysosensors. The UPS nanoprobes offer exciting opportunities for the diagnostic imaging and drug delivery application. The unique pH responsive behavior of UPS block copolymers also inspires us to further investigate the origin of observed ultra-pH sensitivity and underlying structure-property relationships.

2.5-References

1   Webb, B. A., Chimenti, M., Jacobson, M. P. & Barber, D. L. Dysregulated pH: a perfect storm for cancer progression. *Nature Reviews Cancer* **11**, 671-677 (2011).

2   Neri, D. & Supuran, C. T. Interfering with pH regulation in tumours as a therapeutic strategy. *Nature reviews Drug discovery* **10**, 767-777 (2011).

3   Whitten, S. T. & Hilser, V. J. Local conformational fluctuations can modulate the coupling between proton binding and global structural transitions in proteins. *Proceedings of the National Academy of Sciences of the United States of America* **102**, 4282-4287 (2005).

4   Casey, J. R., Grinstein, S. & Orlowski, J. Sensors and regulators of intracellular pH. *Nature reviews Molecular cell biology* **11**, 50-61 (2010).

5   Webb, B. A., Chimenti, M., Jacobson, M. P. & Barber, D. L. Dysregulated pH: a perfect storm for cancer progression. *Nat. Rev. Cancer* **11**, 671-677, doi:10.1038/nrc3110 (2011).

6   Grillo-Hill, B. K., Choi, C., Jimenez-Vidal, M. & Barber, D. L. Increased H(+) efflux is sufficient to induce dysplasia and necessary for viability with oncogene expression. *Elife* **4**, doi:10.7554/eLife.03270 (2015).

7   Matsuyama, S., Llopis, J., Deveraux, Q. L., Tsien, R. Y. & Reed, J. C. Changes in intramitochondrial and cytosolic pH: early events that modulate caspase activation during apoptosis. *Nat. Cell Biol.* **2**, 318-325, doi:10.1038/35014006 (2000).

8   Lagadic-Gossmann, D., Huc, L. & Lecureur, V. Alterations of intracellular pH homeostasis in apoptosis: origins and roles. *Cell Death Differ.* **11**, 953-961, doi:10.1038/sj.cdd.4401466 (2004).

9   Saadoun, S., Papadopoulos, M. C., Hara-Chikuma, M. & Verkman, A. S. Impairment of angiogenesis and cell migration by targeted aquaporin-1 gene disruption. *Nature* **434**, 786-792, doi:10.1038/nature03460 (2005).

10   Denker, S. P. & Barber, D. L. Cell migration requires both ion translocation and cytoskeletal anchoring by the Na-H exchanger NHE1. *J. Cell Biol.* **159**, 1087-1096, doi:10.1083/jcb.200208050 (2002).

11   Gillies, R. J., Liu, Z. & Bhujwalla, Z. 31P-MRS measurements of extracellular pH of tumors using 3-aminopropylphosphonate. *Am. J. Physiol.* **267**, C195-203 (1994).

12   Gillies, R. J., Raghunand, N., Garcia-Martin, M. L. & Gatenby, R. A. pH imaging. A review of pH measurement methods and applications in cancers. *IEEE Eng. Med. Biol. Mag.* **23**, 57-64 (2004).

13   van Sluis, R. *et al.* In vivo imaging of extracellular pH using 1H MRSI. *Magn. Reson. Med.* **41**, 743-750 (1999).

14   Volk, T., Jahde, E., Fortmeyer, H. P., Glusenkamp, K. H. & Rajewsky, M. F. pH in human tumour xenografts: effect of intravenous administration of glucose. *Br. J. Cancer* **68**, 492-500 (1993).

15   Neri, D. & Supuran, C. T. Interfering with pH regulation in tumours as a therapeutic strategy. *Nat. Rev. Drug Discov.* **10**, 767-777, doi:10.1038/nrd3554 (2011).

16   Gatenby, R. A. & Gillies, R. J. Why do cancers have high aerobic glycolysis? *Nat. Rev. Cancer* **4**, 891-899, doi:10.1038/nrc1478 (2004).

17   Helmlinger, G., Sckell, A., Dellian, M., Forbes, N. S. & Jain, R. K. Acid production in glycolysis-impaired tumors provides new insights into tumor metabolism. *Clin. Cancer Res.* **8**, 1284-1291 (2002).

18   Newell, K., Franchi, A., Pouyssegur, J. & Tannock, I. Studies with glycolysis-deficient cells suggest that production of lactic acid is not the only cause of tumor acidity. *Proc. Natl. Acad. Sci. U. S. A.* **90**, 1127-1131 (1993).

19   Yamagata, M., Hasuda, K., Stamato, T. & Tannock, I. F. The contribution of lactic acid to acidification of tumours: studies of variant cells lacking lactate dehydrogenase. *Br. J. Cancer* **77**, 1726-1731 (1998).

20   Jose, C., Bellance, N. & Rossignol, R. Choosing between glycolysis and oxidative phosphorylation: a tumor's dilemma? *Biochim. Biophys. Acta* **1807**, 552-561, doi:10.1016/j.bbabio.2010.10.012 (2011).

21   Vogelstein, B. *et al.* Cancer genome landscapes. *Science* **339**, 1546-1558, doi:10.1126/science.1235122 (2013).

22   Wencel, D., Abel, T. & McDonagh, C. Optical chemical pH sensors. *Analytical chemistry* **86**, 15-29 (2013).

23   Orellana, G. Luminescent optical sensors. *Analytical and bioanalytical chemistry* **379**, 344-346 (2004).

24   Han, J. & Burgess, K. Fluorescent indicators for intracellular pH. *Chemical reviews* **110**, 2709-2728 (2009).

25   Galande, A. K., Weissleder, R. & Tung, C.-H. Fluorescence probe with a pH-sensitive trigger. *Bioconjugate chemistry* **17**, 255-257 (2006).

26   Bradley, M. *et al.* pH sensing in living cells using fluorescent microspheres. *Bioorganic & medicinal chemistry letters* **18**, 313-317 (2008).

27   Wang, R., Yu, C., Yu, F. & Chen, L. Molecular fluorescent probes for monitoring pH changes in living cells. *TrAC Trends in Analytical Chemistry* **29**, 1004-1013 (2010).

28   Chandran, S. S., Dickson, K. A. & Raines, R. T. Latent fluorophore based on the trimethyl lock. *Journal of the American Chemical Society* **127**, 1652-1653 (2005).

29   Sasaki, E. *et al.* Highly sensitive near-infrared fluorescent probes for nitric oxide and their application to isolated organs. *Journal of the American Chemical Society* **127**, 3684-3685 (2005).

30   Peng, X. *et al.* Heptamethine cyanine dyes with a large stokes shift and strong fluorescence: a paradigm for excited-state intramolecular charge transfer. *Journal of the American Chemical Society* **127**, 4170-4171 (2005).

31   Tang, B. *et al.* A near-infrared neutral pH fluorescent probe for monitoring minor pH changes: imaging in living HepG2 and HL-7702 cells. *Journal of the American Chemical Society* **131**, 3016-3023 (2009).

32   Reshetnyak, Y. K., Segala, M., Andreev, O. A. & Engelman, D. M. A monomeric membrane peptide that lives in three worlds: in solution, attached to, and inserted across lipid bilayers. *Biophysical journal* **93**, 2363-2372 (2007).

33   Andreev, O. A. *et al.* Mechanism and uses of a membrane peptide that targets tumors and other acidic tissues in vivo. *Proceedings of the National Academy of Sciences* **104**, 7893-7898 (2007).

34   Kairdolf, B. A. & Nie, S. Multidentate-protected colloidal gold nanocrystals: pH control of cooperative precipitation and surface layer shedding. *Journal of the American Chemical Society* **133**, 7268-7271 (2011).

35   Ling, D. *et al.* Multifunctional tumor pH-sensitive self-assembled nanoparticles for bimodal imaging and treatment of resistant heterogeneous tumors. *Journal of the American Chemical Society* **136**, 5647-5655 (2014).

36   Nasongkla, N. *et al.* Multifunctional polymeric micelles as cancer-targeted, MRI-ultrasensitive drug delivery systems. *Nano letters* **6**, 2427-2430 (2006).

37   Po, H. N. & Senozan, N. The Henderson-Hasselbalch equation: its history and limitations. *J. Chem. Educ.* **78**, 1499 (2001).

38   Boussif, O. *et al.* A versatile vector for gene and oligonucleotide transfer into cells in culture and in vivo: polyethylenimine. *Proceedings of the National Academy of Sciences* **92**, 7297-7301 (1995).

39   Choi, Y. H. *et al.* Polyethylene glycol-grafted poly-L-lysine as polymeric gene carrier. *J. Controlled Release* **54**, 39-48 (1998).

40   Roy, K., Mao, H.-Q., Huang, S.-K. & Leong, K. W. Oral gene delivery with chitosan–DNA nanoparticles generates immunologic protection in a murine model of peanut allergy. *Nat. Med.* **5**, 387-391 (1999).

41   Lee, E. S., Shin, H. J., Na, K. & Bae, Y. H. Poly (L-histidine)–PEG block copolymer micelles and pH-induced destabilization. *Journal of Controlled Release* **90**, 363-374 (2003).

42   Wang, C. *et al.* A nanobuffer reporter library for fine-scale imaging and perturbation of endocytic organelles. *Nature communications* **6** (2015).

3.1-Introduction

3.1.1-Solution behaviors of polymers

3.1.1.1-Dissolution of polymers in aqueous solution

      Dissolution of polymers is an important area of interest in polymer science and engineering because it play a critical role in various applications such as construction of complicated nanostructure, microlithography, plastics recycling, and drug delivery. The dissolution of small molecules like solids is generally governed by the external mass transfer resistance through a liquid layer adjacent to the solid–liquid interface. However, the polymers do not dissolve instantaneously. The dissolution of polymers is controlled by either the disentanglement of the polymer chains or by the diffusion of the chains through the boundary layer adjacent to the polymer–solvent interface. For simpficaiton, the dissolution process of solid polymers in solvent can generally be divided into three stages[1] as shown in **Figure 3.1.1**:

Solid polymer
added to solvent

Swollen polymer
In solvent

Solvated polymer molecules
Diffusing out of swollen mass
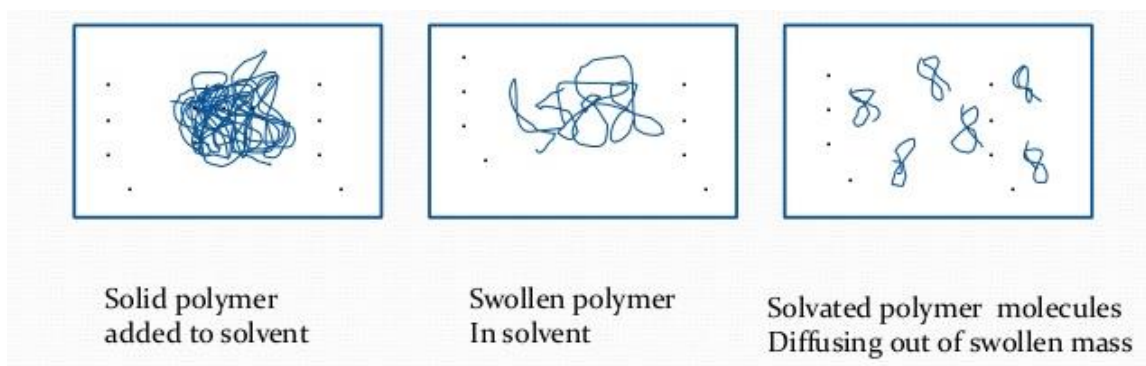
Figure 3.1.1. Different Stages of the dissolution of polymers[1].

For any give polymer, there are solvents that can dissolve the polymers well that are called "good solvent". The solvents that do not dissolve the polymers are known as "non-solvents". For example, poly(methyl methacrylate) can form homogeneous solution in tetrahydrofuran. However, they tend to precipitate in methanol. Both the properties of polymers and solvent will significantly impact the thermodynamic properties of the polymer solutions. Specifically, the molecular weight and polydispersity of polymers will change their solubility remarkably. The structures, composition and conformation may also change the solubility of the polymers. The additives like ions have been shown the capability to change the solution behavior of polymers. Also, people used mixed solvent instead of pure solvent for the dissolution of polymers. Environmental parameters like the temperature and ion strength also change the solution behavior like gelation of polymers.

3.1.1.2-Flory-Huggins theory

The lattice fluid theory was developed to explain the miscibility of two liquids with relatively low molecular weight[2]. On based of that, Flory and Huggins developed the lattice chain theory to describe the solution behaviors of polymers, all known as Flory-Huggins mean-field theory[3-6]. The lattice model was derived from coarse graining model[7], where only the most important molecular details of a system are retained to simply the statistical model. We consider the simplest situation: a monodisperse homopolymer in a pure solvent.

Major assumptions in the construction of lattice models: (a) Volumes of repeating unit of the polymer chain and solvent molecule are equal to on single lattice site; (b) the polymers and solvent molecules are mixed randomly; (c) the only contribution to possible

states are translational configurations (q = q $_{translation}$); (d) molecules of a give type (either repeating unit of polymer and solvent) are indistinguishable.

Definition of key parameters:

n_p= number of polymers chains

N = number of repeating units per chain

n_s = number of solvent molecules

M = total lattice sites = $n_s + Nn_p$

W = number of total possible states in the polymers systems.

Figure 3.1.2 give the derivation of the configuration of a single polymer chain[2]. We repeat the process to place all N repeating units of a single polymer chain on the lattice and will get the final total number of configurations of a single chain, defined as ν_1. The number of possible configuration for the first repeating unit of all n_p chains is defined as ν_{first} as shown in **Figure 3.1.3 a**. The number of possible arrangements of remaining N-1 repeating units can be expressed as subsequence (**Figure 3.1.3 b**)[5]. Based on these, we can get the total number of possible configuration (W) for all np chains (**Figure 3.1.3 c**)[5]. The factor of n_p! was applied to correct the over-counting since we have mentioned that polymer chains are indistinguishable from each other. As shown in **Figure 3.1.4**, we can't differentiate these two configurations with the same polymer distribution but different polymer chains[6].

To put it simple, the Flory–Huggins lattice theory is a simplified mathematical model to describe the thermodynamics of polymer solutions which takes account of the

Place the first repeating unit of polymer chain on the lattice
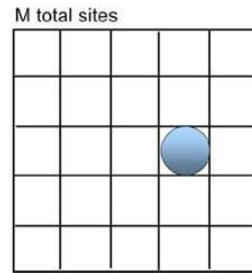
Possible sites to place the second repeating unit of polymer chain
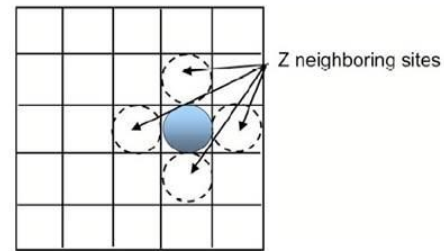
Possible sites to place the third repeating unit of polymer chain
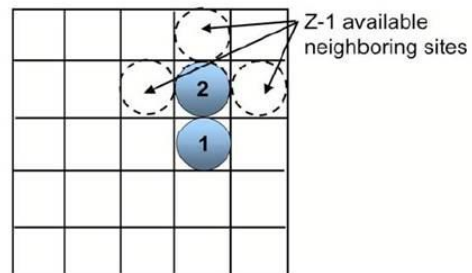
Exclude volume: Number of available neighbor sites is reduced as chains fill up The lattice
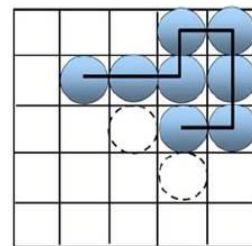
Figure 3.1.2. Configuration of single polymer chain based on Flory-Huggins theory[3].

a

$$v_{first} = M(M-1)(M-2)(M-3)\cdots(M-(n_p-1)) = \frac{M!}{(M-n_p)!}$$

b

$$v_{subsequent} = \left[(z-1)\left(\frac{M-n_p}{M}\right)\right]\left[(z-1)\left(\frac{M-n_p-1}{M}\right)\right]\cdots\left[(z-1)\left(\frac{M-2n_p}{M}\right)\right]\cdots\left[(z-1)\left(\frac{M-N(n_p-1)-(N-1)}{M}\right)\right]$$

$$v_{subsequent} = \left(\frac{z-1}{M}\right)^{n_p(N-1)}\frac{(M-n_p)!}{(M-Nn_p)!}$$

c

$$W = \frac{v_{first}v_{subsequent}}{n_p!}$$

Figure 3.1.3. Counting total number of configurations for all polymer chains[5].
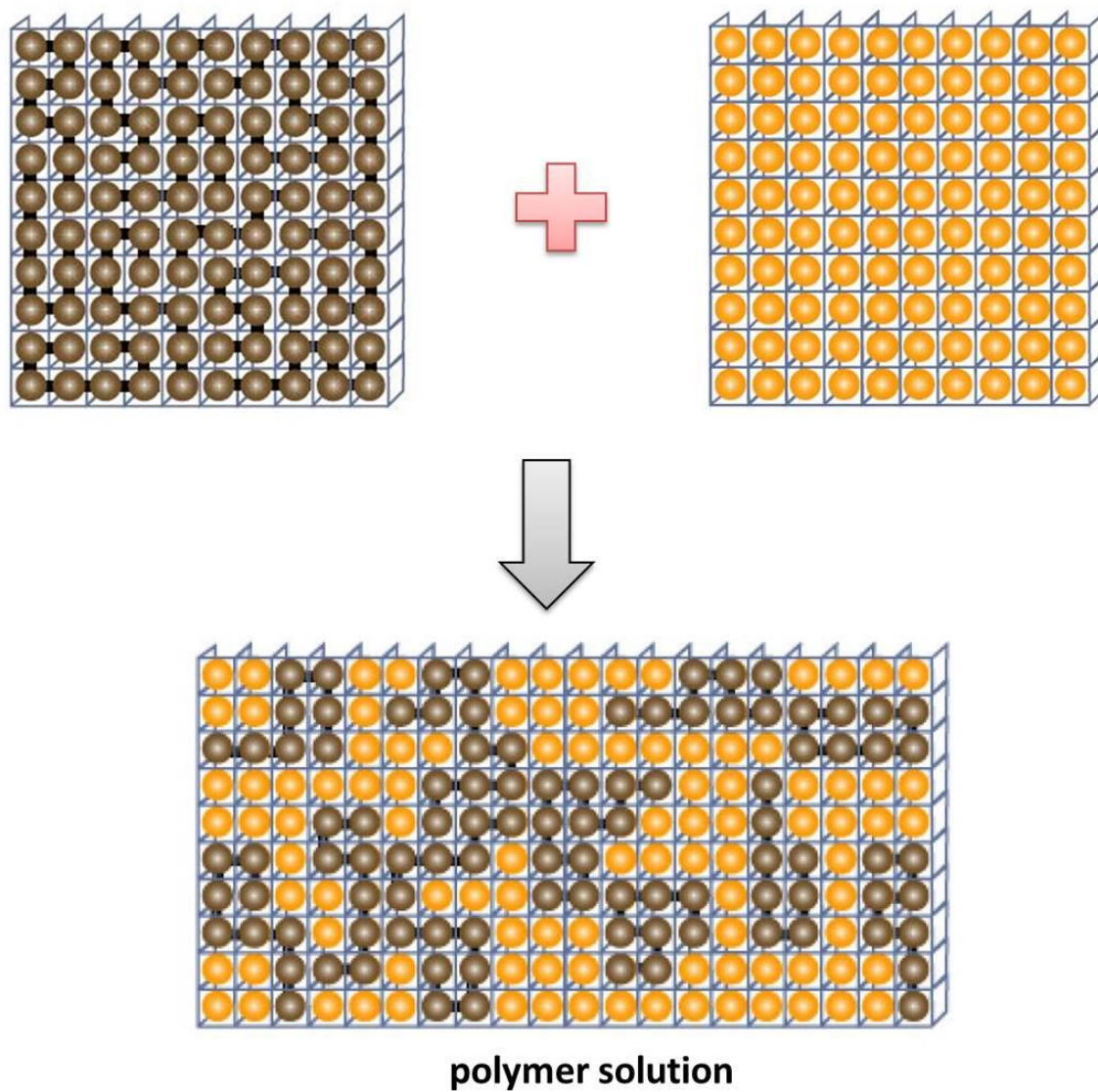
polymer solution

Figure 3.1.4. Schematic illustration of dissolution of polymers based on Flory-Huggins theory[6].

the great dissimilarity in molecular sizes in adapting the expression for the entropy of mixing. The theory offers useful insights for interpreting experiments although it makes multiple assumptions for the mathematical simplification. It has successfully describes the thermodynamics of polymer blends, homo-polymers and di-block copolymers[8-13].

3.1.2-Phase separation and stimuli-triggered supramolecular self-assembly

3.1.2.1-Phase separation in the solution of polymers

The thermodynamic equation for the Gibbs energy change accompanying mixing at constant temperature and (external) pressure is:

$$\Delta G = \Delta Hm - T\Delta Sm$$

A change, denoted by Δ, is the value of a variable for a solution or mixture minus the values for the pure components considered separately. The objective is to find explicit formulas for Hm and ΔSm, the enthalpy and entropy increments associated with the mixing process. The result obtained by Flory and Huggins is:

$$\Delta Gm = RT \, (n_1 \ln\phi_1 + n_2 \ln\phi_2 + n_1\phi_2\chi_{12})$$

n_1 and ϕ_1 are the number of moles and volume fraction of solvent respectively. n_2 and ϕ_2 are the number of moles and volume fraction of polymers. They introduce a parameter χ, also known as Flory-Huggins parameter, to take account of the energy of inter-dispersing polymer and solvent molecules.

For a given polymer concentration c (c = c_1 + c_2). If adiabatic, the system will spontaneously minimize the Gibbs free energy. As a consequences, no phase separation will occur if G(c) < $\phi_1\Delta G(c_1)$ + $\phi_2\Delta G(c_2)$. However, the polymer solution will be unstable if G(c) < $\phi_1\Delta G(c_1)$ + $\phi_2\Delta G(c_2)$, which may be induced by the change of solvent or

temperature. In this situation, phase separation like precipitation or self-assembly will occur to achieve the most thermodynamic stable states.

The nature has shown the capability to construct complicated structures in aqueous environment. One example is the formation of functional and complex proteins from limited choice of amino acids. Inspired by the natural systems, we have built synthetic polymeric structures from various monomers. Polymerization of these monomers affords different kind of homopolymers and copolymers. Also, engineering of these obtained polymers give rise to unusual shapes and architectures like film, vesicles and brush.

Copolymers were constructed from more than one building blocks or monomers. If the sequence of monomer residues follows a statistical rule, we define the polymers as random polymers. In contrast, block copolymers comprise two or more homo-polymer subunits linked by covalent bond. The Flory-Huggins theory is still applicable for the solution behavior of block copolymers, though they are more complicated than homo-polymers. One specific category of block copolymers is the amphiphilic block copolymers, where the polymers contain both hydrophilic and hydrophobic building blocks. The amphiphilic block copolymers have shown the ability to self-organize into multiple nanostructures in aqueous environment. The interfacial balance between solvated components and solvophobic components drives the formation of spherical micelles, worm-like micelles, bilayer vesicles.

3.1.2.2-Preparation of assembled nanostructures from block copolymers

When placed in a specific solution, the solvophobic components tend to form gather together to minimize the unfavorable energy penalty at the polymer-solvent

interfaces[14,15]. The self-organization leads to macroscopic changes in configurations such as the formation of nanostructures[14-28]. The block copolymers can form various types of self-assembled structures, from micelles to nanogels, depending on the solvent selection, preparation methods and composition of polymers. Polyelectrolyte micelles can be obtained by mixing oppositely charged macro-ions, provided that one of the ingredients is a neutral hydrophilic block copolymer[29] (**Figure 3.1.5a**). The PNIPAM-polysaccharide copolymers are soluble in cold water. Upon increase of temperature, the heat-triggered collapse of PNIAAM chains drives the formation of nanogels[16] (**Figure 3.1.5b**). External stimuli like pH may cause the particles to detach entirely from the interface. The breaking of emulsion by pulling the particle off the interface is accompanied with change of configuration[30] (**Figure 3.1.5 c**).

There are two general methods in preparing vesicle or micelles using the self-assembly of polymers. The first one is switching the solvent, which have been widely used in the design of drug delivery systems[19-21]. Initially, amphiphilic polymers are dissolved in organic solvents, followed by the addition of water to induce the nano-precipitation of hydrophobic chains. The hydrophilic blocks are solvated and form the corona of the vesicles. The solvent-switch methods can also be applied by adding organic solvent into water. It is noteworthy that ratio of selected organic solvent and water mixture can significantly impact the size and morphologies of prepared vesicles or
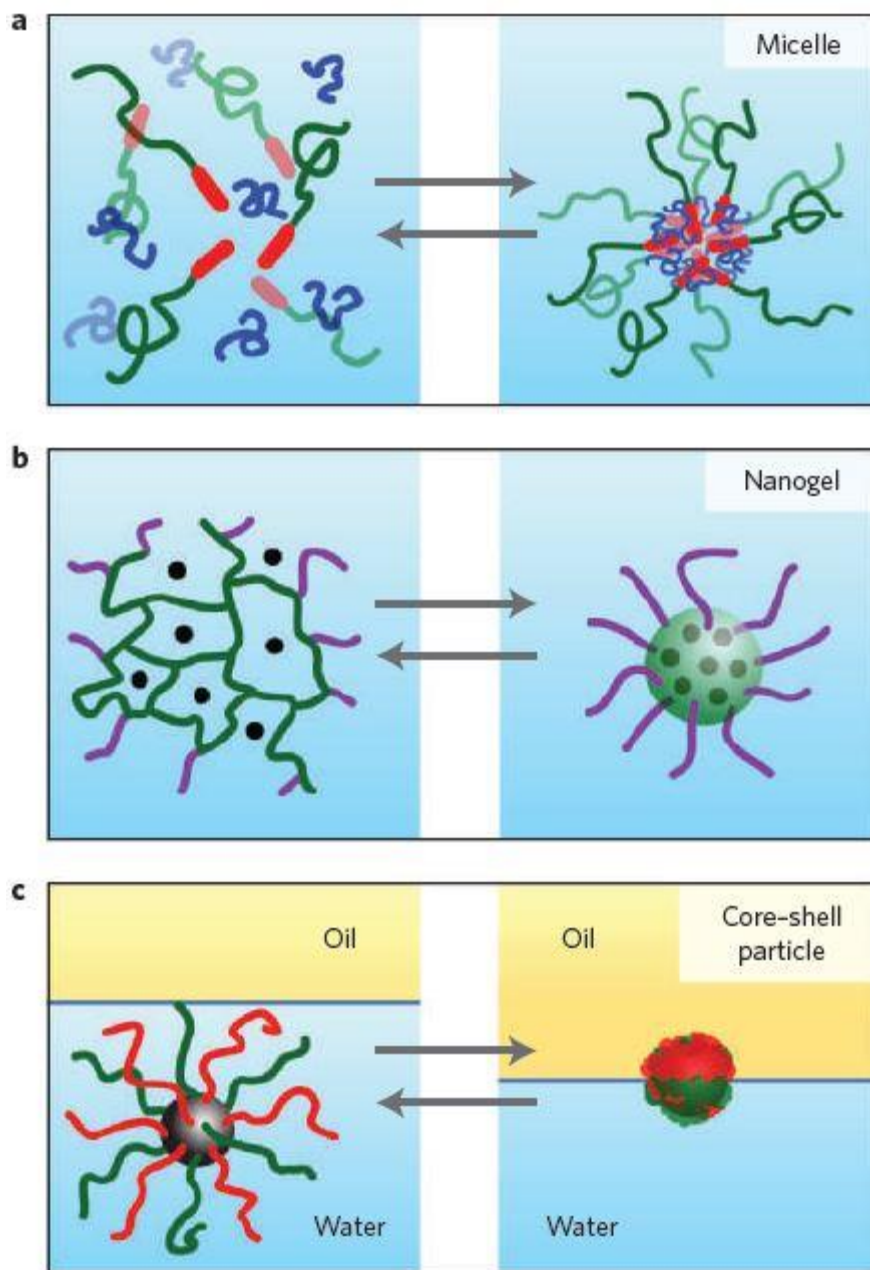
Figure 3.1.5. Configuration changes of stimuli-responsive nanomaterials[22].

micelles. For example, addition of water into poly(styrene)-b-poly(acrylic acids) (PS-PAA) copolymers' dioxane solution drives PS aggregation as a result of increased surface tension. The solvent changes also altered the morphologies of the nanoparticles (**Figure 3.1.6**)[15].

The other method works through tuning the solubility of polymers. One most well established example is the pH tuning in aqueous solution. For polymers with pH response, the ratio of hydrophilicity to hydrophobicity generally changes significantly upon pH tuning. The increase of hydrophobicity will result in the self-assembly of polymers. The Armes group reported a diblock copolymer vesicle self-assembled from poly[2-(methacryloyloxy)ethyl phosphorylcholine]-block-poly[2-(diisopropylamino)ethyl methacrylate] (PMPC-b-PDPA). This block copolymer is soluble in acidic envrionment due to the protonation of the tertiary amine groups (pKa ≈ 6.6) on the PDPA block. Upon pH increasing above 7, the deprotonation of the tertiary amine groups will lead to the formation of polymer vesicles[17,18].

Our design of UPS block copolymers also employs the pH tuning as the strategy to induce the formation of micelles. In this chapter, we systematically investigated the morphological changes of UPS block copolymers in aqueous solution upon pH changes. Multiple methods, including dynamic light scattering, electron microscopy and fluorescence spectroscopy, will be applied to keep track of the self-assembly process of UPS block copolymers. Particularly, key parameters like the critical micelle concentration (CMC), critical micelle protonation degree (CMPD) will be identified.
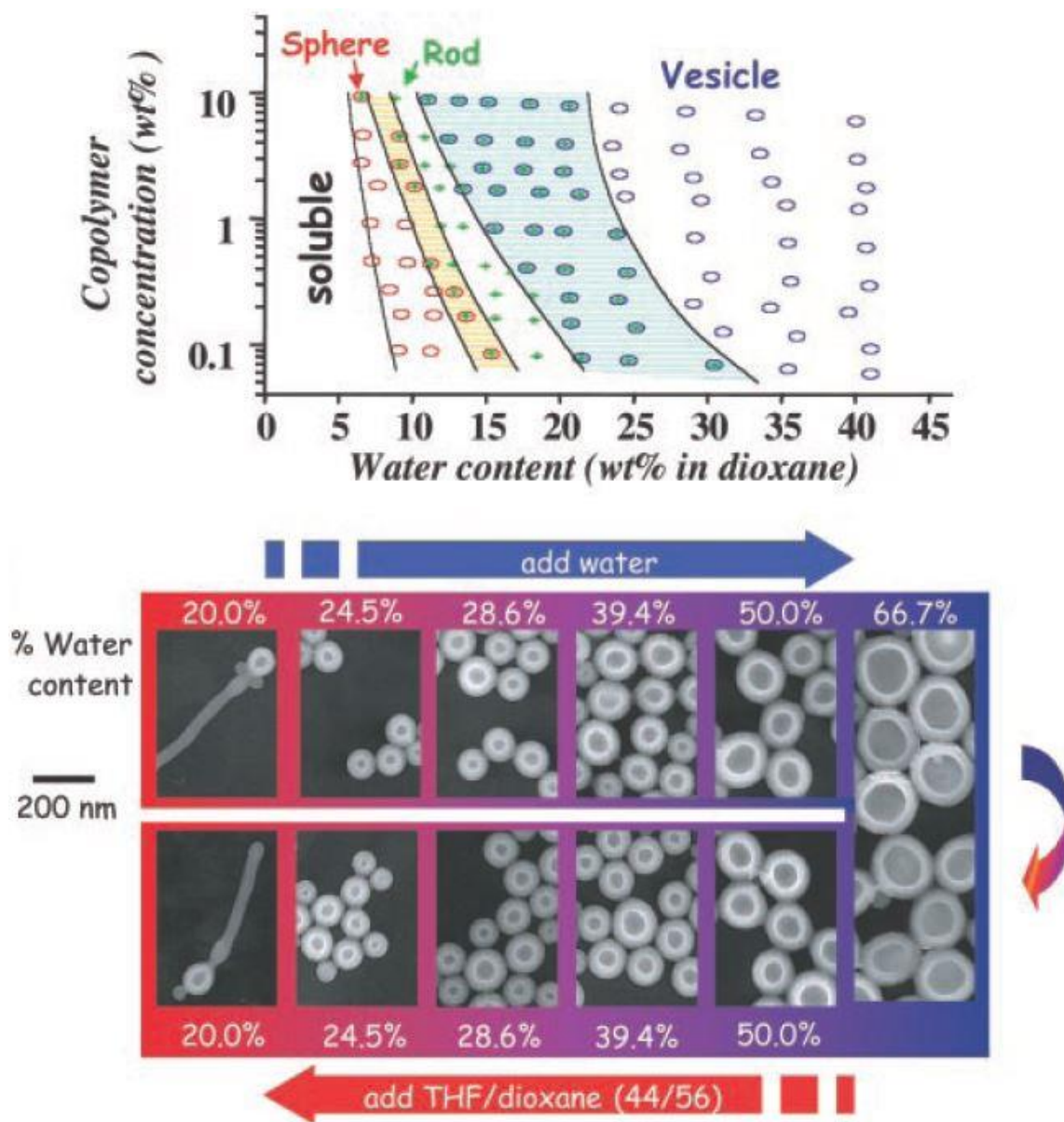
Figure 3.1.6. Morphological phases and vesicle transformations in dilute solutions. (A) Phase diagram of PS_{310}-PAA_{52} in dioxane plus water; the full ternary phase diagram with separate water, dioxane, and copolymer axes looks similar. (B) Reversibility of the vesicle formation and growth process for PS_{300}-PAA_{44}[24].

3.2-Materials and methods

3.2.1-Establishment of polymer library

In this study, we used a series of PEO-b-PR block copolymers with different terminal alkyl groups (PEO-b-PDMA, PEO-b-PDEA, PEO-b-PDPA, PEO-b-PDBA and PEO-b-PD5A). Moreover, we also synthesized PEO-b-PDHA and homo-polymer PDHA as control for the investigation of pH triggered self-assembly of UPS block copolymers.

3.2.2-Preparation of micelle solution

For each copolymer, the stock solution of micelles was prepared following a solvent evaporation method as previously reported3. In the example of PEO-b-nPDPA micelle solution, 20 mg of the copolymer was first dissolved in 2.0 mL THF and then added into 10 mL deionized water dropwise under sonication. The THF was removed through ultrafiltration with (100 KD) membrane for five times. Then deionized water was added to adjust the polymer concentration to 5 mg/mL as a stock solution.

3.2.3-pH titration of different pH sensors

Here we used a representative UPS block copolymer PEO-b-PDPA as an example. PEO-b-PDPA copolymer (80 mg) was first dissolved in 5 mL 0.1 M HCl and diluted to 2.0 mg/ml with DI water. NaCl was added to adjust the salt concentration to 150 mM. pH titration was carried out by adding small volumes (1 μL in increments) of 4.0 M NaOH solution under stirring. The pH increase in the range of 2 to 11 was monitored as a function of total added volume of NaOH. The fully protonated state and complete deprotonation states (protonation degree equaled 100% and 0%) were determined by the

116

two extreme value points of pH titration curves' 1st derivation. The pH values were measured using a Mettler Toledo pH meter with a microelectrode. Titration of other pH sensitive polymers followed similar procedures using the same amine molar concentration.

3.2.4 -TEM and DLS characterization

Samples for TEM and DLS analyses were prepared *in situ* by pH titration. The morphology and size of nanoparticles were characterized by transmission electron microscopy (TEM, FEI Tecnai G2 Spirit Biotwin model). Hydrodynamic diameter (D_h) and scattering count rates were determined by dynamic light scattering (DLS, Malvern Nano-ZS Model, He-Ne Laser, λ=633 nm).

3.2.5-Fluorescence characterization

The fluorescence emission spectra were obtained on a Hitachi fluorometer (F-7500 model, Tokyo, Japan). For each copolymer, the sample was prepared in situ by pH titration at the concentration of 2 mg/m in the presence of 150 mM. The fluorescence intensity was normalized by (F - Fmin)/(Fmax − Fmin).

3.2.6-Measurement of critical micelle concentration (CMC)

CMC of PEO-b-nPDPA block copolyemrs was measured in 0.1 M phosphate buffer saline (PBS, pH 7.4). First, a copolymer stock solution (5 mg/mL) was diluted to different concentrations in the same buffer. In each solution, 5μL pyrene in THF solution (2×10-4 M) was added to 2 mL polymer solution to produce the final pyrene

concentration at 5×10^{-7} M. The fluorescence spectra were recorded on a Hitachi fluoremeter (F-7500 model) with the excitation wavelength of 339 nm and the excitation and emission slits at 10.0 nm and 1.0 nm, respectively. The I1 and I3 values were measured as the maximum emission intensity at ca. 372 and 382 nm, respectively. I1/I3 ratio was plotted as a function of polymer concentration at different pH values. I1/I3 ratio reflects the polarity of the pyrene environment where partition of pyrene in the hydrophobic micelle core leads to decreased I1/I3 values.

3.3-Results and discussions

3.3.1-pH induced micellization of UPS block copolymers

The UPS nanoprobes consist of block copolymers, PEO-b-PR, where PEO is poly(ethylene oxide) and PR is an ionizable tertiary amine block. Ionizable groups can act as tunable hydrophobic groups at different pH values. Amino groups have been incorporated into polymers as ionizable groups to impart pH sensitivity[31]. At low pH, micelles dissociate into cationic unimers with protonated ammonium groups. When pH increases, neutralized PR segments become hydrophobic and self-assemble into core-shell micelles. The formation of micelles and their thermodynamic stability are driven by the delicate balance between the hydrophobic and hydrophilic segments[32]. As shown in **Figure 3.3.1**, the size of PEO-b-PDPA block copolymers were less than 10 nanometers, corresponding to the free size of a single polymer chain. When pH was higher than pKa, we can clearly see the formation of nanoparticles as proved by the TEM images and significantly increased hydrodynamic diameter. In an independent static light scattering characterization, we found that each micelle contained around 800 polymers chains,

118
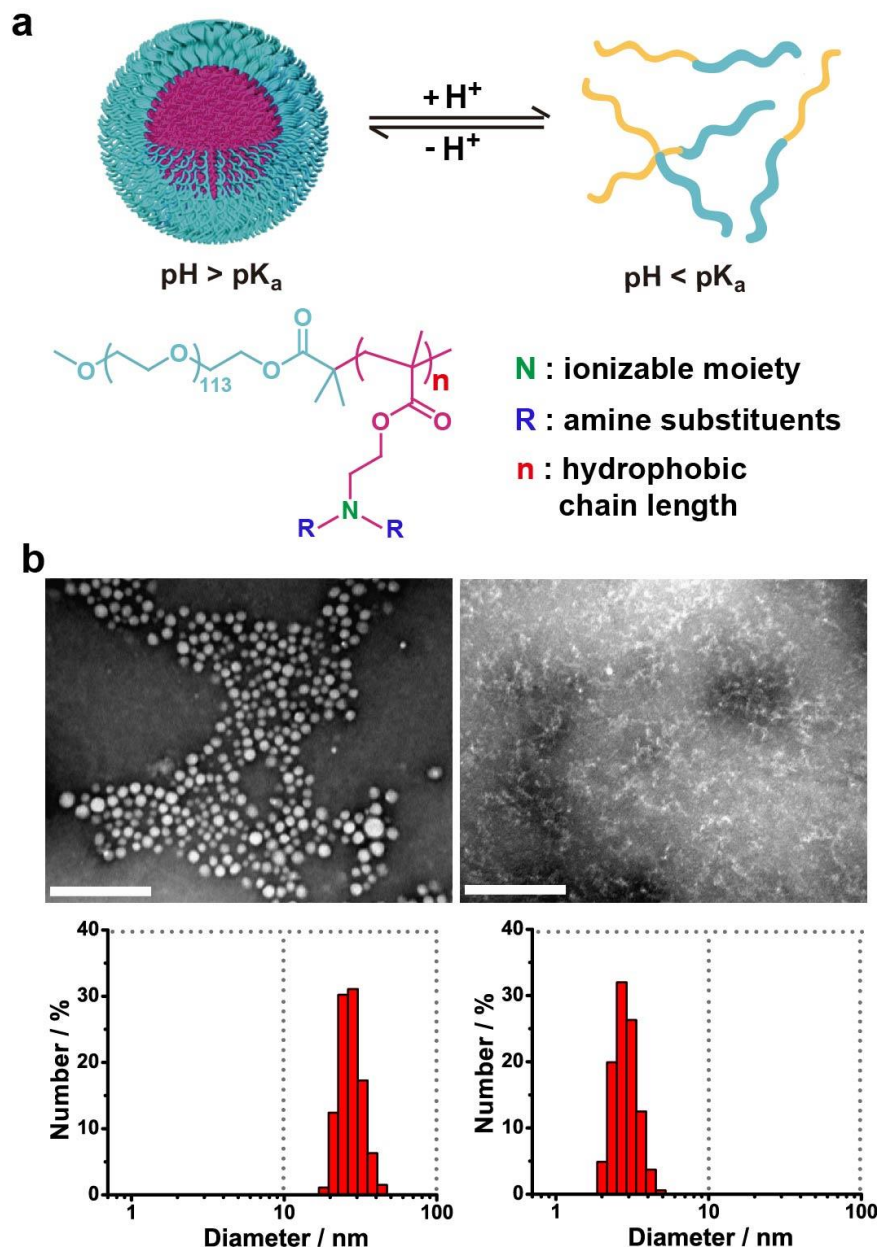
Figure 3.3.1. pH activation of ultra-pH sensitive (UPS) micellar nanoparticles. (a) At pH above pKa, the neutralized PR segment (purple in color) drove the formation of core-shell micelles. Upon pH decrease (< pKa), positively charged ammonium groups in the PR segment (yellow) resulted in micelle dissociation into cationic unimers. (b) TEM and DLS characterization of PEO-b-nPDPA block copolymers at unimer (pH = 5.0) and micelle states (pH 7.4) (scale bar: 200 nm).

contributing to the molecular weight of micelles at 16,000,000. Another interesting fact concerning the UPS nanoparticles was that the micelle prepared form drop-wise pH titration generally showed slightly smaller size compared to that obtained from solvent-evaporation methods. For example, the PEO-b-PDPA micelles were 32 nm in size when prepared via adding DI water into polymer's THF solution. However, micelles from pH titration methods usually had size around 27 nm. In addition, the micelles prepared from pH titration displayed smaller polydispersity in diameter distribution, indicating the formation of micelles were more homogeneous.

3.3.2-Critical micelle concentration (CMC)

The CMC values were measured as the threshold polymer concentration at which micelles were formed in solution[33]. The CMC is an important characteristic of a surfactant. Before reaching the CMC, the surface tension changes strongly with the concentration of the surfactant. After reaching the CMC, the surface tension remains relatively constant or changes with a lower slope. It is noteworthy that the CMC values may be affected by temperature, pressure and ion strength. In our study, all measurements were conducted at room temperature, standard atmosphere and in the presence of 150 mM. The CMC of UPS block copolymers was determined from the measurements of UV absorption of pyrene in polymer solution. The pyrene has two characteristic peak at 372 and 382 nm, whose intensity were known as I_1 and I_3 values. I_1/I_3 ratio reflects the polarity of the pyrene environment where partition of pyrene in the hydrophobic micelle core leads to decreased I_1/I_3 values.
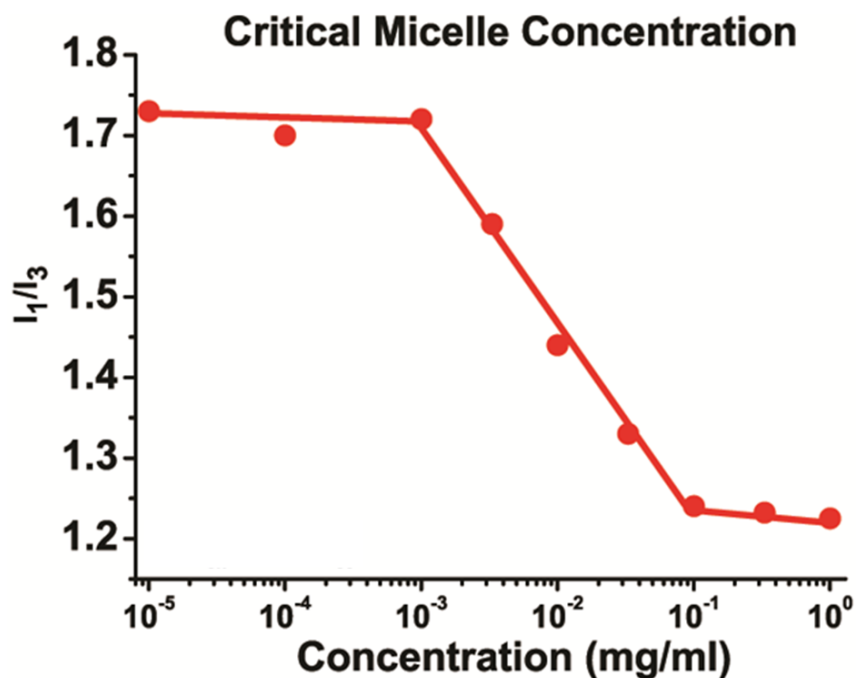
Figure 3.3.2. The critical micelle concentration (CMC) of PEO_{114}-b-$nPDPA_{60}$ copolymer determined from the measurements of UV absorption of pyrene in polymer solution.
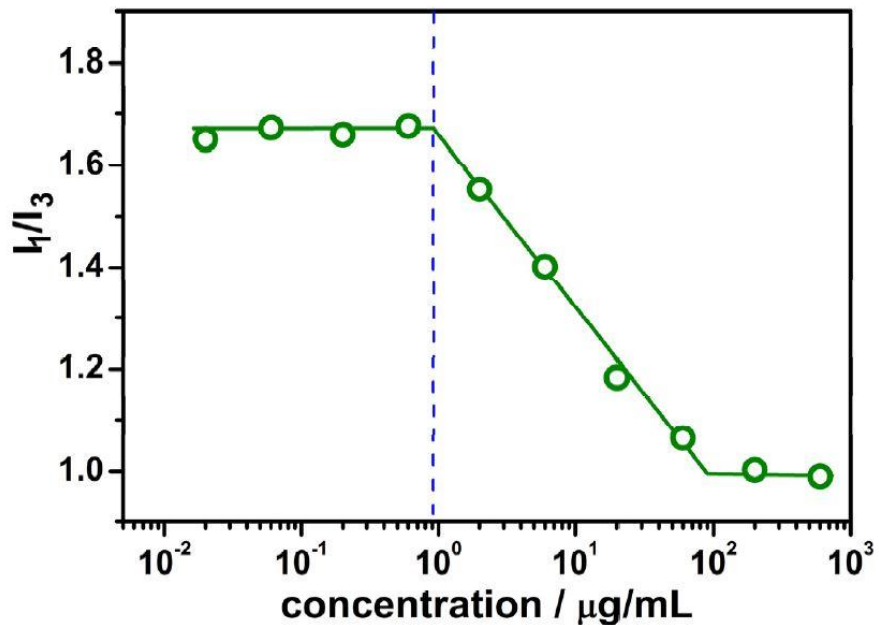
Figure 3.3.3. The critical micelle concentration (CMC) of PEO_{114}-b-$iPDPA_{60}$ copolymer determined from the measurements of UV absorption of pyrene in polymer solution[34].

We plotted I_1/I_3 ratios as a function of polymer concentration. As shown in **Figure 3.3.2**, the I_1/I_3 ratio was almost identical when polymer concentration increased from nearly 0 to 0.001 mg/ml. With further increase of polymer concentration, the I_1/I_3 ratio decreased significantly, suggesting the formation of micelles. Similar procedures were performed for PEO-b-iPDPA. The CMC value of PEO-b-iPDPA (**Figure 3.3.3**) was almost the same with that of PEO-b-nPDPA, although the former had a higher pKa. PEO-b-PDBA and PEO-b-PC7A gave similar CMC values between 0.0009 to 0.003 mg/ml.

3.3.3-Hydrodynamic diameter changes along pH titration coordinates

As we described previously, the pH can tune the hydrophilicity-hydrophobicity ratio via the reversible ionization of pH responsive moieties like tertiary amines in UPS block copolymers. We already know that at low pH, the copolymers stayed at unimer state with tertiary amines 100% protonated. However, the tertiary amines are completely deprotonated at micelle state when pH was increased higher than pKa. This suggested there was a threshold protonation degree at which the micelles were formed. The threshold protonation degree corresponded to critical hydrophobicity-hydrophilicity ratio necessary to drive the formation of micelles.

The supramolecular self-assembly process was usually accompanied with significant parameter changes like size as a result of multiple polymer chains self-organizing into one single nanoparticle. We carefully examined the formation of micelle nanoparticles from PEO-b-nPDPA along the pH titration coordinate. The PEO-b-nPDPA copolymer was first dissolved in HCl and then titrated by addition of NaOH. DLS was used to measure hydrodynamic diameter for particle
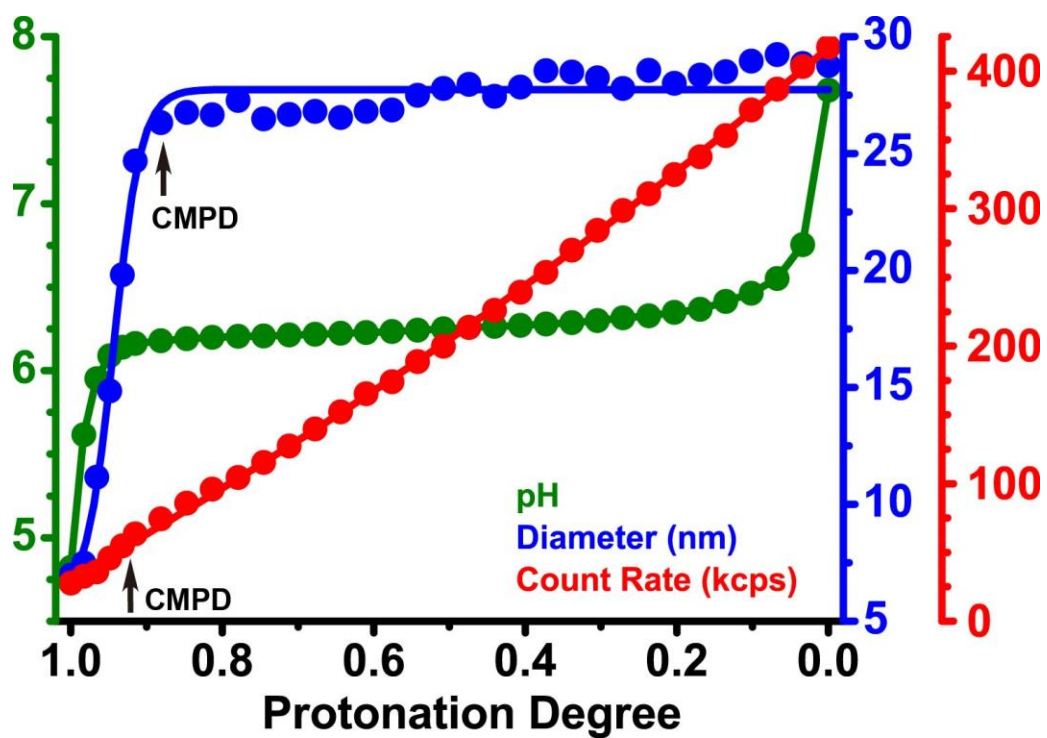
Figure 3.3.4. Hydrodynamic diameter and scattering counter rate measurement along the pH titration coordinate of PEO-b-nPDPA.

size and scattering count rate for nanoparticle concentration. Hydrodynamic diameter increased drastically at a high protonation degree of 91% indicating micelle formation and remained almost unaltered upon further neutralization of tertiary ammonium groups. The count rate increased slightly before 90% protonation and increased almost linearly for the remainder of titration (**Figure 3.3.4**).

We also measured the size changes along the pH titration coordinate of PEO-b-PDEA. We used the same hydrophilic poly(ethylene oxide) segment with 114 repeating units. Both the hydrophobic segment contains 80 PR building blocks. As shown in **Figure 3.3.5**, the hydrodynamic diameter kept unchanged when protonation degree decreased from 100% to 60%. With further decrease of protonation degree, the diameter increased significantly, suggesting the formation of micelles. That is to say, there also existed a threshold protonation degree for PEO-b-PDEA block copolymers. It is worth to note that the CMPD of PEO-b-PDEA was lower than that of PEO-b-PDPA, which made sense since their PR segment repeating units (DEA) were less hydrophobic than that of PEO-b-PDPA. There was no size change along the entire pH titration of PEO-b-PDMA, correlated with the fact the no micelles were formed even the solution pH was as high as 11.

3.3.4- fluorescence quenching along pH titration coordinate

The self-assembly of fluorophore labeled PEO-b-PR block copolymers is accompanied with fluorescence quenching as a result of homo-oligomeric fluorescence resonance energy transfer (HomoFRET). At unimer state, fluorophores emit strong
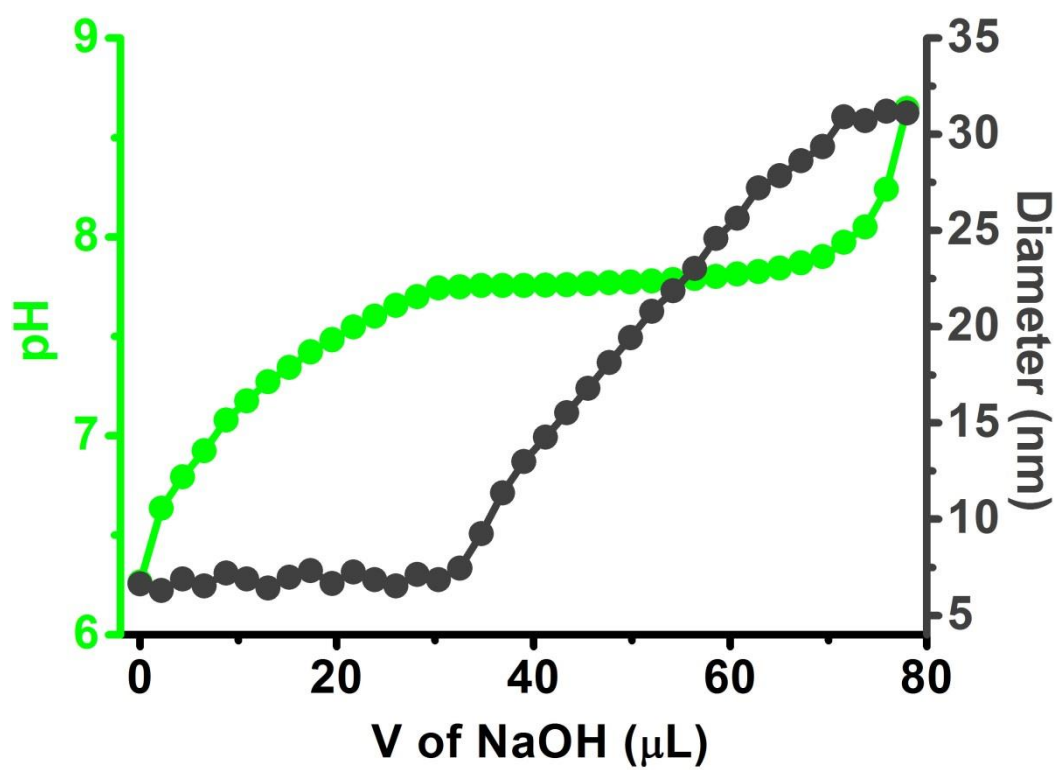
Figure 3.3.5. Hydrodynamic diameter measurement along the pH titration coordinate of

PEO-b-PDEA.

fluorescence. When pH increases, the fluorophore-conjugated PR segment self-assembles into micelle cores and results in fluorescence quenching. We used TMR labeled PEO-b-PDPA to study the fluorescence emission along protonation coordinates. As shown in **Figure 3.3.6**, the fluorescence intensity first decreased slowly until protonation degree reduced to about 92%. Then the fluorescence intensity decreased more drastically. It is known that the quenching of fluorescence is inversely proportional to the sixth power of fluorophore-fluorophore distance. When deprotonation degree decreased to 92%, micelles started to form and the quenching of fluorescence was significantly enhanced. The CMPD values of PEO-b-PDPA copolymer from different measurements by pH titration, micelle size, scattering count rates and fluorescence intensity showed good agreement at 91%, 90%, 92% and 89%, respectively.

3.3.5- Transmission electron microscopy to confirm CMPD

To confirm the CMPD measurement, we took the TEM images of PEO-b-nPDPA polymer solution at protonation degree slightly higher and lower than 90%. As shown in **Figure 3.3.7**, the PEO-b-PDPA all stayed at unimer state without formation of micelles at protonation degree of 95%. However, we observed the formation of core-shell micelles when protonation degree was slightly lowered than CMPD. The surface tension changes strongly with the concentration of amphiphilic block copolymers. And crucial micelle concentration can be used to characterize the critical concentration where the micellization starts. Similarly, the hydrophobicity-hydrophilicity ratio changes remarkably with the protonation degree of pH responsive block copolymers. The critical
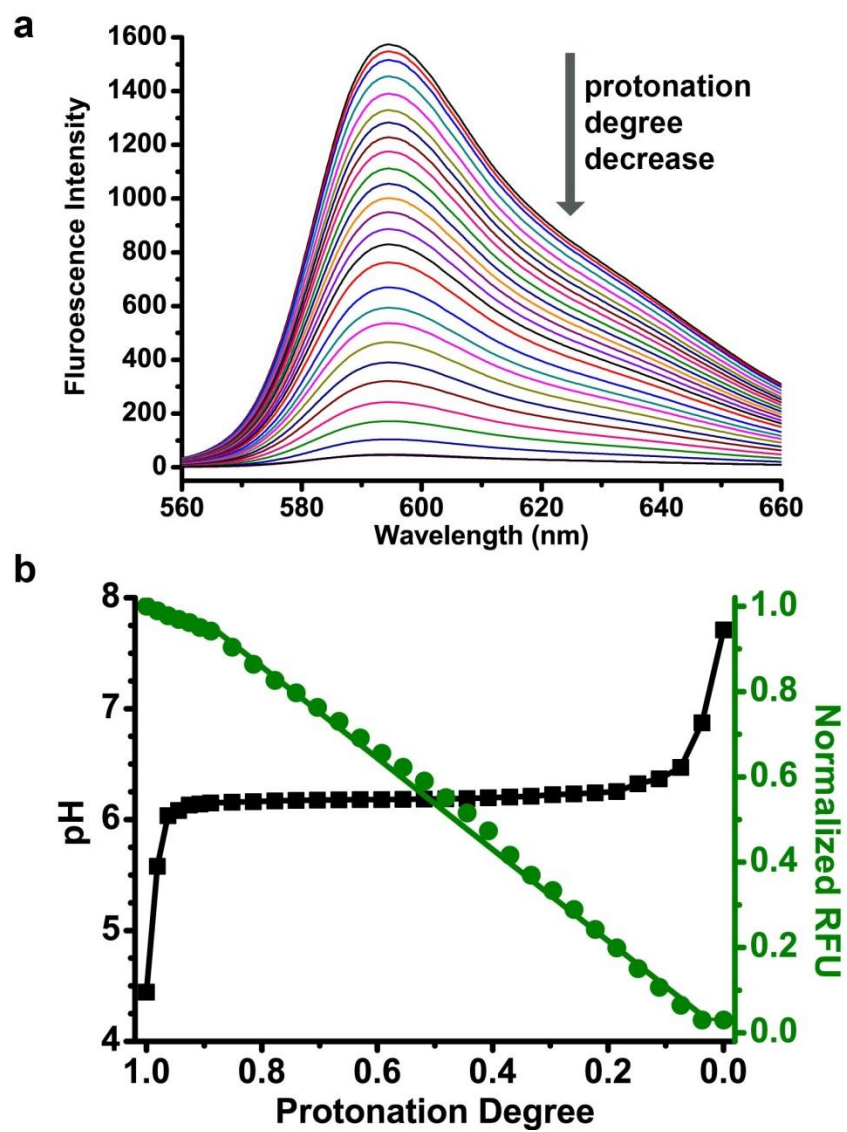
Figure 3.3.6. Normalized fluorescence intensity of TMR labeled PEO-b-nPDPA as a function of protonation degree.
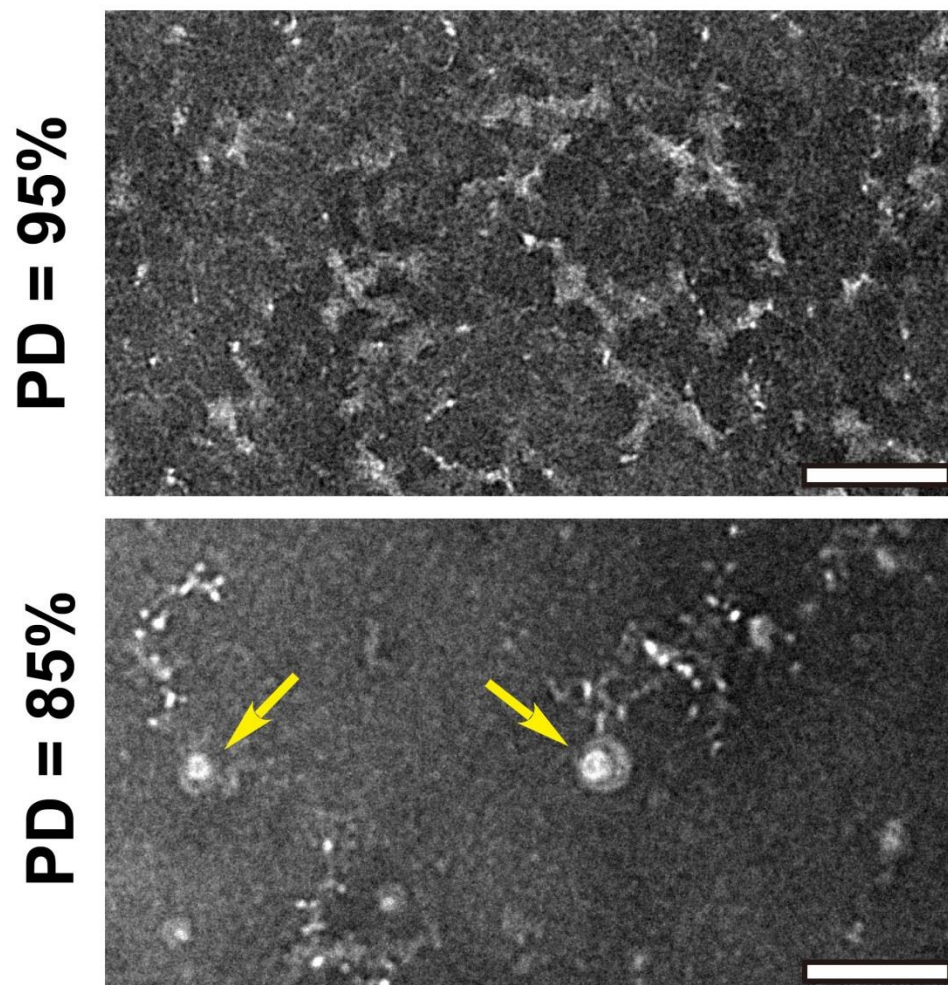
Figure 3.3.7. TEM images of PEO-b-PDPA before (protonation degree at 95%) and after (protonation degree at 85%) critical micelle protonation degree (CMPD = 90%). Micelle formation (yellow arrows) was observed below CMPD. (Scale Bar: 100 nm)

micelle protonation degree can be applied to characterize the critical protonation degree where the hydrophobicity was enough to drive the formation of micelles.

3.3.6- Hydrophobicity threshold for reversible self-assembly

We have showed previously that the PEO-b-PDMA will not form micelles even at very high pH, suggesting there was a threshold necessary to drive the formation of micelles. For the next step, we investigated whether there was a threshold necessary to lead to the dissociation of micelles into unimers. We synthesized PEO-b-PD6A block copolymers with hexyl as terminal alkyl group. The pH titration suggested the PEO-b-PD6A also had strong buffer effect and sharp pH response. But the DLS results suggested that even at pH around 2.0, the PEO_{113}-b-$PD6A_{40}$ did not dissociate into unimers (**Figure 3.3.8**).

Then we were able to conclude the hydrophobicity threshold of PR segment repeating unit necessary for the reversible supramolecular self-assembly triggered by pH changes (**Figure 3.3.9**). When the repeating unit was not hydrophobic enough, the hydrophobicity was too low to drive the formation of micelles. If the repeating unit was extreme hydrophobic, the protonation of tertiary amines still could not overcome the unfavorable energy penalty between hydrophobic repeating units and water.

3.3.7-Hydrophobic threshold for the entire PR segment.

The CMPD concept inspired us to further investigate whether there was a threshold for the entire PR segment. The CMPD for PEO_{114}-b-$PDPA_{80}$ was 90%, corresponding to 8 repeating units were neutralized and 72 repeating units were
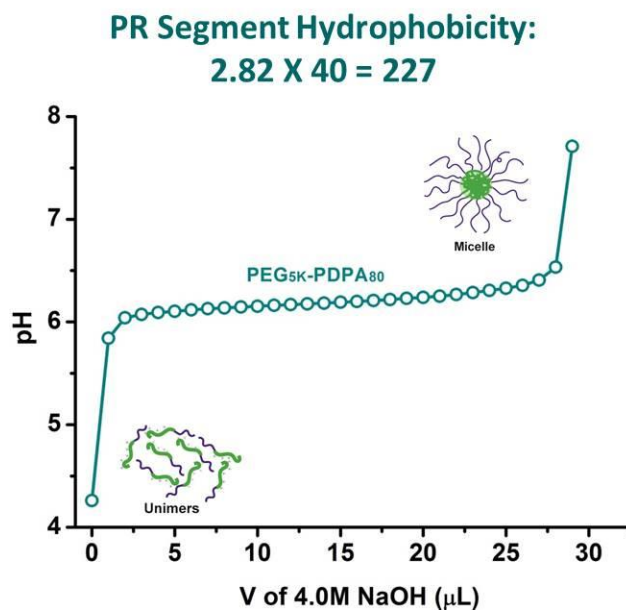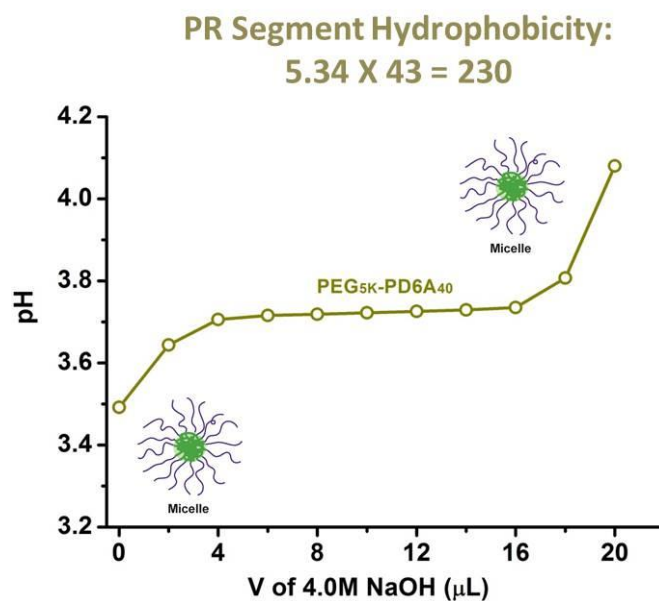
Figure 3.3.8. pH titration curves of PEO_{113}-b-$PD6A_{40}$. The block copolymers stayed at micelle state along the entire pH titration coordinate, even though the hydrophobicity of entire PR segment was the similar.
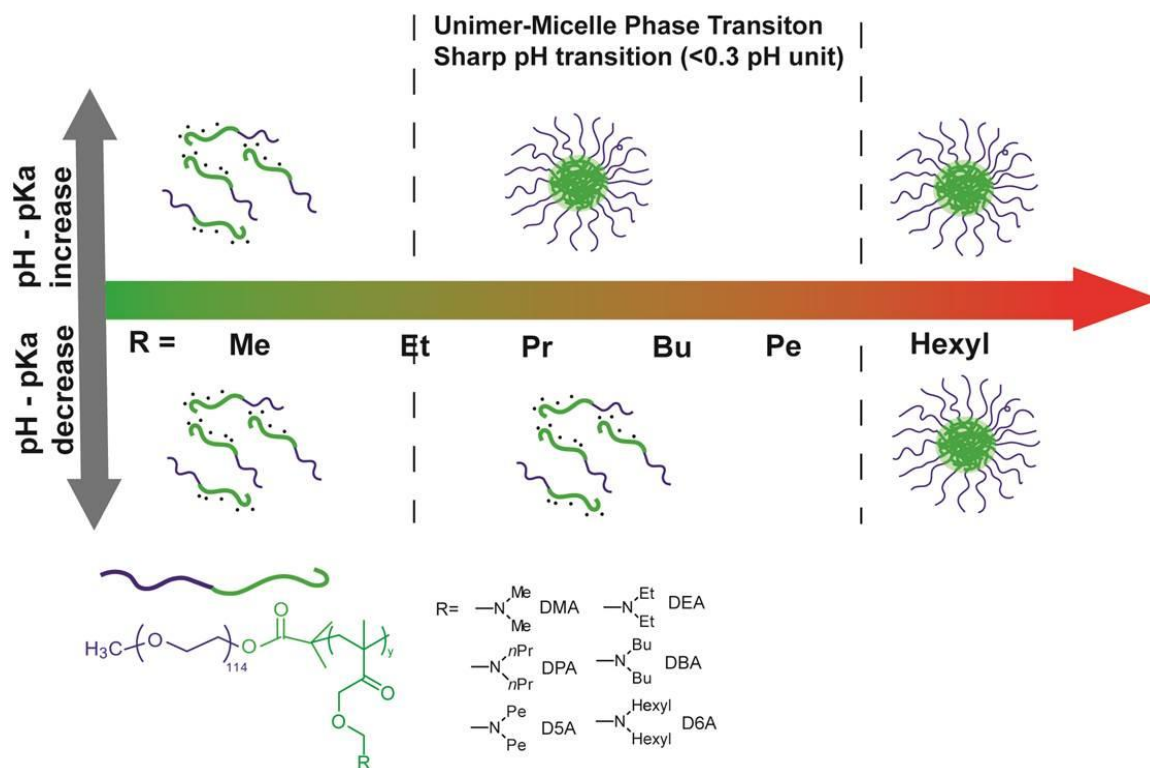
Figure 3.3.9. Hydrophobicity threshold of PR segment repeating unit necessary for the reversible supramolecular self-assembly

protonated. We synthesized PEO_{114}-b-$PDPA_5$ block copolymers, which can still underwent reversible supramolecular self-assembly triggered by pH changes. When 5 of 80 DPA repeating units were neutralized, the PEO_{114}-b-$PDPA_{80}$ will not form micelles. But the PEO_{114}-b-$PDPA_5$ can form micelles. This was reasonable because the remaining DPA repeating units were protonated and probably reduced the hydrophobicity-hydrophilicity ratio due to positive charges. The PEO_{114}-b-$PDPA_{40}$ and PEO_{114}-b-$PDPA_{80}$ had the same hydrophobicity for entire PR segment. Nevertheless, the latter would not dissociate into unimers at low pH. When fully pronated, the hydrophilicity as a result of PEO segment and protonated ammonium groups was probably the same for both polymers. But the hexyl groups contributed to higher hydrophobicity and the hydrophobicity-hydrophilicity ratio was not sufficient enough to drive the formation of micelles. The hydrophobicity-hydrophilicity ratio, instead of hydrophobicity of entire PR segment, may be the best parameter to determine the necessity of pH triggered reversible supramolecular self-assembly of UPS block copolymers.

3.4-References

1   Miller-Chou, B. A. & Koenig, J. L. A review of polymer dissolution. *Progress in Polymer Science* **28**, 1223-1270 (2003).

2   Panayiotou, C. G. Lattice-fluid theory of polymer solutions. *Macromolecules* **20**, 861-871 (1987).

3   Huggins, M. L. Solutions of long chain compounds. *The Journal of chemical physics* **9**, 440-440 (1941).

4   Flory, P. J. Thermodynamics of high polymer solutions. *The Journal of chemical physics* **10**, 51-61 (1942).

5   Doi, M. & Edwards, S. F. *The theory of polymer dynamics*. Vol. 73 (oxford university press, 1988).

6   Flory, P. J. & Krigbaum, W. R. Thermodynamics of high polymer solutions. *Annual review of physical chemistry* **2**, 383-402 (1951).

7   Müller- Plathe, F. Coarse- graining in polymer simulation: from the atomistic to the mesoscopic scale and back. *ChemPhysChem* **3**, 754-769 (2002).

8   Favre, E., Nguyen, Q., Sacco, D., Moncuy, A. & Clement, R. Multicomponent polymer/solvents equilibria: an evaluation of Flory-Huggins theory for crosslinked PDMS networks swelled by binary mixtures. *Chemical Engineering Communications* **140**, 193-205 (1995).

9   Fredrickson, G. H., Liu, A. J. & Bates, F. S. Entropic corrections to the Flory-Huggins theory of polymer blends: Architectural and conformational effects. *Macromolecules* **27**, 2503-2511 (1994).

10   Daoud, M. *et al.* Solutions of flexible polymers. Neutron experiments and interpretation. *Macromolecules* **8**, 804-818 (1975).

11   Scheutjens, J. & Fleer, G. Statistical theory of the adsorption of interacting chain molecules. 1. Partition function, segment density distribution, and adsorption isotherms. *Journal of Physical Chemistry* **83**, 1619-1635 (1979).

12   Karlström, G. A new model for upper and lower critical solution temperatures in poly (ethylene oxide) solutions. *The Journal of Physical Chemistry* **89**, 4962-4964 (1985).

13   Kozak, J. J., Knight, W. S. & Kauzmann, W. Solute- Solute Interactions in Aqueous Solutions. *The Journal of Chemical Physics* **48**, 675-690 (1968).

14   Mai, Y. & Eisenberg, A. Self-assembly of block copolymers. *Chemical Society Reviews* **41**, 5969-5985 (2012).

15   Shen, H. & Eisenberg, A. Morphological phase diagram for a ternary system of block copolymer PS310-b-PAA52/dioxane/H2O. *The Journal of Physical Chemistry B* **103**, 9473-9487 (1999).

16   Morimoto, N., Qiu, X.-P., Winnik, F. M. & Akiyoshi, K. Dual stimuli-responsive nanogels by self-assembly of polysaccharides lightly grafted with thiol-terminated poly (N-isopropylacrylamide) chains. *Macromolecules* **41**, 5985-5987 (2008).

17   Chen, J., Liu, Q., Xiao, J. & Du, J. EpCAM-antibody-labeled noncytotoxic polymer vesicles for cancer stem cells-targeted delivery of anticancer drug and siRNA. *Biomacromolecules* **16**, 1695-1705 (2015).

18   Du, J., Tang, Y., Lewis, A. L. & Armes, S. P. pH-sensitive vesicles based on a biocompatible zwitterionic diblock copolymer. *Journal of the American Chemical Society* **127**, 17982-17983 (2005).

19   Popescu, M.-T., Korogiannaki, M., Marikou, K. & Tsitsilianis, C. CBABC terpolymer-based nanostructured vesicles with tunable membrane permeability as potential hydrophilic drug nanocarriers. *Polymer* **55**, 2943-2951 (2014).

20   Themistou, E., Battaglia, G. & Armes, S. P. Facile synthesis of thiol-functionalized amphiphilic polylactide–methacrylic diblock copolymers. *Polymer Chemistry* **5**, 1405-1417 (2014).

21   Liu, Q., Chen, S., Chen, J. & Du, J. An asymmetrical polymer vesicle strategy for significantly improving T 1 MRI sensitivity and cancer-targeted drug delivery. *Macromolecules* **48**, 739-749 (2015).

22   Stuart, M. A. C. *et al.* Emerging applications of stimuli-responsive polymer materials. *Nature materials* **9**, 101-113 (2010).

23   Zhu, Y., Yang, B., Chen, S. & Du, J. Polymer vesicles: mechanism, preparation, application, and responsive behavior. *Progress in Polymer Science* (2016).

24   Discher, D. E. & Eisenberg, A. Polymer vesicles. *Science* **297**, 967-973 (2002).

25   Hayward, R. C. & Pochan, D. J. Tailored assemblies of block copolymers in solution: it is all about the process. *Macromolecules* **43**, 3577-3584 (2010).

26   Lehn, J. M. Supramolecular chemistry—scope and perspectives molecules, supermolecules, and molecular devices (Nobel Lecture). *Angewandte Chemie International Edition in English* **27**, 89-112 (1988).

27   Darling, S. Directing the self-assembly of block copolymers. *Progress in Polymer Science* **32**, 1152-1204 (2007).

28   Rodriguez-Hernandez, J., Chécot, F., Gnanou, Y. & Lecommandoux, S. Toward 'smart'nano-objects by self-assembly of block copolymers in solution. *Progress in Polymer Science* **30**, 691-724 (2005).

29   Voets, I. K. *et al.* Spontaneous symmetry breaking: formation of Janus micelles. *Soft Matter* **5**, 999-1005 (2009).

30   Edwards, E. W., Chanana, M., Wang, D. & Möhwald, H. Stimuli- Responsive Reversible Transport of Nanoparticles Across Water/Oil Interfaces. *Angewandte Chemie International Edition* **47**, 320-323 (2008).

31   Kim, M. S. *et al.* pH- Responsive PEG- Poly (β- amino ester) Block Copolymer Micelles with a Sharp Transition. *Macromolecular rapid communications* **27**, 447-451 (2006).

32   Lee, E. S., Shin, H. J., Na, K. & Bae, Y. H. Poly (L-histidine)–PEG block copolymer micelles and pH-induced destabilization. *Journal of Controlled Release* **90**, 363-374 (2003).

33   Domínguez, A., Fernández, A., González, N., Iglesias, E. & Montenegro, L. Determination of critical micelle concentration of some surfactants by three techniques. *J. Chem. Educ* **74**, 1227 (1997).

34   Zhou, K. *et al.* Multicolored pH-tunable and activatable fluorescence nanoplatform responsive to physiologic pH stimuli. *Journal of the American Chemical Society* **134**, 7803-7811 (2012).

CHAPTER FOUR-Molecular Pathway of pH-Triggered Supramolecular Assembly

4.1-Introduction

4.1.1-Self-assembly pathway complexity in natural and synthetic macromolecules

One of the defining characteristics of a living system is the ability of component molecular structures to self-assemble with high precision and fidelity. Uncovering the mechanisms through which such processes take place is one of the grand challenges of modern science[1].

4.1.1.1-Proteins

Proteins are the most abundant molecules in biological systems other than water. We contain perhaps more than 100,000 different kinds of protein and they stimulate or control virtually every chemical/biological process on which our lives depend[2-4]. Different proteins are distinguished by a different order of amino acids in the polymeric sequence of various building blocks. Following their biosynthesis, the majority of proteins must be converted into natural folded and compact three dimensional structures in order to function. The unique structure of a specific protein is crucial for its selectivity and diversity in functions.

The folding of proteins into their tightly folded compact structues is one of the most recognized examples of supramolecular self-assembly process in biological systems. understanding this complex process will therefore provide a unique insight into the way in which evolutionary selection has influenced the properties of a molecular system for functional advantage. The wide variety of highly specific structures that result from protein folding and that bring key functional groups into close proximity has enabled

living systems to develop astonishing diversity and selectivity in their underlying chemical processes. In addition to generating biological activity, however, we now know that folding is coupled to many other biological processes, including the trafficking of molecules to specific cellular locations and the regulation of cellular growth and differentiation.

We have been aware that the amino acid sequence of each protein probably contains the information that specifies both the native structure and the pathway to attain that state. However, understanding the molecular pathway through which a polypeptide chain self-assemble to a specific three-dimensional protein structure is still at the heart of molecular biology[5]. The energy landscape theory have been developed for a statistical description of protein folding[3,6-9]. The native states of proteins almost always correspond to the structures that are most thermodynamically stable under physiological conditions[10]. On average, native-like interactions between residues are more stable than nonnative ones. The polypeptide chain is able to find its lowest-energy structure by a process of trial and error. This energy landscape allows the protein to fold to the final native state through any of a large number of pathways and intermediates, rather than being restricted to one specific pathway. The energy landscape theory is supported by both computational simulations of model proteins and experimental studies[6].

Figure 4.1.1 provides a schematic energy landscape for protein folding. The surface is derived from a computer simulation of the folding of a highly simplified model of a small protein[11]. The surface 'funnels' the multitude of denatured conformations to the unique native structure. The critical region on a simple surface such as this one is the saddle point corresponding to the transition state, the barrier that all molecules must cross

138
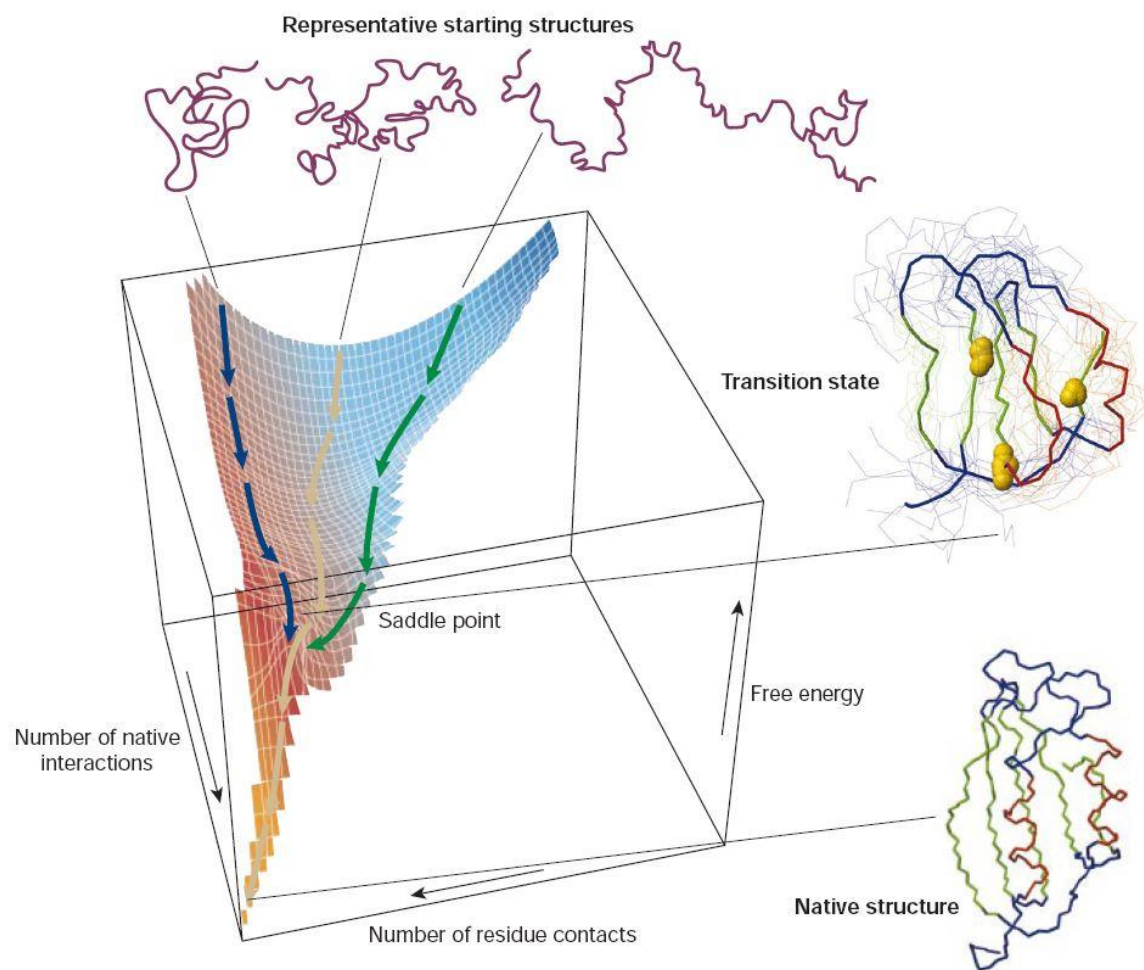
Figure 4.1.1. A schematic energy landscape for protein folding[12].

if they are to fold to the native state. Superimposed on this schematic surface are ensembles of structures corresponding to different stages of the folding process. The transition state ensemble was calculated by using computer simulations constrained by experimental data from mutational studies of acylphosphatase[13]. The yellow spheres in this ensemble represent the three 'key residues' in the structure; when these residues have formed their native-like contacts the moverall topology of the native fold is established. The structure of the native state is shown at the bottom of the surface; at the top are indicated schematically some contributors to the distribution of unfolded species that represent the starting point for folding. Also indicated on the surface are highly simplified trajectories for the folding of individual molecules.

4.1.1.2-Nucleic acids

Like proteins, RNAs that adopt specific functional structures face a similar challenge of attaining these specific structures from a myriad of unfolded conformations. Theoretical studies and computational simulations of minimal peptide models have provided estimates for the folding of proteins that agree well with experimental results[14,15]. The energy landscape theory is also applicable for predicting the folding kinetics of RNA[14-22], although the actual timescales for folding of RNAs may be different from those of proteins[20]. **Figure 4.1.2** gives an hypothetical energy folding landscape of RNA[19]. The graph schematically indicates free energy (G) as a function of conformation (horizontal axis). A subset of the extended molecules undergoes specific nucleation and collapse to the native structure. The remaining population becomes trapped in a collection of compact, metastable intermediates that correspond to local minima in the rough energy landscape. The intermediates contain many native and some non-native

140

Figure 4.1.2. Hypothetical energy folding landscape of RNA[19].
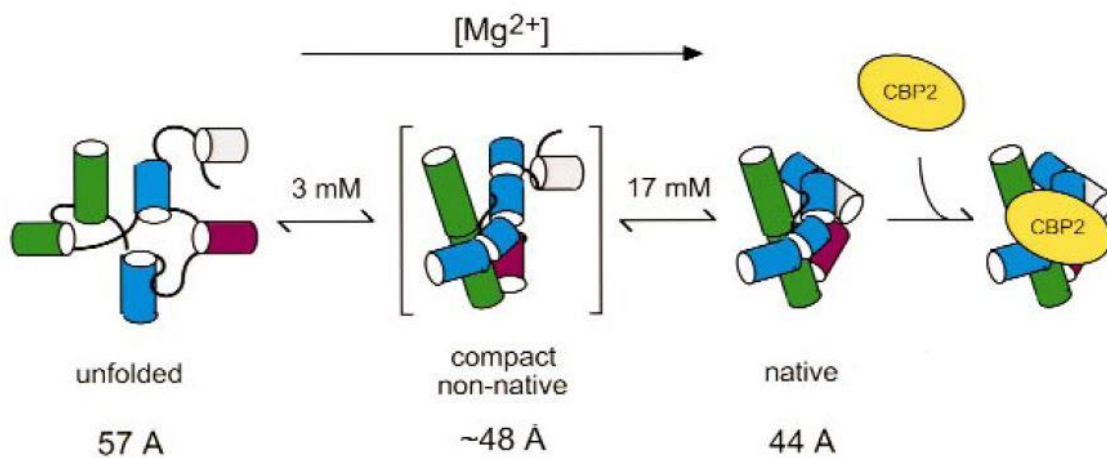
Figure 4.1.3. Folding of yeast mitochondrial bI5 ribozyme[17].

interactions. Transitions from intermediates to native states cross significant energy barriers and occur close to the native structure.

RNA folding pathways are often dominated by partially folded intermediates that persist for long times in vitro[18]. In many cases, the stable tertiary structure of RNAs is only observed in the presence of divalent metal ions or, in some cases, very high concentrations of monovalent ions[23]. Both the kinetics and specificity of folding is expected to be extremely sensitive to ionic conditions. In addition, the electrostatic interactions are expected to dominate the free energy of nucleation and collapse. For example, Mg^{2+} is required to stabilize the native structure in the folding process of *bl5ribozyme*. **Figure 4.1.3** shows the progressive folding of yeast mitochondrial bl5 ribozyme. The ribozyme core becomes increasingly compact in the presence of high concentrations of $MgCl_2$[16]. CBP2 (yellow) is proposed to selectively bind and stabilize the obtained native structure. The structure of the RNA in the collapsed, nonnative phase is unknown, and presumably corresponds to a mixture of conformations.

4.1.1.3-Synthetic polymers

The self-assembly of biological macromolecules is more robust and predictable compared to that of synthetic polymers[1]. However, the protein folding also depends on the solvent, the concentration of salts, pH and temperature[24], similar to the self-assembly of synthetic polymers. This suggests that the supramolecular self-assembly of non-biological macromolecules may also display pathway complexity, even not as complicated as that of proteins. In the last several decades, the self-assembly process of synthetic supramolecular polymers has been studied and even modulated, but our quantitative understanding of the processes involved remains limited.

Wooley group reported the formation of block copolymer self-assemblies via kinetic control[25]. They found that the length of the block segment, and the selectivity of the solvent primarily control the resultant assembled morphology. Through the kinetic manipulation of charged, amphiphilic block copolymers in solution, they are able to generate different nanoscale structures with simple block copolymer chemistry. Richter and his colleagues reported the structural observation and kinetic pathway in the formation of polymeric micelles using a a well-defined amphiphilic block copolymers (poly(ethylene-alt-propylene)-poly(ethylene oxide)). Using a quantitative model, they showed that the self-assembly process can be treated as a nucleation and growth type process where the elemental growth mechanism is an exchange of single molecules. The pathway complexity of supramolecular self-assembly of synthetic polymers was also found in the self-organization of π-conjugated oligomer S-chiral oligo(p-phenylenevinylene) (SOPV)[26], a functional material in variety of organic electronic devices. The self-assembly pathways of SOPV includes the growth of two competing assemblies (**Figure 4.1.4**). The self-assembly of SOPV in a polar solutions is initiated by formation of a hydrogen-bonded dimer. The hydrogen-bonded dimer further self-assembles into helical stacks via a nucleation–elongation growth mechanism. Right-handed P-helices form quickly but are less stable than the left-handed M-helices, which form more slowly.

Self-assembly provides an powerful tool to build functional organic materials with significantly elevated complexity compared to molecules prepared via covalent chemistry[27-30]. Understanding the molecular pathway of supramolecular self-assembly
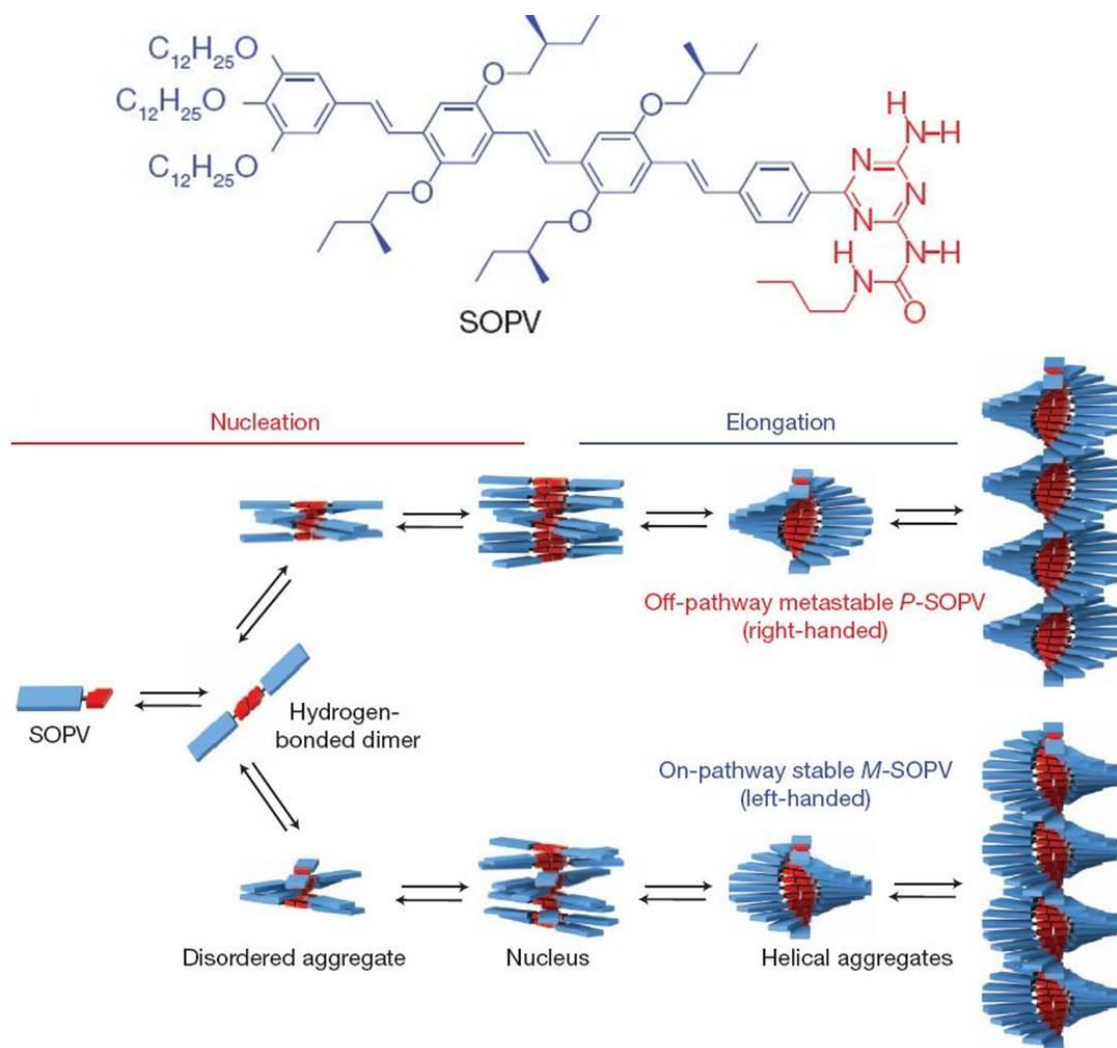
Figure 4.1.4. Pathway complexity in supramolecular polymerization of SOPV[26].

will enable the design of more sophisticated and robust functional materials comparable to biological macromolecules.

4.1.2-Three possible pathways of pH triggered supramolecular self-assembly of

PEO-b-PR block copolymers.

In this study, we systematically investigated the mechanism of pH triggered self-assembly of UPS block copolymers. Intuitively, there are two opposite pathways for pH-triggered supramolecular self-assembly of UPS block copolymers (**Figure 4.1.5**): In the graduate model, below CMPD, majority of block copolymers may first self-assemble into positively charged loose aggregates and upon neutralization, the loose aggregates are gradually deprotonated, shrinking in size and finally turning into neutral, mature micelles; In the divergent model, at any given protonation degree below CMPD, the PEO-b-PDPA copolymers exist in either protonated unimers or neutral, mature micelles with different population distributions. The initial DLS and fluorescence data suggest that micellization undergoes the second pathway as indicated by the relatively unchanged nanoparticle size and linearly correlated count rate and fluorescence intensity to the degree of protonation. In this study, we systematically investigated the molecular pathway of pH triggered supramolecular self-assembly of UPS block copolymers. Particularly, we used PEO-b-nPDPA as the exemplary system.
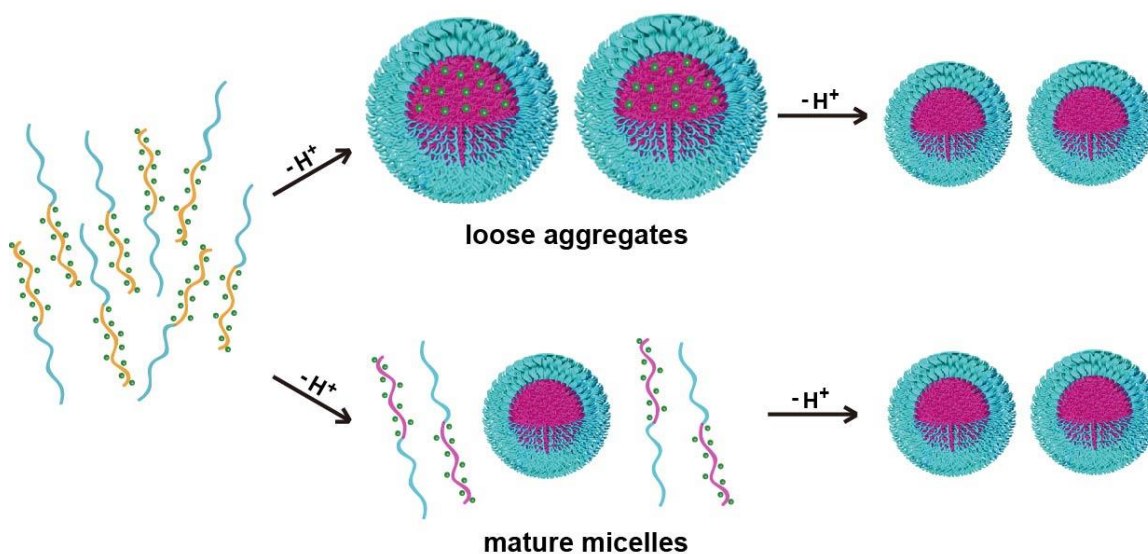
Figure 4.1.5. Two possible pathways for pH-triggered supramolecular self-assembly. In the graduate model (upper panel), the fully charged unimers are initially deprotonated into positively charged loose aggregates. Upon further neutralization, the loose aggregates are gradually deprotonated, shrinking in size and finally turning into neutral, mature micelles. In the divergent model (lower panel), at any given protonation degree below CMPD, the PEO-b-PDPA copolymers exist in either protonated unimers or neutral, mature micelles with different population distributions.

4.2-Materials and methods

4.2.1-Synthesis and characterization of DPA-MA monomers and *PEO-b-nPDPA block copolymers*

First, ethanolamine (12.2g, 0.2 mol) and bromopropane (49.2 g, 0.4 mol) were dissolved in 400 mL acetonitrile, and Na2CO3 (53.0 g, 0.5 mol) was added to the solution. After overnight reaction, the solution was filtered to remove the precipitated NaBr salt and extra Na2CO3. CH3CN solvent was removed by rotovap. The resulting residue was distilled in vacuo (40~45 ℃ at 0.05 mm Hg) as a colorless liquid to obtain 2-(dipropylamino) ethanol. Then 2-(dipropylamino) ethanol (21.3g, 0.1 mol), triethylamine (10.1 g, 0.1 mol), and inhibitor hydroquinone (0.11g, 0.001mol) were dissolved in 100 mL CH2Cl2 and methacryloyl chloride (10.4g, 0.1 mol) was added dropwise into a three-neck flask. The solution was refluxed overnight. After reaction, the solution was filtered to remove the precipitated triethylamine-HCl salts, and CH2Cl2 solvent was removed by rotovap. The resulting residue was distilled in vacuo (47-53 ℃ at 0.05 mm Hg) as a colorless liquid. After synthesis, the monomer was characterized by 1H-NMR. All the NMR spectra were obtained in CDCl$_3$ using tetramethylsilane (TMS) as the internal reference on a Varian 500MHz spectrometer.

PEO-b-nPDPA copolymers were synthesized by atom transfer radical polymerization (ATRP) following similar procedures. The dye free copolymers were used in polymer characterizations. First, DPA-MA (1.70 g, 8 mmol), PMDETA (21 μL, 0.1 mmol) and MeO-PEO114-Br (0.5 g, 0.1 mmol) were charged into a polymerization tube. Then a mixture of 2-propanol (2 mL) and DMF (2 mL) was added to dissolve the monomer and initiator. After three cycles of freeze-pump-thaw to remove the oxygen,

CuBr (14 mg, 0.1 mmol) was added into the polymerization tube under nitrogen atmosphere, and the tube was sealed in vacuo. The polymerization was carried out at 40 ℃ for 8 hours. After polymerization, the reaction mixture was diluted with 10 mL THF, and passed through a neutral Al2O3 column to remove the catalyst. The THF solvent was removed by rotovap. The residue was dialyzed in distilled water and lyophilized to obtain a white powder.

4.2.2-pH titration

PEO-*b*-PDPA copolymer (80 mg) was first dissolved in 5 mL 0.1 M HCl and diluted to 2.0 mg/ml with DI water. NaCl was added to adjust the salt concentration to 150 mM. pH titration was carried out by adding small volumes (1   L in increments) of 4.0 M NaOH solution under stirring. The pH increase in the range of 2 to 11 was monitored as a function of total added volume of NaOH. The fully protonated state and complete deprotonation states (protonation degree equaled 100% and 0%) were determined by the two extreme value points of pH titration curves' 1ˢᵗ derivation. The pH values were measured using a Mettler Toledo pH meter with a microelectrode. Titration of other pH sensitive polymers followed similar procedures using the same amine molar concentration.

4.2.3-Dialysis

PEO-*b*-PDPA copolymers (40 mg) was first dissolved in 2.5 mL 0.1 M HCl and diluted to 2.0 mg/mL with DI water. PEO-*b*-PDPA solutions with protonation degree at 0%, 25%, 50%, 75% and 100% were obtained by adding corresponding volumes of 4.0

M NaOH.   At each protonation degree, 10 mL polymer solution was centrifuged using ultra-centrifugation tube with a molecular weight cutting-off at 100 kDa to approximately 5 mL filtrated sample. pH titration were performed to quantify the amount of polymers and degree of protonation in both residual and filtrate layers. PDMA and PEI were used as control and followed similar procedures using the same amine molar concentration. We repeated the experiments five times and data were shown in mean ±s.d.

4.2.4-NMR Analysis

PEO-*b*-PDPA copolymer (10 mg) was first dissolved in 0.1 M DCl solution in D_2O and diluted to 2.0 mg/ml with D_2O. NaCl was added to a final concentration of 150 mM. pH titration was performed by adding small volumes (1 μL in increments) of 4.0 M NaOD solution under stirring. Following similar procedures as described above, the volume of NaOD needed to adjust protonation degree to 0%, 20%, 40%, 60%, 80% and 100% were calculated based on titration. The NMR spectra were obtained on a Varian 400 MHz ^{1}H NMR Spectrometer at room temperature. NMR analysis of PEO-*b*-PDMA followed a similar procedure using the same amine molar concentration.

4.3-Results and discussions

4.3.1-DLS and fluorescence intensity indications on self-assembly pathway

To differentiate above mechanisms, we first used dynamic light scattering to investigate polymers' hydrodynamic diameter and scattering count rate changes along protonation coordinates. With the addition of base and resulted protonation degree decrease, the hydrodynamic diameter first increased sharply until protonation degree to

149

CMPD. However, the scattering count rate first increased slowly and then started to increase drastically follwoing a inear trend below CMPD. These results excluded the first pathway where the size and count rate should first increase to maximum and then decrease. If the self-assembly went through unimer-micelle mixture transition state, the measured diameter should increase first because unimers are coming together to form micelles with add of base. Then the diameter kept unchanged once micelles were formed since larger nanoparticles were overwhelming in diameter measurement. The count rate increased slowly first because micelles are not formed until CMPD. The linear increase after that resulted from almost the same amount of unimers self-organize into micelles with addition of certain amount of base (**Figure 4.3.1 a**).

We confirmed the unimer-micelle mixture transition state using fluorescence spectrometer with TMR labeled PEO-b-PDPA. At unimer state, fluorophores emit strong fluorescence. When pH increases, the fluorophore-conjugated PR segment self-assembles into micelle cores and leads to fluorescence quenching. As shown in **Figure 4.3.1 b**, the fluorescence first decreased slowly until protonation degree reduced to CMPD. Then the fluorescence decreased drastically following a linear trend. The quenching of fluorescence is inversely proportional to the sixth power of fluorophore-fluorophore distance. If the unimers first formed swollen micelles and then shrink into compact micelles, it's hard to imagine the fluorescence intensity decrease linearly throughout the process. However, if the self-assembly went through unimer-micelle mixture transition state, the fluorescence decreased slowly first because unimer were coming closer with the decrease of protonation degree and resulting slightly increased hydrophobicity. When deprotonation degree decreased to CMPD, micelles are formed and fluorescence
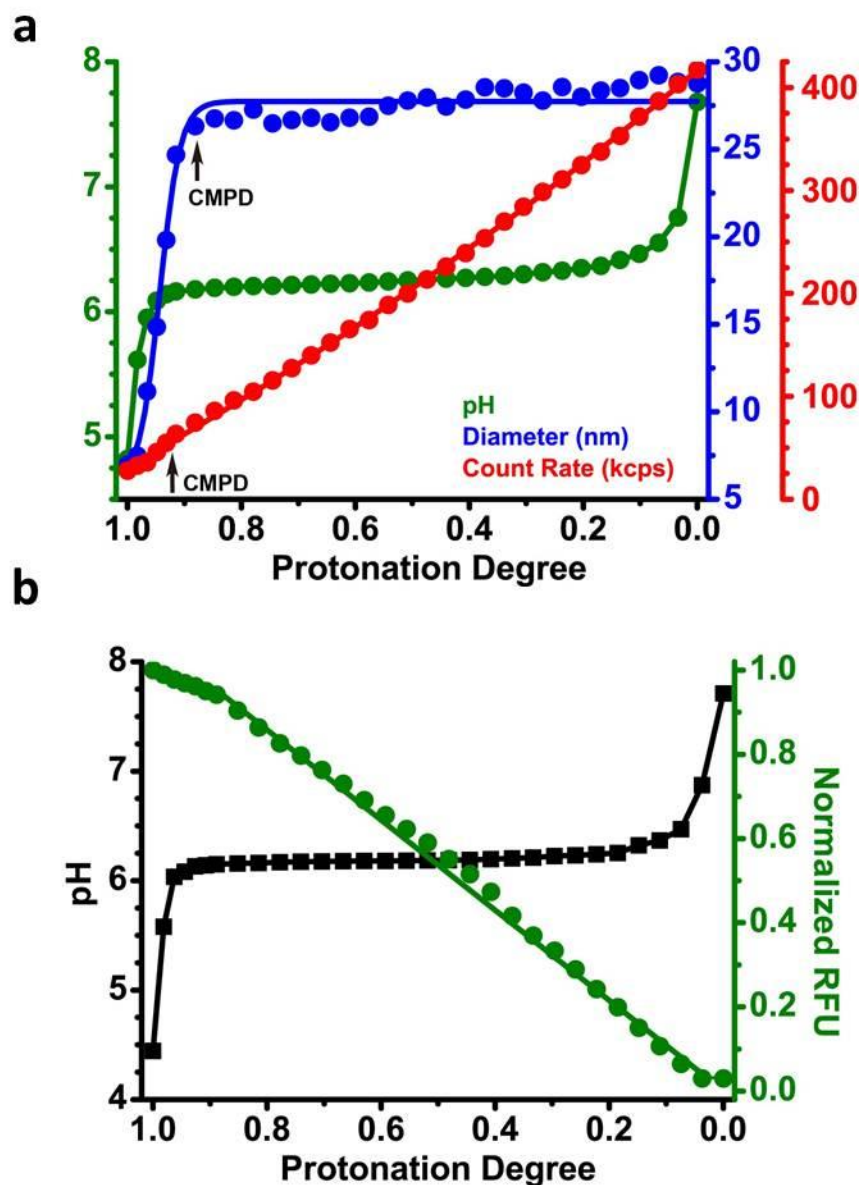
Figure 4.3.1. (a) pH, hydrodynamic diameter and scattering count rate change of PEO-b-PDPA as a function of protonation degree. (b) Normalized fluorescence intensity of TMR conjugated PEO-b-PDPA as a function of protonation degree.

151

quenching is more significant. Also, the same amount of unimers got into micelles with the addition of certain amount of base lead to linear decrease of fluorescence intensity.

4.3.2-Coexistence of micelles and unimers along supramolecular self-assembly

To verify the coexistence of unimers and neutral micelles along the pH titration coordinate, we first applied a dialysis method to separate unimers (22 kD) from micelles (16,000 kD)[31-33] at different degrees of protonation (**Figure 4.3.2**). At different protonation degree, 10 mL TMR labeled PEO-b-PDPA were centrifuged in ultracentrifugation tube until 5 mL filtrate were obtained. The filtrate were acidified to pH=4 and quantified via UV-Vis absorption (**Figure 4.3.3**). Supposedly, all micelles should remain in the upper layer while half of the unimers are filtrated to lower layer. The quantification showed the amount of remaining unimers in the solution decreased almost linearly after critical micelle protonation degree which further confirmed unimer-micelle mixture transition state.

We then performed the dialysis experiments wiht dye-free PEO-b-PDPA block copolymers. PEO-b-PDPA solutions with protonation degree at 0%, 25%, 50%, 75% and 100% were prepared by pH titration. At each protonation degree, 10 mL polymer solution was centrifuged using ultra-centrifugation tube with a molecular weight cutting-off at 100 kDa to approximately 5 mL filtrated sample. pH titration were performed to quantify the amount of polymers and degree of protonation in both residual and filtrate layers. Two polymeric bases with broad pH response (PEO-b-PDMA and PEI) were used for comparison.
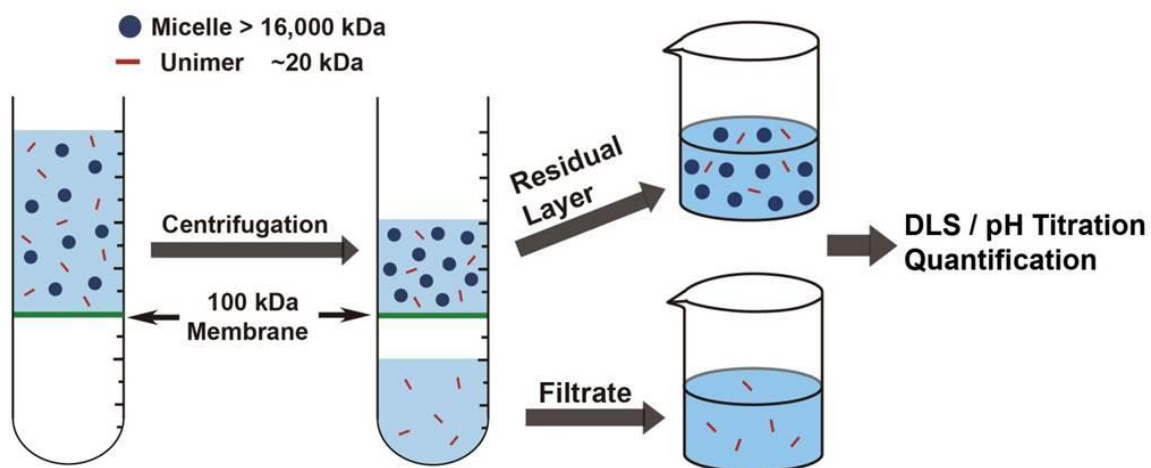
Figure 4.3.2. Schematic illustration of dialysis experiments.
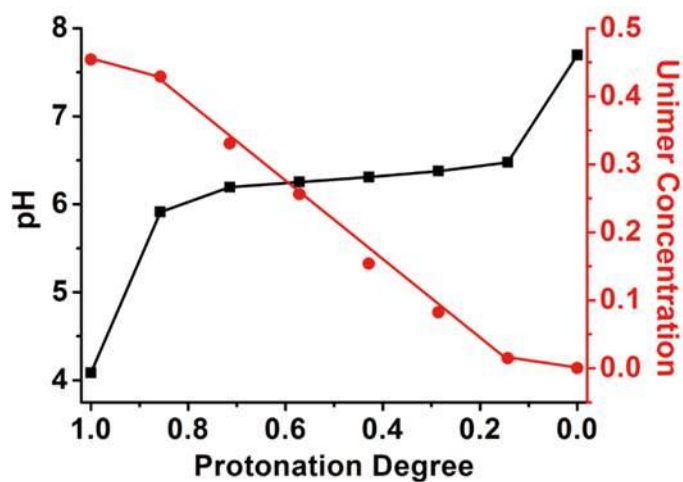
Fiugre 4.3.3. UV-Vis quantification of TMR conjugated PEO-b-PDPA unimers in lower layer after dialysis.
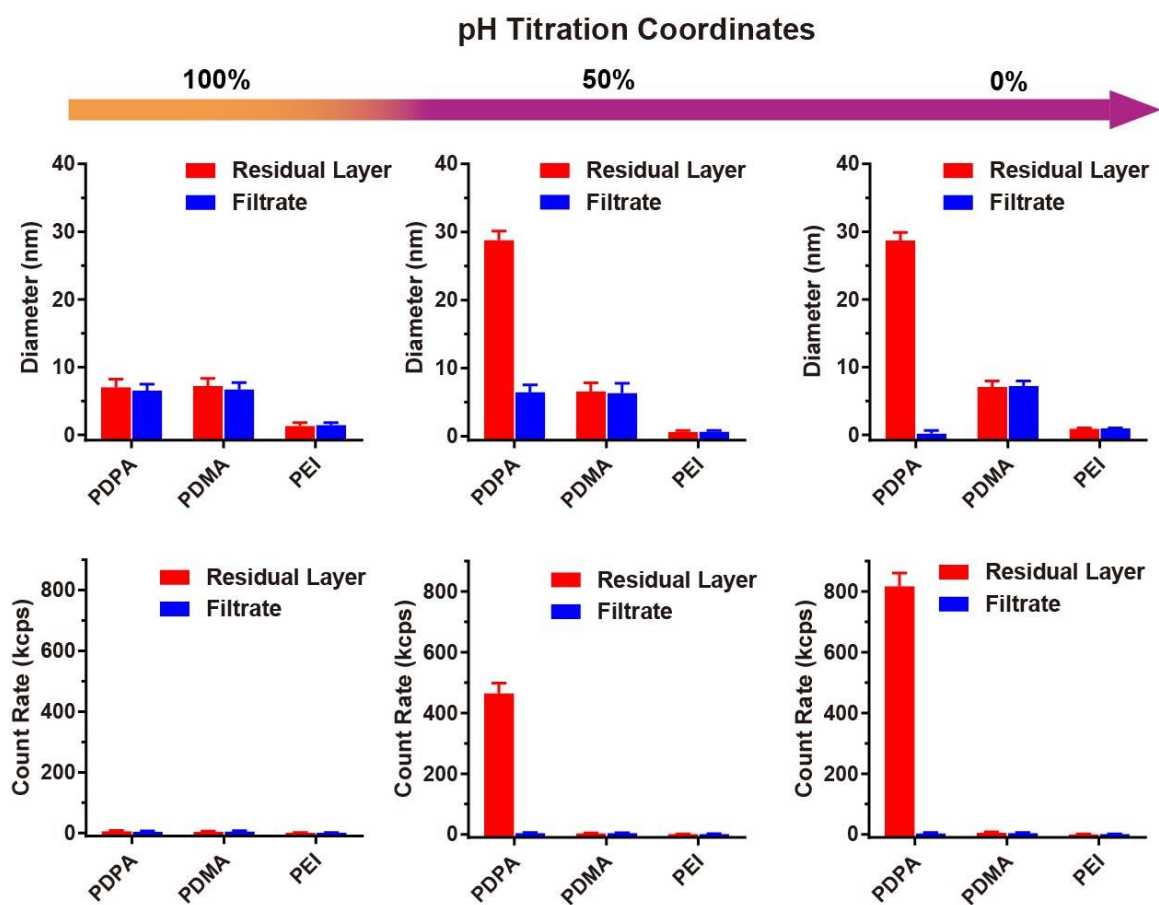
Figure 4.3.4. Hydrodynamic diameters and light scattering count rates of residual and filtrate layers at three protonation degrees (0, 50 and 100%) of PEO-b-PDPA, PEO-b-PDMA and PEI.
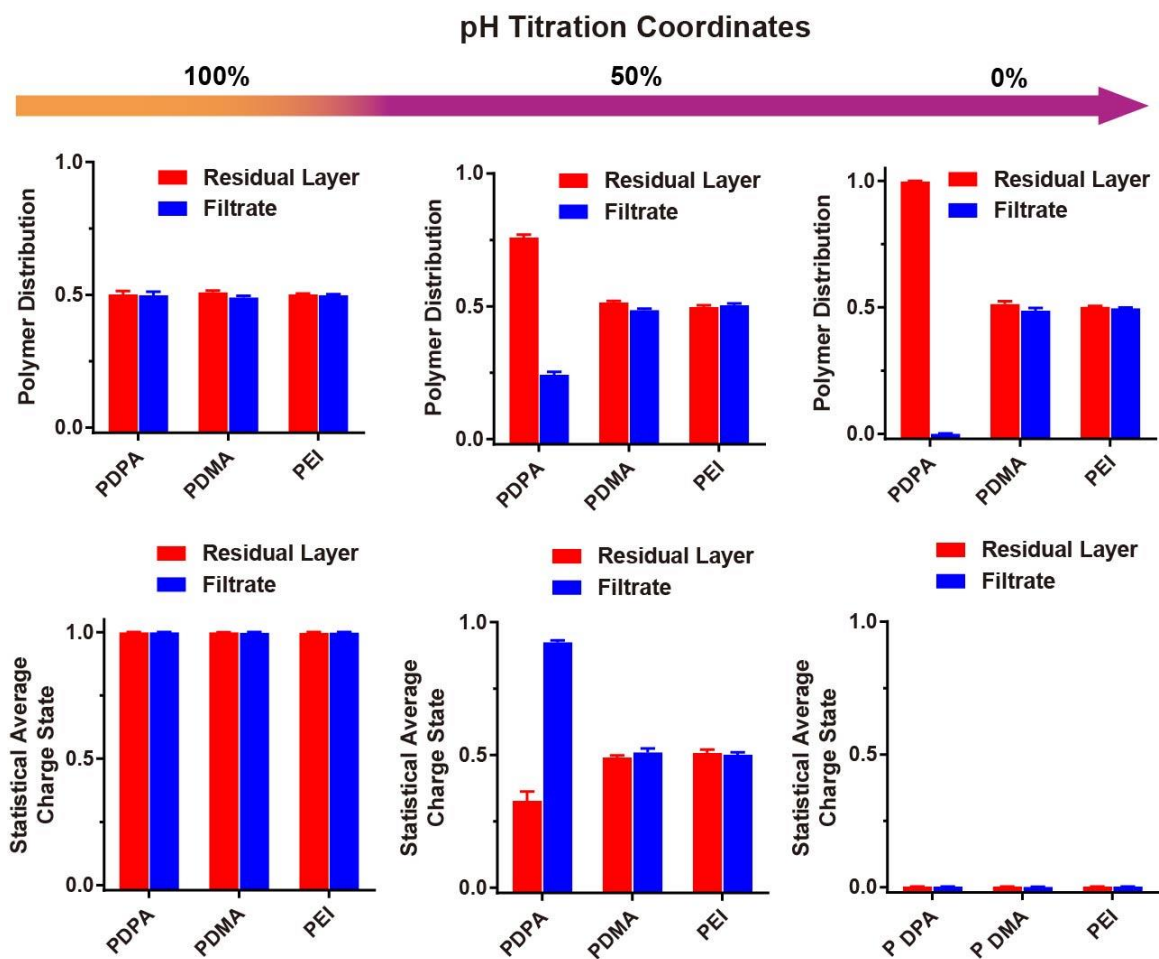
Figure 4.3.5. Polymer mass and charge state distributions in the residual and filtrate layers at three protonation degrees (0, 50 and 100%) of PEO-b-PDPA, PEO-b-PDMA and PEI.
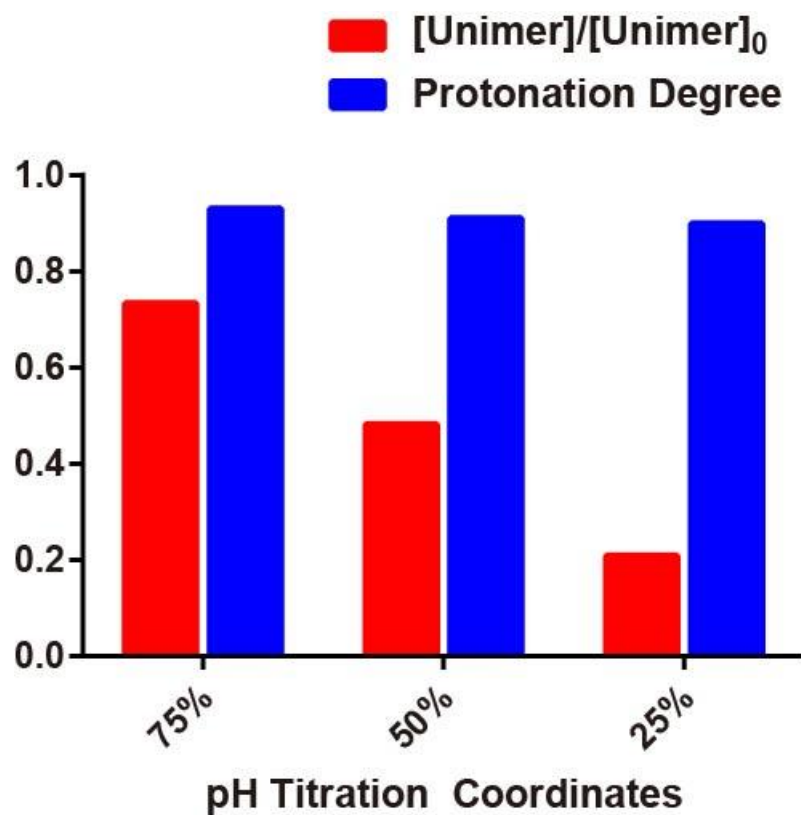
Figure 4.3.6. Unimer molar fraction ([Unimer]/[Unimer]$_0$) in the filtrate layer and their

protonation degrees at different stages of pH titration of PEO-b-PDPA.
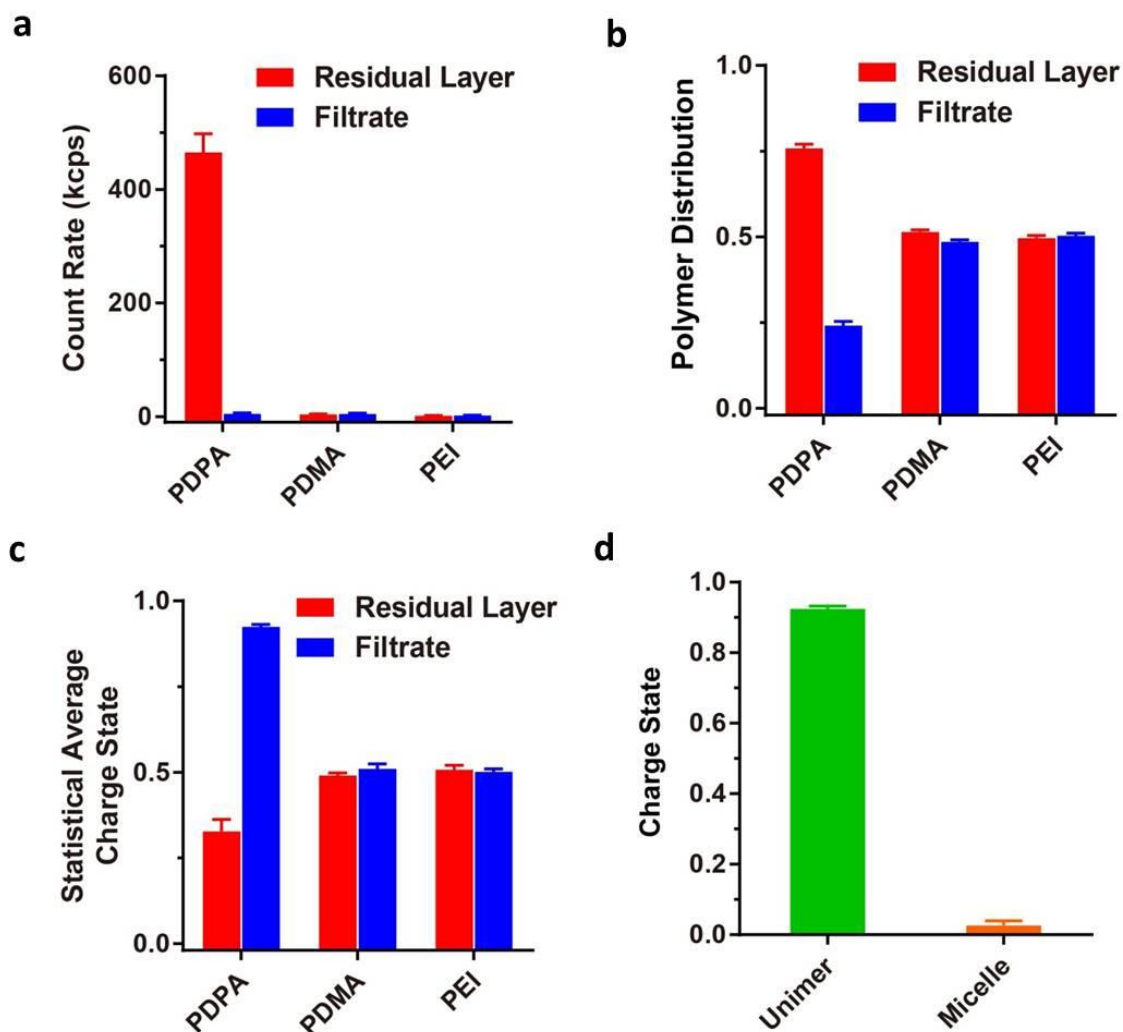
Figure 4.3.7. Divergent proton distribution between unimer and micelle state of PEO-b-PDPA copolymers. PEO-b-PDMA and PEI were used as negative controls without nanophase separation. Light scattering count rates (b), polymer mass distribution (c) and charges states of PEO-b-PDPA polymers (d) are shown at the protonation degree of 50%. e, Quantification of unimer and micelle charge states of PEO-b-PDPA at protonation degree of 50%. Protons distributed divergently where unimers were highly charged (~90%) and micelles were mostly neutral.

Neither polymer sample showed changes in size and scattering count rate along the entire titration course (**Figure 4.3.4**). Quantitative analysis showed that PEO-b-PDMA and PEI polymers distributed equally both in amounts and charge states between the residual and filtrate layers (**Figure 4.3.5**). In contrast, higher amount of PEO-b-PDPA copolymers was retained in the residual layer (**Figure 4.3.4**) due to the retention of micelles (16,000 kD, which is above the molecular weight cut-off (100 kD) of the dialysis membrane). pH titration of residual and filtrate samples showed that PEO-b-PDPA copolymers were highly charged with 90% of tertiary amines protonated in the filtrate sample whereas PEO-b-PDPA copolymers in the micelle state (after subtracting the protonated unimers) in the residual layer were almost neutral (**Figure 4.3.6**). These data suggested that the protons distributed divergently between unimers and micelles, corrresponding to the second prososed self-assembly pathway (**Figure 4.3.7**).

4.3.3-NMR validation of divergent proton distribution along pH triggered

suparmolecular self-assembly of PEO-b-PDPA block copolymers

To further investigate the divergent behavior, we employed ^{1}H NMR to study the proton distribution of PEO-*b*-PDPA along the pH titration path. PEO-*b*-PDMA was used for comparison since their terminal methyl groups were not sufficiently hydrophobic to induce micelle formation.

Upon protonation, the shielding effect from tertiary amines will decrease significantly leading to an increase of the chemical shift of adjacent methylene protons. As shown in **Figure 4.3.8**, **4.3.9** and **4.3.10**, the chemical shift of protons adjacent to

A. Dipropylaminoethanol

B. PEO-*b*-PDMA

C. PEO-*b*-PDPA

		0%	20%	40%	60%	80%	100%
Chemical Shift	a	3.70	3.74	3.78	3.81	3.85	3.89
	b	2.70	2.83	2.94	3.06	3.19	3.30
	c	2.51	2.64	2.76	2.89	3.03	3.15
Chemical Shift	a	4.16	4.20	4.24	4.29	4.34	4.40
	b	2.74	2.86	3.01	3.20	3.37	3.58
	c	2.32	2.44	2.57	2.72	2.84	3.01
Integration	a	96.76	101.74	102.94	102.47	101.90	101.03
	b	99.73	103.07	101.03	101.56	103.71	102.09
	c	325.61	325.92	324.15	323.06	324.70	325.48
Chemical Shift	a	-	4.420	4.420	4.420	4.423	4.432
	b	-	3.59	3.59	3.59	3.59	3.607
	c	-	3.22	3.22	3.22	3.22	3.24
Integration	a	-	26.21	47.31	63.69	84.70	107.66
	b	-	28.52	46.16	65.67	86.07	108.59
	c	-	55.04	102.16	137.08	181.15	228.15

Figure 4.3.8. Chemical shifts and peak integrations of different proton signals in DPA, PEO-b-PDMA and PEO-b-PDPA. All samples were prepared using deuterated D2O, DCl and NaOD. For PEO-b-PDMA and PEO-b-PDPA, peak integration was based on proton signals of interests relative to internal reference of PEO segment. The results from proton "c" was included as examples in the main text.

Figure 4.3.9. [^1]H NMR spectra of DPA at different protonation degree.
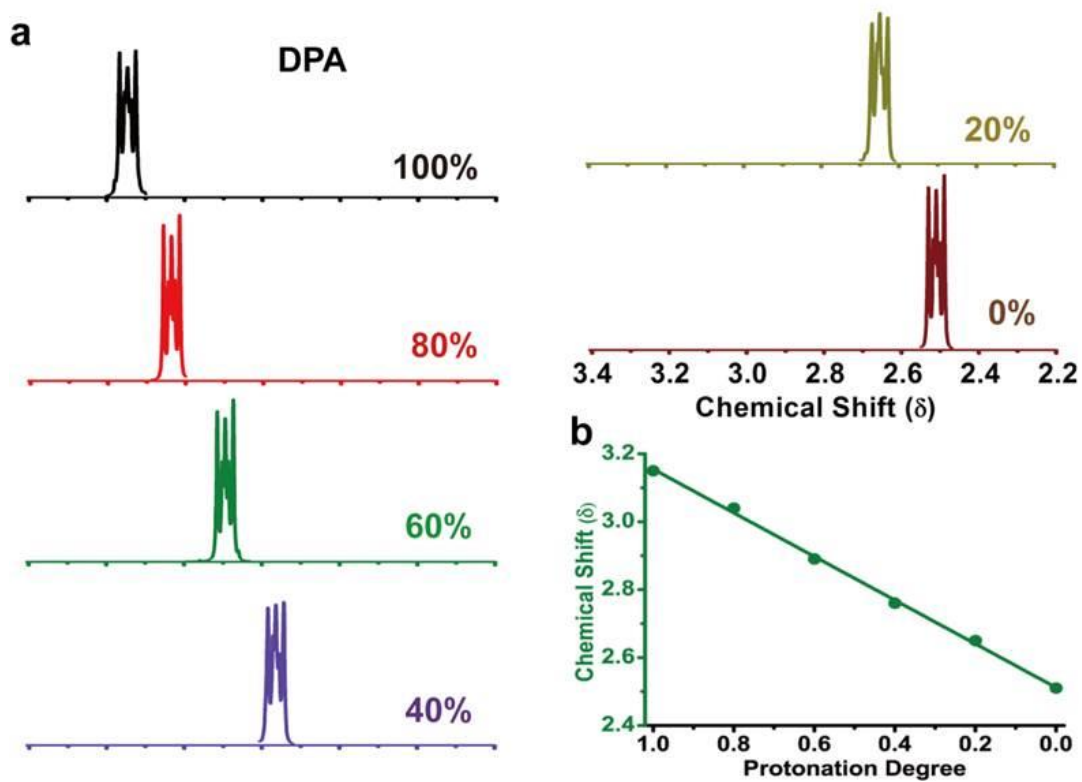
Figure 4.3.10. Chemical shift of methylene protons (c in Figure 5-3-8) of dipropylamino-ethanol (DPA) at different protonation degrees.

tertiary amines displayed remarkable chemical shift in responding to changes of protonation degree.

^{1}H NMR data revealed a striking difference between the titration behaviors of PEO-*b*-PDMA versus PEO-*b*-PDPA copolymers. The PEO-*b*-PDMA copolymer showed a continuous change of chemical shifts of methyl protons along the titration course (**Figure 4.3.11** and **4.3.12**), consistent with the gradual decrease of protonation degree of the total polymer population in solution. The peak area did not change at different degrees of protonation (**Figure 4.3.8**). In contrast, the PEO-*b*-PDPA copolymer displayed a divergent behavior along majority of the pH titration coordinate. The unimer peak did not change its chemical shift but only had decreased intensity of integration (**Figure 4.3.8**, **4.3.11** and **4.3.13** (micelle peaks were not visible due to fast T_2 relaxation). The linear decrease in integration intensity of PEO-*b*-PDPA unimers agrees with linear responses in scattering count rate and fluorescence intensity shown previously.

4.3.4-Molecular pathway of pH triggered supramolecular self-assembly of PEO-b-PDPA block copolymers

Based on these experiments, we constructed a molecular path of pH-triggered supramolecular self-assembly of PEO-*b*-PDPA copolymer (**Figure 4.3.14**). Upon addition of NaOH, the block copolymers are homogeneously deprotonated until reaching CMPD. Below CMPD, further addition of base results in formation of mature micelles where the copolymers inside micelles will lose protons. Soluble copolymers remain highly protonated at a charge state of CMPD in water. Hydrophobic phase separation contributed to the divergent proton distribution at molecular level, which was absent in
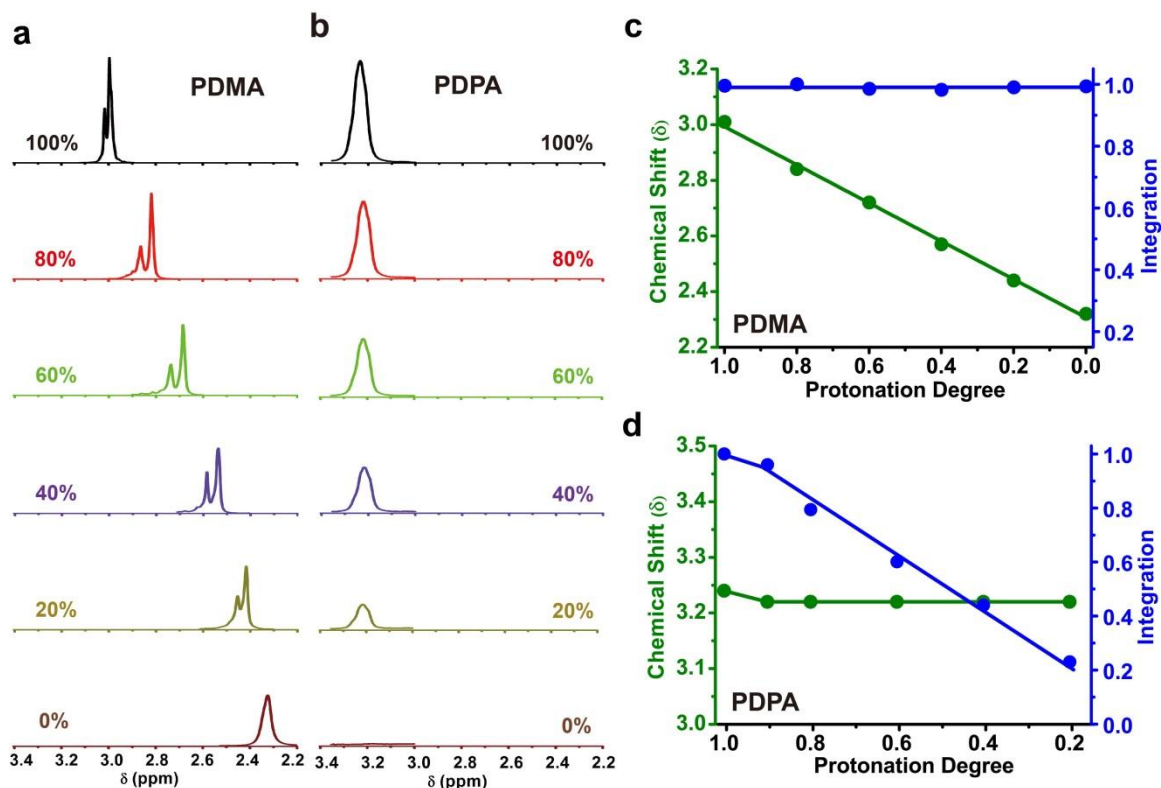
Figure 4.3.11. a-b, ^{1}H NMR spectra (in D$_2$O) of methylene protons of PEO-*b*-PDPA and methyl protons of PEO-*b*-PDMA adjacent to nitrogen atoms at different protonation degrees, respectively. PEO-*b*-PDMA was used as negative control without nanophase separation. **c-d,** Quantification of chemical shift and peak integration of chosen methylene and methyl protons in PEO-*b*-PDMA and PEO-*b*-PDPA, respectively. Integrations were calculated using polyethylene oxide (PEO) segments as internal reference.
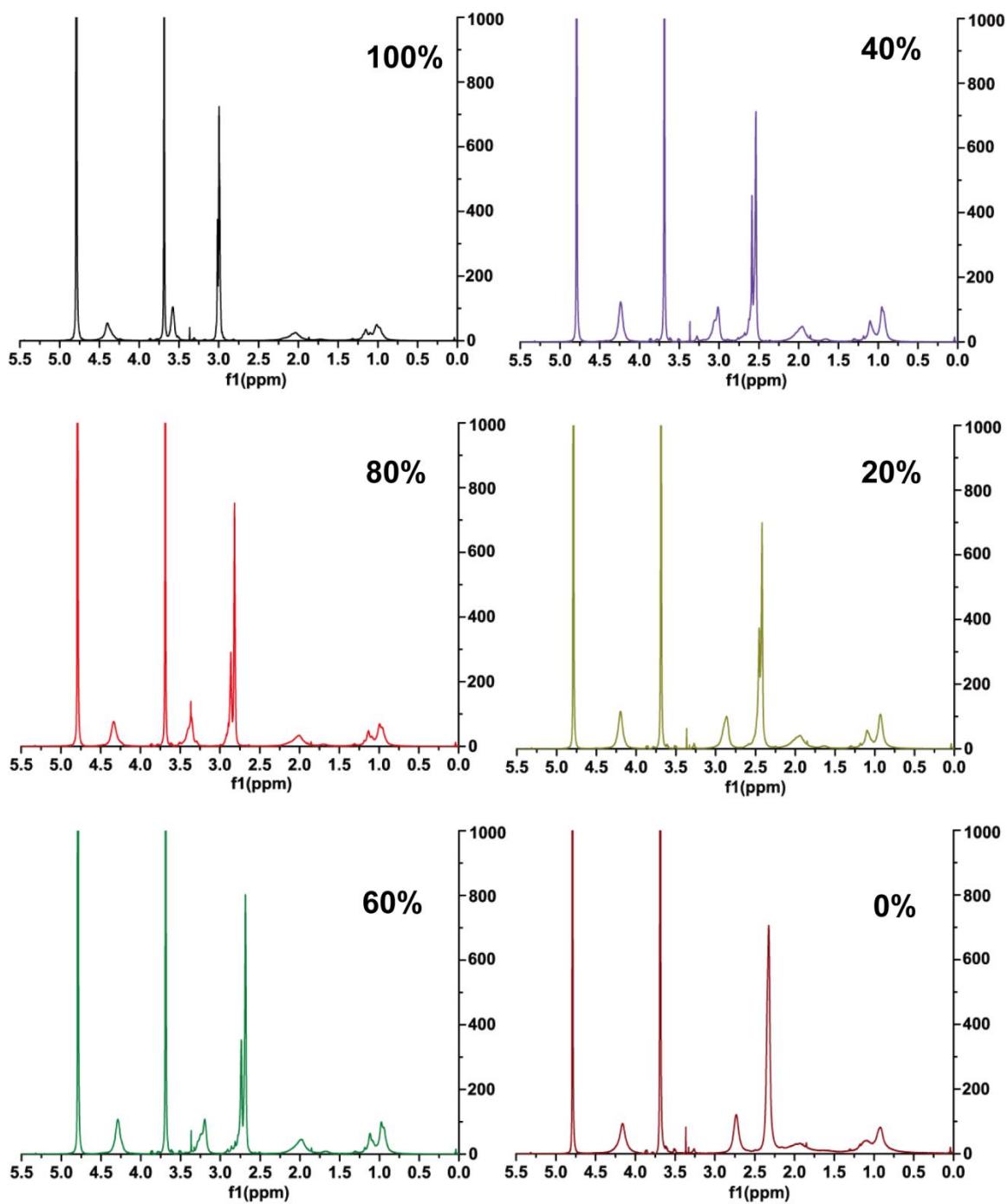
Figure 4.3.12. ^{1}H NMR spectra of PEO-PDMA at different protonation degree.
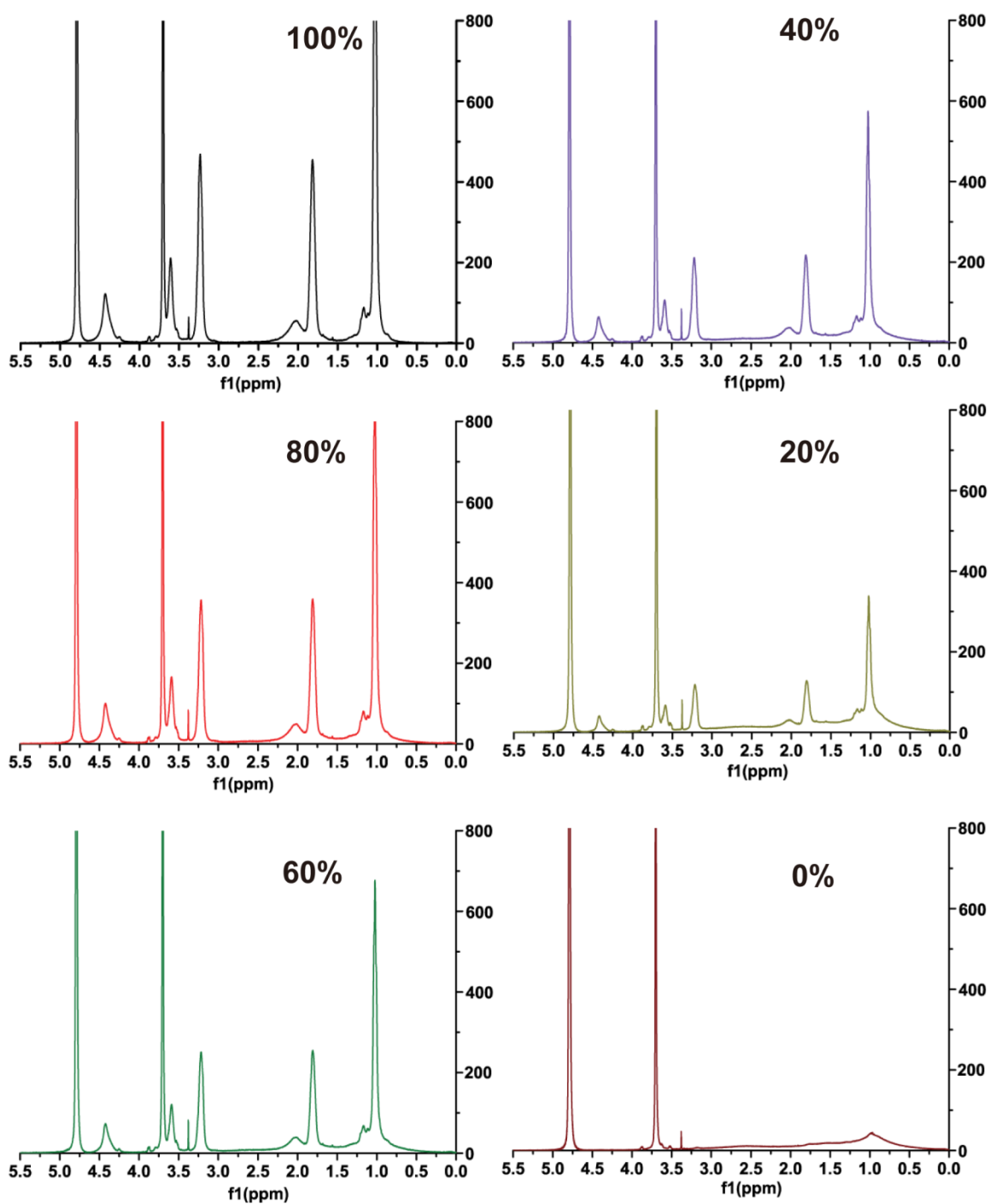
Figure 4.3.13. ^{1}H NMR spectra of PEO-b-PDPA at different protonation degree.

commonly used small molecular and polymeric pH sensors. comparable NMR spectra as well as fluorescence transition curves in either protonation or deprotonation direction (**Figure 4.3.15**).

We also confirmed the critical micelle protonation degree via similar NMR analysis. The chemical shift decreased from 3.24 to 3.22 when protonation degree decreased from 100% to 90%. With further deprotonation, the chemical shift remained unchanged. Before CMPD, the charged ammonium groups were homogeneously deprotonated, resulting in the continuous change of protonation degree of all unimers. Upon the formation of micelles below CMPD, the divergent distribution of protons result in the continuous decrease of amount of unmiers as proved by the integration decrease mentioned previously. However, the protonation degree of unimers that stayed in aqueous solution remained unchanged, leading to identical chemical shift at the protonation degree range from 90% to 0%.

4.3.5- Self-assembly and disassembly of UPS are reversible

Responsive nanomaterials are increasingly important in biomedical applications such as biosensing, molecular imaging and drug delivery. The functionalization of stimuli-responsive nanomaterials like UPS nanoprobes resides in the disassembly of nanoparticles which corresponds to the reserved process of self-assembly. Here we used different methods to characterize self-assembly and disassembly of UPS and verify their reversibility. The pH titration curves of PEO-b-PR (**Figure 4.3.16**) were almost identical indicating the same responsive behavior when exposed to the same external pH. The pH transition where fluorescence going from ON state to OFF state were very similar,
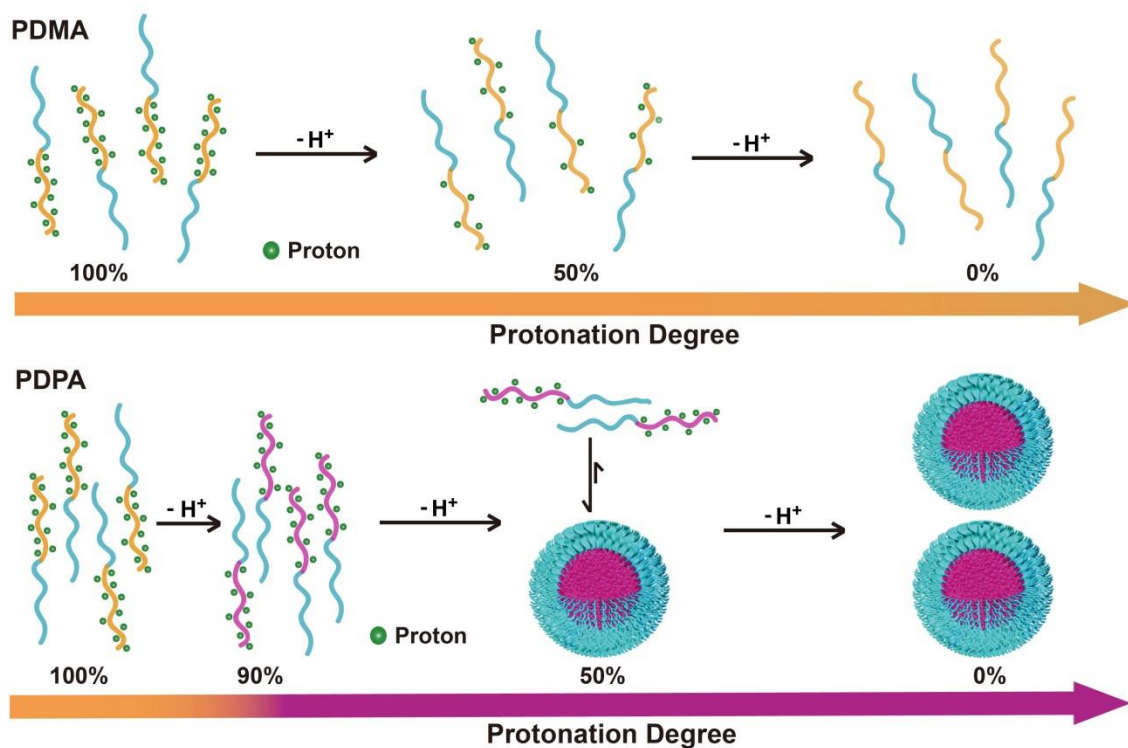
Figure 4.3.14. Schematic illustration of two distinctive deprotonation pathways. Deprotonation of PEO-*b*-PDMA ammonium groups was gradual along the entire pH titration course. Deprotonation of PEO-*b*-PDPA ammonium groups displayed a binary copolymer populations consisting of highly charged unimers in solution and neutral copolymers inside micelles.
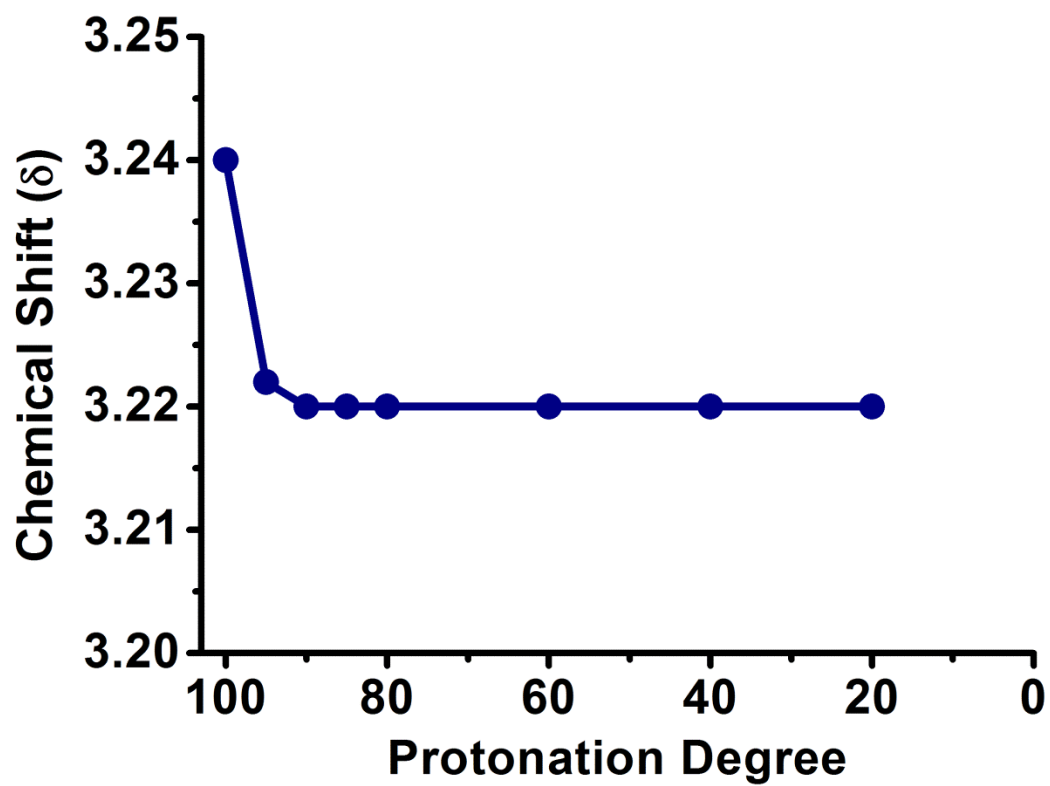
Figure 4.3.15. CMPD determination via ^{1}H-NMR analysis
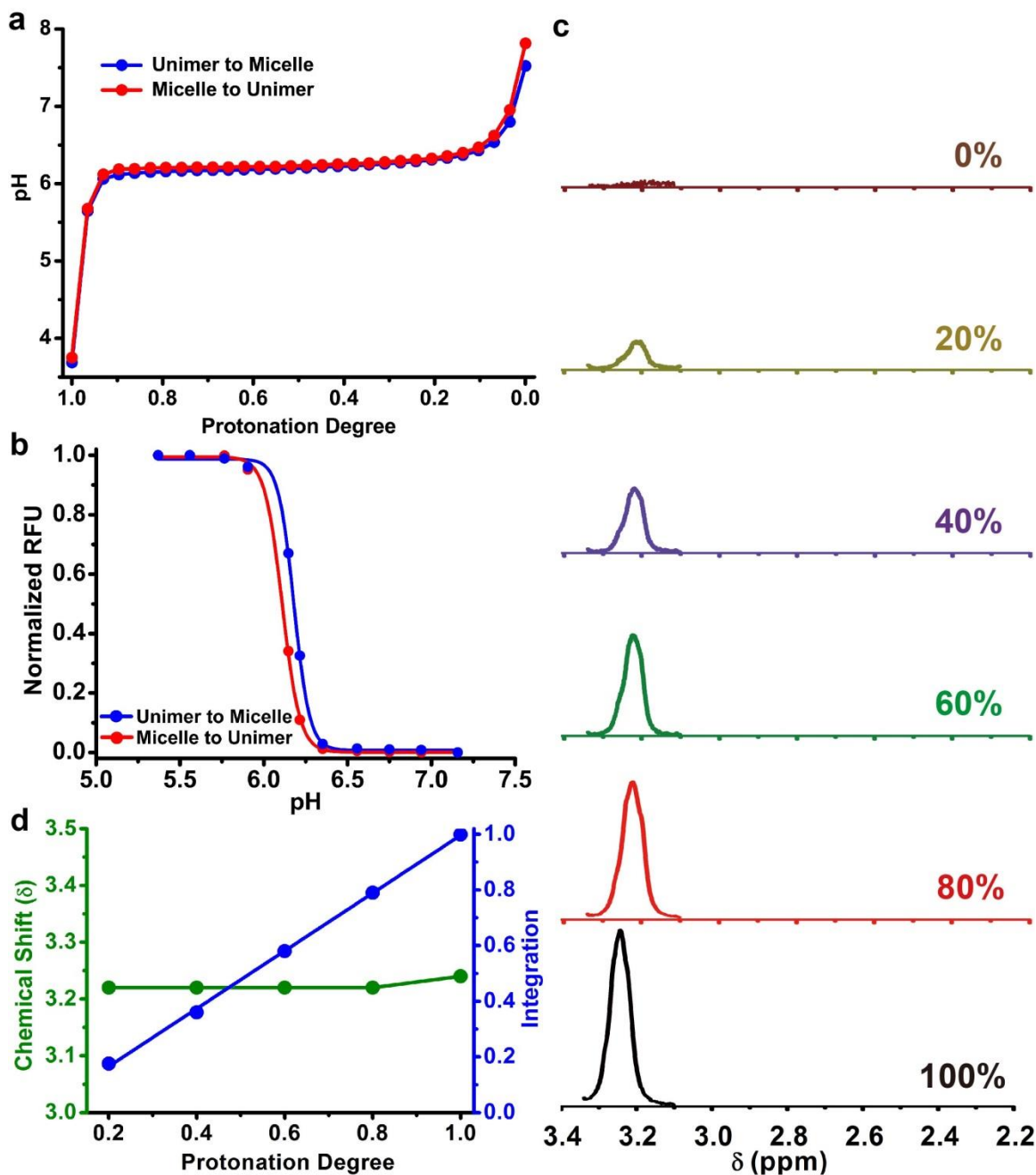
Figure 4.3.16. Microscopic reversibility of pH titration of PEO-*b*-PDPA copolymers. a, pH titration; b, fluorescence emission spectra; c-d, ^{1}H NMR spectra of micelle to unimer transitions (opposite to the titration direction as shown in Figure 5-3-11).
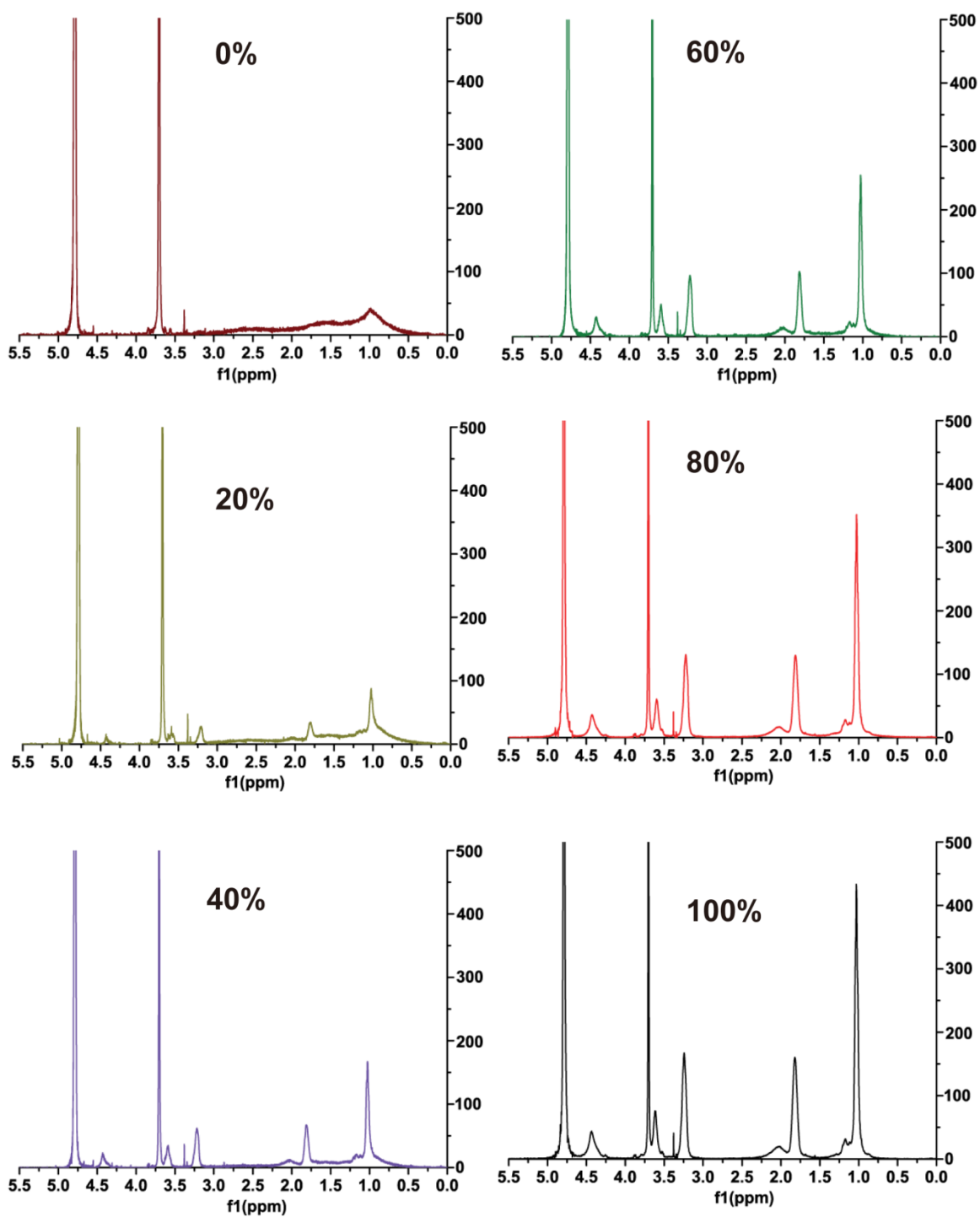
Figure 4.3.17. ^{1}H NMR spectra of PEO-b-PDPA at different protonation degree (from micelles to unimers).

suggesting the activation and deactivation of fluorophore labeled UPS were reversible. The NMR characterization confirmed the coexistence of highly protonated unimers and almost non-protonated micelles along the disassembly of nanoparticles (**Figure 4.3.17**). Further quantification of chemical shift and integration showed that the protonation degree and concentration of unimers were almost identical at the same protonation degree along the self-assembly or disassembly process (**Figure 4.3.11**). Thus the pH-triggered self-assembly and disassembly of UPS were reversible and shared the same transition state.

4.3.6-Conclusion

We investigated the mechanism of pH triggered supramolecular self-assembly using classic pH responsive block copolymers. Unimers started to form micelles at a critical protonation degree: ~90%. The protonation coordinates-resolved analysis also indicates that along the self-assembly polymers coexist in two completely divergent forms: highly protonated unimers and almost non-protonated micelles.

Molecular level illustration of the pH-triggered self-assembly process open paths to the understanding of supramolecular self-assembly mechanisms probably shared by all stimuli-responsive nanomaterials and may lead to the disclosure of underlying complex interplay of non-covalent interactions which would further provide guidelines for the design of novel and improved stimuli-responsive materials.

171

4-4 References

1   Vendruscolo, M., Zurdo, J., MacPhee, C. E. & Dobson, C. M. Protein folding and misfolding: a paradigm of self–assembly and regulation in complex biological systems. *Philosophical Transactions of the Royal Society of London A: Mathematical, Physical and Engineering Sciences* **361**, 1205-1222 (2003).

2   Branden, C. I. *Introduction to protein structure*.   (Garland Science, 1999).

3   Robson, B. & Vaithilingam, A. Protein folding revisited. *Progress in molecular biology and translational science* **84**, 161-202 (2008).

4   Sattin, B. D., Zhao, W., Travers, K., Chu, S. & Herschlag, D. Direct measurement of tertiary contact cooperativity in RNA folding. *Journal of the American Chemical Society* **130**, 6085-6087 (2008).

5   Dobson, C. M. in *Seminars in cell & developmental biology.*   3-16 (Elsevier).

6   Bryngelson, J. D., Onuchic, J. N., Socci, N. D. & Wolynes, P. G. Funnels, pathways, and the energy landscape of protein folding: a synthesis. *Proteins: Structure, Function, and Bioinformatics* **21**, 167-195 (1995).

7   Leopold, P. E., Montal, M. & Onuchic, J. N. Protein folding funnels: a kinetic approach to the sequence-structure relationship. *Proceedings of the National Academy of Sciences* **89**, 8721-8725 (1992).

8   Sharma, V., Kaila, V. R. & Annila, A. Protein folding as an evolutionary process. *Physica A: Statistical Mechanics and its Applications* **388**, 851-862 (2009).

9   Compiani, M. & Capriotti, E. Computational and theoretical methods for protein folding. *Biochemistry* **52**, 8601-8624 (2013).

10   Dobson, C. M., Šali, A. & Karplus, M. Protein folding: a perspective from theory and experiment. *Angewandte Chemie International Edition* **37**, 868-893 (1998).

11   Dinner, A. R., Šali, A., Smith, L. J., Dobson, C. M. & Karplus, M. Understanding protein folding via free-energy surfaces from theory and experiment. *Trends in biochemical sciences* **25**, 331-339 (2000).

12   Dobson, C. M. Protein folding and misfolding. *Nature* **426**, 884-890 (2003).

13   Vendruscolo, M., Paci, E., Dobson, C. M. & Karplus, M. Three key residues form a critical contact network in a protein folding transition state. *Nature* **409**, 641-645 (2001).

14   Chan, H. S. & Dill, K. A. Protein folding in the landscape perspective: Chevron plots and non- Arrhenius kinetics. *Proteins: Structure, Function, and Bioinformatics* **30**, 2-33 (1998).

15   Wolynes, P. G., Onuchic, J. N. & Thirumalai, D. Navigating the folding routes. *SCIENCE-NEW YORK THEN WASHINGTON-*, 1619-1619 (1995).

16   Buchmueller, K. L., Webb, A. E., Richardson, D. A. & Weeks, K. M. A collapsed non-native RNA folding state. *Nature Structural & Molecular Biology* **7**, 362-366 (2000).

17   Sclavi, B., Sullivan, M., Chance, M. R., Brenowitz, M. & Woodson, S. A. RNA folding at millisecond intervals by synchrotron hydroxyl radical footprinting. *Science* **279**, 1940-1943 (1998).

18   Treiber, D. K. & Williamson, J. R. Exposing the kinetic traps in RNA folding. *Current opinion in structural biology* **9**, 339-345 (1999).

19   Woodson, S. A. Compact but disordered states of RNA. *Nature Structural & Molecular Biology* **7**, 349-352 (2000).

20   Thirumalai, D. & Woodson, S. Kinetics of folding of proteins and RNA. *Accounts of chemical research* **29**, 433-439 (1996).

21   Russell, R. & Herschlag, D. Probing the folding landscape of the Tetrahymena ribozyme: commitment to form the native conformation is late in the folding pathway. *Journal of molecular biology* **308**, 839-851 (2001).

22   Sosnick, T. R. Kinetic barriers and the role of topology in protein and RNA folding. *Protein Science* **17**, 1308-1318 (2008).

23   Doudna, J. A. & Doherty, E. A. Emerging themes in RNA folding. *Folding and Design* **2**, R65-R70 (1997).

24   van den Berg, B., Wain, R., Dobson, C. M. & Ellis, R. J. Macromolecular crowding perturbs protein refolding kinetics: implications for folding inside the cell. *The EMBO journal* **19**, 3870-3875 (2000).

25   Cui, H., Chen, Z., Zhong, S., Wooley, K. L. & Pochan, D. J. Block copolymer assembly via kinetic control. *Science* **317**, 647-650 (2007).

26   Korevaar, P. A. *et al.* Pathway complexity in supramolecular polymerization. *Nature* **481**, 492-496 (2012).

27   Whitesides, G. M., Mathias, J. P. & Seto, C. T. Molecular self-assembly and nanochemistry: a chemical strategy for the synthesis of nanostructures. (DTIC Document, 1991).

28   Whitesides, G. M. & Grzybowski, B. Self-assembly at all scales. *Science* **295**, 2418-2421 (2002).

29   Lehn, J. M. Supramolecular chemistry—scope and perspectives molecules, supermolecules, and molecular devices (Nobel Lecture). *Angewandte Chemie International Edition in English* **27**, 89-112 (1988).

30   De Greef, T. F. *et al.* Supramolecular polymerization. *Chemical Reviews* **109**, 5687-5754 (2009).

31   Zhou, K. *et al.* Multicolored pH-tunable and activatable fluorescence nanoplatform responsive to physiologic pH stimuli. *Journal of the American Chemical Society* **134**, 7803-7811 (2012).

32   Wang, Y. *et al.* A nanoparticle-based strategy for the imaging of a broad range of tumours by nonlinear amplification of microenvironment signals. *Nature materials* **13**, 204-212 (2014).

33   Zhou, K. *et al.* Tunable, Ultrasensitive pH- Responsive Nanoparticles Targeting Specific Endocytic Organelles in Living Cells. *Angewandte Chemie* **123**, 6233-6238 (2011).

CHAPTER FIVE-Supramolecular Self-assembly Results in Strong Cooperativity

5.1-Introduction

Polymeric material-based nanoscale assemblies have received considerable attentions in a variety of biomedical applications such as biological sensing, drug delivery, tissue engineering and molecular imaging[1,2]. These efforts have been driven to a large extent by the unmet need to improve the specificity in diagnosis and therapy via precise spatiotemporal control in delivery of therapeutics. Continuous efforts have been dedicated to tailor the three-dimensional architecture of these polymeric assemblies, aiming to augment their function and performance. To achieve these goals, in one way, novel polymeric building blocks are designed to alter the composition, morphology, and surface chemistry. New polymerization and formulation methods have also been developed to control the size, shape and architecture of assembled nanostructures. Capitalizing on the self-organization of polymeric building blocks, many groups including us have been working on the development of assembled nanostructures to address the intrinsic deficiencies of monomolecular materials such as low sensitivity and selectivity and lack of specific targeting and accumulation in disease area.

These nanoscale structures were assembled from individual building block via a multitude of non-covalent interactions, the same as those in the supramolecular assembly of protein and nucleic acids. The packing of preceding building block may more or less affect the assembly of ensuing building blocks that was usually nonexistent in small molecules. Moreover, the subtle interplay of these non-covalent interactions during the self-assembly process also contributes to the cooperativity absent in monomolecular materials. The cooperativity gives rise to unique and superior physical and chemical

properties in multiple nanosystems over a broad range of biomedical applications. In this section, we will discuss the cooperativity in several well-established self-assembled nanoplatform and why cooperativity is critical for their performance and biomedical application.

Advances in genomics, proteomics and bioinformatics have facilitated the development of new therapeutic biomaterials with increased potency and decreased side effects. The aim of nanomedicine has always been to maximize the therapeutic efficacy while minimizing the potential side effects such as toxicity. One distinctive characteristics of polymeric materials is the intrinsic cooperativity arising from the intramolecular or intermolecular interactions, which may serve as another unique but powerful strategy to address the deficiencies and limitation of small molecular therapeutics.

With each passing year, we are able to expand the scope of synthetic chemistry for the development of new nanomaterials for biomedical applications. On the other hand, researchers from pharmacology radiology and oncology have been working on exploring the therapeutic potential of these materials in both academic studies and in clinical trials. Despite the great promise in public health and personal medicine, there still exists several big gaps that impedes moving the nanomaterials from bench work to industrial applications. One is the lack of the mechanistic understanding and experimental control of the reversible supramolecular self-assembly process, where molecular building blocks spontaneously self-organize into nano-scaled structures. The physiochemical properties and self-assembly of polymeric materials have inspired the development of a multitude of formulation methods, aiming to improve the drug loading efficacy, biodistribution and

minimize the off-target effect of administered therapeutic nanoparticles[3]. The lack of control and prediction of in vivo behaviors of nanomedicines also required fundamental understanding of how the self-assembled nanostructures respond to the host-environment like tumor on the molecular level.

It is of critical importance to establish the logic of design of self-assembled nanomedicine. One powerful approach is the construction of mathematical models. The modeling can help rationalize the structure-property correlations and provide guidelines for the optimization of key design parameters. In this study, we will assess the cooperativity in pH-triggered supramolecular self-assembly of UPS block copolymers. An allosteric model is constructed to validate the strong H cooperativity and help evaluate key design parameters that affect the pKa and H transition sharpness of UPS block copolymers.

5.2-Materials and methods

5.2.1-*Synthesis and characterization of PEO-b-PR block copolymers with different terminal alkyl groups*

PEO-b-PR copolymers were synthesized by atom transfer radical polymerization (ATRP) following similar procedures. The dye free copolymers were used in polymer characterizations. PEO-b-PDPA is used as an example to illustrate the procedure. First, DPA-MA (1.70 g, 8 mmol), PMDETA (21 μL, 0.1 mmol) and MeO-PEO114-Br (0.5 g, 0.1 mmol) were charged into a polymerization tube. Then a mixture of 2-propanol (2 mL) and DMF (2 mL) was added to dissolve the monomer and initiator. After three cycles of freeze-pump-thaw to remove the oxygen, CuBr (14 mg, 0.1 mmol) was added into the

polymerization tube under nitrogen atmosphere, and the tube was sealed in vacuo. The polymerization was carried out at 40 °C for 8 hours. After polymerization, the reaction mixture was diluted with 10 mL THF, and passed through a neutral Al2O3 column to remove the catalyst. The THF solvent was removed by rotovap. The residue was dialyzed in distilled water and lyophilized to obtain a white powder.

5.2.2-Synthesis and characterization of PEO-b-PDPA block copolymers with different hydrophobic chain length

PEO-b-nPDPA copolymers were synthesized by atom transfer radical polymerization (ATRP) following similar procedures. The dye free copolymers were used in polymer characterizations. Different initiator and monomers ratios were applied to control the hydrophobic chain length. A series of PEO-b-PDPAx (with x = 5, 10, 20, 60,100) were prepared and used for the assessment of pH cooperativity. GPC was used to measure the molecular weight and polydispersity. ^{1}H-NMR was used to quantify the hydrophobic chain length with poly(ethylene glycol) (PEG) as internal standard.

5.2.3-Quantification of different types of cooperativity

Recently, Hunter and Anderson delineated different kinds of cooperative behaviors and scenarios in multicomponent complexes (**Figure 6.2.1**)[4]. The discrete allosteric model is best understood, where binding a ligand to a multi-site receptor will affect the binding affinity of next ligand via change of shape or conformation. Allosteric enzymes change shape between active and inactive shapes upon the binding of substrates at the active site, and of regulatory molecules at other sites. The second type is the

nucleation-growth of polydisperse oligomers. Such cooperative oligomerization is found in the self-assembly of amyloid peptides[5], actin strands[6] and some polymers[7]. Similar to discrete allosteric scenario, the cooperativity arises from that the initial binding will make the later binding more favorable. The third type of cooperativity occurs in the self-assembly of closed systems such as folding of proteins or formation of DNA duplex. This system exhibits a different kind of cooperativity form first two. The cooperative assembly results from the difference between the intermolecular and intramolecular interactions. Such molecular architecture-driven cooperativity is also known as chelate cooperativity[8]. The fourth type of cooperativity is found in processes where ligands break up a supramolecular assembly. One such example is the unfolding of proteins as induced by the addition of guanidine hydrochloride. Whitesides et al have reported extensive studies on the cooperativity formation of supramolecular ladders via denaturation[9-11].

5.2.4-Quantification of cooperativity in allosteric binding systems

To determine whether a protein-ligand process exhibits no cooperativity, positive cooperativity, or negative cooperativity, we usually perform an experiment to measure the binding of the ligand to the protein at various concentrations of ligand. Define θ_A as the total fraction of a protein binding sites that are occupied by the ligands. For a process with no cooperativity, it takes around 100-fold change in ligand concentration when the site-occupancy increases from 10% to 90%. If a system displays positive cooperativity, it takes smaller change in concentration for the occupation percentage increases from 10% to 90% due the increased binding affinity. For allosteric systems like protein-ligand binding, there is more quantitative method to determine the cooperativity by plotting the binging profile on a Hill plot[12]. In practice, the Hill plot is obtained by plotting $\log(\theta_A$

180
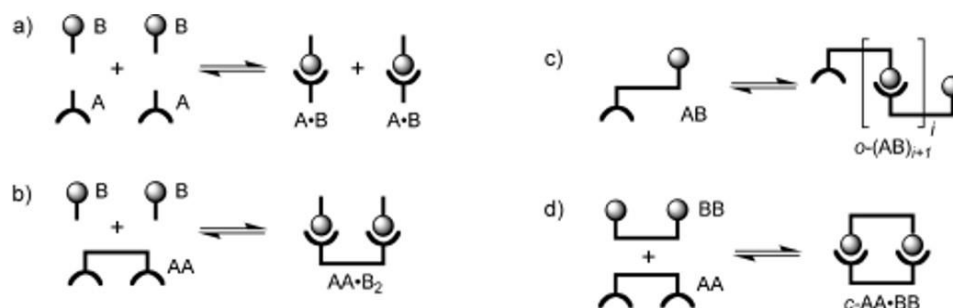
Figure 5.2.1. Cooperativity in different complexation equilibria. (a) the reference system. (b). Discrete allosteric system. (c) Poly-disperse oligomerization (d) self-assembled system[4].

$/(1- \theta_A))$ versus logarithmic concentration of ligands. The Hill coefficient nH, corresponding to the slope of this plot measured at 50% saturation, is used to quantify the cooperativity strength experimentally. A Hill coefficient of one indicates no cooperativity, a Hill coefficient of greater than one indicates positive cooperativity and a Hill coefficient of less than one indicates negative cooperativity.

5.3-Results and discussions

5.3.1- Development of the cooperative deprotonation model

We adopted an allosteric model[13] to describe the cooperative deprotonation process. The sequential neutralization of fully protonated polymers can be characterized by a series of microscopic Ki, which corresponds to the ith dissociation constant of the polyatomic acids.

$$H_{n-i+1}A \overset{K_i}{\rightleftharpoons} H_{n-i}A + H^+ \qquad \text{S1}$$

Cooperative parameters

In the simplest case of dibasic acid (n=2), the neutralization of protons can be characterized by two microscopic dissociation constant K_1 and K_2 as defined by Equation S2 and S3, where 2 and ½ are statistical factors[14].

$$2K_1 = \frac{[HA^-][H^+]}{[H_2A]} \qquad \text{S2}$$

$$1/2K_2 = \frac{[A^{2-}][H^+]}{[HA^-]} \qquad \text{S3}$$

At molecular level, the cooperativity of dibasic acid dissociation process can be described by the interaction parameter α, which is defined as[15]:

$$\alpha = K_2 / K_1 \qquad \text{S4}$$

182

For the dissociation of polyatomic acid as in our system, a series of cooperative parameters α are defined by Equation 4 as shown in the main text. The apparent dissociation constant K is defined as geometric mean of individual dissociation constants[16] (Equation 5).

$$K = \sqrt[n]{K_1 K_2 \ldots K_n} \qquad\qquad \textbf{S5}$$

Assuming identical cooperative parameter α for each dissociation step (Equation S6), Equation S5 can be simplified as Equation 7. This equation allows the theoretical-experimental correlation between the microscopic cooperative parameter α and macroscopically measurable pKa (logarithmic K). The theoretical modeling suggests that cooperative dissociation of fully protonated PEO-*b*-PR with more ammonium groups per polymer chain will have higher K (or Ka) and lower pKa.

$$\alpha = \alpha_1 = \alpha_2 = \cdots\cdots = \alpha_{n-1} \qquad\qquad \textbf{S6}$$

$$K = \sqrt{\alpha^{n-1}}\, K_1 \qquad\qquad \textbf{S7}$$

Hill Coefficient. Practically, Hill plot is used to evaluate the allosteric cooperativity. First, the sequential neutralization of fully protonated UPS nanoprobes are described in dissociation isotherms. Here we use (pH - pKa) as the x-axis and protonation degree (θ_A) as the y-axis to plot the dissociation isotherms. In this case, the point at which 50% of tertiary amines are protonated occurs at 0 on the x-axis according to Henderson-Hasselbalch Equation[17]:

$$pH - pKa = \log \frac{[A^-]}{[HA]} \qquad\qquad \textbf{S8}$$

Increase of pH leads to dissociation of protons, corresponding to the decreased θ_A.

For classic allosteric binding of monovalent ligand B to multi-site receptors A….A , the dependence of the binding site occupancy θ_A can be generalized as[4]:

$$\theta_A = \frac{(K[B])^n}{1+ (K[B])^n} \qquad\qquad \text{S9}$$

Hill plot is based on a rearranged version of this equation to characterize the strength of cooperative binding interactions by ploting $\log(\theta_A /(1- \theta_A))$ versus logarithmic ligand concentration $\text{Log}[B]$[4]:

$$\text{Log}\left(\frac{\theta_A}{1 - \theta_A}\right) \approx n \, \text{Log}(K'[B]) \qquad\qquad \text{S10}$$

The deprotonation is opposite process of protons binding to tertiary amines, which means the $K=1/K'$. So the cooperativity in allosteric deprotonation of fully charged PEO-*b*-PR copolymers can be quantified by plotting $\log(\theta_A /(1- \theta_A))$ versus $(pKa-pH)$ in a Hill plot:

$$\text{Log}\left(\frac{\theta_A}{1 - \theta_A}\right) \approx n(pKa - pH) \qquad\qquad \text{S11}$$

The Hill coefficient n_H, corresponding to the slope of this plot measured at 50% saturation, is a useful parameter to quantify the cooperativity strength. The allosteric systems with positive cooperativity have the number of binding sites n as the limit of n_H. In the absence of cooperativity, the n_H is equal to 1. Positive cooperaitvity gives a slope larger than 1 (n_H >1), which corresponds to narrower ligand concentration range nacessary for receptors to go from bound free state to fully occupied state. The Hill plot modeling suggests that polyatomic acids with more ammonium groups per polymer chain will have higher n_H and sharper pH transition.

5.3.2-Comparison of pH-cooperaitivty in different pH sensors

We adopted an allosteric model to measure the cooperative strength of deprotonation (**Figure 5.3.1**)[18]. The neutralization of fully protonated unimers can be characterized by a series of microscopic K_i, which corresponds to the ith dissociation constant of polyatomic acids. The antagonistic or synergistic effect during deprotonation is described by the cooperative parameter α_i, which is defined as K_{i+1}/K_i (**Equation (4)**). The apparent dissociation constant K for the entire deprotonation process is defined by **Equation (5)**. Assuming identical cooperative parameter α for each ionization step, K can be simplified as **Equation (7)**. This equation allows a simplified theoretical-experimental correlation between the microscopic cooperative parameter α with macroscopically measurable pKa. In practice, the Hill plot is used to evaluate the cooperativity of ligand binding. Protonation degree (θ_A, **Equation (9)**) is used to describe the extent of protonation of tertiary amines[4]. The cooperativity in allosteric deprotonation process can be quantified by plotting $\log(\theta_A/(1-\theta_A))$ versus (pKa - pH) (**Equation (10)**). The Hill coefficient n_H, which corresponds to the slope of this plot measured at 50% saturation, is used to describe the cooperativity strength.

Quantitative analysis revealed that small molecular base DPA had a typical non-cooperative behavior with a Hill coefficient close to 1 (**Figure 5.3.2**). In contrast, PEO-*b*-PDPA with 100 repeating units of ammonium groups per polymer chain displayed exceptionally strong positive cooperativity with $n_H = 51$, compared to 2.3-3.0 for oxygen binding to hemoglobin[19]. Cooperative deprotonation of multiple ammonium groups per polymer chain can dramatically increase the acidification constant as shown in **Equation (3)**. The pKa value indeed decreased from 10.1 for monovalent DPA
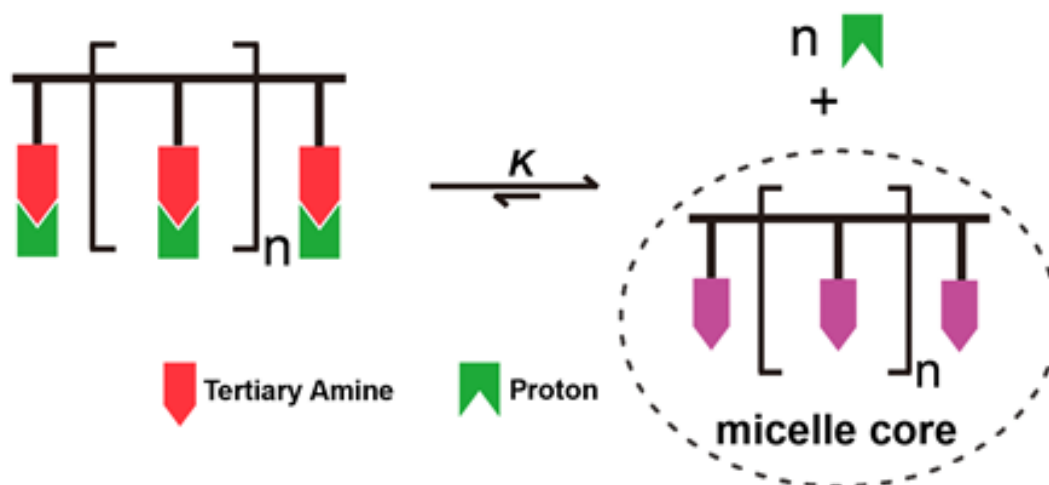
Figure 5.3.1. Allosteric modeling of cooperativity in pH-triggered supramolecular self-assembly of UPS block copolymers.
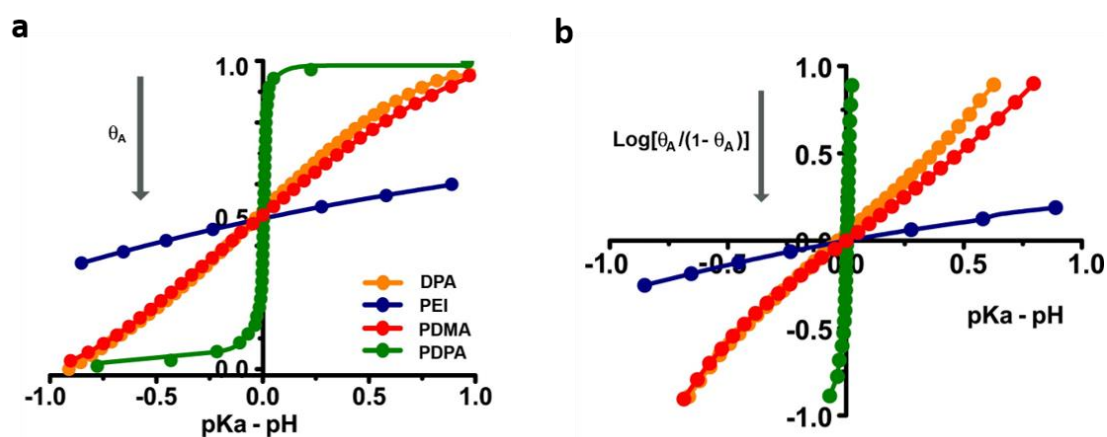
Figure 5.3.2. a-b, Cooperativity analysis based on Hill plot of small molecular base DPA, polymeric bases of PEI, PEO-b-PDMA and PEO-b-PDPA. DPA and PEO-b-PDMA showed non-pH cooperativity. PEI displayed negative pH cooperativity and PEO-b-PDPA showed strong positive cooperativity.

ammonium group to an apparent 6.2 for PEO-*b*-PDPA with 100 ammonium groups per polymer chain - almost 4 order of magnitude increases for the Ka constant. Comparison of PEO-*b*-PDMA copolymer with similar repeating units (~100) showed a Hill coefficient close to 1, indicating non-pH cooperativity. PEI was found to have strong negative cooperativity with Hill coefficient close to 0.2, which is consistent with previously reported neighboring exclusion effect during protonation of PEI[20].

5.3.3-Comparison of pH-cooperaitivty in different hydrophobic chain length

Next, we investigated the influence of polymer chain length on pH cooperativity (**Figure 5.3.3**). We found that increasing the number of repeating units in the hydrophobic PR segment significantly sharpened the pH response and increased n_H (**Figure 5.3.4**). In addition, pKa values of PEO-*b*-PDPA copolymers decreased from 6.66 to 6.26 with the number of repeating unit increased from 5 to 100 (**Figure 5.3.5**). Increase of positive cooperativity by hydrophobic chain length may provide an additional strategy in fine tuning pKa and sharpness of pH response, which will help improve the performance of pH sensors.

Copolymer	$M_{w,GPC}$ $(\times 10^{-4} D)^a$	$M_{n,GPC}$ $(\times 10^{-4} D)^a$	PDI^a	Repeating units In the PR block	$M_{n,1H\,NMR}$ $(\times 10^{-4} D)^b$
PEO-*b*-nPDPA$_5$	0.87	0.66	1.32	6	0.63
PEO-*b*-nPDPA$_{10}$	1.07	0.83	1.29	10	0.72
PEO-*b*-nPDPA$_{20}$	1.32	1.09	1.22	22	0.98
PEO-*b*-nPDBA$_{60}$	2.29	2.01	1.14	64	1.86
PEO-*b*-nPDPA$_{100}$	3.33	2.71	1.23	98	2.59

[a] Number-average (Mn), weight-average molecular weight (Mw) and polydispersity index (PDI) (PDI=Mw/Mn) were determined by GPC using THF as the eluent. [b] Determined by ^{1}H-NMR.

Figure 5.3.3. Characterization of PEO-b-PDPA block copolymers with different hydrophobic chain length.
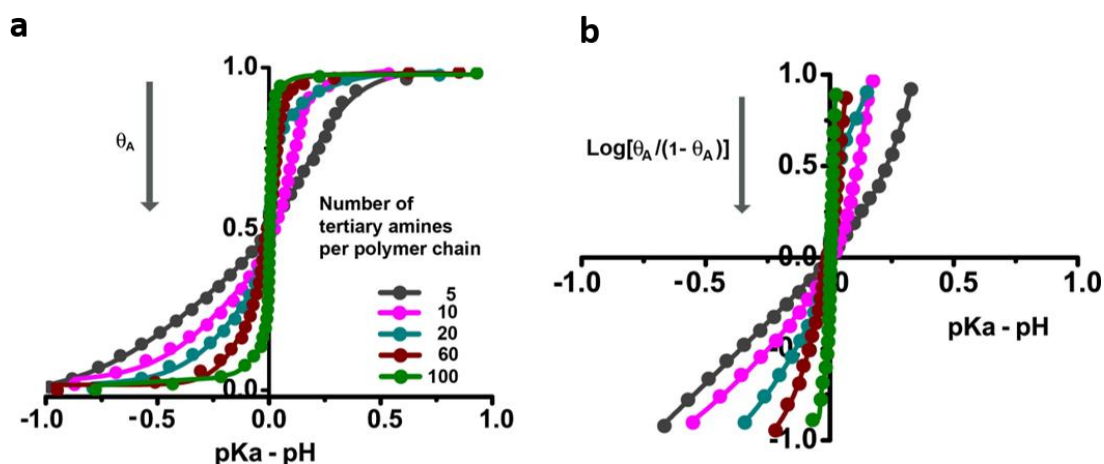
Figure 5.3.4. a-b, Cooperativity analysis of PEO-b-PDPA copolymers with different number of repeating units in the hydrophobic segment. Increase of hydrophobic chain length led to stronger positive cooperativity and sharper pH response.
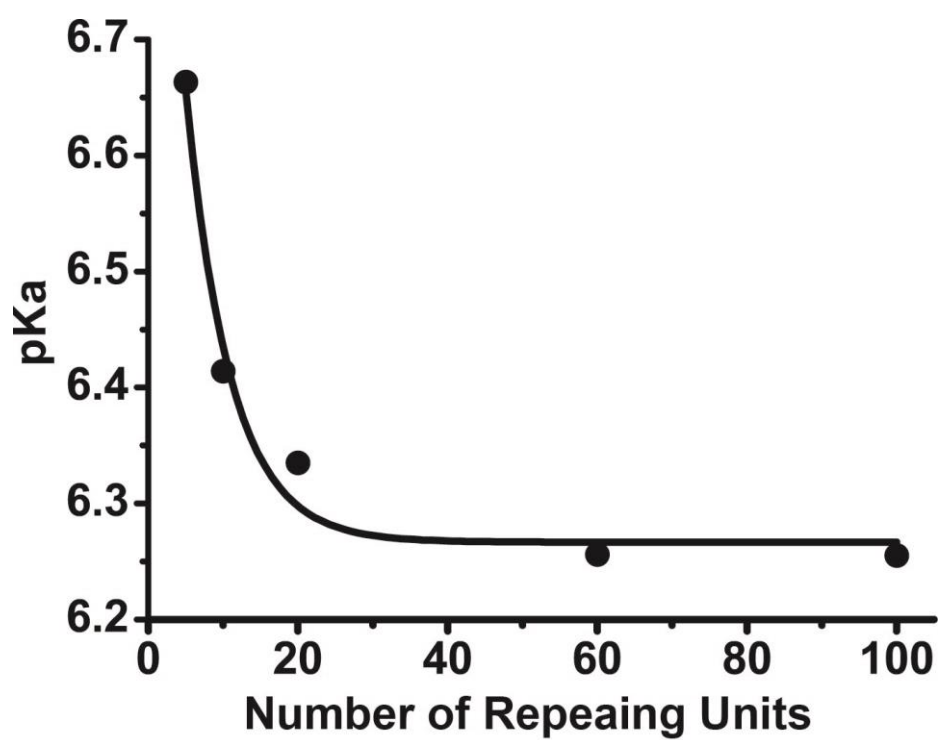
Figure 5.3.5. pKa of PEO-b-PDPA copolymers decreases with increasing polymer chain length. Longer hydrophobic chain length leads to lower pKa.

5.3.4-pH cooperativity results from hydrophobic phase separation

For pH sensors, there are two key parameters, the pKa and the pH transition sharpness. Here I compared our UPS nanoparticles with a commonly used small molecular pH sensor. Lysosensor Green shows 150-fold change in fluorescence intensity over 2 pH unit, that's broad pH response. One of our UPS nanoparticles with similar pKa shows more than 100-fold change in fluorescence intensity over 0.2 pH unit. So basically, the small molecular H sensors can only provide grey scale differentiation. However, our UPS nanoparticles show binary fluorescent on/off switch. The sharp pH transition of UPS nanoparticles is very unique and we want to know why. I also investigate several commonly used polymer pH sensors. They all show broad pH response like the small molecular pH sensors.

Figure 5.3.6 showed the pH responsive behavior of two polymers. The PEO-b-PDMA is water soluble and shows broad pH response like small molecular pH sensors. But the PEO-b-PDPA shows very sharp pH transition. These two polymers have the same backbone. The only difference is that the PDPA is slightly hydrophobic and can form micelles at high pH. These results provides direct evidence that the hydrophobic phase separation lead to the observed sharp pH transition of UPS block copolymers.

5.3.5-Molecular insights of the hydrophobic phase separation-driven ultra-pH sensitivity

Figure 5.3.7 and **Figure 5.3.8** provided the molecular description of the protonation process of commonly used small molecular and polymeric pH sensors. For water soluble pH sensors, the protonation display no cooperativity. Along the entire

190

protonation process, the pH sensors were solubilized in water. Although there might be proton exchange or chain conformation changes, protonation of previous amines will not change the proton binding affinity of remaining amines. These sensors exhibit broad pH response over 2.0 pH units as predicted by henderson hasselbalch equation. Their pKa will shift a little bit, depending on the substituents.

Figure 5.3.9 showed the origin of strong pH cooperativity of UPS nanoparticles. Initially, the micelles create a hydrophobic core where protons are unfavorable. It's like they build a hydrophobic barrier to prevent the protons from getting in. Protons will not be able to break through the hydrophobic barrier until a critical threshold, a critical proton concentration or pH value. After the hydrophobic barrier is broken, the hydrophobic chain is exposed to the aqueous solution and protons. This is unfavorable and results in huge energy penalty. The only way to minimize the energy penalty is to protonate the tertiary amines and to make the polymers soluble in water. Once the tertiary amines are protonated, the hydrophobic micelle cores swell a little bit because of the repulsion between positive charges. The swelling of micelles makes the hydrophobic chain more exposed to the aqueous solution and lead to more energy penalty. The energy penalty will further drive the protonation of tertiary amines. This positive feedback process keeps going on until micelles completely dissociate into water soluble single polymer chains. The pH cooperativity significantly sharpens the pH transition. Commonly used pH sensitive polymers do not have such hydrophobic barrier and pH cooperativity in the protonation process.
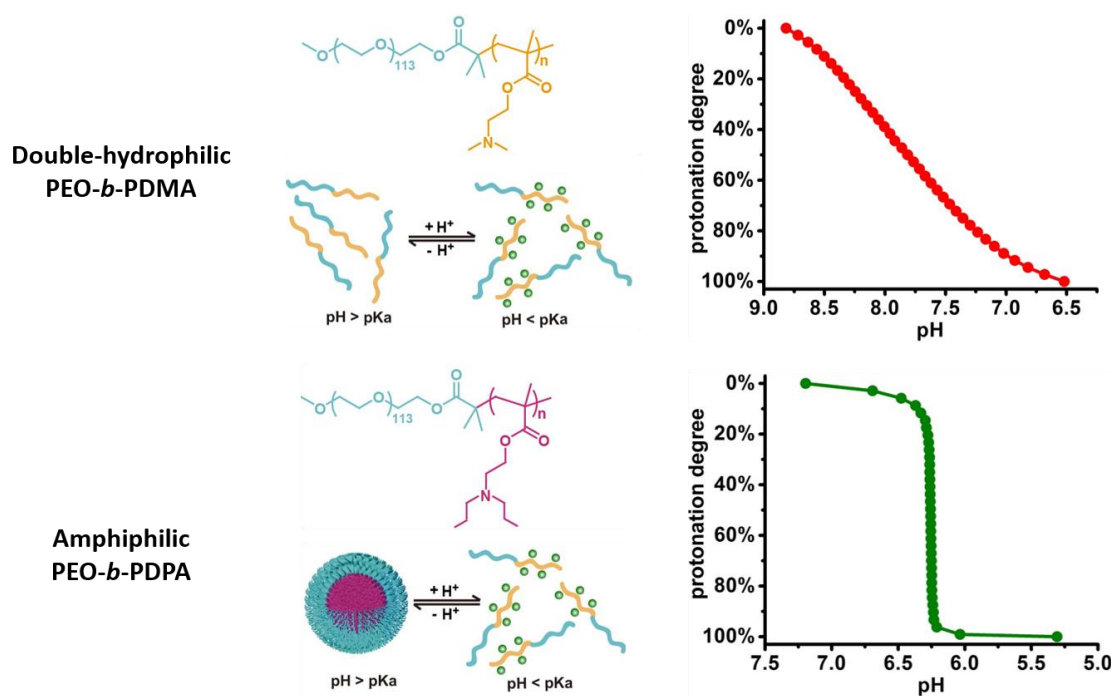
Figure 5.3.6. Comparison of pH transition sharpness of PEO-b-PDMA and PEO-b-PDPA. Hydrophobic phase separation lead to the sharp H transition of UPS block copolymers like PEO-b-PDPA.

192
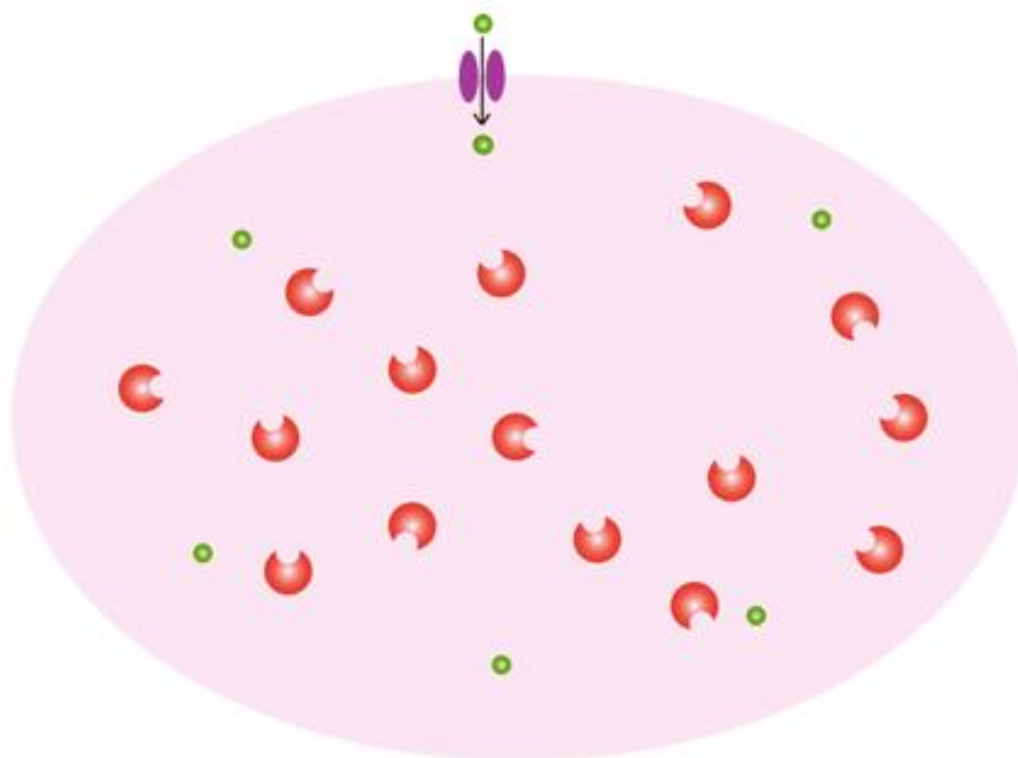
Figure 5.3.7. Schematic illustration of protonation of small molecular pH sensors.
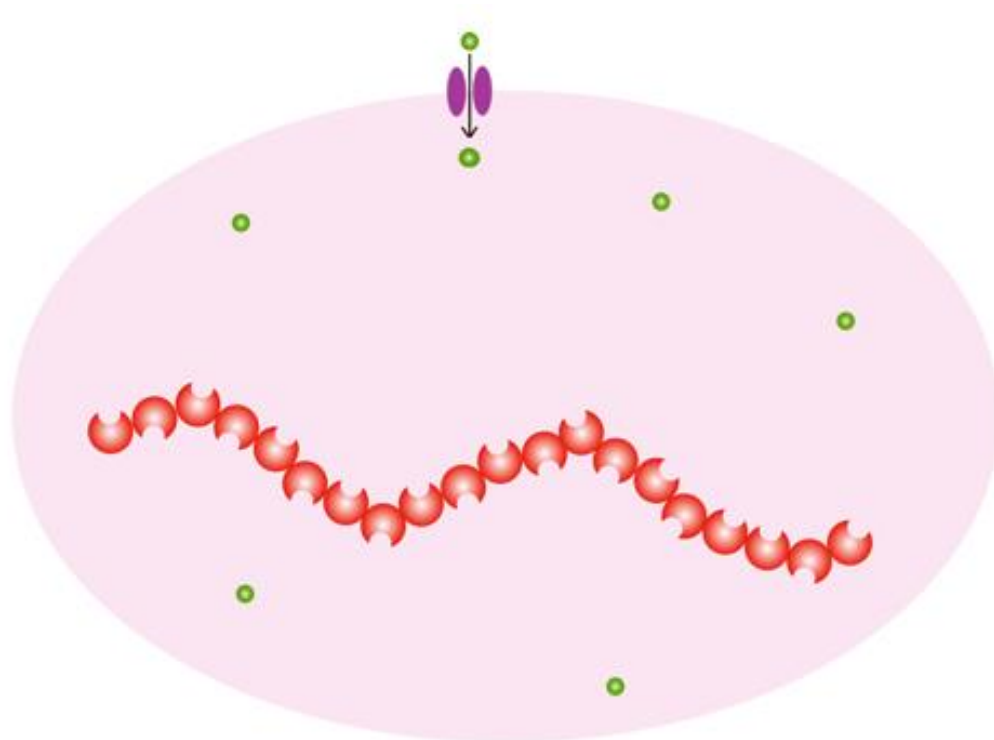
Figure 5.3.8. Schematic illustration of protonation of water soluble polymeric pH sensors.
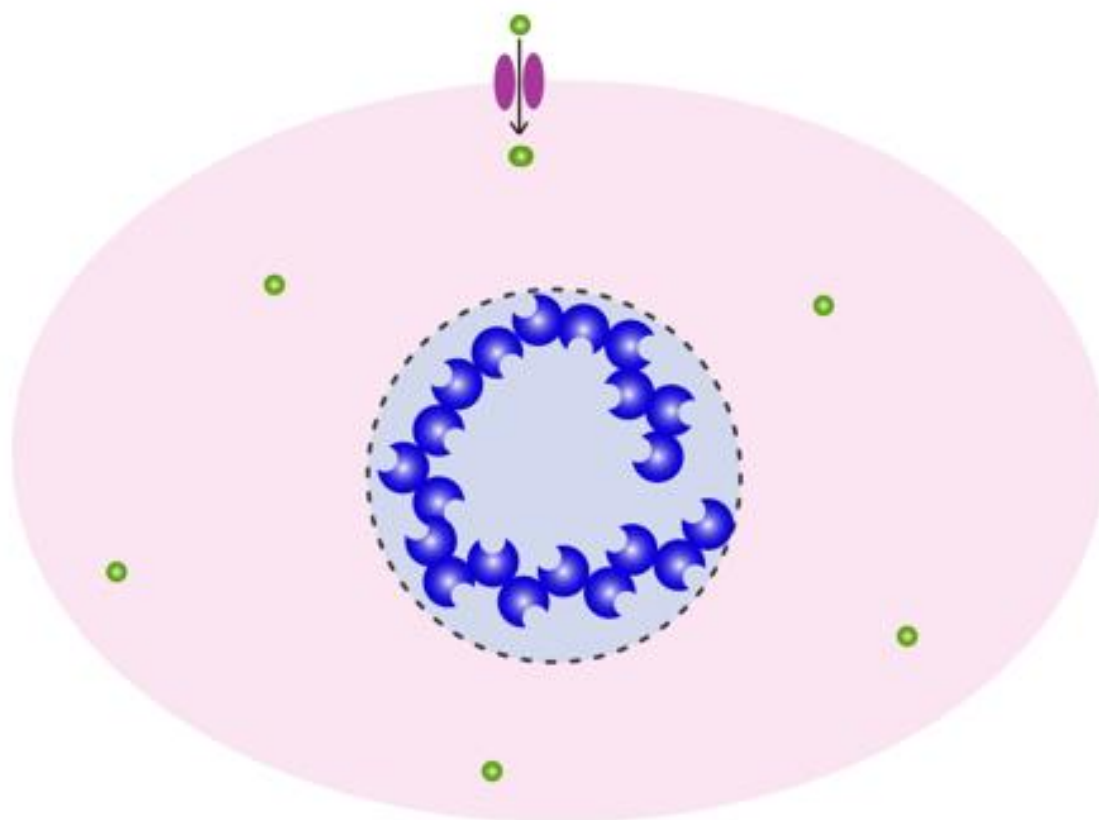
Figure 5-3-9. Schematic illustration of protonation of UPS nanoparticles

5.3.6. Discussion

In biological sensing, achieving high sensitivity and specificity of detection remains a great challenge due to the frequently small differences between pathological and normal physiological signals and the difficulty in signal amplification without introducing noise. Unimolecular sensors (e.g., Lysosensor) have a continuous response to the biological target concentration. Like all analog sensors, they are capable of distinguishing fine gradations in biological signals. However, analog sensors often suffer from low detection sensitivity and specificity due to lack of signal amplification without noise introduction. Recently, responsive nanomaterials have rapidly advanced in a variety of optical, electrical and mechanical systems for a wide range of applications such as biosensing, self-healing, and drug delivery[2,21]. Compared to single molecules, nanomaterials often display positive cooperativity arising from non-covalent self-assembly chemistry. This cooperative response can lead to transistor-like biosensors that can be leveraged to amplify or switch signals[22]. One such example is the nanoparticle-based optical bioaffinity assay where small changes in input biochemical signals such as DNA concentration resulted in a dramatically amplified optical signals from aggregating gold nanoparticles[23,24]. The ultra-pH sensitive (UPS) nanoprobes also displayed switchable fluorescent on/off response to pH changes[25-27]. Despite these examples, the design principles for rational conversion of responsive nanomaterials into binary switchable biosensors are still lacking.

One major obstacle to achieving this goal is the complexity of the multitude of weak, reversible and non-covalent interactions with responsive nanomaterials in the aqueous environment[28], which makes it difficult to understand the molecular mechanism

of stimuli response. Unlike covalent chemistry, supramolecular self-assembly employs non-covalent bonds (e.g., electrostatic and hydrophobic interactions, hydrogen bonds, etc.) to achieve a thermodynamically stable nanostructure[28,29]. This strategy has the advantage of reaching sizes (10^4-10^{10} Da) not easily achievable by covalent chemistry, and the resulting system is typically more responsive to environmental stimuli due to the lower energy barriers in the formation or dissociation of non-covalent complexes than the making or breaking of covalent bonds. A hallmark of self-assembled system is positive cooperativity[4,28,30], which can arise from the interplay of two or more synergistic interactions, with the resulting system often displaying emergent properties (e.g. ultra-pH response) absent from the sum of individual components.

In this study, we elucidated the molecular pathway of pH-induced supramolecular self-assembly of an ultra-pH sensitive PEO-*b*-PDPA copolymer. We discovered that hydrophobic nanophase separation is responsible for the catastrophic deprotonation of charged unimers into neutral copolymers inside polymeric micelles. The divergent proton distribution characteristic of PEO-*b*-PDPA copolymers was not observed in commonly used small molecular and polymeric bases (e.g., PEI). The strong pH cooperativity can explain the significantly decreased pKa and sharpened pH response from the unimolecular DPA base. Combining of theoretical modeling and experimental validation identified key structural parameters such as repeating unit hydrophobicity and polymer chain length that impact pKa and the sharpness of pH transition. Cooperativity arising from micellization was also observed in an independent sensing experiment of perchlorate anions, demonstrating the potential universality of this approach.

In conclusion, results from this study provide molecular insights to help establish the general principles in applying non-covalent self-assembly chemistry to achieve molecular cooperativity for the development of future nanomaterials-based sensors with binary stimuli response. Conversely, the UPS nanoparticles offer a relatively simple model system to further study molecular cooperativity (e.g., interplay of enthalpy and entropy during the reversible self-assembly process), which may offer insights in more complex phase transition systems such as thermosensitive NIPAM[31] and elastin-like polymers[32].

5.4-References

1   De las Heras Alarcón, C., Pennadam, S. & Alexander, C. Stimuli responsive polymers for biomedical applications. *Chemical Society Reviews* **34**, 276-285 (2005).

2   Stuart, M. A. C. *et al.* Emerging applications of stimuli-responsive polymer materials. *Nature materials* **9**, 101-113 (2010).

3   Lammers, T., Aime, S., Hennink, W. E., Storm, G. & Kiessling, F. Theranostic nanomedicine. *Accounts of chemical research* **44**, 1029-1038 (2011).

4   Hunter, C. A. & Anderson, H. L. What is cooperativity? *Angewandte Chemie International Edition* **48**, 7488-7499 (2009).

5   Terzi, E., Hölzemann, G. & Seelig, J. Self-association of β-amyloid peptide (1–40) in solution and binding to lipid membranes. *Journal of molecular biology* **252**, 633-642 (1995).

6   Zhao, D. & Moore, J. S. Nucleation–elongation: a mechanism for cooperative supramolecular polymerization. *Organic & biomolecular chemistry* **1**, 3471-3491 (2003).

7   Jonkheijm, P., van der Schoot, P., Schenning, A. P. & Meijer, E. Probing the solvent-assisted nucleation pathway in chemical self-assembly. *Science* **313**, 80-83 (2006).

8   Zhang, B. Enthalpic domination of the chelate effect in cyclodextrin dimmers. *J. Am. Chem. Soc.* **115**, 9353-9354 (1993).

9   Mammen, M., Simanek, E. E. & Whitesides, G. M. Predicting the relative stabilities of multiparticle hydrogen-bonded aggregates based on the number of hydrogen bonds and the number of particles and measuring these stabilities with titrations using dimethyl sulfoxide. *Journal of the American Chemical Society* **118**, 12614-12623 (1996).

10   Taylor, P. N. & Anderson, H. L. Cooperative self-assembly of double-strand conjugated porphyrin ladders. *Journal of the American Chemical Society* **121**, 11538-11545 (1999).

11   Camara-Campos, A., Hunter, C. A. & Tomas, S. Cooperativity in the self-assembly of porphyrin ladders. *Proceedings of the National Academy of Sciences of the United States of America* **103**, 3034-3038 (2006).

12   Weiss, J. N. The Hill equation revisited: uses and misuses. *The FASEB Journal* **11**, 835-841 (1997).

13   Perlmutter-Hayman, B. Cooperative binding to macromolecules. A formal approach. *Accounts of Chemical Research* **19**, 90-96 (1986).

14   Ercolani, G., Piguet, C., Borkovec, M. & Hamacek, J. Symmetry numbers and statistical factors in self-assembly and multivalency. *The Journal of Physical Chemistry B* **111**, 12195-12203 (2007).

15   Connors, K. A., Paulson, A. & Toledo-Velasquez, D. Complexing of. alpha.-cyclodextrin with sym-4, 4'-disubstituted biphenyls. *The Journal of Organic Chemistry* **53**, 2023-2026 (1988).

16   Chang, R. *Physical chemistry for the chemical and biological sciences*. (University Science Books, 2000).

17   Po, H. N. & Senozan, N. The Henderson-Hasselbalch equation: its history and limitations. *J. Chem. Educ.* **78**, 1499 (2001).

18   Li, Y. *et al.* Molecular basis of cooperativity in pH-triggered supramolecular self-assembly. *Nature communications* **7** (2016).

19   Perutz, M. F. Mechanisms of cooperativity and allosteric regulation in proteins. *Q. Rev. Biophys.* **22**, 139-237 (1989).

20   Koper, G. J. & Borkovec, M. Proton binding by linear, branched, and hyperbranched polyelectrolytes. *Polymer* **51**, 5649-5662 (2010).

21   Webber, M. J., Appel, E. A., Meijer, E. W. & Langer, R. Supramolecular biomaterials. *Nat. Mater.* **15**, 13-26, doi:10.1038/nmat4474 (2016).

22   Lei, J. & Ju, H. Signal amplification using functional nanomaterials for biosensing. *Chem. Soc. Rev.* **41**, 2122-2134 (2012).

23   Mirkin, C. A., Letsinger, R. L., Mucic, R. C. & Storhoff, J. J. A DNA-based method for rationally assembling nanoparticles into macroscopic materials. *Nature* **382**, 607-609 (1996).

24   Elghanian, R., Storhoff, J. J., Mucic, R. C., Letsinger, R. L. & Mirkin, C. A. Selective colorimetric detection of polynucleotides based on the distance-dependent optical properties of gold nanoparticles. *Science* **277**, 1078-1081 (1997).

25   Zhou, K. *et al.* Tunable, Ultrasensitive pH- Responsive Nanoparticles Targeting Specific Endocytic Organelles in Living Cells. *Angewandte Chemie International Edition* **50**, 6109-6114 (2011).

26   Wang, Y. *et al.* A nanoparticle-based strategy for the imaging of a broad range of tumours by nonlinear amplification of microenvironment signals. *Nature materials* **13**, 204-212 (2014).

27   Ma, X. *et al.* Ultra-pH-sensitive nanoprobe library with broad pH tunability and fluorescence emissions. *J. Am. Chem. Soc.* **136**, 11085-11092 (2014).

28   Whitesides, G., Mathias, J. & Seto, C. Molecular self-assembly and nanochemistry: a chemical strategy for the synthesis of nanostructures. *Science* **254**, 1312-1319, doi:10.1126/science.1962191 (1991).

29   Whitesides, G. M. & Grzybowski, B. Self-assembly at all scales. *Science* **295**, 2418-2421 (2002).

30   Whitty, A. Cooperativity and biological complexity. *Nat. Chem. Biol.* **4**, 435-439 (2008).

31   Schild, H. G. Poly (N-isopropylacrylamide): experiment, theory and application. *Prog. Polym. Sci.* **17**, 163-249 (1992).

32   Quiroz, F. G. & Chilkoti, A. Sequence heuristics to encode phase behaviour in intrinsically disordered protein polymers. *Nat. Mater.* (2015).

CHAPTER SIX-Key Design Parameters for the Design of UPS Nanoprobes

6.1-Introduction

6.1.1-Program the stimuli-responsiveness in nanomaterials

Proteins that undergo phase transitions triggered by biological stimuli play critical roles in many self-assembly events and involved functionalities in nature[1,2]. Nuclear pore complexes allow passage of cargoes bound to nuclear transport receptors, but suppress nucleocytoplasmic fluxes of inert macromolecules above 30 kDa. It was found that reversible cross-linking between Phe and Gly (FG)–rich nucleoporin repeats was responsible for observed selectivity[3]. Analogously, nanomaterials that display stimuli-triggered self-assembly have inspired the development of novel approaches for regenerative medicine, targeted delivery of therapeutics and disease diagnosis[4]. The progress in understanding the sequence-structure relationships in proteins has enabled the prediction of the folding process[5] and intrinsic disorder[6] by computational approaches. In contrast, the phase transition behavior in synthetic self-assemblies in much less understood. The development of functional nanomaterials has a growing emphasis on identification and optimization of specific design parameters crucial to performance. It is of great importance to identify, evaluate and optimize key design parameters that affect the stimuli-triggered self-assembly. The supramolecular self-assembly arises from a multitude of molecular interactions that exist ubiquitously in both natural and synthetic macromolecular systems. Self-assembly based on selective and precise control of non-covalent interactions provides powerful and versatile tools for the development of complicated nanostructures at the molecular level.

Upon external physical or chemical stimuli, responsive nanomaterials can respond and adapt to surrounding environment through conformational or chemical changes. In many cases, the conformational changes come in the form of external signal-triggered supramolecular self-assembly. At the molecular level, supramolecular self-assembly is the spontaneous association of molecules under equilibrium conditions into thermodynamically stable and structurally well-defined nanostructures joined by non-covalent bonds[7,8]. Supramolecular chemistry offers a toolbox of multiple non-covalent interactions for the formation of well-defined nanostructures[9]. These interactions range from relatively weak forces such as hydrophobic interactions, hydrogen bonding, or $\pi-\pi$ stacking interactions to ionic bonds. The keys to develop functional nanomaterials via external signal-induced self-assembly are to understand and control the non-covalent connections between building blocks or molecules, and to understand and overcome the intrinsically unfavorable thermodynamic barrier involved in bringing many molecules together in a single aggregate of a nanoparticle[10]. A major challenge in studying self-assembly in natural and synthetic systems is the interdependence of many non-covalent interactions and their compensating effects on the composite behaviors of the nanosystem[11]. To pinpoint specific contribution from individual non-covalent interaction, we need to establish a model system in which key parameters can be changed easily and independently. In addition, mechanistic investigation will help identify and evaluate key design parameters crucial for the performance of stimuli-responsive nanomaterials in biomedical applications.

6.1.2.- Factors in Controlling the Melting Curves of Spherical Nucleic Acids

Spherical nucleic acids (SNAs) can report the presence of target single strand DNA via oligonucleotides that are chemically anchored onto the surface of gold nanoparticle surface. A high DNA surface density on the nanoparticle will stabilize the particles and potentially increase the hybridization efficiency, resulting in cooperativity in the melting process[12]. The surface density of the probe oligonucleotides can be increase linearly with the mole percentage of the DNA strand in the deposition solution over a broad concentration range. And the transition temperature was found directly proportional to the surface probe density when keeping the nanoparticle and target concentration unchanged.

One attractive property of nanomaterials is large surface-to-volume ratio, which obviously directly relate to size. Generally, smaller nanoparticles will have larger surface-to-volume ratio. The nanoparticle size is expected to affect the phase transition of SNAs since the oligonucleotides are incorporated onto the surface of inner solid cores. The transition temperature decreased from 50 ℃ to 47 ℃ when the gold particle size increased from 13nm to 50 nm. Interestingly, the large SNAs generally exhibited sharp melting transitions compared to small ones.

Salt is known to affect the self-assembly behavior of natural macromolecules like proteins, especially at elevated concentration. The melting curves of natural single strand DNA exhibit a salt concentration dependence[13]. The melting analyses in NaCl solution suggested that salt concentration substantially affects the Tm of the SNAs. The transition temperature of SNAs increased from 41 to 61.5 ℃ with the salt concentration increasing from 0.05 to 1.0 M while keeping the nanoparticle and target concentration unchanged. In

addition, increase of salt concentration also lead to the formation of larger aggregates, as confirmed by light-scattering results[14]. This can probably attributed to a screening effect of the salt, which can minimize electrostatic repulsion between the oligonucleotide-modified gold nanoparticles and permit further hybridization between nanoparticles.

The aggregation of SNAs is triggered by hybridization of complementary DNA strands, which results in distinct color changes from red to purple and enables the colorimetric detection. The electromagnetic coupling between nanoparticles that significantly affect the surface plasmon resonance is distance dependent. Moreover, the distance between particles also impacts the van der Waals and electrostatic interactions between the particles. Thus, it is reasonable to assume the inter-particle distance may affect the hybridization process and ensuing melting behaviors. The melting analysis showed that longer inter-particle distance resulted in higher transition temperature of SNAs. Further mechanistic investigation suggested that the electrostatic interaction was expected to be the dominant factors in regulating distance-dependent melting behaviors. Ribonucleic acids (RNAs) are key components in many cellular processes including differentiation, growth and aging. Double strand RNA have shown promising therapeutic efficacy due to high cellular uptake and enhanced stability[15]. Similar to DNA, RNAs can also be incorporated onto the surface of gold nanoparticle to generate the RNA SNAs, which consist of dense shells of double-stranded RNA on nanoparticle surfaces.

6.1.3. Factors in Controlling the Phase Transition Temperature of PNIPAM Poly(N-isopropylacrylamide) Derivatives

Poly(N-isopropylacrylamide) (PNIPAM) is known for its unique phase transition behavior as noted by a lower critical solution temperature (LCSTs). It is generally accepted that the temperature-triggered phase transition is governed by cooperative dehydration of side chains. Compared to natural macromolecules such as proteins or nucleic acids, the structure and composition of synthetic polymers can be easily modified and engineered, which will help elucidate the structure-property correlation in the polymeric systems. Extensively work has been done in order to understand the phase transition process of PNIPAM and corresponding structure-property relationships.

Fujishige et al discovered that the transition occurs independently of either the molecular weight of the polymer (5×10^4 to 840×10^4) or its concentration (0.01 to 1 wt %)[16], but lots of reports suggested that the LCST can be changed upon shifting the hydrophilic/hydrophobic balance[17]. Different kinds of N-alkyl-substituted poly(meth) acrylamides have been developed and their LCST phase transition were investigated[18]. Poly(N-n-propylacrylamide) (PNNPAM)[19,20] had a LCST at 10 °C compared to 32 °C of PNIPAM, suggesting increasing the hydrophobicity may decrease the transition temperature. The LCST of poly(N-cyclopropylacrylamide) (PNCPAM), in which iso-propyl of PINPAM is replaced by less hydrophobic cyclo-propyl, occurs around 53 °C. Poly(N,N-diethylacrylamide) (PDEAM) displayed a phase transition temperature similar to PNIPAM at 33 °C[21]. The LCST of poly(N,N-ethylmethyl acrylamide) (PNEMAM) shifted significantly to much higher 70 °C. It is worth noting that the poly(N,N-dimethyl acrylamide) do not showed phase transition behavior bellowing the

boiling point of water[22]. The hydrophobicity of PNIPAM can also be tuned by incorporating an additional alkyl group in the backbone instead of side chains. Poly(N-isopropyl methacrylamide) have a LCST at 45 ℃, which indicates that increasing hydrophobicity of the back bone will increase the transition temperature and is opposite to that in side chain.

The great promise of PINPAM in biomedical application has inspired further development of other thermos-responsive polymers and these thermos-responsive system also showed similar structure-properties correlations in terms of phase transition temperature and stimuli-triggered supramolecular self-assembly. Gibson group reported the synthesis and investigation of a series of poly(acrylamide)-based thermo-responsive polymers with cyclic alkyl groups as N-substitutes[23]. Poly(N-vinylpiperidone) (PVPip) , with six-member-ring side chain, showed LCST between 65-90 degrees[24]. The phase transition temperature of poly(N-vinylcaprolactam) (PVCap) shifted to lower 40 degree with an seven-member-ring side chain[25,26]. Though the PVPip and PVCap demonstrated similar hydrophobicity-dependent phase transition behavior, they also showed significant molecular weight-dependent LCST shift, different from PNIPAM. When the molecular weight of PVPip increased from 4100 Da to 83000 Da, the LCST decreased from 99 ℃ to 67 ℃. The LCST of PVCap shifted from 49 ℃ to 36 ℃ when the molecular weight increased from 1400 Da to 17000 Da.

Zhang group synthesized a series of N-ester-substituted poly(acrylamide) and performed a systematic investigation of their LCST behavior[27]. In one of their polymer library-poly(N-acryloylglycine methyl ester) (PNAGME), the melting temperature displayed strong molecular weight dependence. The LCST shifted from 57 ℃ to 42 ℃

when the polymerization degree increased from 20 to 180. They also observed that increase the concentration of salt like NaCl would shift the LCST to lower temperature.

A new category of thermo-responsive nanomaterials have also been developed by coating thermos-responsive polymers onto the surface of different solid nanoparticles. Edwards et al. demonstrated that increasing the temperature of poly(poly(ethylene glycol) methacrylate) (PPEGMA) coated gold nanoparticles above the LCST of the polymer facilitates the transport of the nanoparticles across an oil/water interface[28]. Boyer et al. prepared a series of thermosensitive copoly(oligoethylene oxide) acrylates and these copolymers exhibited tunable LCST behavior over the range of 15−90 °C dependent on their monomer compositions[29]. Tenhu group reported the development of thermos-responsive nanoparticles via grafting PNIPAM brushes on the surface of gold nanoparticles (AuNPs)[30]. Increase the molecular weight of PNIPAM resulted in the decrease of LCST. They also found that decrease of size of gold nanoparticle core may lead to slight increase of phase transition temperature. Klok and co-workers also observed similar size-dependent LCST transitions of polymer-coated gold nanoparticles[31].

6.1.4-Key design parameters in controlling pH-responsive behaviors of UPS block copolymers

Besides the introduction of acid labile moieties like acetal groups[32,33], the incorporation of ionizable groups such as amines or carboxylic acids serves as the general strategy in the development of pH sensitive nanomaterials[34-38]. The nanoprobes consist of a block copolymer, PEO-*b*-PR, where PEO is poly(ethylene oxide) and PR is an ionizable

tertiary amine block. Our UPS nanoprobes achieved over 100 fold fluorescence intensity increase within 0.3 pH units, which is critical for broad tumor imaging and endosome maturation studies[39,40]. The hydrophobic and $\pi-\pi$ stacking interactions can be intensified by increasing the hydrophobic chain length and incorporating aromatic moieties in the copolymer, respectively. The hydrogen bonding network and hydration of macromolecular solutes in aqueous solution are also dependent on the presence of salt and its concentration. The strength of ionic bonds between charged polymers and counter ions are known to be ion species dependent. By selectively tailoring specific structural (e.g., substituents of amines) and solution parameters (ion species and concentrations), we are able to strengthen or weaken ion pair interactions in pH-triggered supramolecular self-assembly of UPS block copolymers.

In this chapter, we will provide a systematic investigation of key factors that impact the pH responsive behavior and resulting self-assembly of UPS block copolymers. This study aims to provide fundamental understanding of the effect of multiple non-covalent interactions (e.g., hydrophobic interactions, $\pi-\pi$ stacking, hydrogen and ionic bonding) on the pH-triggered supramolecular self-assembly. It also offers useful insights for further development of polymeric pH sensors with predictable and tunable transition pH.

6.2-Materials and methods

6.2.1.-Preparation of micelle solution

For each copolymer, the stock solution of micelles was prepared following a solvent evaporation method as previously reported[41]. In the example of PEO-*b*-nPDPA micelle solution, 20 mg of the copolymer was first dissolved in 2.0 mL THF and then added into 10 mL deionized water dropwise under sonication. The THF was removed through ultrafiltration with (100 KD) membrane for five times. Then deionized water was added to adjust the polymer concentration to 5 mg/mL as a stock solution.

6.2.2-Fluorescence Measurement

The fluorescence emission spectra were obtained on a Hitachi fluorometer (F-7500 model, Japan). For each copolymer, the sample was initially prepared in Milli-Q water at the concentration of 2 mg/mL. Then the stock solution was diluted in 0.2 M sodium phosphate buffers (containing 0.15 M sodium chloride) at different pH values. The TMR conjugated nanoprobes were excited at 545 nm, and the emission spectra were collected from 560 to 750 nm. The emission and excitation slits were both 5 nm. The emission intensity at 580 nm was used to quantify the ultra-pH response for different nanoprobe concentrations as shown in Figure 7d.

6.2.3-Measurement of critical micelle concentration (CMC)

CMC of PEO-b-nPDPA block copolyemrs was measured in 0.1 M phosphate buffer saline (PBS, pH 7.4). First, a copolymer stock solution (5 mg/mL) was

diluted to different concentrations in the same buffer. In each solution, 5μL pyrene in THF solution (2×10^{-4} M) was added to 2 mL polymer solution to produce the final pyrene concentration at 5×10^{-7} M. The fluorescence spectra were recorded on a Hitachi fluoremeter (F-7500 model) with the excitation wavelength of 339 nm and the excitation and emission slits at 10.0 nm and 1.0 nm, respectively. The I_1 and I_3 values were measured as the maximum emission intensity at ca. 372 and 382 nm, respectively. I_1/I_3 ratio was plotted as a function of polymer concentration at different pH values. I_1/I_3 ratio reflects the polarity of the pyrene environment where partition of pyrene in the hydrophobic micelle core leads to decreased I_1/I_3 values.

6.2.4-TEM and DLS characterization

Samples for TEM and DLS analyses were prepared in situ by pH titration. The morphology and size of nanoparticles were characterized by transmission electron microscopy (TEM, FEI Tecnai G2 Spirit Biotwin model). Hydrodynamic diameter (Dh) and scattering count rates were determined by dynamic light scattering (DLS, Malvern Nano-ZS Model, He-Ne Laser, λ=633 nm).

6.3-Results and discussions

6.3.1-Establishment of UPS block copolymer library for the investigation of structure-property correlations

We used the atom transfer radical polymerization (ATRP) method with CuBr as a catalyst and *N,N,N',N',N''*-pentamethyl-diethylenetriamine (PMDETA) ligand for the copolymer syntheses. The UPS block polymers used in current study was shown in **Figure 6.3.1**. The PEO-*b*-PR copolymers with homopolymeric PR block were synthesized using a single methacrylate monomer as previously described[42]. At low pH, micelles dissociate into cationic unimers with protonated ammonium groups. When pH increases, neutralized PR segments become hydrophobic and the block copolymers self-assemble into core-shell micelles. The delicate balance between the hydrophobic and hydrophilic segments as a result of external pH changes drives the formation of thermodynamically stable micelles. The phase transition pH, where reversible supramolecular self-assembly occurs, depends on the pKa values of UPS block copolymers around which tertiary amines are reversibly protonated. The extraordinarily sharp pH transition makes the pKa of UPS block copolymers almost identical to the phase transition pH as described previously[42].

pH titration offers critical information on how pH sensors respond to external pH changes along the titration coordinate. We performed the pH titration experiments by adding HCl solution into UPS block copolymers' micelle solution prepared following a solvent evaporation procedure[42]. Without specific indication, pH titrations were performed in the presence of 150 mM NaCl to mimic the physiological level of salt concentration. We treated the initial micelle solution as having a protonation degree of 0%

213

when no HCl was added. We considered the tertiary amines as 100% protonated when the addition of HCl yielded the sharpest change of pH (**Figure 6.3.2**). The apparent pKa value was determined as the pH at which 50% of all the tertiary amines were protonated[43].
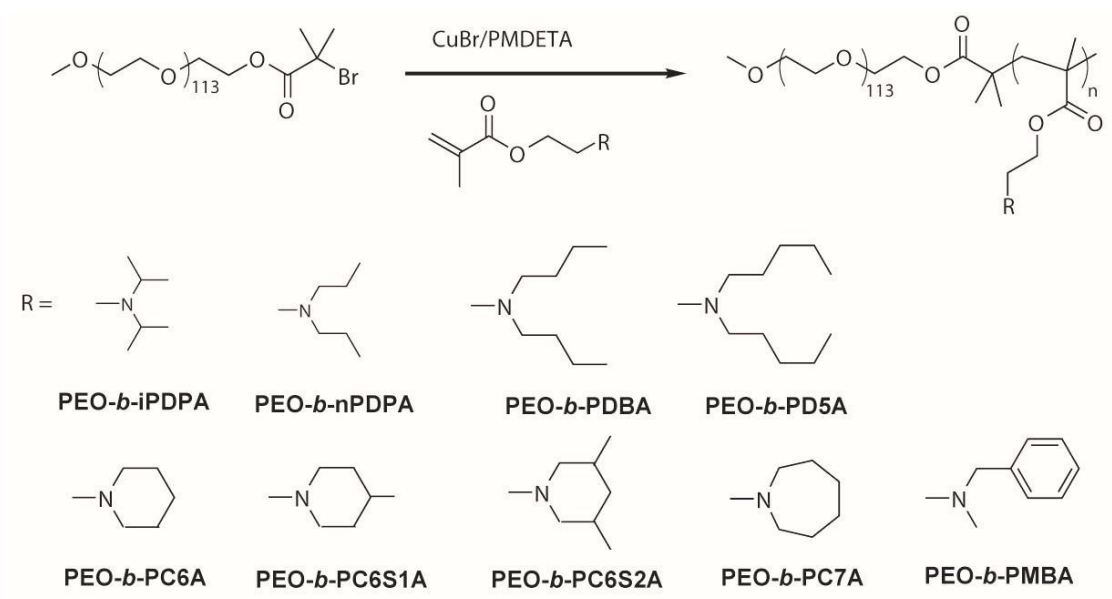
Figure 6.3.1. Schematic syntheses and structures of PEO-b-PR diblock copolymers. PR is the hydrophobic segment with ionizable tertiary amines.
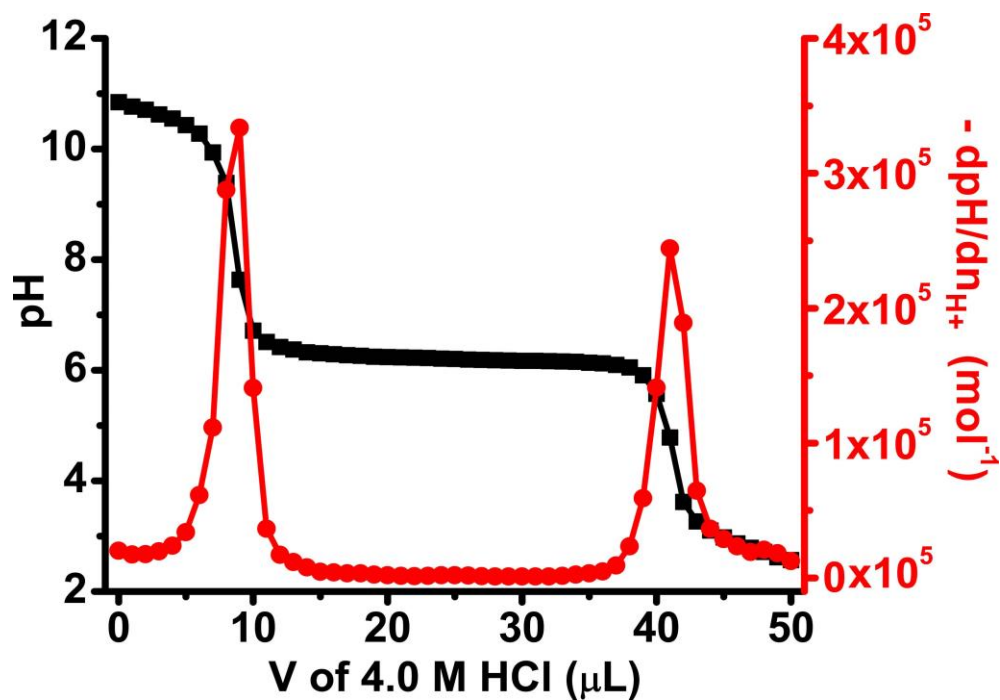
Figure 6.3.2. Figure S3. pH titration of PEO-b-nPDPA block copolymers. We considered the tertiary amines as 100% protonated when the addition of HCl yielded sharpest change of pH. The calculated –dpH/dnH+ was plotted as a function of added HCl. The peak corresponded to the protonation degree at 100% where the amines were 100% converted to ammonium groups.

6.3.2-Effect of hydrophobic interactions on pH responsive behavior

Naturally existing self-assembly systems like proteins and synthetic assemblies designed for biomedical applications like UPS nanoprobes are primarily used in aqueous media. In aqueous solution, the hydrophobic interactions constitute the predominant driving force for the polymeric molecules to self-organize into nanostructures. We began the investigation of structure-property relationship by determining how changing hydrophobic interactions affected the pH responsive behavior and self-assembly of UPS block copolymers. Early studies in thermo-responsive polymers have shown that hydrophobicity of polymers had substantial impact on the transition temperature of nanomaterials[44-46].

An obvious strategy in increasing hydrophobic interactions of amphiphilic PEO-*b*-PR block copolymers is to increase the hydrophobic chain length. For proof of concept studies, we synthesized a series of PEO_{114}-*b*-$nPDPA_x$ block copolymers with fixed hydrophilic poly(ethylene oxide) chains but systematic changes in the hydrophobic PR chain length (x = 5, 10, 20, 60 and 100). The transition pH of PEO_{114}-*b*-$nPDPA_{100}$ block copolymers, with the longest hydrophobic segment, yielded the lowest pKa at 6.2 (**Figure 6.3.3a**). In contrast, PEO_{114}-*b*-$nPDPA_5$, with the shortest hydrophobic chain length, displayed the highest transition pH around 6.7. The plot of pKa values as a function of hydrophobic chain length of PEO-*b*-nPDPA copolymers showed a dramatic hydrophobic chain length-dependent transition pH shift (**Figure 6.3.3b**). It is also interesting to note that longer hydrophobic chain length also resulted in increased pH sharpness, as measured by $pH_{10-90\%}$ (the pH range where protonation degree of all tertiary amines decreases from 90% to 10%) (**Figure 6.3.3 and 6.3.4**).

Strengthening the hydrophobic interactions can also be achieved by increasing the hydrophobicity of amine substituents of UPS block copolymers. To accomplish this goal, we used a series of ultra-pH sensitive PEO_{114}-b-PR_{80} block copolymers with identical poly(methacrylate) backbone and similar chain length but different linear terminal alkyl groups on the side chain. All polymers showed a strong buffer effect as proven by the plateau along the majority of the pH titration coordinates (**Figure 6.3.5a**). The PEO-b-PD5A with the most hydrophobic pentyl group yielded the lowest pKa at 4.4. Meanwhile, the PEO-b-iPDPA with the least hydrophobic isopropyl group as an amine substituent showed the highest pKa, close to 6.6. PEO-b-nPDPA and PEO-b-PDBA had pH transitions at 6.2 and 5.3, respectively. These results demonstrated that PEO-b-PR block copolymers with more hydrophobic amine substituents have a lower pKa. We calculated the octanol-water partition coefficients (LogP) of the repeating unit of the PR segment (neutral form) and used them as a quantitative measure of molecular hydrophobicity and strength of hydrophobic interactions. The plot of pKa values as a function of LogP (**Figure 6.3.5b**) showed a linear correlation.

To confirm the effect of enhancing hydrophobic interactions on the transition pH of UPS block copolymers, we synthesized another series of PEO_{114}-b-PR_{80} block copolymers with the same backbone and similar chain length, but cyclic terminal alkyl groups. For PEO-b-PC6A, we observed the highest pH transition at 7.3. Incorporation of one or two extra methyl groups on the piperidine ring resulted in lower transition pH values of 6.8 and 6.1, respectively (**Figure 6.3.5c**). A plot of pKa values as a function of LogP also showed a linear correlation (**Figure 6.3.5d**). Besides six-membered rings as cyclic substituents, we also synthesized another block copolymer, PEO-b-PC7A, with

seven-membered rings as cyclic substituents. C7A repeating units had similar hydrophobicity (LogP = 2.33) as that of C6S1A (2.25) and they indeed showed very close pKa value around 6.9 (**Fig. 6.3.6**).

Based on the above experiments, we concluded that stronger hydrophobic interactions (both in amine substituents and hydrophobic chain length) generally lead to the decrease of transition pH of UPS block copolymers. An increase of hydrophobic interactions will stabilize the nanoparticles and shift the equilibrium to the direction of neutralization of protonated tertiary amines, corresponding to the decrease of pKa. In this case, the pH-triggered supramolecular self-assembly occurred at lower pH. This is in accordance with early reports that the lower critical solution temperature (LCST) of poly(*N*-isopropylacrylamide)(PNIPAM) based copolymers can be controlled by changing the hydrophobic chain length[47-49].
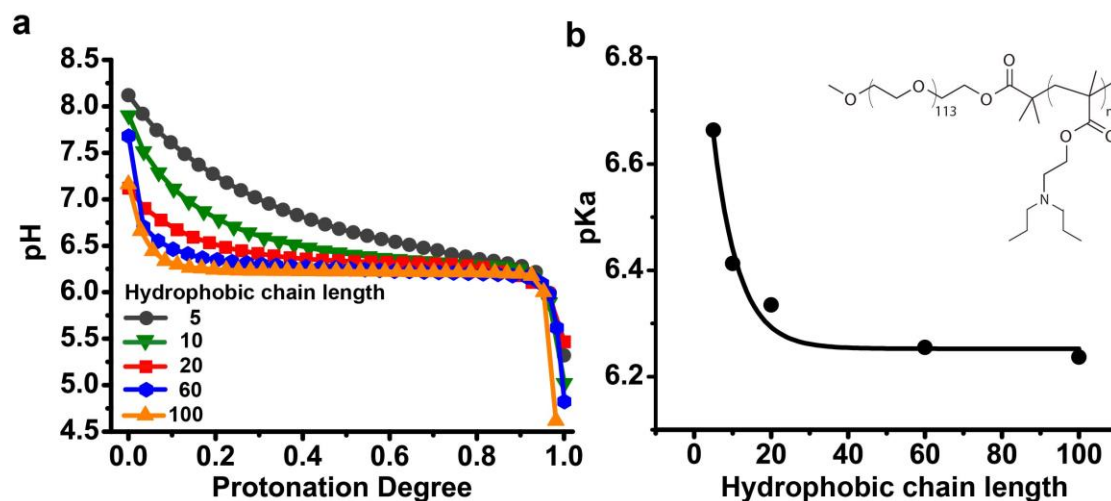
Figure 6.3.3. The effect of hydrophobic chain length on the transition pH of UPS block copolymers. pH titration curves (a) and pKa values (b) of PEO-b-nPDPA block copolymers with the number of PDPA repeating units at 5, 10, 20, 60 and 100. Increase of hydrophobic chain length not only lowers the pKa but also sharpens the pH transition.
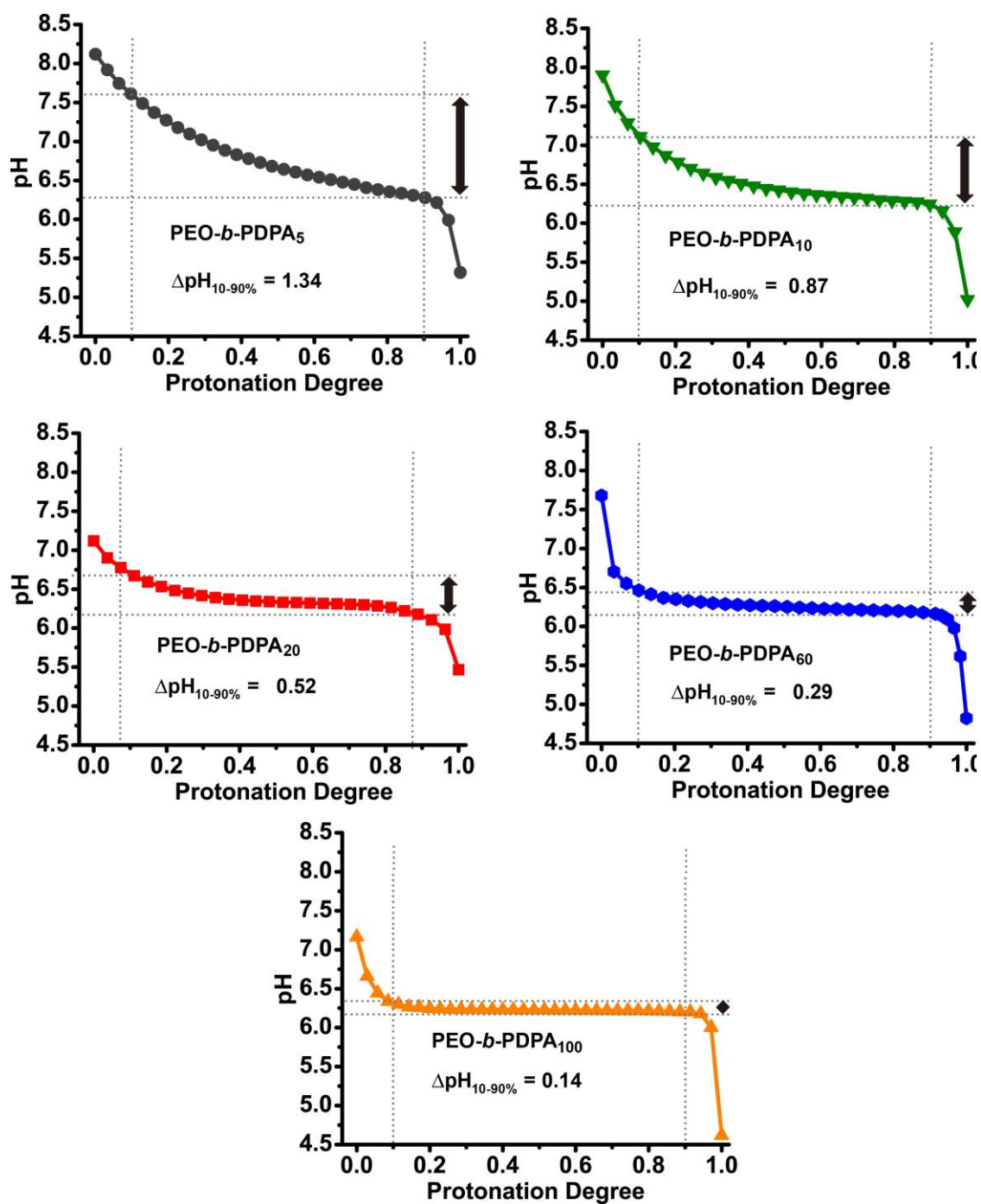
Figure 6.3.4. pH transition sharpness ($\Delta pH_{10-90\%}$) of PEO-*b*-nPDPA block copolymers with different hydrophobic chain lengths.
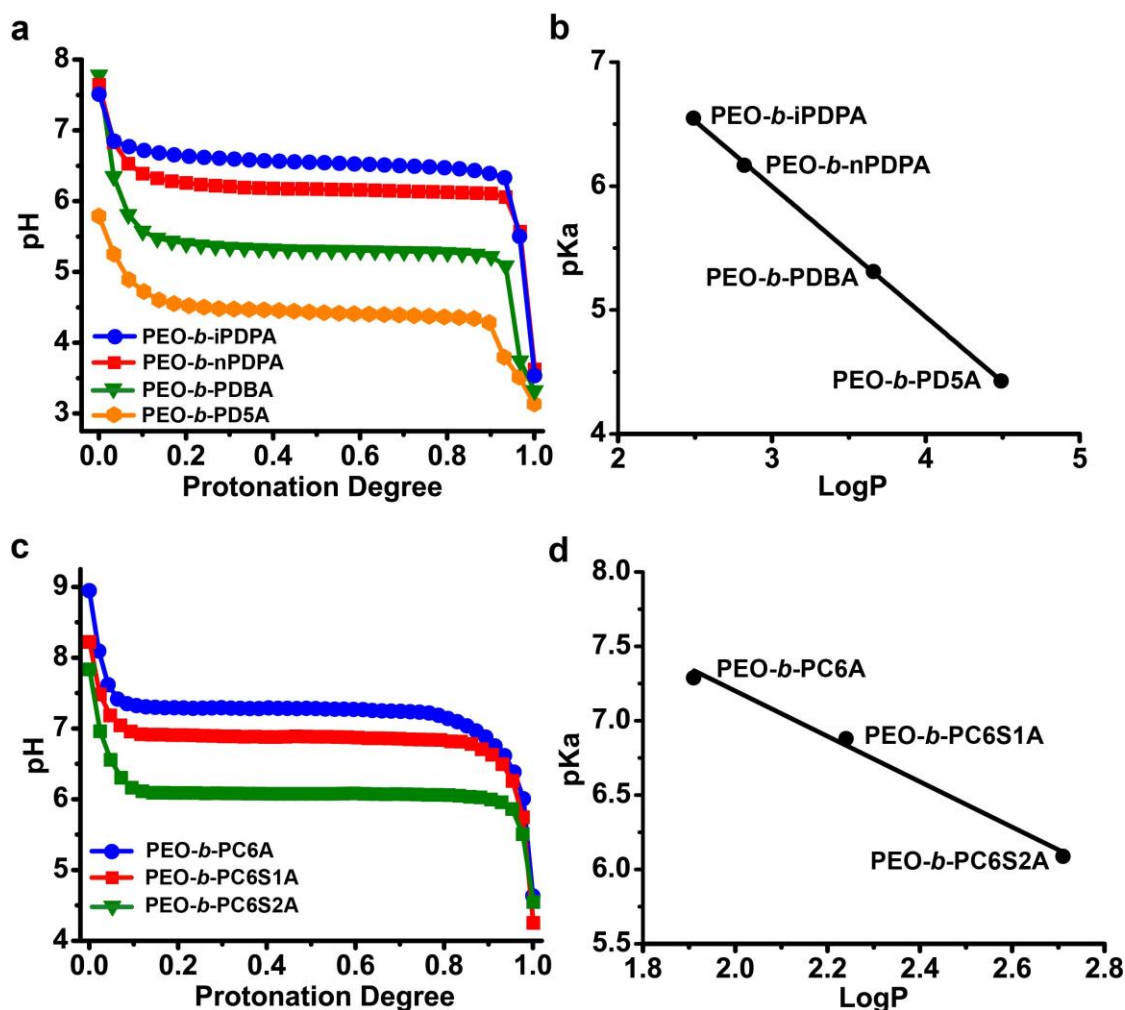
Figure 6.3.5. The effect of hydrophobicity of tertiary amine substituents on the pKa of

UPS block copolymers. pH titration curves (a) and pKa values (b) of a series of

PEO-b-PR block copolymers with the same poly(methacrylate) backbone but different

acyclic amine substituents. pH titration curves (c) and pKa values (d) of a series of

PEO-b-PR block copolymers with the same poly(methacrylate) backbone but different

cyclic amine substituents. The pKa values were correlated with the hydrophobicity

parameter (LogP) of the repeating unit of PR segment (b,d).Increase of hydrophobic

chain length not only lowers the pKa but also sharpens the pH transition.
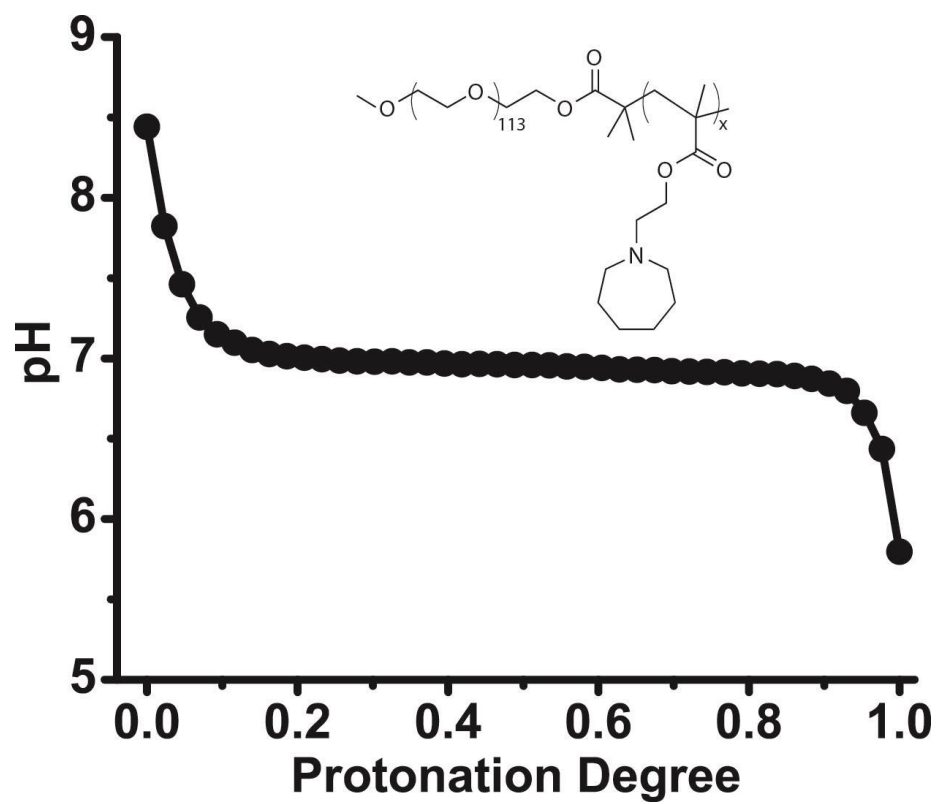
Figure 6.3.6. pH titration of PEO-b-PC7A block copolymers.

6.3.3-Effect of π–π stacking on pH responsive behavior

π–π stacking has been reported to direct the formation of structured ensembles via the self-assembly of individual magnetic particles[50,51]. We investigated whether the incorporation of aromatic rings also affected the pKa values of UPS block copolymers. PEO-*b*-PMBA block copolymers were synthesized via polymerization of (methylbenzylamino) ethyl methacrylate (MBA, LogP = 2.91) monomers. The hydrophobicity of amine substituents of PEO-*b*-PMBA was similar to that of PEO-*b*-nPDPA, but the pKa value (4.86) was significantly lower (**Figure 6.3.7**). This suggested that the introduction of aromatic rings and resulting π–π stacking may further decrease the pKa of UPS block copolymers, in addition to hydrophobic interactions.

To further investigate the π–π stacking effect on the pH response of UPS block copolymers, we synthesized a series of PEO-*b*-P(MBA-*r*-C7A) copolymers. The molar fraction of the two monomers can be precisely controlled prior to polymerization, leading to a random copolymerized P(MBA-*r*-C7A) block with predesigned MBA molar ratio. The pH titration experiments showed that incorporation of more hydrophobic MBA monomers into PEO-*b*-P(MBA-*r*-C7A) copolymers resulted in the decrease of pKa (**Figure 6.3.8a**). Further quantification by plotting the pKa values of PEO-*b*-P(MBA-*r*-C7A) copolymers as a function of MBA molar ratio showed a linear correlation (**Figure 6.3.8b**).
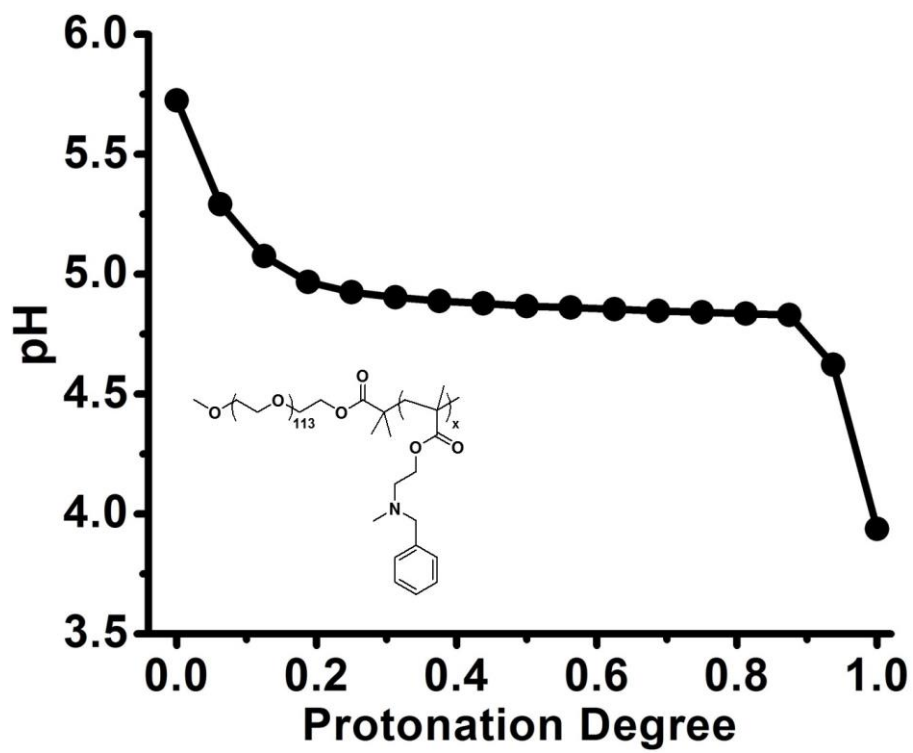
Figure 6.3.7. pH titration of PEO-b-PMBA (lower panel) block copolymers.
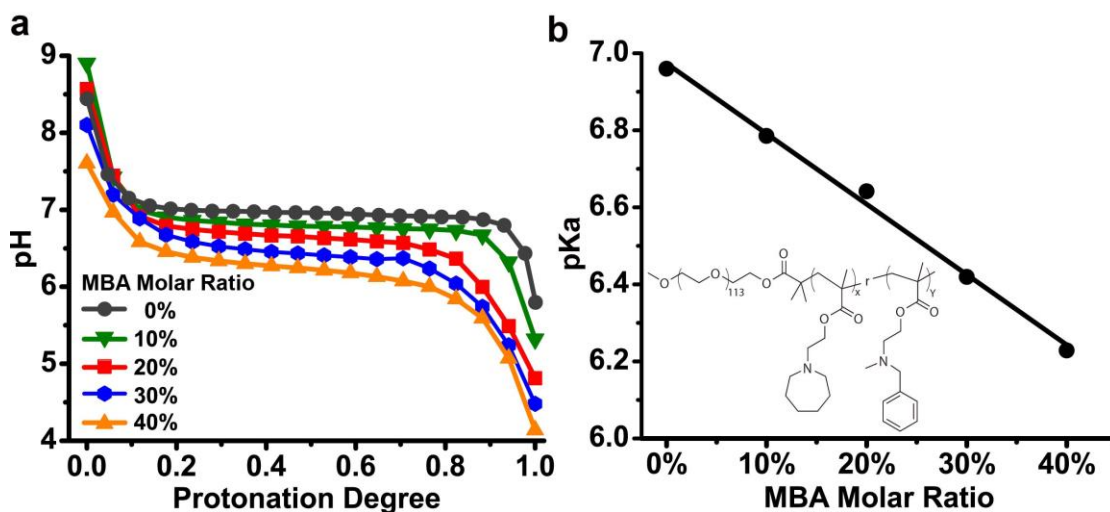
Figure 6.3.8. The effect of incorporation of (methylbenzylamino) ethyl methacrylate (MBA) monomer in the PEO-b-P(C7A-r-MBA) copolymers on the transition pH of the copolymers. pH titration curves (a) and dependence of pKa on MBA molar ratio (b) were shown.

6.3.4-Summary of effect of tertiary amines substituents in changing pH responsive behavior

Upon external physical or chemical stimuli, responsive nanomaterials can respond and adapt to surrounding environment through conformation or chemical changes such as self-assembly. The pH-triggered reversible micellization of UPS block copolymers represents a supramolecular self-assembly process, which employs a multitude of non-covalent interactions (e.g., electrostatic and hydrophobic interactions, hydrogen bond, $\pi-\pi$ stacking, etc.) to achieve thermodynamically stable nanostructures. Non-covalent interactions besides hydrophobicity may also impact the pH responsive behavior and shift the pKa of UPS block copolymers in aqueous solution. **Figure 6.3.9** summarized the pKa values of all the UPS block copolymers used in this study as a function of their hydrophobicity of PR segment repeating units. The hydrophobicity of PR segment repeating units in PEO-*b*-P(C7A-*r*-MBA) copolymers was calculated as the statistical average of C7A and MBA repeating units. All PEO-*b*-PR block copolymers with aliphatic alkyl groups as amine substituents, either linear or cyclic, followed linear pKa-LogP correlation. The pKa of PEO-*b*-PR block copolymers did not change much by replacing the six-membered ring cyclic substituents (C6S1A) with seven-membered rings (C7A) as long as the hydrophobicity of repeating units stayed the same. The geometry of the alkyl substituents, namely PEO-*b*-iPDPA vs. PEO-*b*-nPDPA, appeared to affect the pKa of the copolymers, but fit in the same linear curve in the pKa-LogP plot. Interestingly, the incorporation of $\pi-\pi$ stacking via an introduction of aromatic rings also affect the pH responsive behavior of UPS block copolymers, as proved by the fact that the pKa values of PEO-*b*-P(C7A-*r*-MBA) copolymers did not fit in the linear correlation

227

of pKa-LogP that existed in PEO-*b*-PR block copolymers with only aliphatic alkyl substituents. The observed drastic decrease in pKa of PEO-*b*-P(MBA-*r*-C7A) copolymers as a function of hydrophobicity of PR segment repeating units suggested the stacking further lowered the pKa of UPS block copolymers. At the micelle state, the aromatic rings on PR segment were close to each other to form aromatic stacking. At the unimer state, the π–π stacking effect was significantly minimized because the aromatic rings were far from each other as a result of electrostatic repulsion between cationic ammonium groups. Incorporation of π–π stacking stabilized the nanoparticles and shifted the equilibrium to the direction of neutralization of protonated tertiary amines, corresponding to the decrease of pKa. These data also suggested π–π stacking as an additional strategy in fine-tuning the transition pH of the UPS block copolymers.
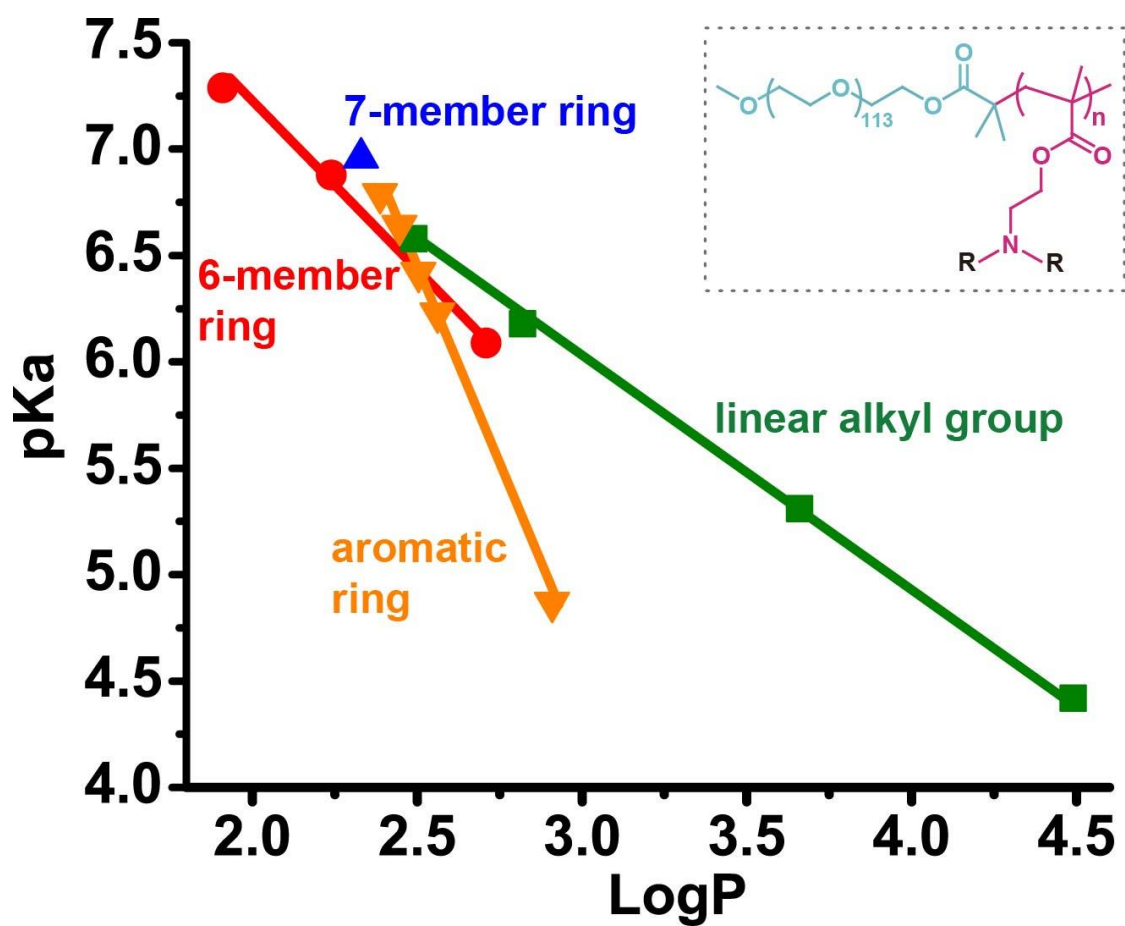
Figure 6.3.9. Correlation of the pKa values of PEO-b-PR block copolymers with the

hydrophobicity parameter (LogP) of PR segment repeating units.

6.3.5-Effect of hydrogen bonding and ionic bonds on pH responsive behavior

Self-organization of molecules via multiple intra- and intermolecular hydrogen bonds have served as an important strategy in the development of self-assembled structures[7,52]. Ions have been known to greatly affect multiple chemical and biological processes in aqueous solution because of their ability to interfere with hydrogen bonding networks and solvent polarity of water[53,54]. Early reports indicated the increase of NaCl concentration resulted in the decrease of LCST of thermo-responsive PNIPAM[53]. We first investigated whether a change of ion concentration could impact the pH response of UPS block copolymers. Here we used PEO-*b*-nPDPA block copolymer and NaCl as a model system. A series of pH titration experiments of PEO-*b*-nPDPA block copolymers in aqueous solution were performed in the presence of various NaCl concentrations (**Figure 6.3.10a**). As the NaCl concentration increased from 1 to 150 mM while keeping the polymer concentration the same, the apparent pKa values of PEO-*b*-PDPA block copolymers increased from 5.1 to 6.2 (**Figure 6.3.10a**). Quantitative correlation indicated an exponential increase of pKa as a function of NaCl concentration (**Figure 6.3.10d**).

Hofmeister anions have been well known for their effects on the solubility of proteins in aqueous solution, though the underlying mechanism remains elusive[55,56]. The Hofmeister anion series have been divided into water structure makers (kosmotropes) and breakers (chaotropes) with distinct effect on protein solubility. SO_4^{2-} and ClO_4^- anions are classical kosmotropes and chaotropes, respectively. Cl^- is considered as a neutral anion. We investigated whether ion species can have a different effect on the transition pH of UPS block copolymers. A series of pH titration experiments of PEO-*b*-nPDPA micelle solutions were performed using H_2SO_4 and $HClO_4$ in the presence of Na_2SO_4 and

NaClO$_4$ salts, respectively. As shown in **Figure 6.3.10b**, increase of SO$_4^{2-}$ concentration also resulted in the increase of pKa values, although not as notable as Cl$^-$. Most notably, increase of ClO$_4^-$ concentration resulted in the most drastic pKa increase (**Figure 6.3.10c**). Quantitative analysis showed that the pKa values of PEO-*b*-nPDPA were directly proportional to the logarithmic of ionic strength. The slopes of pKa values as a function of ion strength (dpKa/dLog[I]) for SO$_4^{2-}$, Cl$^-$ and ClO$_4^-$ were 0.16, 0.49 and 0.85, respectively (**Figure 6.3.10d**).

These data demonstrate that both the anion species and concentration had significant impact on the transition pH of PEO-*b*-PR block copolymers. Increase of salt concentration generally leads to the increase of transition pH of UPS block copolymers. The salt effect on the transition temperature of thermo-responsive nanostructures has been studied in multiple systems[12,46]. However, such effect on the responsive behavior of pH-sensitive nanomaterials is less investigated. As addressed by previous reports[53], interactions among anions, macromolecules and hydration water molecules all have potential impact on the stimuli-triggered supramolecular self-assembly behaviors of responsive nanomaterials.

We attempt to rationalize the effect of Hofmeister anions on the pH responsive behaviors of PEO-*b*-nPDPA by three plausible mechanisms (**Fig. 6.3.11**). First, the hydrated anions are capable of polarizing adjacent water molecules which may form hydrogen bonds to the nitrogen atoms on the tertiary amines. The polarization is likely to weaken the hydrogen bond and make the lone pair electron of amine nitrogen more accessible to protons. In this case, increase of salt concentration will favor the protonation of tertiary amines and lead to the increase of pKa values. Second, anions may

also interfere with the hydration of hydrophobic surfaces by water molecules by increasing the surface tension at the water/hydrophobic interface. This dehydration effect will lead to the decrease of pKa because of decreased solubility of hydrocarbons. The decrease of pKa as a result of salt-induced increase of surface tension can partly offset the H bond-induced pKa increase. The order of anions' ability in decreasing H-bond interactions between water and tertiary amines and strengthening surface tension is: $SO_4^{2-} > Cl^- > ClO_4^-$. Third, direct bonding between anions and cationic ammonium groups can neutralize the positive charges of protonated tertiary amines through formation of ion-pairs. The neutralization will shift the equilibrium to the direction of protonation of amines, corresponding to the increase of pKa. The ability to form stable ion pair interactions is much stronger with chaotropic anions (e.g., ClO_4^-, I^-) than kosmotropic anions (SO_4^{2-}). As we reported previously[54], the order of ion pair strength between ammonium groups and specific anions is: $ClO_4^- > Cl^- > SO_4^{2-}$, consistent with prior reports on the binding of anions to amides of PNIPAM[53].   We attribute that the ion pair interactions play a more dominant role than the other two factors for the observed influence of ClO_4^- anions on the pKa shift of PEO-*b*-nPDPA copolymer. PEO-*b*-PR block copolymers may serve as a good model system for the further delineation of solvation effect, hydrogen bonding and ionic interactions between Hofmeister anion series and synthetic macromolecules.
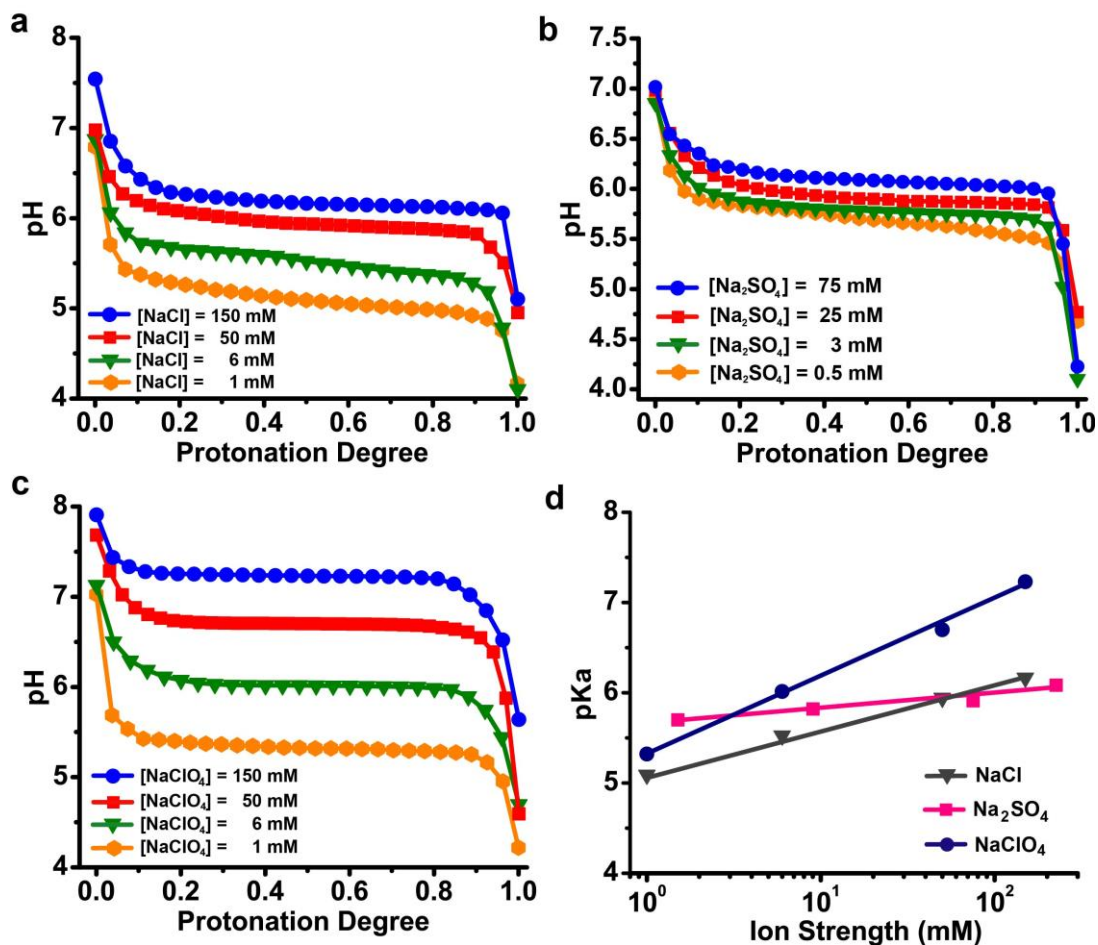
Figure 6.3.10. The effect of anion species and concentration on the transition pH of UPS block copolymers. pH titration curves of PEO-b-nPDPA polymers in the presence of NaCl (a), Na2SO4 (b) and NaClO4 (c) at different salt concentrations. (d) Quantitative analysis of pKa values of PEO-b-nPDPA block copolymers as a function of ionic strength of aqueous solution. Increase of salt concentrations generally leads to increase in pKa. ClO4- had the most impact whereas SO42- had the least effect on pKa increase.
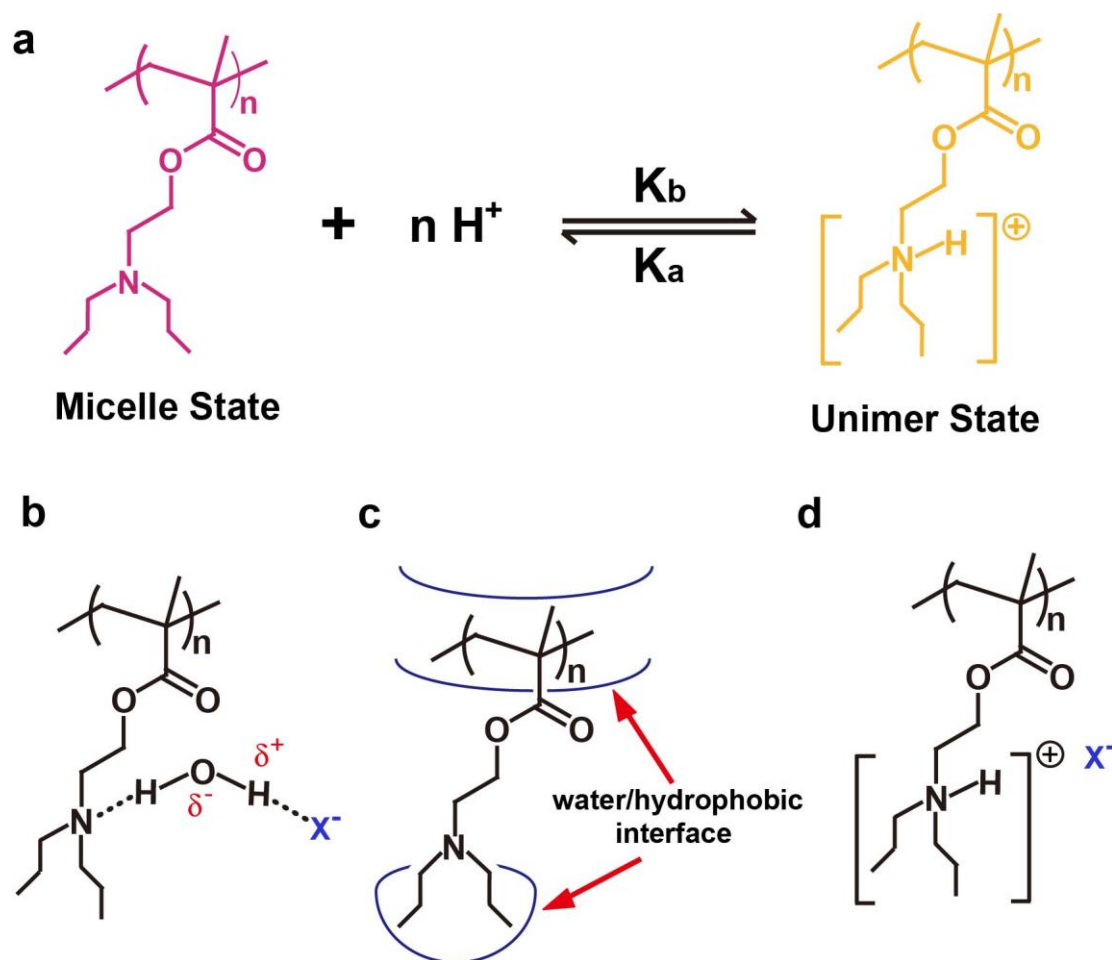
Figure 6.3.11. Interactions among anions, PEO-*b*-nPDPA block copolymers and hydration waters. (a) Structural illustration of PEO-*b*-nPDPA block copolymers in unimer or micelle state. For simplification, only hydrophobic PDPA segment was shown. (b) Hydrogen bonding of tertiary amines and hydration water molecules. The hydrogen bonding can be destabilized through polarization by anions, X^-. (c) The hydration of hydrophobic surfaces on PDPA segment is associated with surface tension at the water/ hydrophobic interface. The hydration of hydrophobic surfaces can also be modified by anions, X^-. (d) Direct ion pair interactions between protonated ammonium groups and chaotropic anions.

6.3.6-Effect of polymer concentration on pH responsive behavior

       The effect of ion species and concentration in affecting the pKa values of UPS block copolymers suggest the solution parameters also play a critical role in the pH-triggered supramolecular self-assembly process. Functional nanomaterials for biomedical applications are usually designed to transport therapeutic or diagnostic modalities from the point of administration to the site of action. One potential challenge is to assure that dose dilution in the journey from injected sites to the action sites, such as in blood, will not compromise the performance of the nanomaterials. To address this question, we investigated whether the polymer concentration, a key solution parameter of polymers in water, may affect the transition pH of UPS block copolymers. We used PEO-*b*-nPDPA as a representative system in this study. The critical micelle concentration (CMC) of PEO-*b*-nPDPA, measured in the 0.2 M sodium phosphate buffer at pH = 7.4, was around 1 g/ml (**Figure 6.3.12**). We performed all the experiments in the concentration range above the CMC.

       In the presence of low NaCl concentration (e.g.,1 mM), the pKa values of PEO-*b*-nPDPA increased significantly with the increase of polymer concentration (**Figure 6.3.13a and 6.3.13c**). More specifically, when the polymer concentration was increased from 0.2 to 10 mg/ml, pKa values jumped from 4.7 to 5.3 (**Figure 6.3.13a and 6.3.13c**). In the presence of 150 mM NaCl to mimic the physiological conditions, however, the pKa values of PEO-*b*-nPDPA copolymers stayed the same at 6.2 (**Figure 6.3.13b and 6.3.13c**). High salt concentration normalized the variations in pH transition from different polymer concentrations.

To further validate the observation, we conjugated a fluorescent dye, tetramethylrhodamine (TMR), to the hydrophobic PDPA segment to evaluate the fluorescent transition pH as a function of polymer concentration in the presence of 150 mM NaCl. At high pH, neutralization of ammonium groups lead to the formation of micelles and resulting quenching of fluorescence. At low pH, protonation of tertiary amines resulted in the dissociation of micelles into unimers, accompanied by resurrection of fluorescence. The fluorescence intensity of PEO-*b*-nPDPA-TMR copolymers was measured in a series of sodium phosphate buffers with different buffering pH. Plot of normalized fluorescence intensity as a function of pH suggested the fluorescence on/off transition pH stay almost the same (**Figure 6.3.13d and Figure 6.3.14**) over 100-fold change in polymer concentration (0.02 to 2 mg/ml), consistent with the above pH titration data. It is worth noting that the administrated concentration of UPS nanoprobes for *in vivo* tumor imaging studies varies from 0.5 to 2.0 mg/ml. The nanoprobe concentration in plasma 24 h after intravenous injection was approximately 0.02 to 0.1 mg/ml[39]. These data suggest that physiological level of salt concentration (i.e., 150 mM NaCl) may be critical to reduce variability from probe dilution and maintain the nanoprobe integrity in biological studies. Besides tumor imaging, the administered concentration of responsive polymers may vary significantly for different applications such as drug delivery or biosensing. Elucidation of polymer concentration-transition pH relationships will help predict and improve the performance of pH responsive nanomaterials.
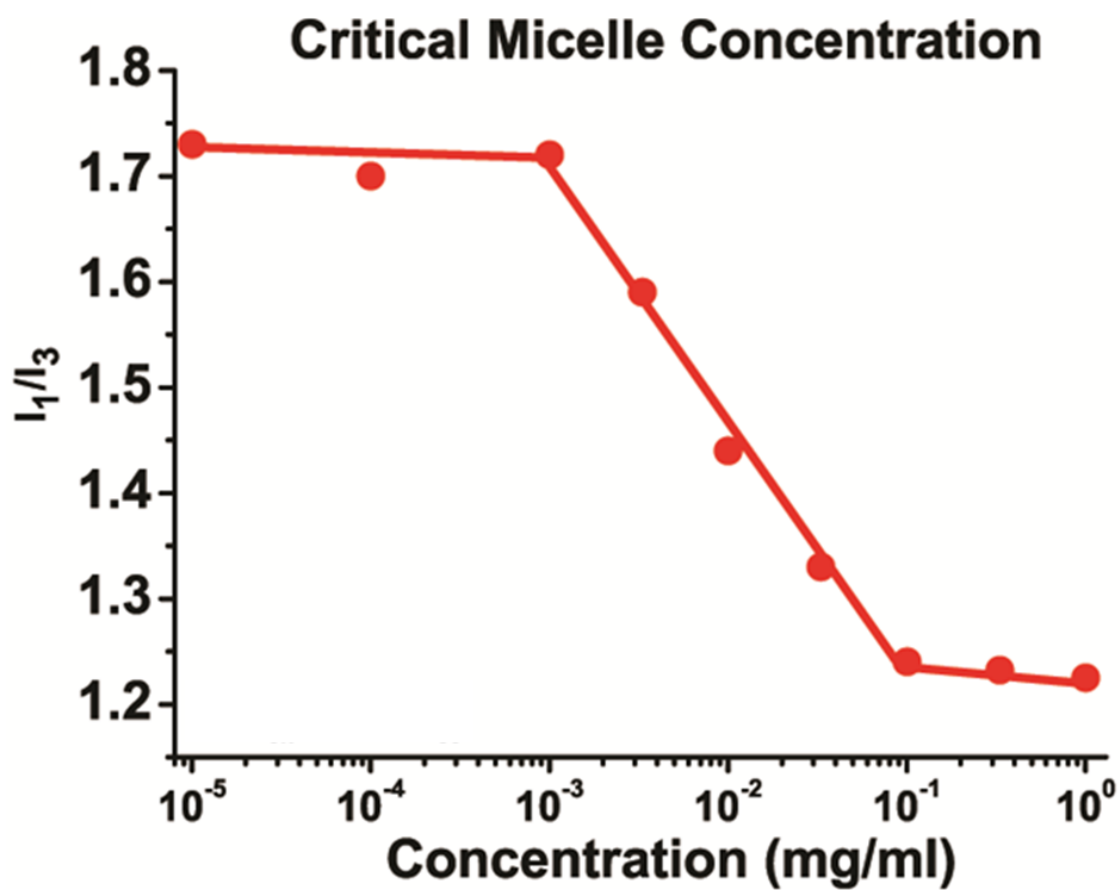
Figure 6.3.12. The critical micelle concentration (CMC) of PEO_{114}-*b*-$PDPA_{60}$ block copolymer determined from the measurements of UV absorption of pyrene in polymer solution.
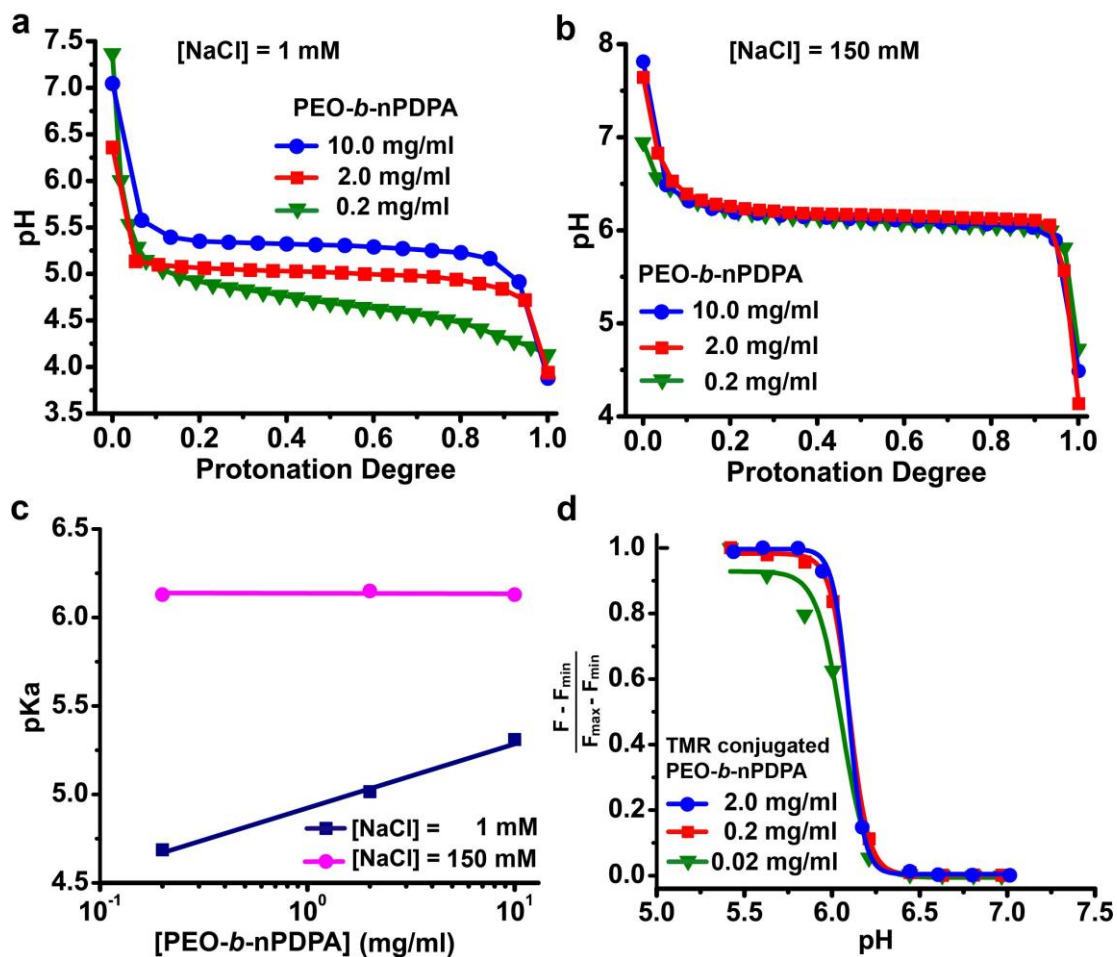
Figure 6.3.13. The effect of polymer concentration on the transition pH of UPS block copolymers. pH titration curves of PEO-*b*-nPDPA block copolymers in the presence of 1 mM NaCl (a) and physiological level of 150 mM NaCl (b). (c) Quantification of pKa values as a function of PEO-*b*-nPDPA concentration. (d) Normalized fluorescence intensity of TMR-conjugated PEO-*b*-nPDPA block copolymers at different polymer concentration. In the presence of high NaCl concentration, the pKa and fluorescent transition pH stayed approximately the same over 100-fold change in polymer concentration.
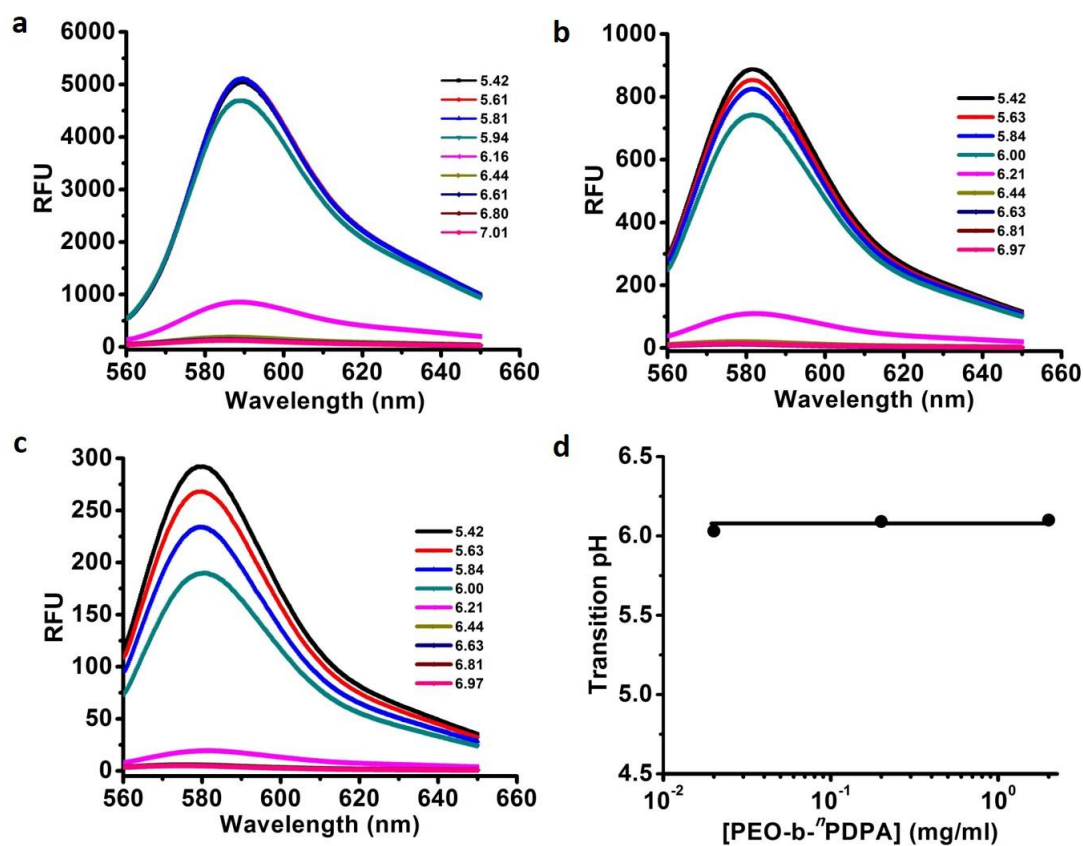
Figure 6.3.14. Fluorescence intensity of PEO-*b*-nPDPA-TMR block copolymers at different polymer concentrations in sodium phosphate buffer at pH=7.4: (a) 2.0 mg/ml; (b) 0.2 mg/ml; (c) 0.02 mg/ml. (d) Fluorescence on/off transition pH of TMR conjugated PEO-*b*-nPDPA block copolymers at different polymer concentrations (0.02 to 2.0 mg/ml).

6.3.7-Discussion

In this study, we systematically investigated a multitude of non-covalent interactions that impacted the pH responsive behavior and resulting supramolecular self-assembly of amphiphilic UPS block copolymers. Increase of both hydrophobic interactions and $\pi-\pi$ stacking effect stabilized the micelles, which favors the neutralization of protonated tertiary amines resulting in the decrease of pKa values. Formation of ion pairs between protonated ammonium groups and chaotropic anions drove the protonation of tertiary amines and led to the increase of pKa values of UPS block copolymers. A series of key parameters that affected the responsive behaviors of UPS block copolymers such as chain length, hydrophobicity of substituents of tertiary amines and salt concentration were identified and evaluated, which help establish useful guidelines for rational development of nanomaterials based pH sensors with predictable and tunable transition pH. Without NaCl, transition pH of UPS block copolymers was polymer concentration-dependent. In the presence of 150 mM NaCl, the transition pH of UPS block copolymers remain unchanged over 100-fold range in polymer concentration. Ensuring the performance of pH sensors across a wide dose range is crucial for biomedical applications such as molecular imaging and drug delivery.

Introduction of stimuli-responsive moieties has become a general strategy in the design of responsive, functional nanomaterials. Temperature-sensitive materials usually contain amide bonds surrounded by hydrophobic groups (e.g., PNIPAM[17], elastin-like peptides[46]). pH responsive materials are composed of amines[57], carboxylic acids[58], or pH-sensitive labile bonds[38]. Disulfide bonds are used to synthesize redox-responsive systems[59]. These stimuli-triggered supramolecular self-assembly sensors arise from a

multitude of molecular interactions that exist ubiquitously in various natural and synthetic macromolecular systems. Self-assembly based on selective and precise control of non-covalent interactions provides powerful and versatile tools for the development of complicated nanostructures at the molecular level. The development of functional nanomaterials has a growing emphasis on identification and optimization of specific design parameters crucial to performance. The key parameters that affect the pH-triggered self-assembly from this study may also serve as useful guideline for tailoring the structure of other stimuli-responsive systems. Moreover, different responsive groups can be introduced in the same polymeric structures for the development of multi-responsive nanomaterials[60].

6.4-Reference

1   Toretsky, J. A. & Wright, P. E. Assemblages: functional units formed by cellular phase separation. *J Cell Biol* **206**, 579-588 (2014).

2   Weber, S. C. & Brangwynne, C. P. Getting RNA and protein in phase. *Cell* **149**, 1188-1191 (2012).

3   Frey, S., Richter, R. P. & Görlich, D. FG-rich repeats of nuclear pore proteins form a three-dimensional meshwork with hydrogel-like properties. *Science* **314**, 815-817 (2006).

4   Stuart, M. A. C. *et al.* Emerging applications of stimuli-responsive polymer materials. *Nature materials* **9**, 101-113 (2010).

5   Dill, K. A. & MacCallum, J. L. The protein-folding problem, 50 years on. *Science* **338**, 1042-1046 (2012).

6   Habchi, J., Tompa, P., Longhi, S. & Uversky, V. N. Introducing protein intrinsic disorder. *Chemical reviews* **114**, 6561-6588 (2014).

7   Stoffelen, C. & Huskens, J. Soft Supramolecular Nanoparticles by Noncovalent and Host–Guest Interactions. *Small* **12**, 96-119 (2016).

8   Stupp, S. I. & Palmer, L. C. Supramolecular chemistry and self-assembly in organic materials design. *Chemistry of Materials* **26**, 507-518 (2013).

9   Mattia, E. & Otto, S. Supramolecular systems chemistry. *Nature nanotechnology* **10**, 111-119 (2015).

10   Whitesides, G., Mathias, J. & Seto, C. Molecular self-assembly and nanochemistry: a chemical strategy for the synthesis of nanostructures. *Science* **254**, 1312-1319, doi:10.1126/science.1962191 (1991).

11   Whitesides, G. M. & Grzybowski, B. Self-assembly at all scales. *Science* **295**, 2418-2421 (2002).

12   Jin, R., Wu, G., Li, Z., Mirkin, C. A. & Schatz, G. C. What controls the melting properties of DNA-linked gold nanoparticle assemblies? *Journal of the American Chemical Society* **125**, 1643-1654 (2003).

13   Pohl, F. M. & Jovin, T. M. Salt-induced co-operative conformational change of a synthetic DNA: equilibrium and kinetic studies with poly (dG-dC). *Journal of molecular biology* **67**, 375-396 (1972).

14   Storhoff, J. J. *et al.* What controls the optical properties of DNA-linked gold nanoparticle assemblies? *Journal of the American Chemical Society* **122**, 4640-4650 (2000).

15   Burnett, J. C. & Rossi, J. J. RNA-based therapeutics: current progress and future prospects. *Chemistry & biology* **19**, 60-71 (2012).

16   Fujishige, S., Kubota, K. & Ando, I. Phase transition of aqueous solutions of poly (N-isopropylacrylamide) and poly (N-isopropylmethacrylamide). *Journal of Physical Chemistry* **93**, 3311-3313 (1989).

17   Schild, H. G. Poly (N-isopropylacrylamide): experiment, theory and application. *Progress in polymer science* **17**, 163-249 (1992).

18   Roy, D., Brooks, W. L. & Sumerlin, B. S. New directions in thermoresponsive polymers. *Chemical Society Reviews* **42**, 7214-7243 (2013).

19   Ito, D. & Kubota, K. Solution properties and thermal behavior of poly (N-n-propylacrylamide) in water. *Macromolecules* **30**, 7828-7834 (1997).

20   Feil, H., Bae, Y. H., Feijen, J. & Kim, S. W. Effect of comonomer hydrophilicity and ionization on the lower critical solution temperature of N-isopropylacrylamide copolymers. *Macromolecules* **26**, 2496-2500 (1993).

21   Idziak, I., Avoce, D., Lessard, D., Gravel, D. & Zhu, X. Thermosensitivity of aqueous solutions of poly (N, N-diethylacrylamide). *Macromolecules* **32**, 1260-1263 (1999).

22   Cao, Y., Zhu, X., Luo, J. & Liu, H. Effects of substitution groups on the RAFT polymerization of N-alkylacrylamides in the preparation of thermosensitive block copolymers. *Macromolecules* **40**, 6481-6488 (2007).

23   Ieong, N. S. *et al.* Polymers with molecular weight dependent LCSTs are essential for cooperative behaviour. *Polymer Chemistry* **3**, 794-799 (2012).

24   Ieong, N. S. *et al.* The missing lactam-thermoresponsive and biocompatible poly (N-vinylpiperidone) polymers by xanthate-mediated RAFT polymerization. *Macromolecules* **44**, 886-893 (2011).

25   Weaver, J. *et al.* Stimulus-responsive water-soluble polymers based on 2-hydroxyethyl methacrylate. *Macromolecules* **37**, 2395-2403 (2004).

26   Phillips, D. J. & Gibson, M. I. Degradable thermoresponsive polymers which display redox-responsive LCST Behaviour. *Chemical Communications* **48**, 1054-1056 (2012).

27   Chen, S., Zhang, Y., Wang, K., Zhou, H. & Zhang, W. N-Ester-substituted polyacrylamides with a tunable lower critical solution temperature (LCST): the N-ester-substitute dependent thermoresponse. *Polymer Chemistry* **7**, 3509-3519 (2016).

28   Edwards, E. W., Chanana, M., Wang, D. & Möhwald, H. Stimuli- Responsive Reversible Transport of Nanoparticles Across Water/Oil Interfaces. *Angewandte Chemie International Edition* **47**, 320-323 (2008).

29   Boyer, C., Whittaker, M. R., Luzon, M. & Davis, T. P. Design and synthesis of dual thermoresponsive and antifouling hybrid polymer/gold nanoparticles. *Macromolecules* **42**, 6917-6926 (2009).

30   Shan, J., Zhao, Y., Granqvist, N. & Tenhu, H. Thermoresponsive properties of N-isopropylacrylamide oligomer brushes grafted to gold nanoparticles: effects of molar mass and gold core size. *Macromolecules* **42**, 2696-2701 (2009).

31   Gibson, M. I., Paripovic, D. & Klok, H. A. Size- Dependent LCST Transitions of Polymer- Coated Gold Nanoparticles: Cooperative Aggregation and Surface Assembly. *Advanced Materials* **22**, 4721-4725 (2010).

32   Heller, J., Penhale, D. & Helwing, R. Preparation of polyacetals by the reaction of divinyl ethers and polyols. *Journal of Polymer Science: Polymer Letters Edition* **18**, 293-297 (1980).

33   Gillies, E. R. & Fréchet, J. M. A new approach towards acid sensitive copolymer micelles for drug delivery. *Chemical Communications*, 1640-1641 (2003).

34   Lee, E. S., Shin, H. J., Na, K. & Bae, Y. H. Poly (L-histidine)–PEG block copolymer micelles and pH-induced destabilization. *Journal of Controlled Release* **90**, 363-374 (2003).

35   Roy, K., Mao, H.-Q., Huang, S.-K. & Leong, K. W. Oral gene delivery with chitosan–DNA nanoparticles generates immunologic protection in a murine model of peanut allergy. *Nature medicine* **5**, 387-391 (1999).

36   Choi, Y. H. *et al.* Polyethylene glycol-grafted poly-L-lysine as polymeric gene carrier. *Journal of controlled release* **54**, 39-48 (1998).

37   Boussif, O. *et al.* A versatile vector for gene and oligonucleotide transfer into cells in culture and in vivo: polyethylenimine. *Proceedings of the National Academy of Sciences* **92**, 7297-7301 (1995).

38   Pang, X. *et al.* pH-responsive polymer–drug conjugates: Design and progress. *Journal of Controlled Release* **222**, 116-129 (2016).

39   Wang, Y. *et al.* A nanoparticle-based strategy for the imaging of a broad range of tumours by nonlinear amplification of microenvironment signals. *Nature materials* **13**, 204-212 (2014).

40   Wang, C. *et al.* A nanobuffer reporter library for fine-scale imaging and perturbation of endocytic organelles. *Nature communications* **6** (2015).

41   Nasongkla, N. *et al.* Multifunctional polymeric micelles as cancer-targeted, MRI-ultrasensitive drug delivery systems. *Nano letters* **6**, 2427-2430 (2006).

42   Zhou, K. *et al.* Tunable, Ultrasensitive pH- Responsive Nanoparticles Targeting Specific Endocytic Organelles in Living Cells. *Angewandte Chemie International Edition* **50**, 6109-6114 (2011).

43   Po, H. N. & Senozan, N. The Henderson-Hasselbalch equation: its history and limitations. *Journal of Chemical Education* **78**, 1499 (2001).

44   Chen, S., Zhang, Y., Wang, K., Zhou, H. & Zhang, W. N-Ester-substituted polyacrylamides with a tunable lower critical solution temperature (LCST): the N-ester-substitute dependent thermoresponse. *Polymer Chemistry* (2016).

45   Wang, K., Song, Z., Liu, C. & Zhang, W. RAFT synthesis of triply responsive poly [N-[2-(dialkylamino) ethyl] acrylamide] s and their N-substitute determined response. *Polymer Chemistry* (2016).

46   Quiroz, F. G. & Chilkoti, A. Sequence heuristics to encode phase behaviour in intrinsically disordered protein polymers. *Nature materials* (2015).

47   Li, S., Su, Y., Dan, M. & Zhang, W. Thermo-responsive ABA triblock copolymer of PVEA-b-PNIPAM-b-PVEA showing solvent-tunable LCST in a methanol–water mixture. *Polymer Chemistry* **5**, 1219-1228 (2014).

48   Schilli, C. M. *et al.* A New Double-Responsive Block Copolymer Synthesized via RAFT Polymerization: Poly (N-isopropylacrylamide)-b lock-poly (acrylic acid). *Macromolecules* **37**, 7861-7866 (2004).

49   Zhang, W., Shi, L., Wu, K. & An, Y. Thermoresponsive micellization of poly (ethylene glycol)-b-poly (N-isopropylacrylamide) in water. *Macromolecules* **38**, 5743-5747 (2005).

50   Jin, J. *et al.* Self- Assembly of Uniform Spherical Aggregates of Magnetic Nanoparticles through π–π Interactions. *Angewandte Chemie International Edition* **40**, 2135-2138 (2001).

51   Zang, L., Che, Y. & Moore, J. S. One-dimensional self-assembly of planar π-conjugated molecules: adaptable building blocks for organic nanodevices. *Accounts of chemical research* **41**, 1596-1608 (2008).

52   Sherrington, D. C. & Taskinen, K. A. Self-assembly in synthetic macromolecular systems via multiple hydrogen bonding interactions. *Chemical Society Reviews* **30**, 83-93 (2001).

53   Zhang, Y., Furyk, S., Bergbreiter, D. E. & Cremer, P. S. Specific ion effects on the water solubility of macromolecules: PNIPAM and the Hofmeister series. *Journal of the American Chemical Society* **127**, 14505-14510 (2005).

54   Li, Y. *et al.* Chaotropic- Anion- Induced Supramolecular Self- Assembly of Ionic Polymeric Micelles. *Angewandte Chemie International Edition* **53**, 8074-8078 (2014).

55   Jungwirth, P. & Cremer, P. S. Beyond hofmeister. *Nature chemistry* **6**, 261-263 (2014).

56   Gurau, M. C. *et al.* On the mechanism of the Hofmeister effect. *Journal of the American Chemical Society* **126**, 10522-10523 (2004).

57   Bae, Y., Fukushima, S., Harada, A. & Kataoka, K. Design of environment-sensitive supramolecular assemblies for intracellular drug delivery: Polymeric micelles that are responsive to intracellular pH change. *Angewandte Chemie International Edition* **42**, 4640-4643 (2003).

58   Schmaljohann, D. Thermo-and pH-responsive polymers in drug delivery. *Advanced drug delivery reviews* **58**, 1655-1670 (2006).

59   Nakahata, M., Takashima, Y., Yamaguchi, H. & Harada, A. Redox-responsive self-healing materials formed from host–guest polymers. *Nature communications* **2**, 511 (2011).

60   Zhuang, J., Gordon, M. R., Ventura, J., Li, L. & Thayumanavan, S. Multi-stimuli responsive macromolecules and their assemblies. *Chemical Society Reviews* **42**, 7421-7435 (2013).

CHAPTER SEVEN - Specific Anion-Induced Micellization

7.1-Introduction

Salt is known to affect the solubility and self-assembly of biological macromolecules such as proteins[1]. The structure and dynamics of water in the vicinity of different solutes have been studied for decades. One of the most challenging phenomena is the Hofmeister effect[2,3]. Frank Hofmeister observed that different salts have different efficiencies in salting-out proteins, while some salts have no effect[3]. The ions are divided into structure makers (kosmotropes) and structure breakers (chaotropes), with the former decreasing and the latter increasing the solubility of proteins in aqueous solution[4].

They also play a critical role in tuning the physiochemical properties of synthetic polymers. Paul Cremer group have been working on the specific ion effect on the thermos-responsive behavior of PINPAM over the last decade. They found that increasing the concentration of NaCl lead to the decrease of LCST. They then expand the ion effect on PNIPAM to the entire Hofmeister series[5]. Basically, the LCST decrease upon the increase of salt concentration and the ability of a particular anion to lower the LCST generally followed the Hofmeister series (**Figure 7.1.1**)[6]. Mechanistic investigation indicate that strongly and weakly hydrated anions affect the LCST of PNIPAM via different mechanisms. The chaotropic ions lower the LCST via a surface-tension effect, which causes hydrophobic collapse. For kosmotropes, the surface-tension effects and the polarization of hydration water molecules are both at work. The "salting-in" or "salting-out" effects associated with the Hofmeister trend is usually more pronounced for anions than cations. In another study, Zhang et al found that the effect of Hofmesiter anions on the LCST of PINPAM was molecular weight-dependent[7].
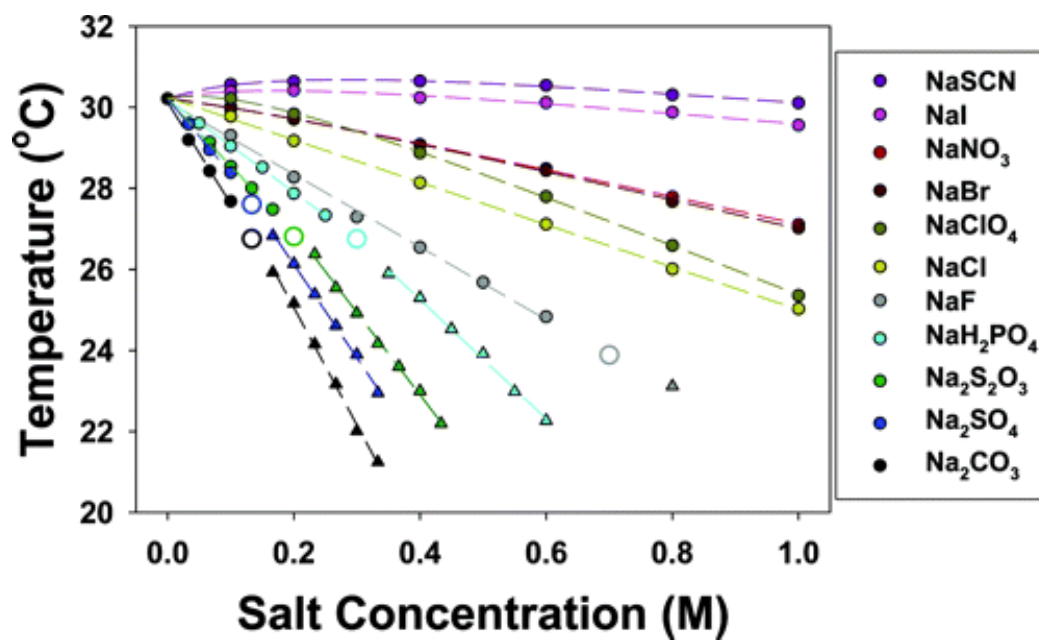
Figure 7.1.1. The LCST values of PNIPAM measured for sodium salts at concentrations from 0 to 1.0 M[6].

In this study, we report a serendipitous discovery of chaotropic anion-induced micellization of protonated PEO-b-PR copolymers at pH below pH$_t$ (right panel in Figure 1). Surprisingly, an anti-Hofmeister trend was observed, where chaotropic anions resulted in micellization but not the kosmotropic anions[8-10], in contrary to their effects in protein aggregation.

7.2-Materials and methods

7.2.1-Syntheses of PEO-b-(PR-r-TMR/Cy5) block copolymers

AMA monomer was incorporated in the copolymers for the conjugation of dyes. Synthesis of PEO-*b*-(PR-r-AMA) copolymers followed the procedure described above. Three primary amino groups were introduced into each polymer chain by controlling the feeding ratio of AMA monomer to the initiator (ratio = 3). In a representative procedure, PEO-*b*-(PR-r-AMA) (50mg) was dissolved in 2 mL DMF. Then the NHS-ester (2.0 equivalence for TMR-NHS and 1.0 equivalence for Cy5-NHS) was added. After overnight reaction, the copolymers were purified by preparative gel permeation chromatography (PLgel Prep 10 m 10E3 Å 300×250 columns by Varian, THF as eluent at 5 mL/min) to remove the free dye molecules. The produced PEO-*b*-(PR-*r*-Dye) copolymers were lyophilized and kept at -20 ℃ during storage. It is important to note that the dye would undergo both Hetero FRET as well self-quenching when block copolymers self-assembled into micelles. So the dye conjugation number for each polymer chain is important for the FRET experiment. In our experiment, we controlled the conjugation number of TMR and Cy5 to be 2 and 1 per polymer chain, respectively.

7.2.2-Preparation of micelle nanoparticles

For each copolymer, the stock solution of micelles was prepared following a solvent evaporation method as previously reported[11]. In the example of PEO-*b*-(PDPA-r-TMR) micelle solution, 20 mg of the copolymer was first dissolved in 1.0 mL THF and then added into 8 mL deionized water dropwise under sonication. The THF was removed through ultrafiltration with (100 KD) membrane for five times. Then

251

deionized water was added to adjust the polymer concentration to 5 mg/mL as a stock solution. PEO-*b*-PDMA stock solution could be made by directly dissolve copolymer in deionized water.

Micelle solution samples for FRET experiment were prepared in a similar method. Preparation of PEO-*b*-(PDPA-TMR/Cy5) samples was described as a representative procedure. First, 0.1 mL PDPA-TMR and 0.1 mL PDPA-Cy5 stock solution was added to 1.8 mL deionized water. Then 1.8 μL of 1.0 M HCl was added to dissolve the water-insoluble block copolymer and adjust solution pH to 4. The Cl^- from HCl in the starting sample was < 2 mM, which could be neglected for their ability to perturb micellization according to our experimental results.

7.2.3-FRET experiment

The fluorescence emission spectra were obtained on a Hitachi fluorometer (F-7500 model). The samples were excited at 545 nm, and the emission spectra were collected from 560 to 750 nm. The FRET experiment for PEO-*b*-PDPA self-assembly behavior with the introduction of different anions followed similar procedure. ClO_4^- was used as an example: 0.2 μL of 10 M $NaClO_4$ solution was added to 2.0 mL 0.5 mg/mL dye-conjugated PDPA (PDPA-TMR/PDPA-Cy5 = 1:1) solution at pH=4 and adjusted the ClO_4^- concentration to 1 mM. Then small volume of 10 M $NaClO_4$ solution was added incrementally to increase the ClO_4^- concentration to 3.2, 5.6, 10 mM. After 10 mM, solid $NaClO_4$ was added to the solution to increase the ClO_4^- concentration to avoid sample dilution. The total volume of added $NaClO_4$ is less than 2 μL, which can be

neglected compared to total volume of 2 mL. The fluorescence emission spectrum was collected after 4 min vortex following each addition of $NaClO_4$.

7.2.4-TEM and DLS characterization

Samples for TEM and DLS analyses were prepared following procedures described above. The transition pH of PEO-*b*-PDPA was 6.2. First, 0.1 mL PDPA-TMR and 0.1 mL PDPA-Cy5 stock solution was added to 1.6 mL deionized water. Solid $NaClO_4$ and NaCl were then added to the solution and dissolved after vortex. HCl and NaOH solution (1 M) were used to adjust the solution pH to 5.0 and 7.4. Deionized water was added to adjust the total volume to 2 mL. The morphology and size of nanoparticles were characterized by transmission electron microscopy (TEM, JEOL 1200EX model). Hydrodynamic diameter (D_h) was determined by dynamic light scattering (DLS, Malvern MicroV Model, He-Ne Laser, $\lambda=632$ nm).

7.2.5-Anion Competition Experiment

The preparation of micelle samples followed the same procedures described in FRET experiment. Solid NaCl and Na_2SO_4 powders were dissolved in the aqueous solution to achieve the initial anion concentration. The initial concentrations of Cl^- were 0, 50, 100, 200, 500, 1000 and 2000 mM. The initial concentrations of SO_4^{2-} were 0, 25, 50, 100, 200 and 500 mM. The fluorescence emission spectra were collected 4 mins after vortex following the addition of $NaClO_4$. We fit the results with a sigmoidal curve. The half maximal FRET efficiency concentration of perchlorate was defined as FC_{50} to quantify the competition ability of Cl^- and SO_4^{2-}.

7.2.6-ClO$_4^-$ -induced micelle self-assembly of PEO-b-PR copolymers

A series of PEO-*b*-PR copolymers with different alkyl side chains were used in this study. The preparation of micelle samples followed that described in the FRET experiment section. In this series of experiments, we buffered the ionic strength of the solution by using a 100 mM of NaCl concentration. This was used to minimize the ionic strength contribution from NaClO$_4$ since more hydrophobic PEO-*b*-PR copolymer (e.g. **5**) requires less concentration to induce micelle self-assembly. After the experiments, the FRET efficiency was calculated as previously described in the FRET section.

7.3-Results and discussions

7.3.1-Chaotropic anion-induced micellization

We first established a fluorescence energy resonance transfer (FRET) method to investigate the micelle self-assembly process. FRET is highly sensitive in detecting conformational and phase transitions of polymers/proteins because the energy transfer efficiency is inversely proportional to the sixth power of the donor-acceptor distance.[12,13] In our method, we conjugated block copolymers (**1-5** in **Figure 7.3.1** and **7.3.2**)[14,15] with either a donor or acceptor dye. Initially we chose PEO-*b*-poly(dipropylaminoethyl methacrylate) (**3**, pH_t=6.2) as a model copolymer, and tetramethyl rhodamine (TMR, $\lambda_{ex}/\lambda_{em}$= 545/580 nm)/Cy5 ($\lambda_{ex}/\lambda_{em}$ = 647/666 nm) as donor/acceptor, respectively.[16,17]

At pH 4, the tertiary amines in **3** (pH_t = 6.2) were pronated and the resulting copolymers were soluble in water as dispersed cationic unimers. No FRET effect was observed due to the large distance between the unimers (therefore TMR and Cy5) in solution. Addition of chaotropic anions (e.g. ClO_4^-, SCN^- and I^-) resulted in the decrease of fluorescence intensity from TMR and increase of emission intensity of Cy5 (**Figure 7.3.3**), indicating the formation of polymeric micelles. Micelle formation was hypothesized to bring TMR and Cy5 to close proximity within the micelle core, thereby dramatically increasing FRET efficiency (**Figure 7.3.4b**). In contrary, kosmotropic anions (e.g. SO_4^{2-}, $H_2PO_4^-$) did not lead to any FRET transfer (**Figure 7.3.5**) even at concentrations close to their solubility limits (**Figure 7.3.6**).

The FRET effects were quantified to compare different anions in their abilities to induce micellization (**Figure 7.3.4c**). FRET efficiency was normalized as $(F_A/F_D)/(F_A/F_D)_{max}$, where F_A and F_D were the fluorescence intensity of TMR and Cy5 at different anion concentrations, respectively; $(F_A/F_D)_{max}$ was the maximum value of F_A/F_D

(3.3) at high ClO_4^- concentrations. FRET efficiency was plotted as a function of concentration for different anions. Results displayed an anti-Hofmeister trend where chaotropic anions were able to induce unimer association (i.e. micellization) whereas the kosmotropic anions were not (**Figure 7.3.4c**). This is in contrary to the classical Hofmeister effect in protein solubilisation, where kosmotropic ions are known to induce protein aggregation in water but not the chaotropic ions.[2,18]

Copolymer **3** displayed different detection sensitivity toward the chaotropic anions. Data show FRET sensitivity followed the order of $ClO_4^- > SCN^- > I^- > NO_3^-$. We define FC_{50} as the anion concentration that the FRET efficiency was increased to 50%. The values of FC_{50} were 11, 68 and 304 mM for ClO_4^-, SCN^-, and I^-, respectively. For NO_3^-, only weak FRET effect was observed at its saturation concentration (~3 M). More detailed examination shows that only 3-fold ClO_4^- concentration change (i.e. from 6 to 18 mM, **Figure 7.3.4c**) was necessary to increase FRET efficiency from 10% to 90%. This narrowed concentration dependence suggests an increased cooperative response similar to the ultra-pH response as reported previously[19-22].
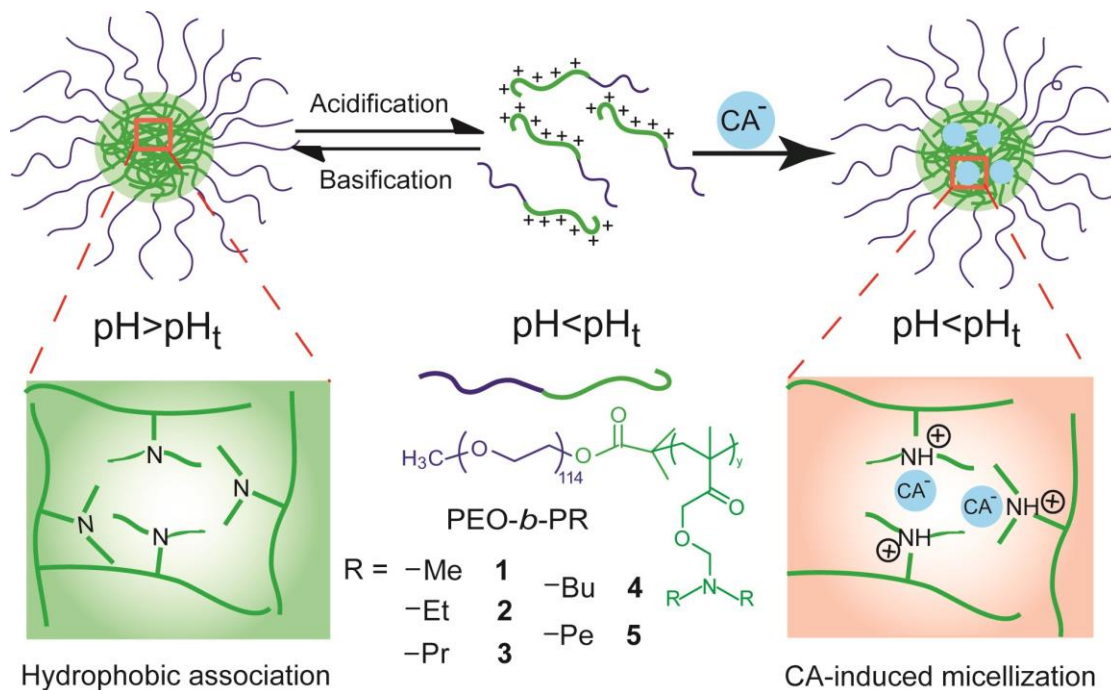
Figure 7.3.1. Self-assembly of ionizable polymeric micelles by two independent mechanisms. The left panel shows the induction of micellization by pH increase, where the PR segments become neutralized and hydrophobic to drive micelle formation. Surprisingly, addition of chaotropic ions (CA, such as ClO4-) at low pH also leads to micellization with ammonium PR segments (right panel). Structures of a series of PEO-b-PR copolymers (1-5) with different hydrophobic side chains are shown in the inset.

Copolymer	PR name	Yield (%)	$M_{w,GPC}$ $(\times 10^{-4} D)^a$	$M_{n,GPC}$ $(\times 10^{-4} D)^a$	PDI^a	Repeating units In the PR block	$M_{n,1H\,NMR}$ $(\times 10^{-4} D)^b$
1	PDMA	86	2.28	1.87	1.22	92	1.99
2	PDEA	87	2.42	1.97	1.23	88	2.17
3	PDPA	88	2.45	2.06	1.19	80	2.25
4	PDBA	78	2.84	2.32	1.22	72	2.47
5	PD5A	72	3.11	2.58	1.20	82	2.75

[a] Number-average (M_n), weight-average molecular weight (M_w) and polydispersity index (PDI) (PDI=M_w/M_n) were determined by GPC using THF as the eluent. [b] Determined by ^{1}H-NMR.

Figure 7.3.2. Characterization of PEO-b-(PR-r-AMA) block copolymers.

Figure 7.3.3. Fluorescence spectra of FRET polymer pairs of PEO-*b*-P(DPA-*r*-TMR)/ PEO-*b*-P(DPA-*r*-Cy5) at different concentrations of chaotropic anions.   The samples were excited at λ_{ex}=545nm and emission spectra were collected from 560-750 nm. All the experiments were conducted at pH=4, below the transition pH of PEO-*b*-PDPA (pH_t=6.2).
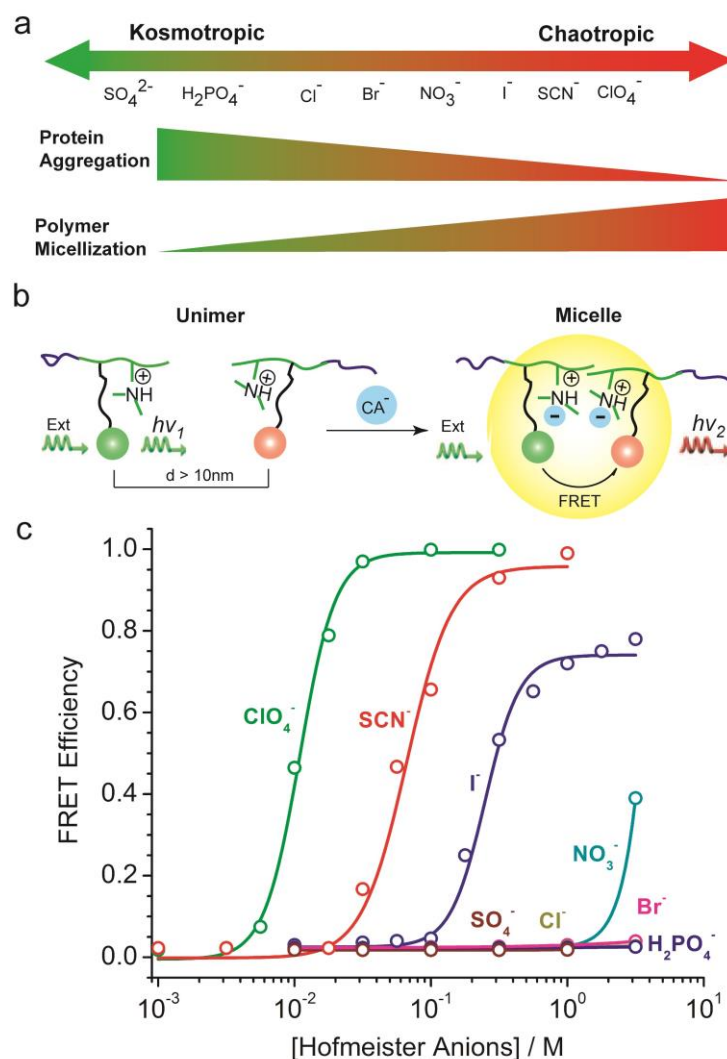
Figure 7.3.4. (a) Chaotropic anions induce micelle self-assembly from PEO-*b*-PR copolymers with protonated PR segment, a reversed "salt-out" effect from their abilities to solubilize proteins (salt-in). (b) Illustration of FRET design to investigate CA-induced micelle self-assembly. Addition of CA results in micelle formation and efficient energy transfer from donor (TMR) to acceptor (Cy5) dyes. (c) Chaotropic anion-induced micelle self-assembly showing the anti-Hofmeister trend. Kosmotropic anions, known to cause protein aggregation, did not induce micelle self-assembly.
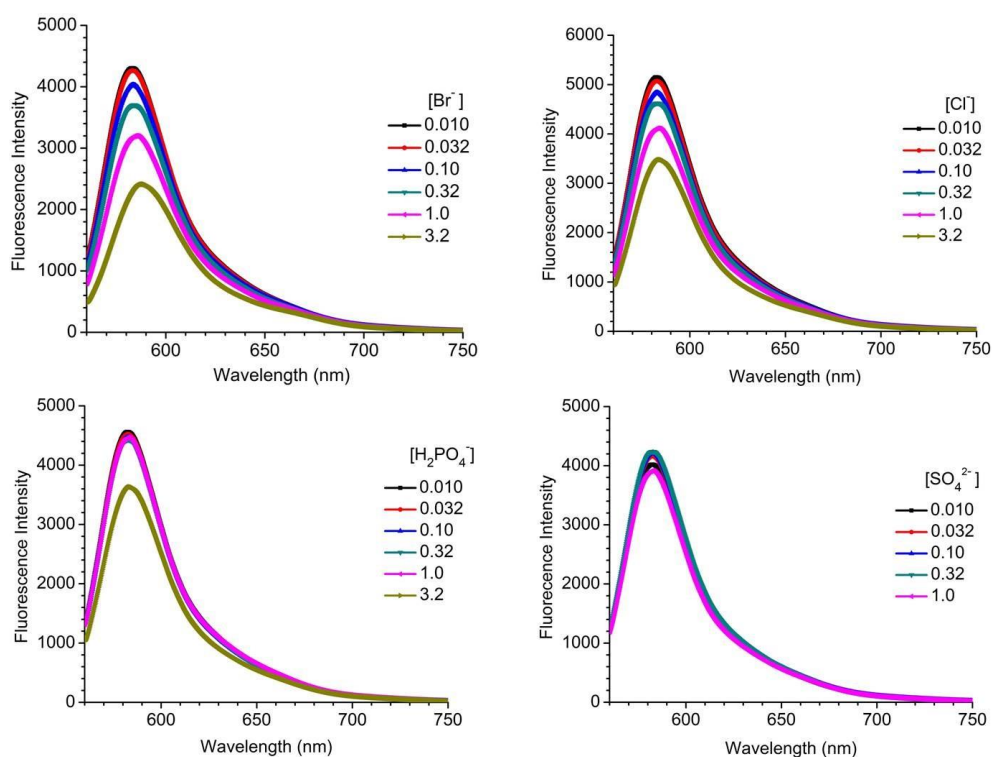
Figure 7.3.5. Fluorescence spectra of FRET polymer pairs of PEO-b-P(DPA-r-TMR)/

PEO-b-P(DPA-r-Cy5) at different concentrations of kosmotropic and borderline

anions.   The samples were excited at λex=545nm and emission spectra were collected

from 560-750 nm. All the experiments were conducted at pH=4, below the transition

pH of PEO-b-PDPA (pHt=6.2).

Salt	Saturated solubility (M)	Salt	Saturated solubility (M)
$NaClO_4$	17.2	NaBr	8.8
NaSCN	17.1	NaCl	6.1
NaI	11.9	NaH_2PO_4	7.2
$NaNO_3$	5.0	Na_2SO_4	1.4

Solubility data were obtained from solubility handbook by Khaled Gharib from open sources:
[1] http:/ / srdata. nist. gov/ solubility/ index. aspx
[2] http:/ / food. oregonstate. edu/ learn/ sugar. html
[3] http:/ / www. kayelaby. npl. co. uk/
[4] http:/ / chemfinder. cambridgesoft. com

Figure 7.3.6. Saturated solubility of sodium salts of Hofmeister anions.

7.3.2-TEM validation of ClO$_4^-$ -induced micellization

        To further confirm chaotropic anion-induced micellization, we employed transmission electron microscopy (TEM) and dynamic light scattering (DLS) to investigate the changes in morphology and hydrodynamic- diameter during micelle transition, respectively. We used chloride anion (Cl$^-$) as a negative control. In the presence of 50 mM Cl$^-$, copolymer **3** stayed as a unimer at pH 5.0 (below its pH$_t$ at 6.2, **Figure 7.3.7a**). In contrast, copolymer **3** self-assembled into spherical micelles when Cl$^-$ was replaced with ClO$_4^-$ (**Figure 7.3.7b**). DLS analyses showed increase of hydrodynamic diameters from 7 ± 2 to 26 ± 3 nm when the anions were changed from Cl$^-$ to ClO$_4^-$, respectively (**Figure 7.3.7**). This size increase reflects the transition of copolymer **3** from unimer state to the micelle state, consistent with the FRET and TEM data. At pH 7.4, copolymer **3** was present as spherical micelles with hydrodynamic diameters at 27 ± 2 and 28 ± 3 nm in the presence of Cl$^-$ and ClO$_4^-$ anions, respectively (**Figure 7.3.8** and **Figure 7.3.9**). For non-ionizable amphiphilic block copolymers such as PEO-*b*-poly(D,L-lactic acid) (PEO-*b*-PLA), neither pH change nor ClO$_4^-$ addition had any effects on the micelle state (**Figure 7.3.10**).
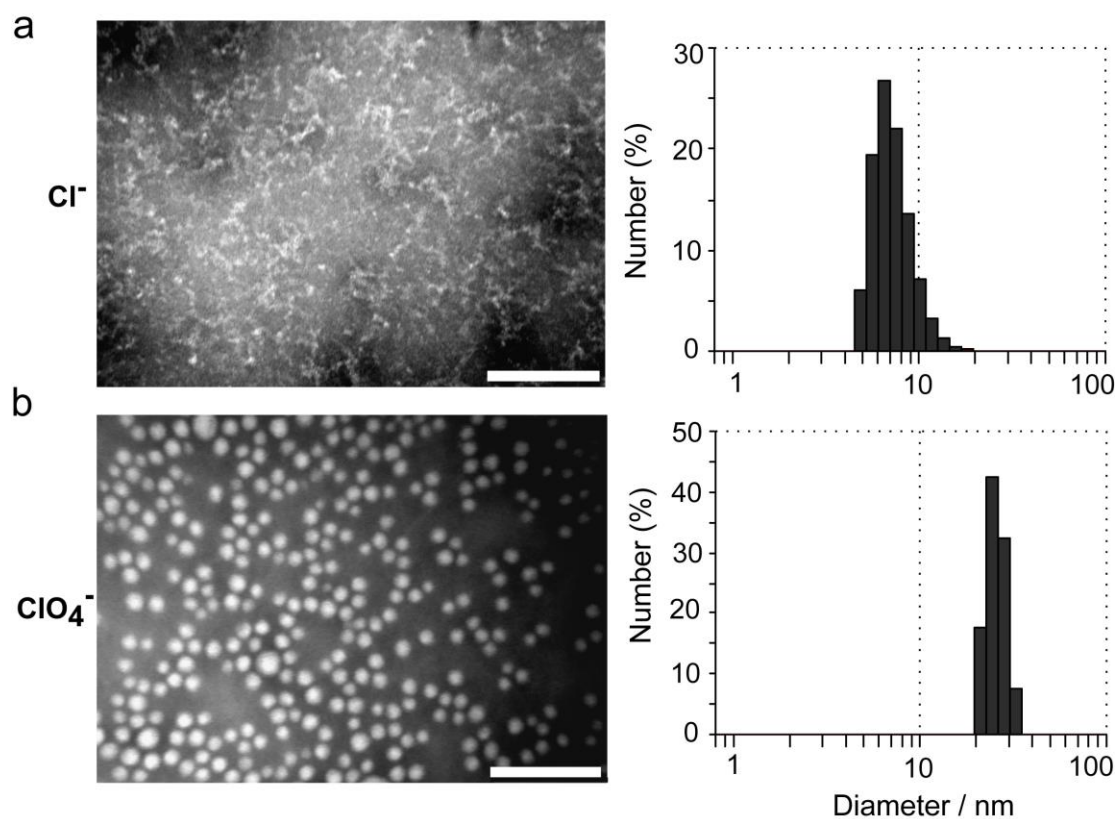
Figure 7.3.7. TEM and DLS analyses of micelle transition of copolymer 3 in the presence of Cl$^-$ (a) and ClO$_4^-$ anions (b).   Concentrations of both anions were controlled at 50 mM (pH = 5.0).   The scale bars are 100 nm in the TEM images.
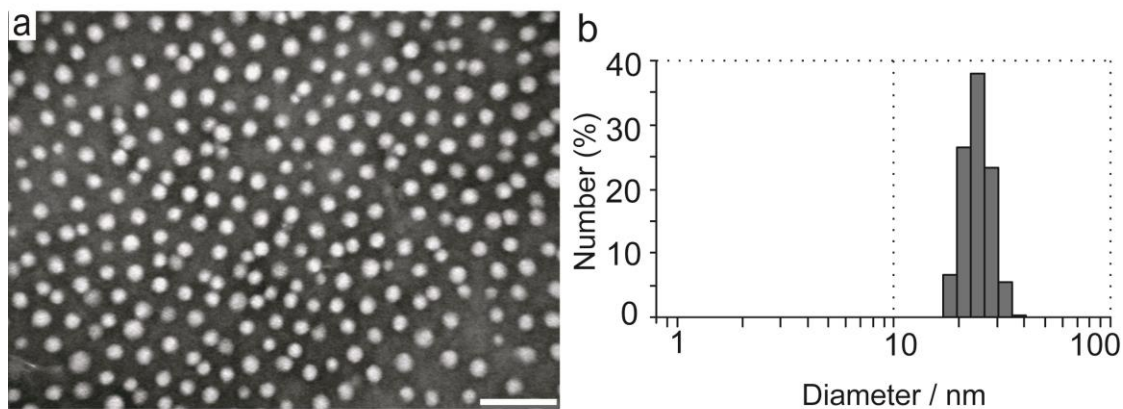
Figure 7.3.8. (a) TEM and (b) DLS analyses of micelle morphology and hydrodynamic diameter of copolymer **3** micelles in the presence of Cl⁻ (50 mM) at pH 7.4. The scale bar is 100 nm in the TEM image.
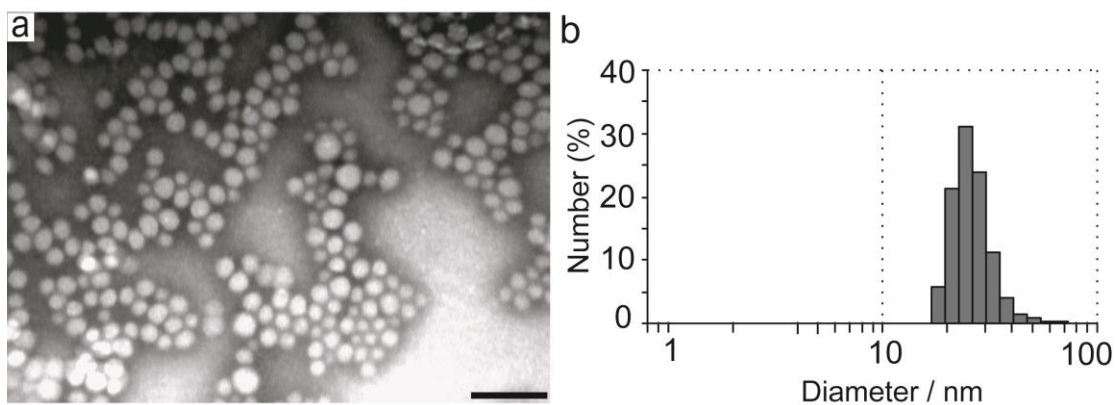
Figure 7.3.9. (a) TEM and (b) DLS analyses of micelle morphology and hydrodynamic diameter of copolymer **3** micelles in the presence of ClO_4^- (50 mM) at pH 7.4. The scale bar is 100 nm in the TEM image.
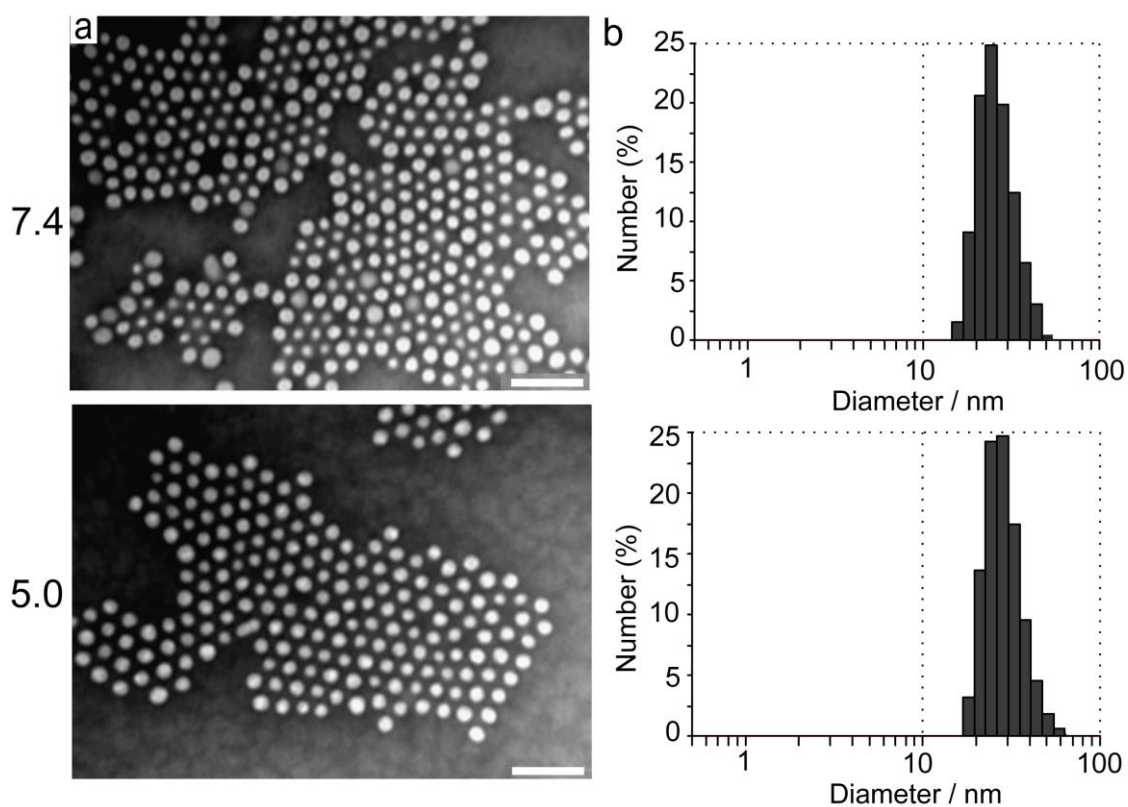
Figure 7.3.10. (a) TEM and (b) DLS analyses of micelle morphology and hydrodynamic diameters of PEO-*b*-PLA copolymer in the presence of ClO_4^- (50 mM) at pH 7.4 and 5.0. The scale bars are 100 nm in the TEM images.

7.3.3-Competing effect in the anion-induced micellization

We then studied the chaotropic anion-induced self-assembly in the presence of competing kosmotropic or borderline anions. In this experiment, copolymer **3** was dissolved at pH 4 with different initial concentrations of competing SO_4^{2-} or Cl^-. Then chaotropic anions ClO_4^- were added to induce micellization (**Figure 7.3.11 - 7.3.14**). **Figure 7.3.15a** showed the representative example of FRET efficiency as a function of ClO_4^- concentration. Addition of SO_4^{2-} anions was able to decrease the sensitivity of ClO_4^- in micelle induction. We quantified the FC_{50} values to evaluate the effect of competing anions (**Figure 7.3.15b**). We observed an interesting bell curve as a function of the ionic strength of the competing anions. At low ionic strength (<0.1 M), addition of competing anions decreased the ability of ClO_4^- to induce micelle formation, consistent with their competition with the ammounium groups of the PR segment. At high ionic strength (>0.5 M) of SO_4^{2-} or Cl^-, however, we observed an enhancement of ClO_4^- induced self-assembly. We attribute this effect to the more ordered bulk water structures at high kosmotropic ion concentrations, which makes the hydrophobic association during micelle self-assembly more favorable.
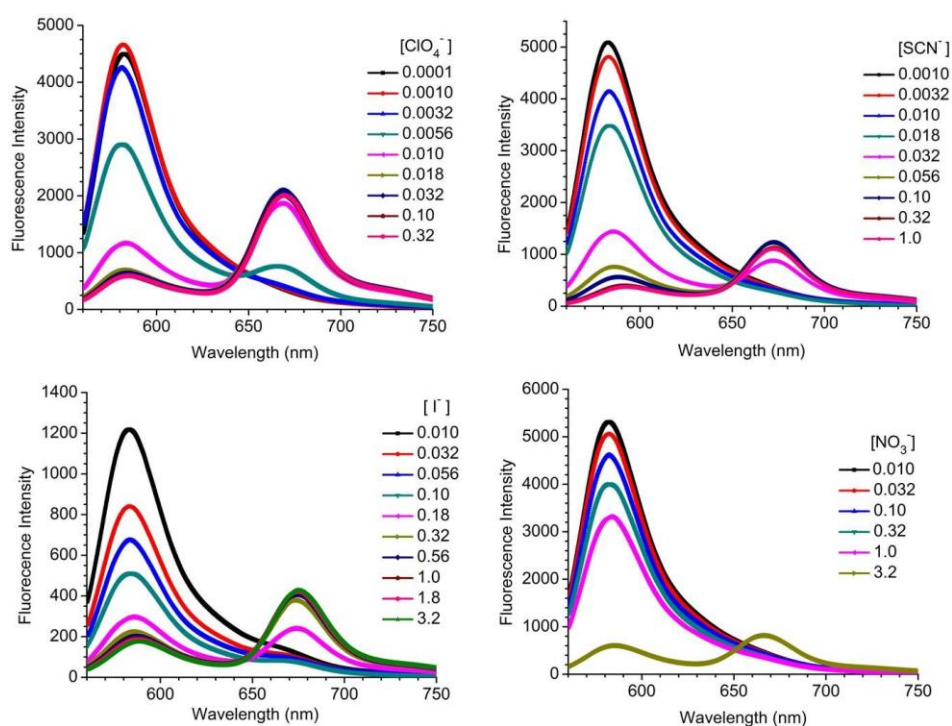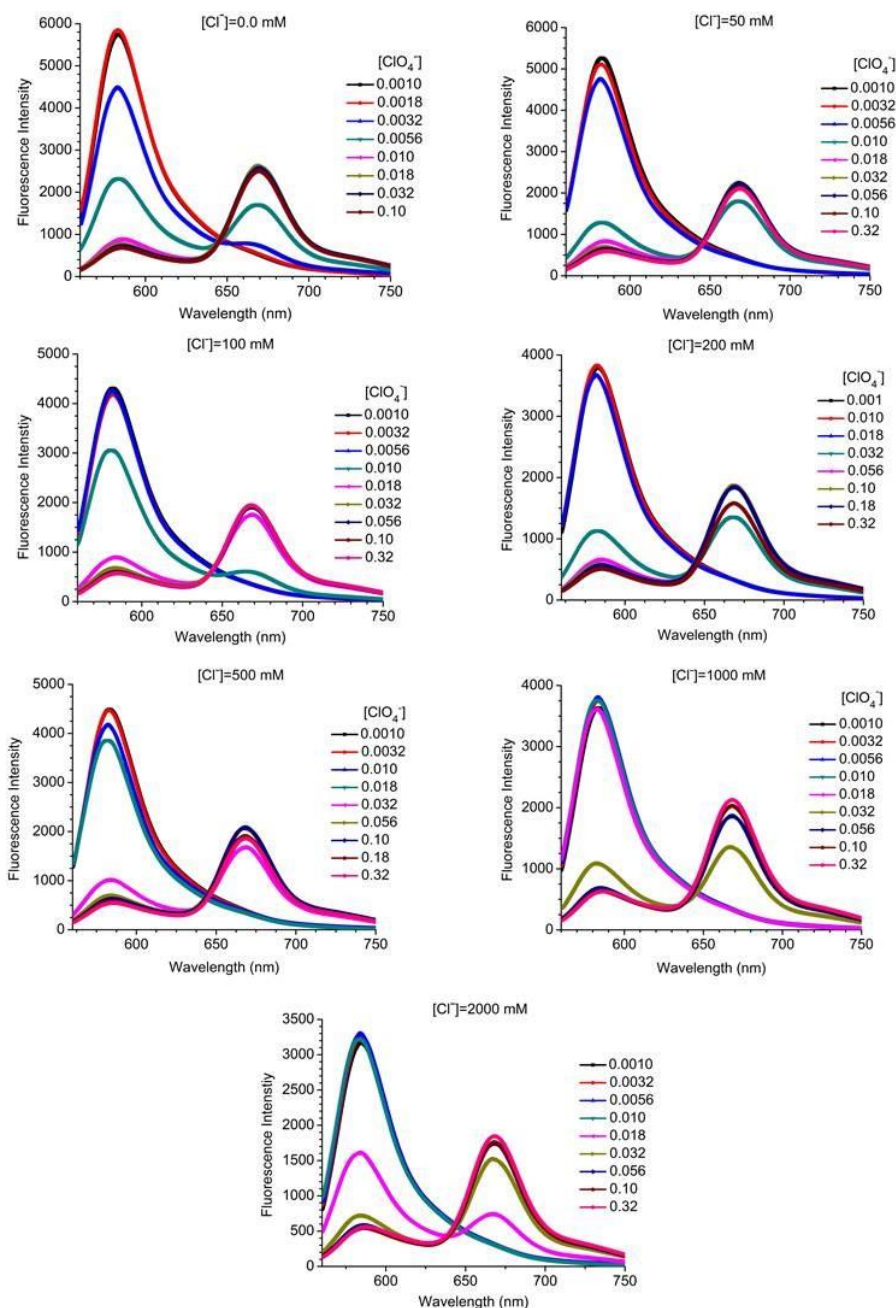
Figure 7.3.11. Fluorescence spectra of FRET polymer pairs of PEO-*b*-P(DPA-*r*-TMR) /PEO-*b*-P(DPA-*r*-Cy5) at different initial concentration of Cl⁻ (0-2,000 mM). Different concentrations of ClO_4^- (in M) anions were added to induce micelle formation. The samples were excited at λ_{ex}=545nm and emission spectra were collected from 560-750 nm. All the experiments were conducted at pH=4, below the transition pH of PEO-*b*-PDPA (pH$_t$=6.2).
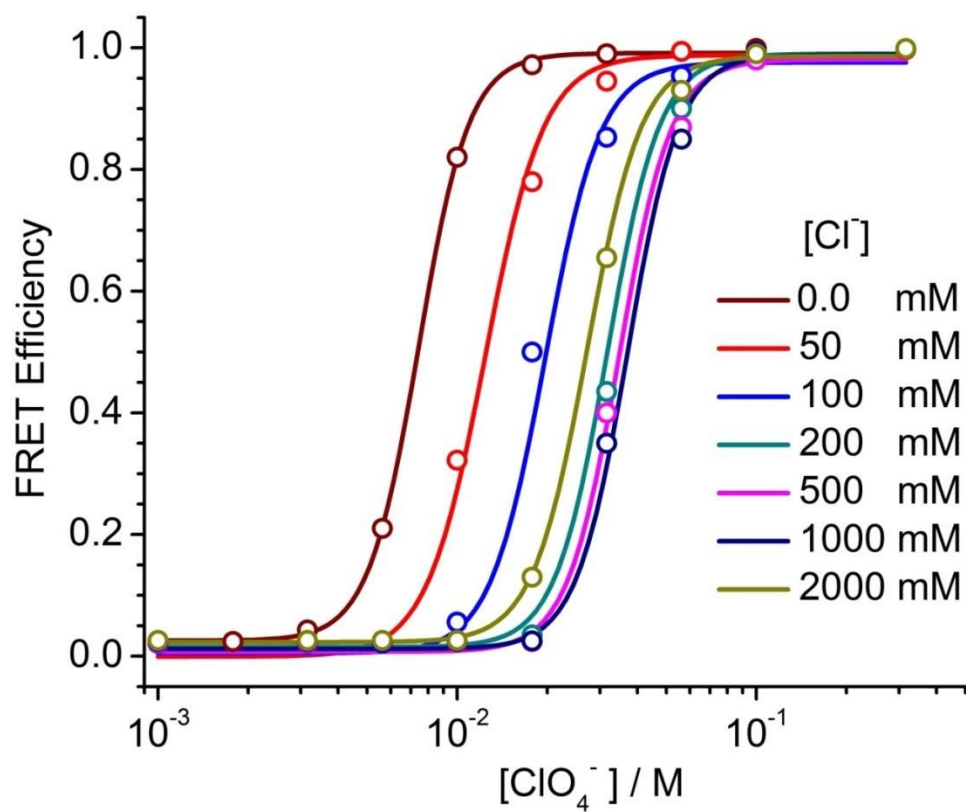
Figure 7.3.12. FRET transfer efficiency as a function of ClO_4^- concentration at different competing Cl^- concentrations (0-2,000 mM).
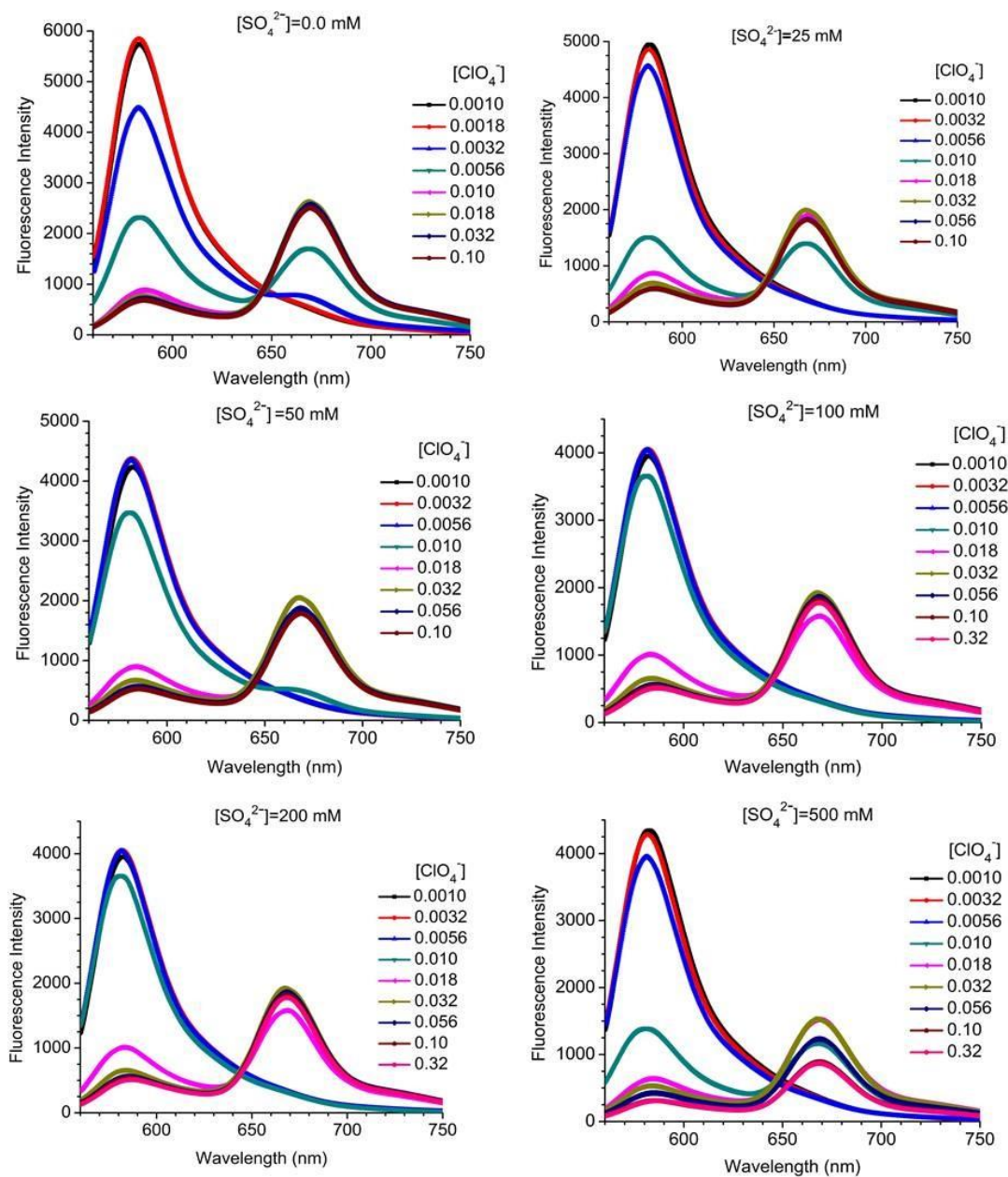
Figure 7.3.13. Fluorescence spectra of FRET polymer pairs of PEO-*b*-P(DPA-*r*-TMR)/PEO-*b*-P(DPA-*r*-Cy5) at different initial concentration of SO_4^{2-} (0-500 mM). Different concentrations of ClO_4^- (in M) anions were added to induce micelle formation. The samples were excited at λ_{ex}=545nm and emission spectra were collected from 560-750 nm. All the experiments were conducted at pH=4, below the transition pH of PEO-*b*-PDPA (pH$_t$=6.2).
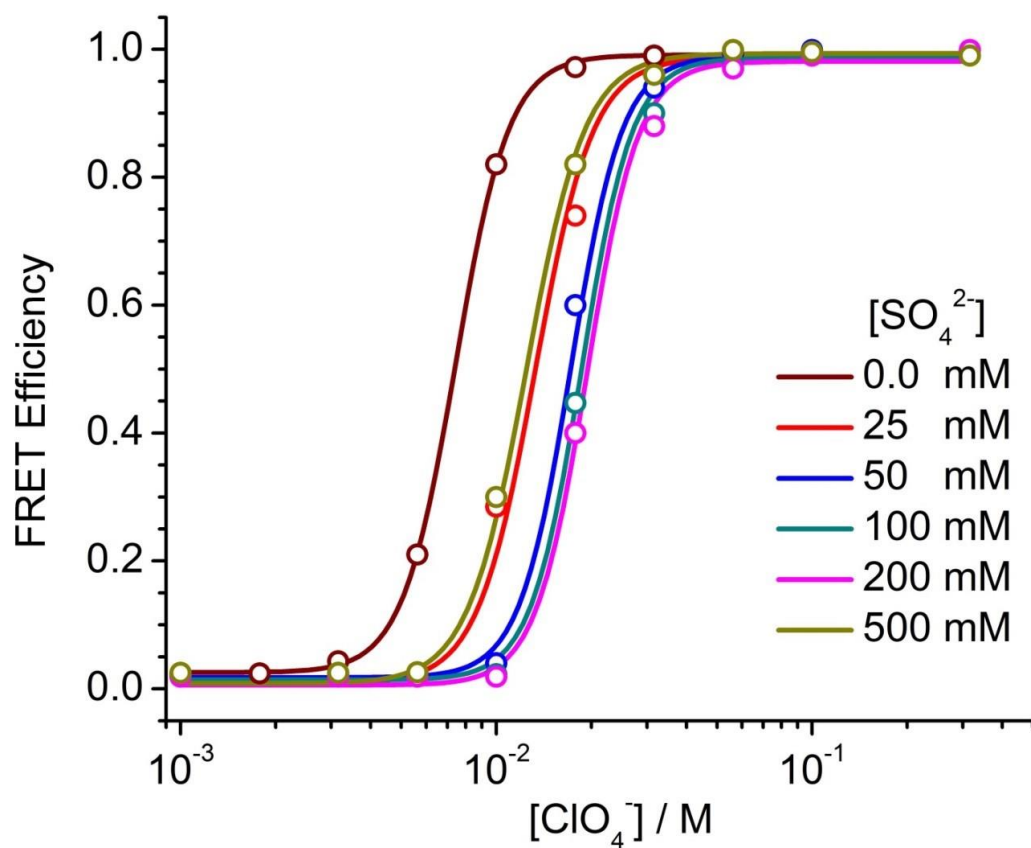
Figure 7.3.14. FRET transfer efficiency as a function of ClO_4^- concentration at different competing SO_4^{2-} concentrations (0-500 mM).
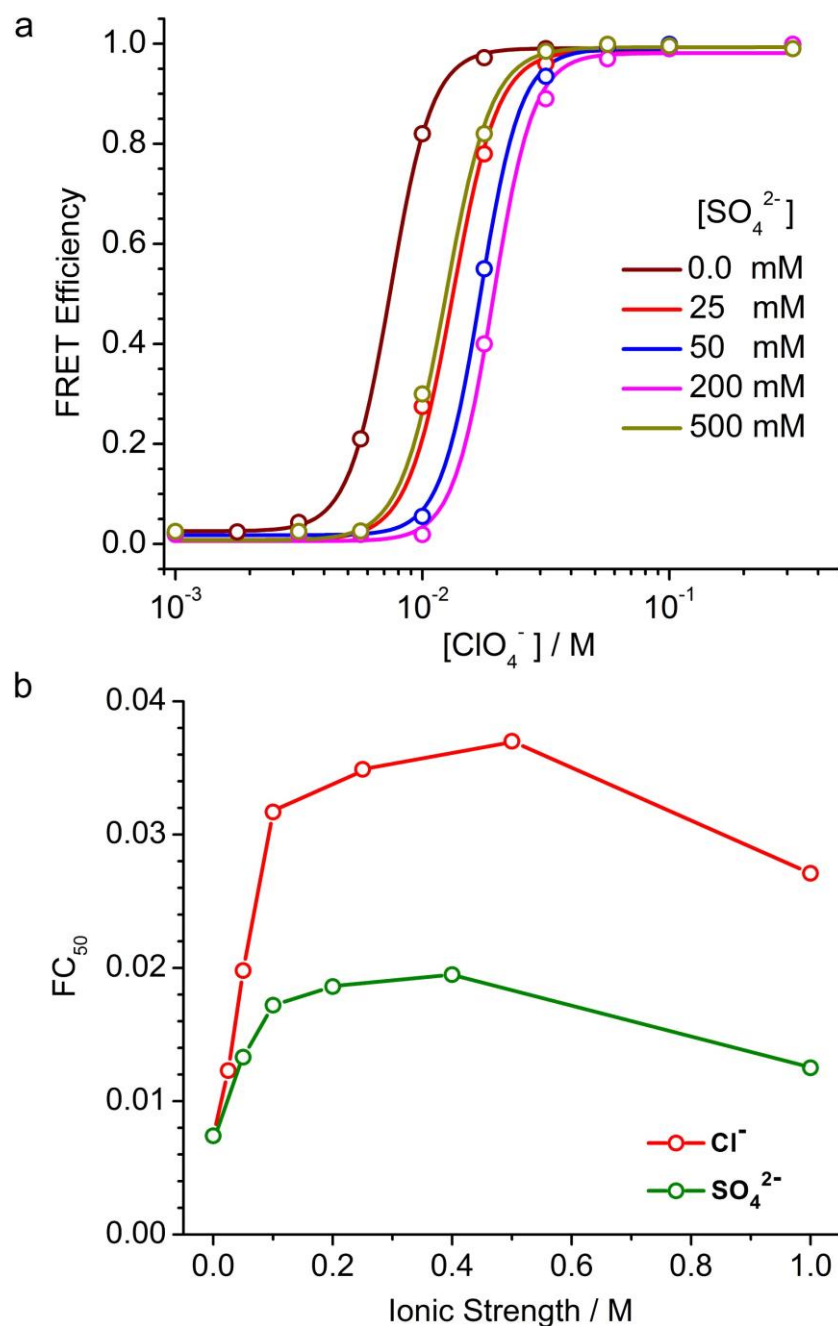
Figure 7.3.15. (a) ClO_4^--induced self-assembly of copolymer **3** in the presence of different concentrations of competing SO_4^{2-} anions. (b) The FRET efficiency (FC_{50}) from ClO_4^--induced self-assembly as a function of ionic strength of competing Cl^- and SO_4^{2-} anions. The solution pH was controlled at 4 in these studies.

7.3.4-Anion-induced micellizaiton also showed hydrophobicity dependence

We then investigated the effect of hydrophobic strength of PR segment on chaotropic anion-induced micelleization (**Figure 7.3.16a**).   We synthesized a series of PEO-*b*-PR copolymers bearing different alkyl chain lenths from methyl to pentyl groups on the tertiary amines.   Results show a clear dependence of ClO_4^--induced self-assembly on the hydrophobicity of the PR segment (**Figure 7.3.17**). With the least hydrophobic side chains (i.e. methyl), no micellization was observed even at the highest ClO_4^- concentrations (1 M).   In contrary, the most hydrophobic side chains (pentyl in **5**) resulted in the most sensitive micellization induction by ClO_4^-.   The FC_{50} values were 2, 4, 35, 134 mM when the side chains were pentyl, butyl, propyl and ethyl groups, respectively (**Figure 7.3.16a**).

Results from the above studies illustrate a highly unusual micelle self-assembly process from block copolymers with teriary ammonium groups induced by chaotropic anions.   There are several unique features in the current nanosystem: first, chaotropic anions were able to form stable ion pairs with positively charged ammonium groups in the hydrophobic micelle core environment. Assuming majority of the ammonium groups are in the ionized state, this translates into ~60,000 ion pairs per micelle nanoparticle (calculation based on 800 polymer chains per micelle[8b] and 70-80 repeating units of amino group-containing monomers per polymer chain).   Second, only chaotropic anions were able to induce micelle formation whereas the kosmotropic (SO_4^{2-}) and borderline (Cl^-) anions did not pertain this ability.   This trend appears to counter that in classical protein solublization studies. Third, the ability of chaotropic anions to induce micellization appears to show positive cooperativity similar to ultra-pH sensitive

response. Our previous study showed fluorescence activation (10% to 90% response) occured within 0.25 pH unit (or 2-fold in $[H^+]$). Current study show FRET transfer happened in a span of 3-fold $[ClO_4^-]$ change. Lastly, competition experiments with kosmotropic and borderline anions illustrated a bell curve behavior, which points to the complexity and subtle nature of the micelle self-assembly process in the current system.

We built an empirical model (**Figure 7.3.16b**) to depict the factors that contribute to the micelle self-assembly process. We hypothesize that the hydrophobic interactions from increasing alkyl chain lengths provide the dominant driving force for micelle formation. This is supported by the lack of micelle formaton when the side chain of the tertiary amines is methyl group (as indicated by the dashed line on the left arm of Figure 5b). Similarly, neutralized copolymer **1** did not form micelles at pH above its pH_t.[2d] Meanwhile, anions also play a critical role in micellization. Kosmotropic anions, which are known to have strong hydration shells and weak polarization characteristics,[23] are energetically less favoralbe in the formation of ion pairs[24] and stabilization of ion pairs in the hydrophobic core. Chaotropic anions, with their strong polarizability and low energy cost at removing hydration sheath[25,26], allows for formation of stable ion pairs in the hydrophobic micelle core. Further studies are necessary to elucidate the thermodynamic contributions in enthalpy and entropy to the overall free energy of micelle phase transitions by the chaotropic anions.
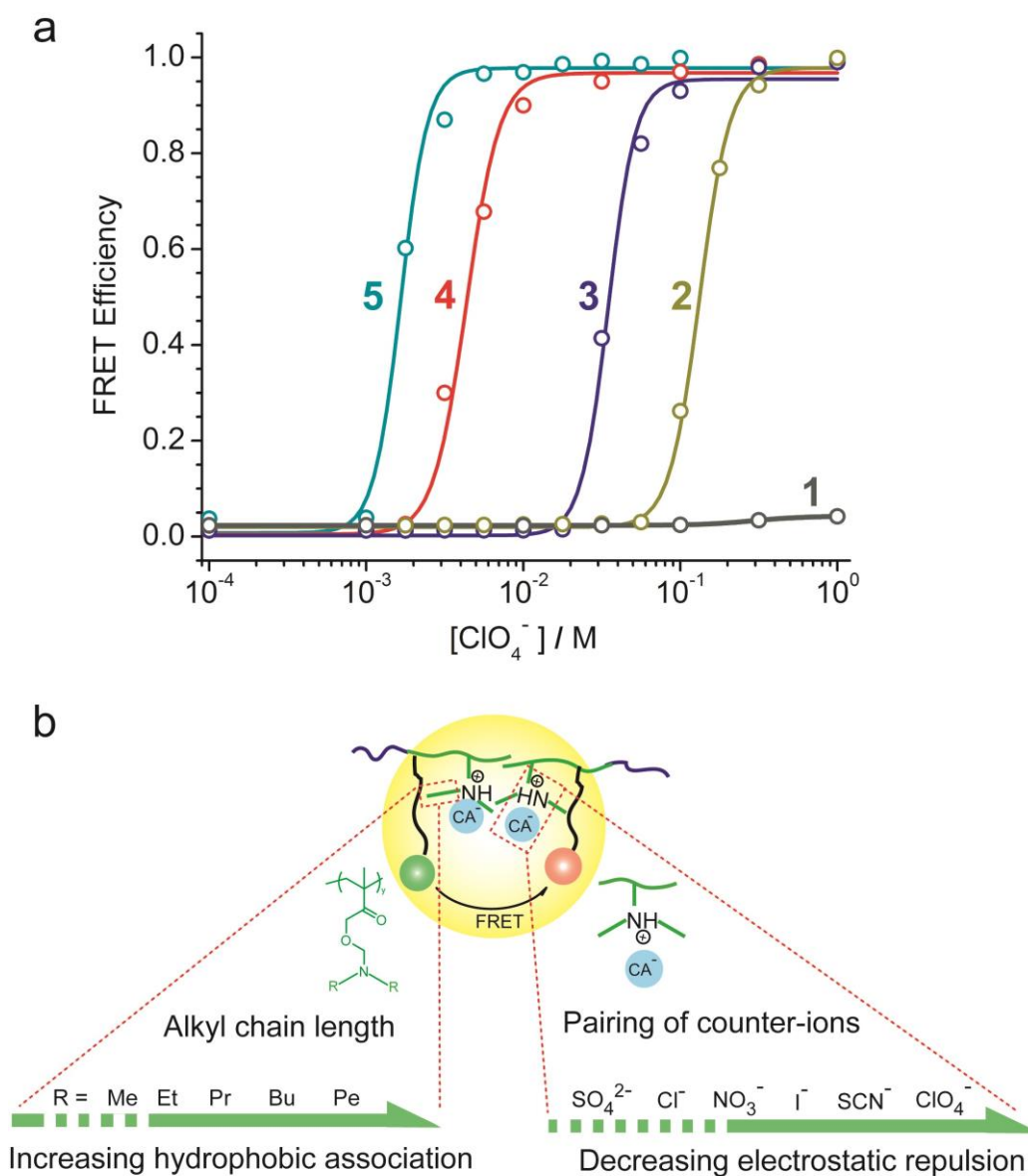
Figure 7.3.16. (a) Hydrophobic strength of PR segment affects the ability of ClO_4^- in micelle induction. More hydrophobic PR segment (e.g. pentyl groups in 5) increases the ClO_4^- sensitivity to induce micelle formation. (b) An empirical model depicting two important contributing factors (hydrophobic alkyl chain length and chaotropic anions) on the self-assembly of ionic polymeric micelles.
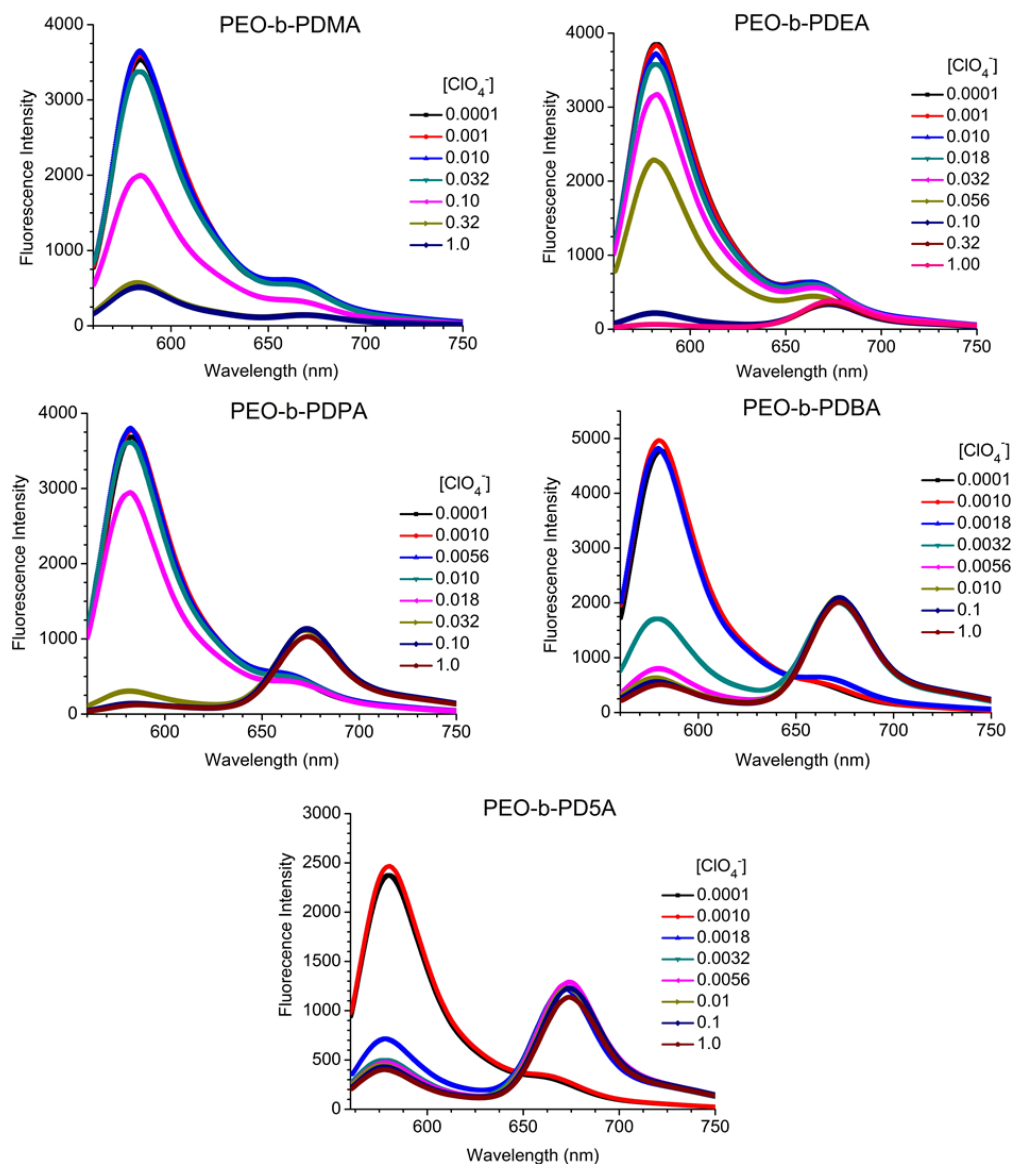
Figure 7.3.17. Fluorescence spectra of FRET polymer pairs of PEO-*b*-P(R-*r*-TMR)/ PEO-*b*-P(R-*r*-Cy5) of different hydrophobic strengths (PR segments were varied from methyl to pentyl side chains). Different concentrations of ClO_4^- (in M) anions were added to induce micelle formation. The samples were excited at $\lambda_{ex}=545$nm and emission spectra were collected from 560-750 nm. All the experiments were conducted at pH=4, which was below the transition pH of PEO-*b*-PDPA (pH$_t$=6.1).

7.3.5-Quantification of cooperativity in anion-induced micellization

The chaotropic anions-induced micellization also lead to sharp fluorescence on/off switch as a function of anion concentration, similar to that in pH-triggered binary optical transition of UPS block copolymers. Inspired by the observation, we investigate whether binding cooperativity contribute to the sharpened binding transition.

In the absence of cooperativity, the transition from free anion state to fully bound state will take place over 100-fold ligand concentration as in most monovalent receptor-ligand interactions. The fluorescence sensing data for ClO_4^- showed less than 3-fold in the concentration span of ClO_4^- for 10-fold signal change in fluorescence. PEO-*b*-PD5A copolymer with more hydrophobic side chains displayed higher sensitivity and stronger cooperativity in ClO_4^- sensing than PEO-*b*-PDPA (**Figure 7.3.18**). Moreover, PEO-*b*-PDPA copolymer with higher number of repeating unit (100) showed higher sensitivity and cooperativity than PEO-*b*-PDPA with shorter chain length (40) (**Figure 7.3.19**). These data showed that hydrophobic nanophase separation can also drive cooperative sensing of ClO_4^- anions, indicating its broad potential in the design of binary on/off switchable chemical or biological sensors.

7.3.6-Conclusion

In conclusion, we report a surprising micelle self-assembly process enabled by chaotropic anions with block copolymers containing hydrophobic, cationic ammonium groups. Unlike conventional micelles with simple hydrophobic cores, the current ionic micelles contain a large number of ion pairs in the core environment. The resulting micelles provide a good model system to study the fundamental process of

supramolecular self-assembly through the interplay of non-covalent forces (e.g. electrostatic, van der Waals and hydrophobic interactions) in the aqueous environment. From the application standpoint, results from this study may also open up new opportunities of using stabilized ion-pair interactions for the delivery of charged drug molecules using tailored micelle systems.
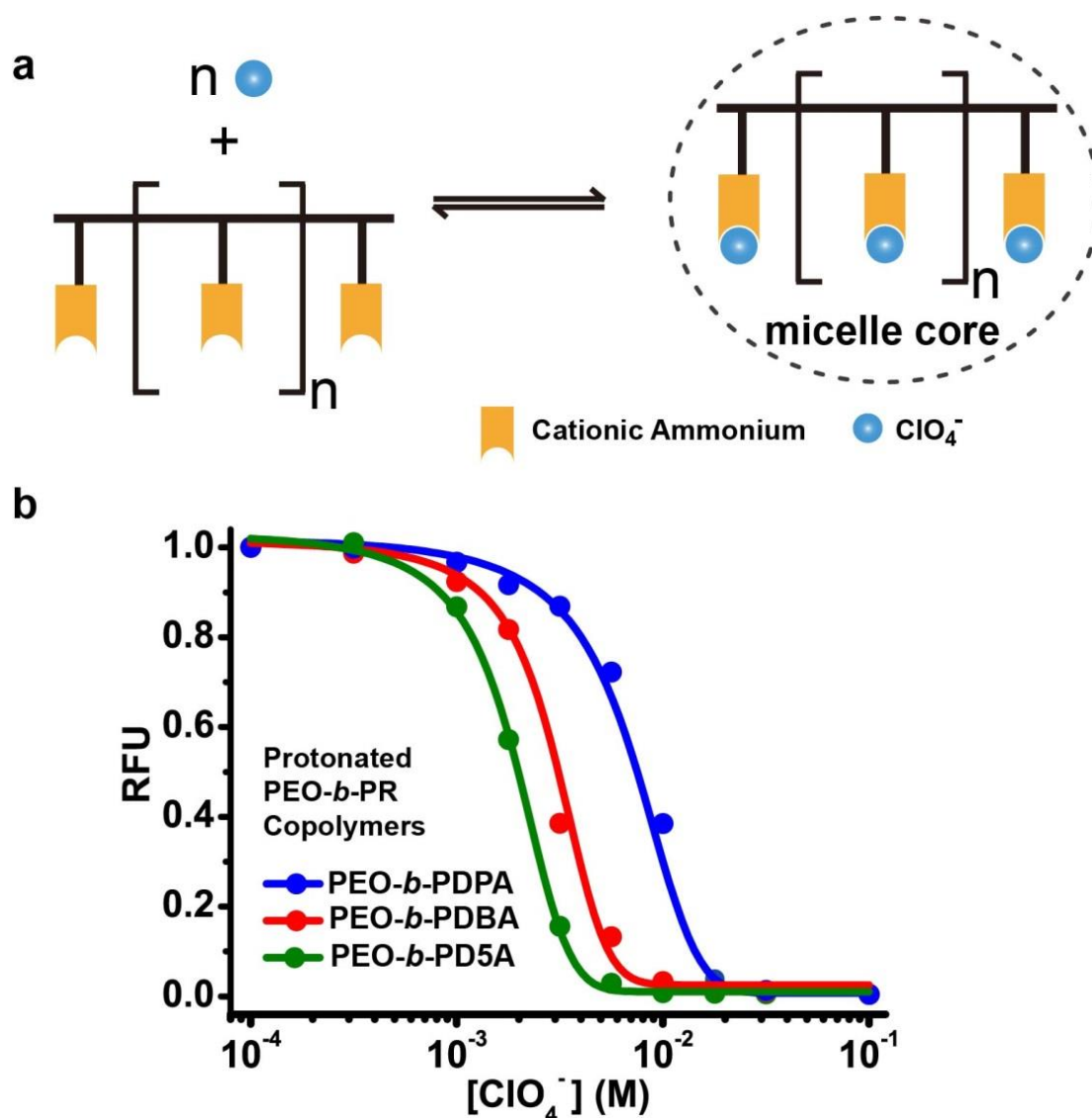
Figure 7.3.18. a, Schematic illustration of ClO_4^- binding to protonated PEO-*b*-PR block copolymers, which is treated as monovalent ligands binding to multi-site receptors. **b**, Normalized fluorescent intensity of TMR-conjugated cationic PEO-*b*-PR block copolymers as a function of ClO_4^- concentration. Copolymers with more hydrophobic side chains had lower critical concentration necessary for the formation of micelles. In the absence of cooperativity, the transition from bound-free state to fully occupied state will require over 100 fold ligand concentration. The fluorescent on/off transition of dye-conjugated PEO-*b*-PR copolymers requires ~3-fold in ClO_4^- concentrations, indicating positive binding cooperativity.
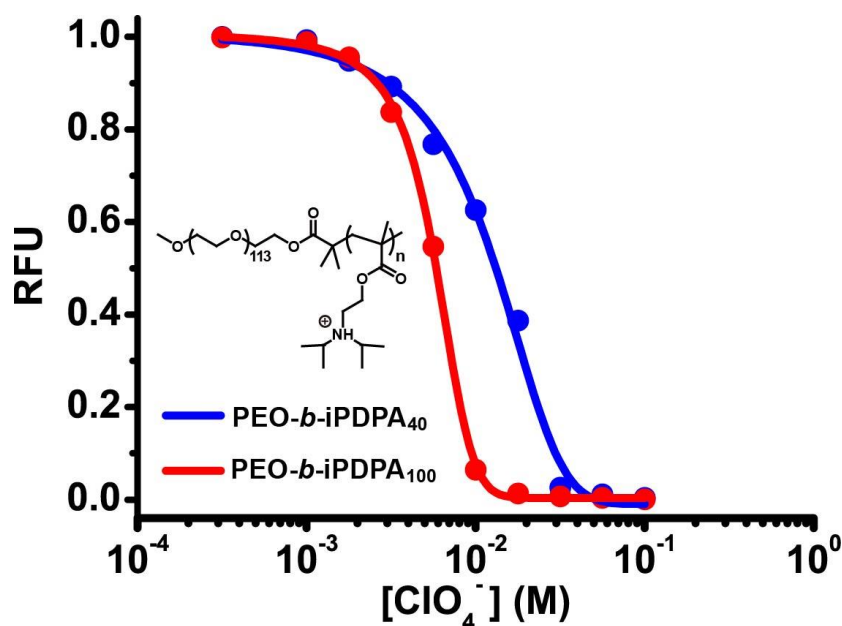
Figure 7.3.19. Normalized fluorescent intensity of dye-conjugated cationic PEO-*b*-[i]PDPA (isopropyl group as terminal alkyl groups) copolymers as a function of ClO_4^- concentration. For positive cooperative binding between monovalent ligands and multi-site receptors, increasing the binding sites per chain will increase binding cooperativity. Sharper on/off transition and increased detection sensitivity as a result of increased hydrophobic chain length confirm the positive cooperativity in the ClO_4^- and cationic PEO-*b*-PR interactions.

7.4-Reference

1   Arakawa, T. & Timasheff, S. N. Mechanism of protein salting in and salting out by divalent cation salts: balance between hydration and salt binding. *Biochemistry* **23**, 5912-5923 (1984).

2   Hofmeister, F. Zur lehre von der wirkung der salze. *Archiv für experimentelle Pathologie und Pharmakologie* **25**, 1-30 (1888).

3   Parsegian, V. A. Hopes for Hofmeister. *Nature* **378**, 335-336 (1995).

4   Jungwirth, P. & Cremer, P. S. Beyond hofmeister. *Nature chemistry* **6**, 261-263 (2014).

5   Zhang, Y. & Cremer, P. S. Chemistry of Hofmeister anions and osmolytes. *Annual review of physical chemistry* **61**, 63-83 (2010).

6   Zhang, Y., Furyk, S., Bergbreiter, D. E. & Cremer, P. S. Specific ion effects on the water solubility of macromolecules: PNIPAM and the Hofmeister series. *Journal of the American Chemical Society* **127**, 14505-14510 (2005).

7   Zhang, Y. *et al.* Effects of Hofmeister anions on the LCST of PNIPAM as a function of molecular weight. *The journal of physical chemistry. C, Nanomaterials and interfaces* **111**, 8916 (2007).

8   Zhang, Y. & Cremer, P. S. Interactions between macromolecules and ions: The Hofmeister series. *Curr. Opin. Chem. Biol.* **10**, 658-663, doi:10.1016/j.cbpa.2006.09.020 (2006).

9   Parsons, D. F., Bostrom, M., Lo Nostro, P. & Ninham, B. W. Hofmeister effects: interplay of hydration, nonelectrostatic potentials, and ion size. *Phys. Chem. Chem. Phys.* **13**, 12352-12367, doi:10.1039/c1cp20538b (2011).

10   Kunz, W., Lo Nostro, P. & Ninham, B. W. The present state of affairs with Hofmeister effects. *Curr. Opin. Colloid Interface Sci.* **9**, 1-18, doi:http://dx.doi.org/10.1016/j.cocis.2004.05.004 (2004).

11   Nasongkla, N. *et al.* Multifunctional polymeric micelles as cancer-targeted, MRI-ultrasensitive drug delivery systems. *Nano Lett.* **6**, 2427-2430, doi:10.1021/nl061412u (2006).

12   Jares-Erijman, E. A. & Jovin, T. M. FRET imaging. *Nat Biotech* **21**, 1387-1395 (2003).

13   Sapsford, K. E., Berti, L. & Medintz, I. L. Materials for fluorescence resonance energy transfer analysis: beyond traditional donor-acceptor combinations. *Angew. Chem. Int. Ed.* **45**, 4562-4589, doi:10.1002/anie.200503873 (2006).

14   Tsarevsky, N. V. & Matyjaszewski, K. "Green" Atom Transfer Radical Polymerization: From Process Design to Preparation of Well-Defined Environmentally Friendly Polymeric Materials. *Chem. Rev.* **107**, 2270-2299, doi:10.1021/cr050947p (2007).

15   Ma, Y. *et al.* Well-Defined Biocompatible Block Copolymers via Atom Transfer Radical Polymerization of 2-Methacryloyloxyethyl Phosphorylcholine in Protic Media. *Macromolecules* **36**, 3475-3484, doi:10.1021/ma021762c (2003).

16   Ha, T. *et al.* Single-molecule fluorescence spectroscopy of enzyme conformational dynamics and cleavage mechanism. *Proc. Natl. Acad. Sci. U. S. A.* **96**, 893-898 (1999).

17   Grunwell, J. R. *et al.* Monitoring the Conformational Fluctuations of DNA Hairpins Using Single-Pair Fluorescence Resonance Energy Transfer. *J. Am. Chem. Soc.* **123**, 4295-4303, doi:10.1021/ja0027620 (2001).

18   Collins, K. D. & Washabaugh, M. W. The Hofmeister effect and the behaviour of water at interfaces. *Q. Rev. Biophys.* **18**, 323-422, doi:doi:10.1017/S0033583500005369 (1985).

19   Zhou, K. *et al.* Tunable, ultrasensitive pH-responsive nanoparticles targeting specific endocytic organelles in living cells. *Angew Chem Int Ed Engl* **50**, 6109-6114, doi:10.1002/anie.201100884 (2011).

20   Zhou, K. *et al.* Multicolored pH-tunable and activatable fluorescence nanoplatform responsive to physiologic pH stimuli. *J. Am. Chem. Soc.* **134**, 7803-7811, doi:10.1021/ja300176w (2012).

21   Huang, X. *et al.* Multi-chromatic pH-activatable 19F-MRI nanoprobes with binary ON/OFF pH transitions and chemical-shift barcodes. *Angew. Chem. Int. Ed.* **52**, 8074-8078, doi:10.1002/anie.201301135 (2013).

22   Wang, Y. *et al.* A nanoparticle-based strategy for the imaging of a broad range of tumours by nonlinear amplification of microenvironment signals. *Nat. Mater.*, doi:10.1038/nmat3819 (2013).

23   Leontidis, E. Hofmeister anion effects on surfactant self-assembly and the formation of mesoporous solids. *Curr. Opin. Colloid Interface Sci.* **7**, 81-91, doi:http://dx.doi.org/10.1016/S1359-0294(02)00010-9 (2002).

24   Collins, K. D. Charge density-dependent strength of hydration and biological structure. *Biophys. J.* **72**, 65-76, doi:10.1016/s0006-3495(97)78647-8 (1997).

25   Underwood, A. L. & Anacker, E. W. Counterion lyotropy and micelle formation. *J. Colloid Interface Sci.* **117**, 242-250, doi:http://dx.doi.org/10.1016/0021-9797(87)90188-3 (1987).

26   Zhang, Y. & Cremer, P. S. The inverse and direct Hofmeister series for lysozyme. *Proc. Natl. Acad. Sci. U. S. A.* **106**, 15249-15253, doi:10.1073/pnas.0907616106 (2009).

CHAPTER EIGHT-In Vivo Activation of UPS Nanoparticles

8.1-Introduction

Most biological signals (e.g., pH, ROS) are analog in nature with perpetual changes in space and time[1-6]. Conventional biosensors (e.g., small molecular pH probes) are analog sensors which offer reversible and continuous response to the changes in biological signals. Analog sensors often suffer from low specificity to differentiate pathological versus normal signals because they are not effective at signal amplification without noise introduction[7]. Responsive nanomaterials have emerged as promising candidates to address such challenge in a wide range of applications such as biological sensing, self-healing, and drug delivery[8-12]. Compared to single molecules, nanomaterials often display positive cooperativity arising from non-covalent self-assembly chemistry[13]. Despite successful development of various nanosystems, nanomaterials-based biosensors that can consistently convert subtle differences into a discrete signal are still lacking.

Electronic transistors have revolutionized the electronics and computer industries by their ability to amplify or switch signals as discrete or digital outputs[5,14]. Digital signals can be processed, amplified, and transmitted without adding noise or distortion[15]. Our transistor-like ultra-pH sensitive nanoparticles (~25 nm in diameter) with binary off/on reporters that are finely tunable in a broad range of physiological pH (4.0-7.4)[16]. The ultra pH-sensitive property is a unique nanoscale phenomenon arising from catastrophic phase transitions during pH-triggered self-assembly of amphiphilic copolymers[17]. At molecular level, an all-or-nothing protonation distribution in cationic unimers or neutral micelles, respectively, was observed in contrary to conventional

283

polymeric bases (e.g., PEI, polylysine). The resulting pH cooperativity rendered the nanoprobes a dramatically sharpened pH response ($\Delta pH_{off/on}< 0.2$ pH), compared to 2 pH units for small-molecular pH sensors. We recently adopted a pH nanotransistor with a pKa of 6.9 ($PNT_{6.9}$) as a pH threshold sensor to image acidic tumor pH signals. A nearly binary digitization of tumor signals was achieved over the muscle background for margin delineation, which allowed real time, image-guided surgery with significantly improved long-term survival (>70% cures) in mice bearing head and neck tumors (**Figure 8.1.1**)[18].
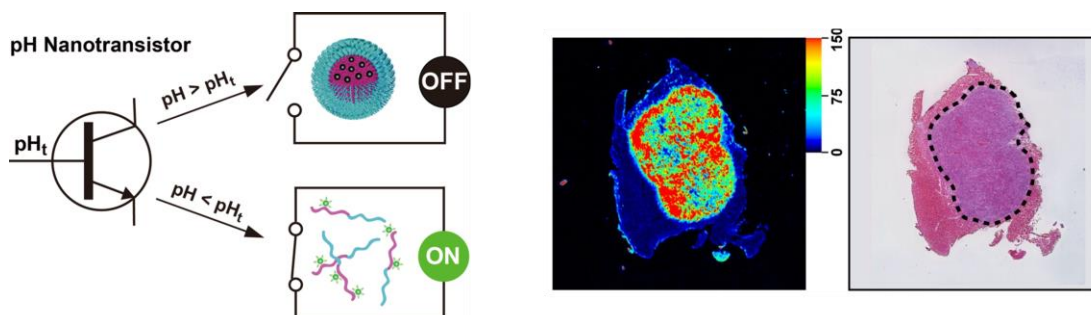
Figure 8.1.1. (Left) Schematic illustration of pH-nanotransistors. (right) representative fluorescence imaging and corresponding H & E validation of tumor margin delineation performance of PNT

Despite the molecular understanding of pH cooperativity during pH-triggered molecular self-assembly and demonstration of outstanding tumor margins delineation performance, there is still a knowledge gap between these two studies in how the pH transistor probes are able to achieve binary tumor margin delineation *in vivo*. In this study, we will investigate the biochemical mechanism of pH transistor nanoprobes to digitize tumor over normal muscle signals. We will specifically focus on testing the hypothesis that "irreversible" activation of pH transistor nanoprobes is responsible for the binary demarcation of tumor/muscle tissues for improved tumor diagnosis.

8.2-Materials and methods

8.2.1-Synthesis of dye-conjugated PEO-b-PEPA block copolymers

AMA-MA was used for the conjugation of dyes or fluorescence quenchers. Synthesis of PEO-b-(PEPA-r-AMA) copolymers followed the procedure described previously. Three primary amino groups were introduced into each polymer chain by controlling the feeding ratio of AMA monomer to the initiator (ratio = 3). After synthesis, PEO-b-(PR-r-AMA) (10 mg) was dissolved in 2 mL DMF. Then the NHS-ester (1.5 equivalences for TMR-NHS, Cy5-NHS or ICG-OSU) was added. After overnight reaction, the copolymers were purified by ultra-centrifugation. The produced PEO-b-(PR-r-Dye/FQ) copolymers were lyophilized and kept at -20 ℃ for storage.

8.2.2.-Preparation of micelle solution

For each copolymer, the stock solution of micelles was prepared following a solvent evaporation method as previously reported[19]. 20 mg of dye-conjugated PEO-b-PEPA block copolymer was first dissolved in 2.0 mL THF and then added into 10 mL deionized water dropwise under sonication. The THF was removed through ultrafiltration with (100 KD) membrane for five times. Then deionized water was added to adjust the polymer concentration to 5 mg/mL as a stock solution.

8.2.3-pH reversal experiment

The stock solution of dye-conjugated PEO-b-PEPA block copolymers were diluted to 0.5 mg/ml with PBS buffer (pH = 6.5). Their fluorescence emission spectra were obtained on a Hitachi fluorometer (F-7500 model). Then the pH of the same sample was

adjusted to 7.4 with addition of 0.4 M NaOH solution and fluorescence emission spectra of obtained solution was measured. Finally, the pH of the same sample solution was brought back to 6.5, followed by measurement of fluorescence emission. The fluorescence intensity was plotted in a histogram (pH = 6.5, 7.4 and 6.5 (reversal)).

8.2.4-Dialysis

Dye-conjugated PEO-*b*-PDEA copolymers (2.0 mg) was first dissolved in PBS buffer to obtain 0.5 mg/mL polymer solution. 2.0 mL polymer solution was centrifuged using ultra-centrifugation tube with a molecular weight cutting-off at 100 kDa to approximately 1.0 mL filtrated sample. DLS were used to measure the size of the filtrate and remaining solution. Then the filtrate and remaining solution were diluted with MeOH to 0.02 mg/ml and UV-Vis was applied to quantify the molar concentration of the dye-conjugated PEO-b-PEPA block copolymers.

8.2.5- Confocal imaging

HN5 and other cancer cells were first plated in glass bottom dishes (MatTek, MA) in 2 mL complete DMEM medium. In a typical procedure, the cancer cells in complete medium were kept at 4°C for 10 min, then 100 μg/mL of dye-conjugated PEO-b-PEPA nanoparticles was added and kept for 30 min at 4 ℃. The medium was

removed and washed thrice. Thereafter, cells were incubated with complete medium for 3 h at 37 ℃. TMR, Cy5 and ICG were excited at 543, 633 and 750 nm, respectively. Corresponding filters were used for TMR, Cy5 and ICG imaging.

8.2.6-Margin validation.

For orthotopic head and neck tumours, HN5, FaDu or HCC4034 cells (2×10^6 per mouse) were injected into the right thigh. One week after inoculation, animals were used for imaging studies. Tumor and surrounding tissues were collected 24 h after probe injection. The collected samples were frozen in optimum cutting temperature (OCT) medium and 8 μm frozen section slides. Frozen sections were prepared from the specimens for H & E staining and histology validation. Histological evaluation was performed independently by a surgical pathologist without knowing the fluorescence assignment for each sample.

8.3-Results and Discussion

8.3.1-Dye-dependent self-assembly of UPS block copolymers

As described above, we used indocyanine green (ICG)-conjugated UPS block copolymers to evaluate the tumor margin delineation performance. ICG is a commonly used cyanine dye used in medical diagnostics and imaging. It has been widely applied for determining hepatic function, cardiac output, and liver blood flow[20-22]. Its maximum emission (~800 nm) falls into near infrared region and enabled deeper penetration ability than commonly used fluorophores such as Rhodamine and Cy5.

However, one obvious drawback of ICG in biomedical applications is low solubility in water and instability in blood circulation and tumor microenvironment[23]. The free ICG tend to form dimers and oligomers at mass concentration above > 3.9 μg/ml. When the concentration is over 1.0 mg/ml, free ICG will aggregate in aqueous solution. Both dimerization and aggregation results in self-quenching of fluorescence. ICG was also found to undergo degradation in aqueous solution, following first-order kinetics[24]. Exposure to light and high temperatures tend to accelerate such degradation and the intensity of exposed light also affected degradation. ICG aqueous solution was found to be more stable in dark, at low temperatures, and at higher ICG concentrations. In addition, ICG can also interact with both lipophilic and hydrophilic molecules. In physiological environment, ICG binds almost completely (>98%) to most of the major plasma proteins such as albumin, globulins and lipoproteins. As a result, the half-life of free ICG is only 3-4 min.

We first investigated whether the conjugated ICG on the hydrophobic segment will lead to oligomerization or aggregation of UPS block copolymers at the unimer state in the

presence of serum albumin. DLS was applied to track the hydrophobic diameter and scattering intensity of a representative PEO-b-PEPA-ICG block copolymers. Dye-free PEO-b-PEPA and PEO-b-PEPA-TMR was adopted as control. Cy5 was not applicable due the interference with the laser beam of DLS equipment. The albumins are a family of globular proteins and their size is around 5 nm in aqueous solution. As shown in **Figure 8.3.1**, the dye-free and TMR-conjugated PEO-b-PEPA displayed reversible self-assembly triggered by external pH. The size and scattering intensity decreased significantly at low pH (unimers state). However, ICG-conjugated PEO-b-PEPA block copolymers exhibited striking different behavior where the scattering intensity at unimer state was higher than that in micelles state, indicating the unimers may form loose aggregations. As the ICG can oligomerize as well as bind to serum proteins like albumin, we evaluated the aggregation behavior of ICG-conjugated PEO-b-PEPA block copolymers without serum albumin. We are surprised to find that the PEO-b-PEPA-ICG can also form aggregation in simple saline solution.

We concluded that the ICG-conjugated PEO-b-PEPA block copolymers tend to form aggregation at unimers state, either with other polymers or with serum proteins like albumin. After activation at tumor microenvironment, the UPS nanoparticles dissociated into cationic unimers. These unimers can form loose aggregations linked by ICG or they can bind to serum proteins and get internalized into cellular plasma. Although there may exist fluctuation of proton concentration and the local pH value may increase above the pKa of UPS$_{6.9}$ block copolymers, we don't expect the unimers to reversibly self-assemble into core-shell micelles. Instead, they probably get trapped in tumor microenvironment and eventually internalized by the tumor cells.
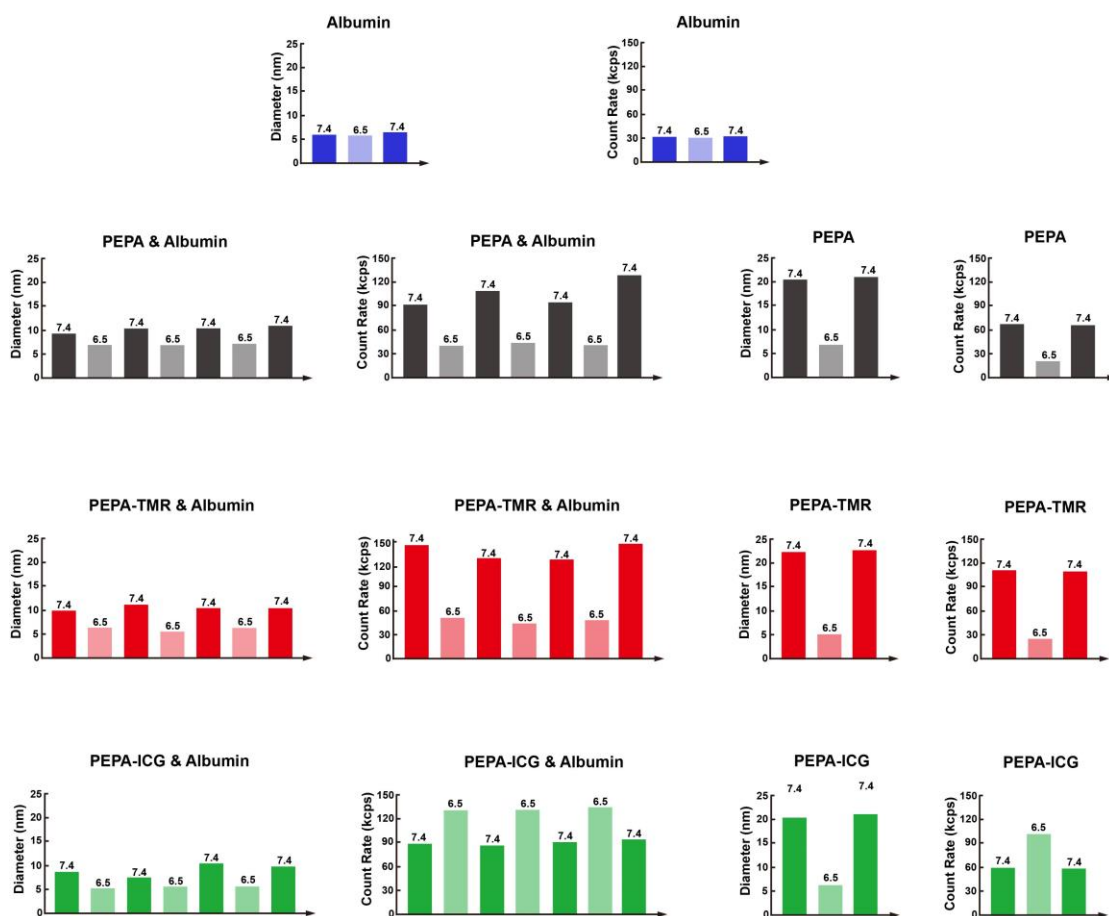
Figure 8.3.1. Measurement of hydrodynamic diameter and scattering intensity of dye-conjugated PEO-b-PEPA block copolymers in PBS buffers with and without albumin.

8.3.2-Irreversible activation of UPS nanoparticles in the presence of serum proteins

Previous studies have shown that UPS nanoprobes maintained its intact structure (e.g., size and spherical morphology) and low fluorescence in the presence of serum proteins at pH 7.4 for over 24 hours. Pharmacokinetic studies of ^{3}H-labelled I-UPS$_{6.9}$ nanoprobe showed a 8.6±2.7 h b-phase elimination half-life[18], compared to <5 mins for free ICG, which further supported the stability of ICG conjugated PEO-b-PEPA nanoprobes in blood. Fluorescence imaging performance is critical for imaging-based diagnostic applications such as tumor margin delineation.

In this study, we examined the reversibility of fluorescence emission of the ICG-conjugated PEO-b-PEPA nanoprobes in the presence or absence of 100% human serum (**Figure 8.3.2**). Results show in the absence of serum, the fluorescence intensity of PEO-b-PEPA-ICG returned to the base level after pH is reversed from 6.5 to 7.4. In contrast, in the presence of serum, the fluorescence intensity was kept at the on state after pH reversal (**Fig. 8.3.3**). At low albumin concentration, the fluorescence stayed around 50% of maximum values at on state after pH reversal. With the increase of albumin concentration, the tendency of irreversible arrest of fluorescent signals increased. In the presence of physiological mimic albumin concentration, the fluorescence intensity after pH reversal was above 80% of that in on state. These data suggested that the fluorescent activation of dye-conjugated UPS nanoparticles was irreversible. Moreover, the irreversibility showed dye-dependence. Most hydrophilic TMR dye displayed least tendency in arresting the fluorescent signals. In contrast, the ICG-conjugated PEO-b-PEPA showed strongest tendency to lock down the fluorescent signal at the on state, probably due to binding of serum proteins and formation of aggregations.
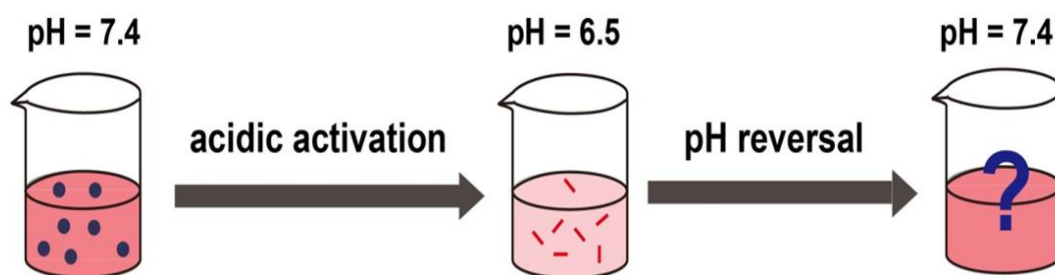
Figure 8.3.2. Schematic illustration of pH-dependent fluorescence reversal experiment of dye-conjugated PEO-b-PEPA block copolymers.
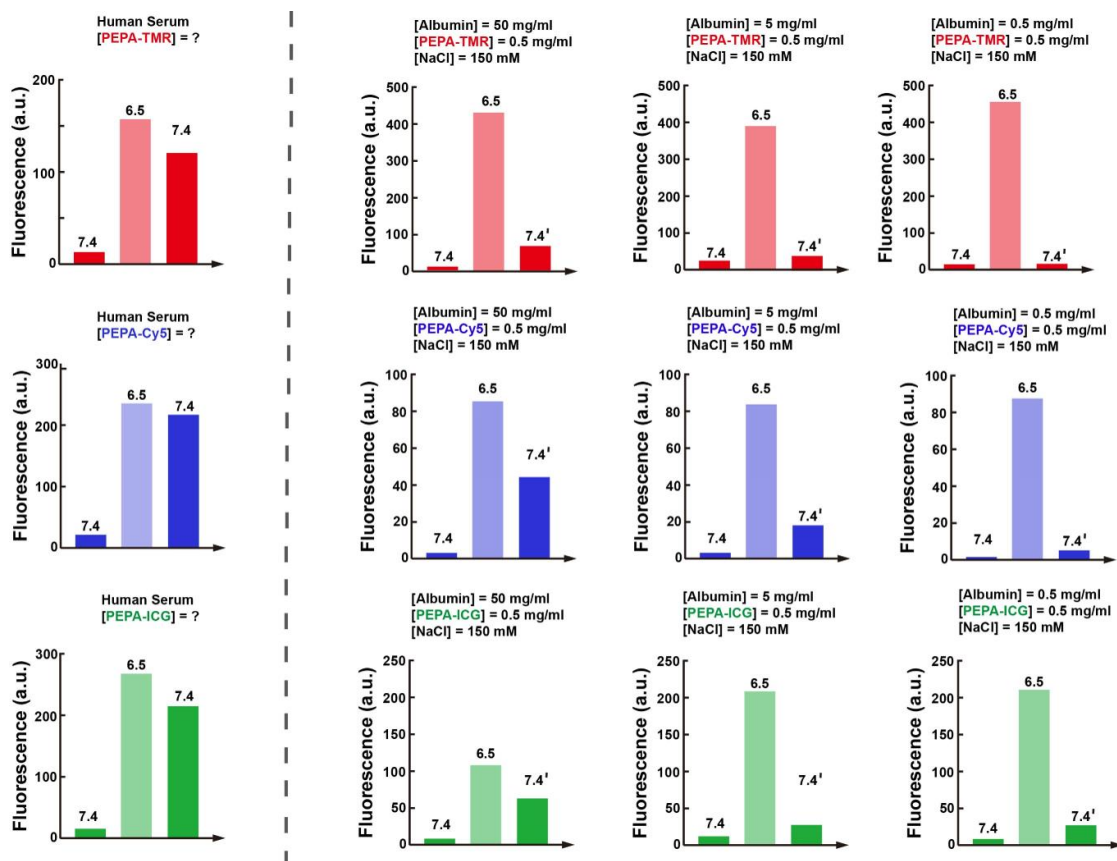
Figure 8.3.3. pH-dependent fluorescence reversal experiment of dye-conjugated

PEO-b-PEPA block copolymers in the presence of albumin at different concentration

8.3.3-Dye-dependent intracellular accumulation

Albumin is a major component (55%) of serum proteins and is also selectively endocytosed by cancer cells to catabolize into amino acids for tumor growth and survival. Previous results elucidated that albumin alone was sufficient to cause irreversibility. In this study, we investigated whether the pH irreversibility was caused by ICG or protonated PEPA copolymer binding to albumin (pI 4.7-5.5, which is negatively charged) and ensuing increased internazliation. We also compared the effect of ICG-conjugated UPS nanoparticles with tetramethyl rhodamine (TMR) and Cy5-conjugated ones. It is known that albumin binds to ICG strongly (10^{-7} M by isothermocalorimetry measurement)[25], but not TMR or Cy5. If the pH reversibility is retained TMR-UPS, it suggests that protonated PEPA polymer interaction with albumin is the dominant factor; otherwise ICG may be more directly responsible. As shown in **Figure 8.3.4**, ICG-conjugated UPS nanoparticles showed a higher level of intracellular accumulation. The results in both HN5 and FaDu cell lines showed that the incorporation of ICG lead to increased cell uptake compared to TMR and Cy5.

Fluorescence microscopy of frozen HN5 tumor sections showed the internalization of the ICG-conjugated PEO-b-PEPA nanoprobes inside the punctate organelles in the cancer cells 24 h after the intravenous injection (cell membranes and nucleus were stained to assist the location of nanoprobes). It is known that cancer cells avidly take up albumin as a food source through scavenger receptor or FcRn-mediated endocytosis pathways[26]. We further investigated whether albumin-bounded activated-PEO-b-PEPA-ICG might facilitate nanoprobe uptake inside cancer cells.
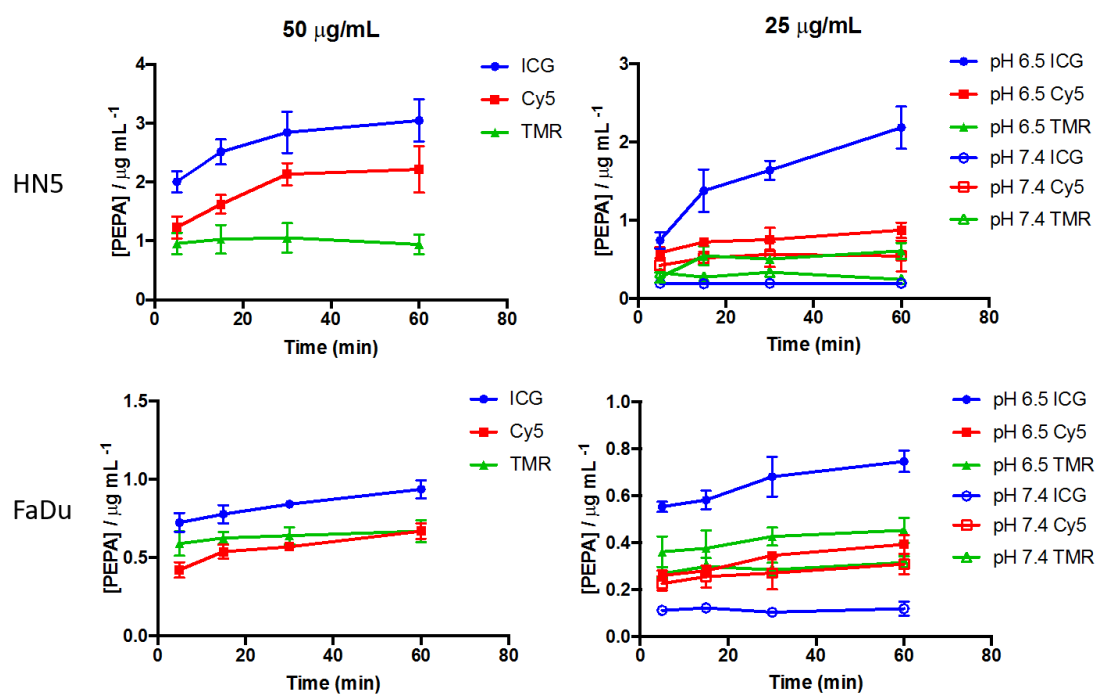
Figure 8.3.4. Internalization level of dye-conjugated PEO-b-PEPA nanoparticles at different pH.

We pretreated ICG-conjugated PEO-b-PEPA nanoparticles to pH 6.5 in the absence and presence of albumin and then bring up the pH to 7.4. In this way, we were able to study the impact of albumin binding on the internalization level of ICG-conjugated UPS nanoparticles. Serum albumin hindered instead of promoting the internalization of nanoparticles regardless of extracellular pH (**Figure 8.3.5**). But albumin may change the endocytosis route of ICG-conjugated nanoprobes.

In addition to UPS trapping by albumin, negatively charged cell surface (either lipids or glycocalyx) may also irreversibly arrest the cationic unimers from reassembly even after pH reversal. We then investigated whether the interaction between cell surface and cationic UPS block copolymers would affect their cell uptake. We first reduced the cell culture temperature to 4 degrees after cells reach confluency in the cell culture plate. We then removed the FBS-containing cell culture medium and washed the cells three times with PBS buffer at pH 7.4. While keeping the temperature at 4 degrees, we added the solution of PEO-b-PEPA-ICG nanoparticle solution (100 µg/mL, well below the IC_{50} concentration of 2 mg/mL) at either pH 6.5 or 7.4. TMR and Cy5 conjugated PEPA nanoparticles as well as PEO-labeled nanoparticles were used as a control to evaluate whether the membrane interaction is dye-dependent. After incubation for 30 mins, we used confocal microscopy to study the localization of dye-conjugated nanoprobes.

To investigate whether membrane adhesion could lead to cell internalization, we first allowed the activated UPS block copolymers binding to cell surface at 4 degree at pH 6.5, then we replaced the medium to 7.4 and raised the cell culture temperature to 37 degrees and allowed endocytosis to occur. We used confocal microscopy to investigate the localization of fluorescent signals over time.
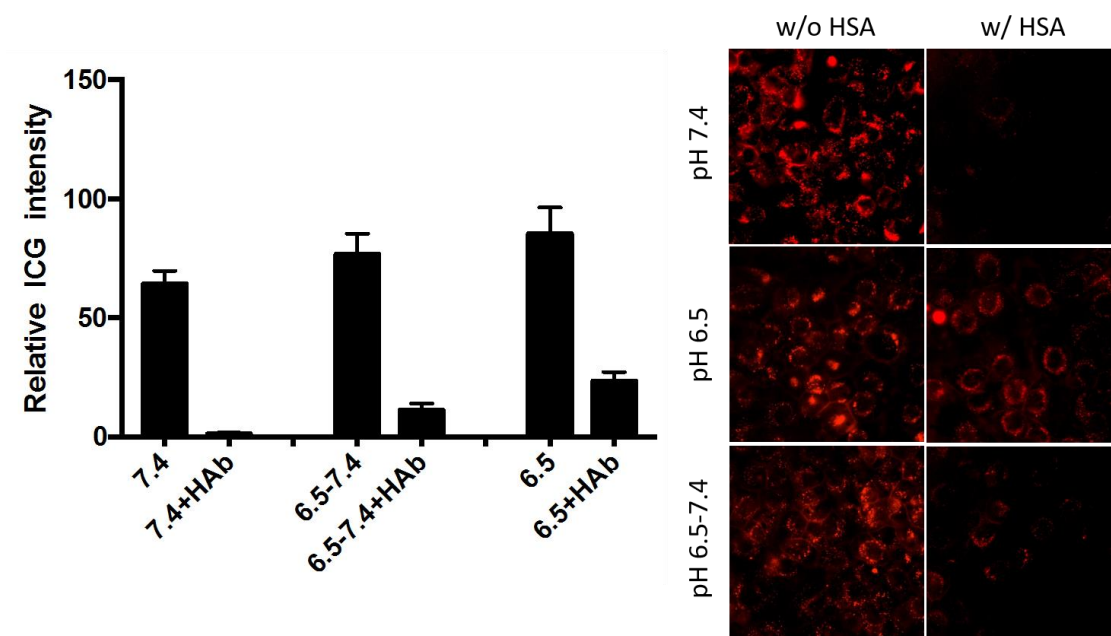
Figure 8.3.5. Internalization level of ICG-conjugated PEO-b-PEPA-ICG nanoparticles at different surrounding pH.

The results suggested that ICG-conjugated nanoparticles showed similar level of membrane interaction as PEO-b-PEPA-Cy5 at 4 degree (**Figure 8.3.6**) but higher level of membrane interaction at 37 degree (**Figure 8.3.7**). To investigate whether this interaction was primarily electrostatic in nature, we used different concentration of polycations (polylysine) to compete for cell binding. The preliminary results suggested that addition of poly-lysine reduced the cell uptake of ICG-conjugated UPS nanoparticles. Higher concentration of poly-lysine lead to lower uptake of PEO-b-PEPA-ICG nanoprobes.

In addition to albumin and cancer cells, other biological components in the tumor microenvironment include other serum proteins (globulins) after vascular extravasation, tumor secreted proteins (e.g., heat shock proteins) or extracellular matrix (e.g., fibronectin). Further studies are still need to investigate their contributions to the irreversible activation of UPS nanoprobes.

To conclude, albumin didn't increase the level of internalization of ICG-conjugated UPS nanoparticles, but it may change their endocytosis route. PEO-b-PEPA-ICG nanoparticles also showed a higher level of intracellular accumulation and membrane interaction as compared with TMR or Cy5 conjugated nanoprobes, which may contribute to its clearer tumor margin delineation outcome in vivo. Electrostatic interaction was one of the factors that contributes to the interaction of PEPA-ICG with cell membrane.
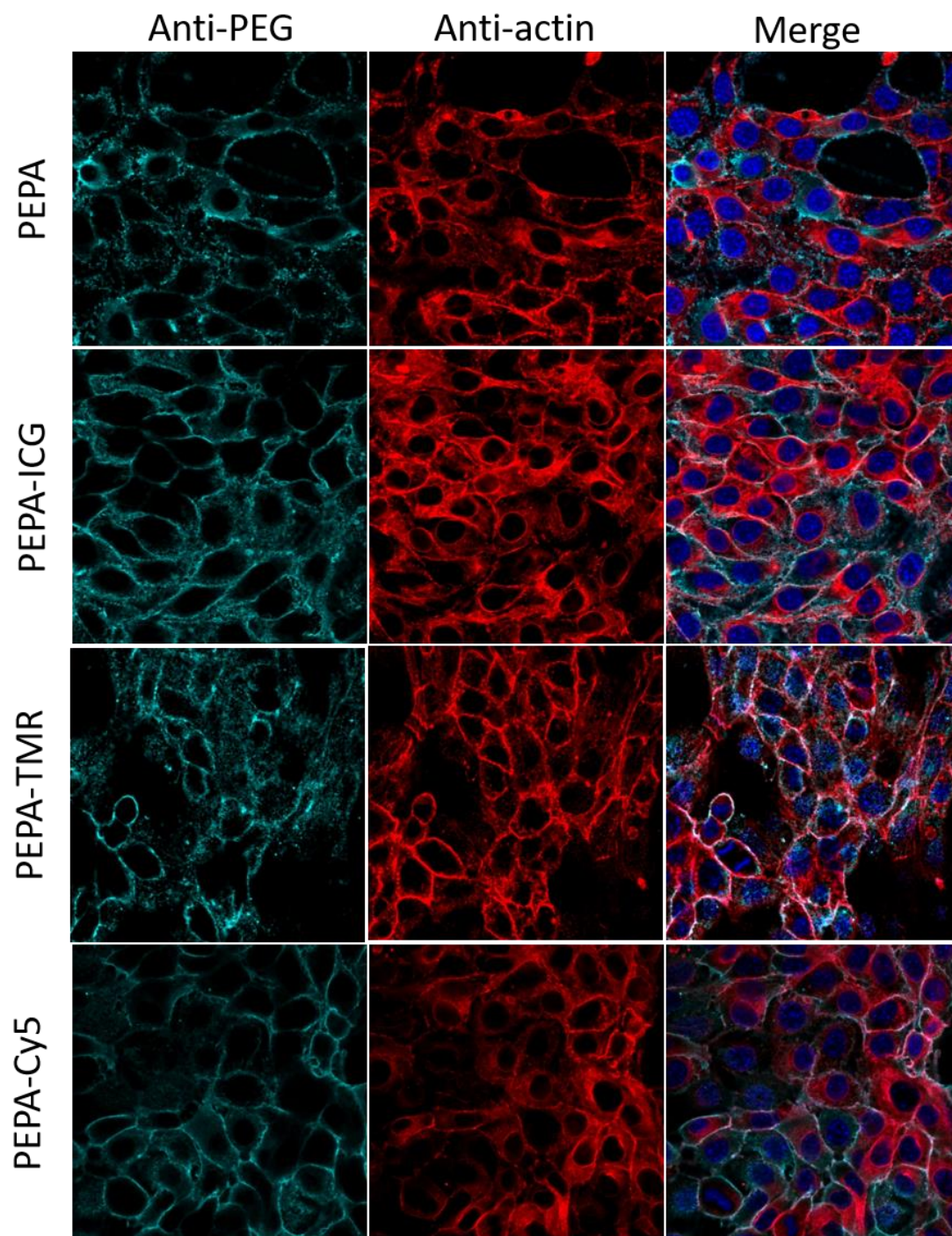
Figure 8.3.6. Membrane interaction level of dye-conjugated PEO-b-PEPA nanoparticles at 4 degree.
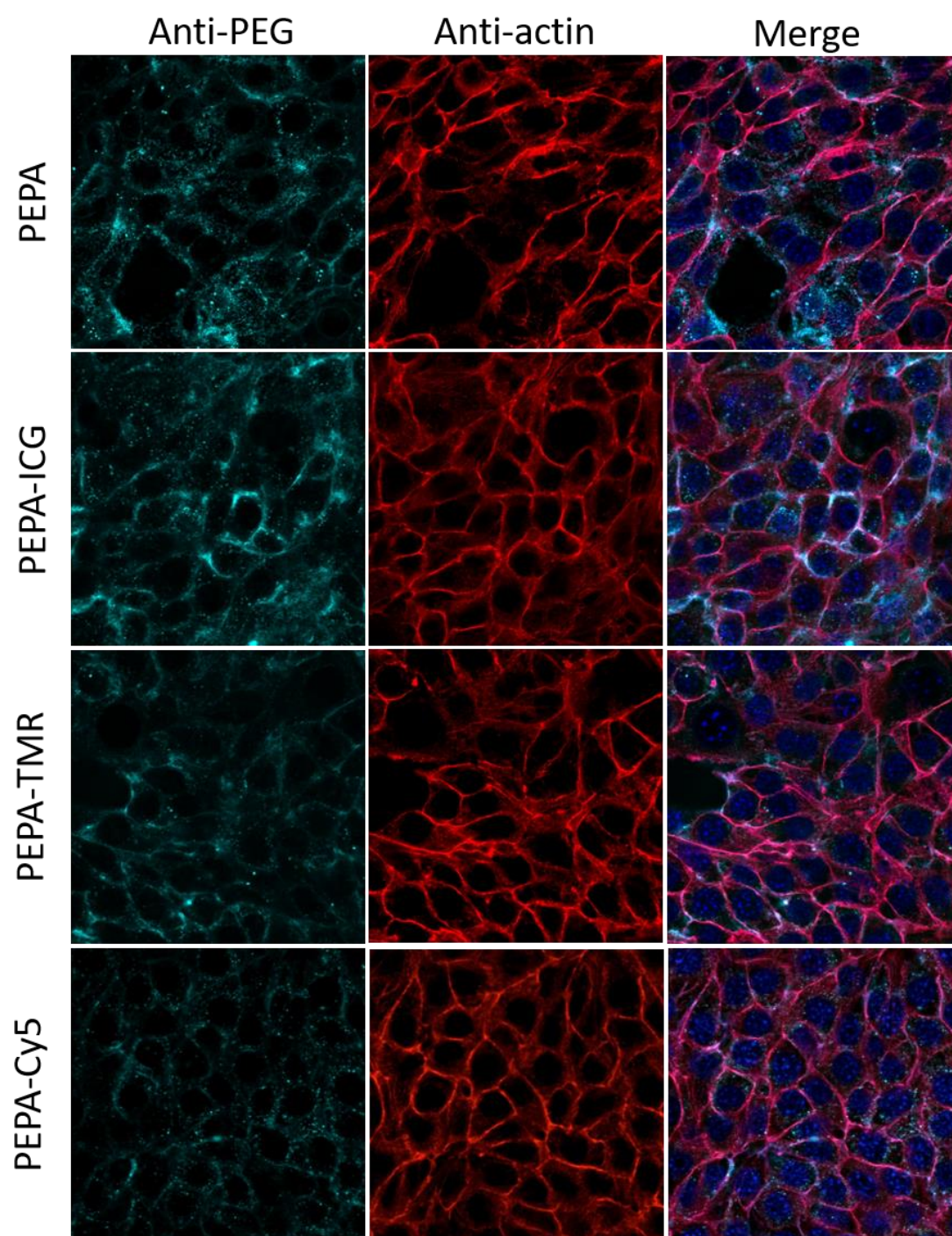
Figure 8.3.7. Membrane interaction level of dye-conjugated PEO-b-PEPA nanoparticles at 37 degree.

8.3.4-Dye-dependnet fluorescence activation patterns

Previous in vitro results have shown that ICG-conjugated UPS nanoparticles displayed better intracellular accumulation and cell membrane interactions than that of TMR and Cy5-conjugate nanoprobes. Both effect will help arrest the fluorescence signals of activated UPS nanoparticles at on state and probably improve the tumor precision. In this study, we will validate such dye-dependent in vivo tumor margin-delineation effect.

The ICG-conjugated PEO-b-PEPA nanoparticles precisely differentiated the cancerous tissues from surrounding normal tissues in huge xenograft tumors (n=3) (**Figure 8.3.8**). Large tumors with irregular morphology were impossible to be localized by commonly used small molecular or polymeric pH sensors. The fluorescence intensity variations among different regions of tumors suggested proton fluctuation, indicating tremendous tumor heterogeneity.

To validate whether fluorophores may affect the imaging performance, we co-injected ICG and Cy5-conjugated UPS nanoparticles. The mixed micelles were prepared via solubilizing PEO-b-PEPA-Cy5 and PEO-b-PEPA-ICG in THF following addition of DI water under sonication. As shown in **Figure 8.3.9**, the tumor margin based on ICG channel was very clear. In contrast, the tumor margin based on Cy5 channel was a little bit blurry with lower fluorescence intensity. In another study, we co-injected TMR, Cy5 and ICG-conjugated PEO-b-PEPA nanoparticles. The ICG channel showed much stronger fluorescence intensity than TMR and Cy5, probably due the hetero-FRET effect between these three fluorophores that quenches the signals of TMR and Cy5. In further study, we will inject these three dye-conjugated PEPA nanoparticles independently and evaluate the dye-dependent tumor margin delineation effect.
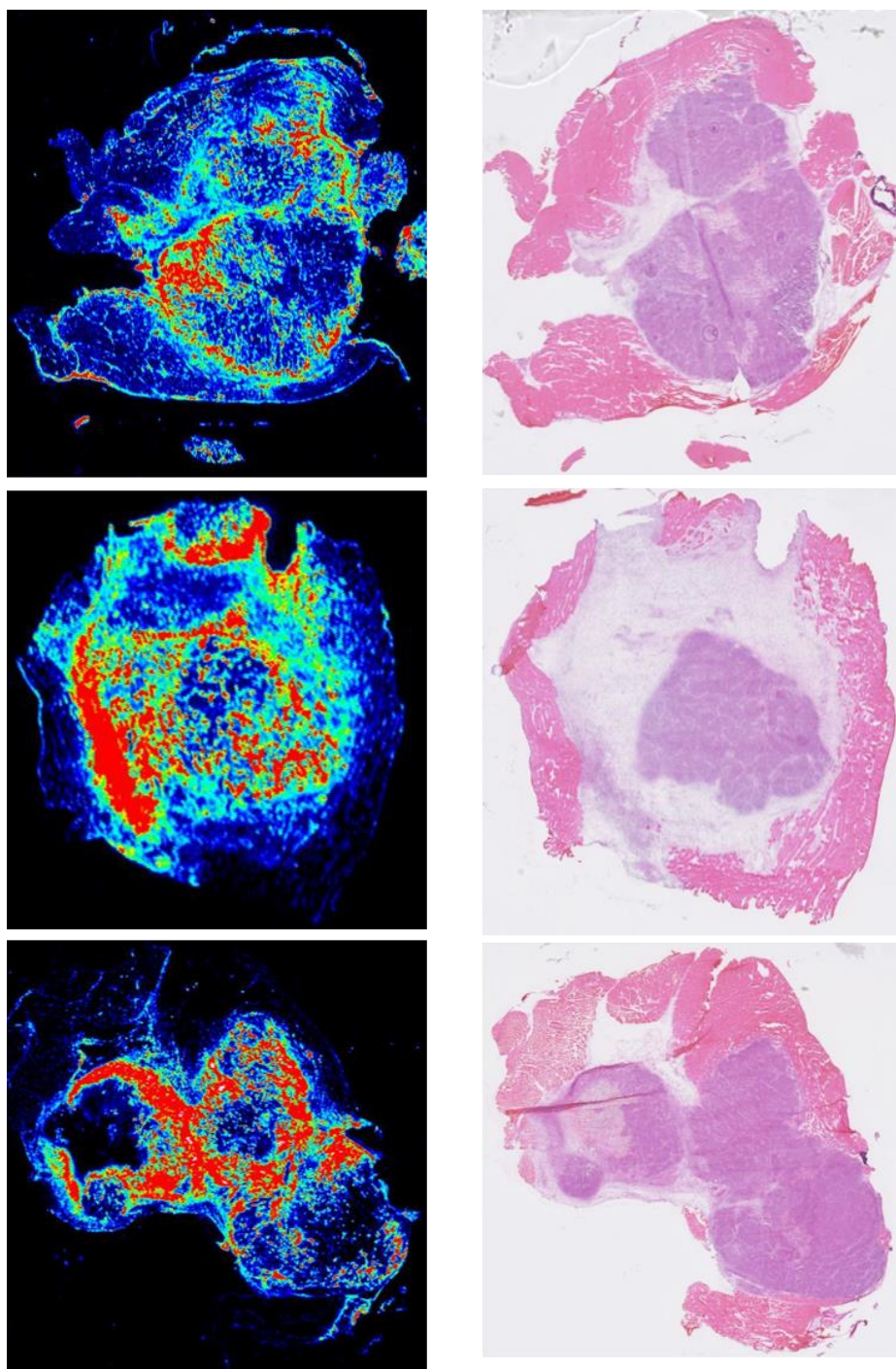
Figure 8.3.8. Tumor margin delineation effect of ICG-conjugated PEO-b-PEPA nanoparticles. The tumors were subcutaneously planted at the right thigh of mice.
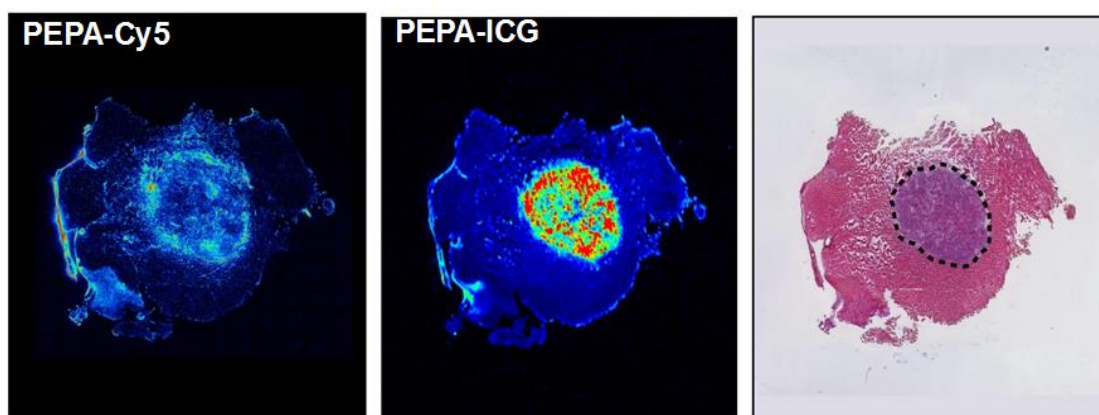
Figure 8.3.9. Comparison of tumor margin delineation effect of Cy5 and ICG conjugated PEO-b-PEPA nanoparticles, following co-injection of mixed micelles.

8.3.5-Discussion

Recently, Kataoka and coworkers have elegantly illustrated a vascular burst effect of nanoparticle extravasation from tumor vasculature, indicating vascular leakiness in solid tumors is a not a perpetual event but a transient phenomenon[27]. Similarly, many studies have also reported that tumor acidic pH is also dynamic in nature with high intratumoral heterogeneity in space and time (Tumor pH = f(x,y,z,t)). We argue that reversible small molecular extracellular pH sensors are more effective at reporting transient pH changes in the tumor microenvironment, however, they are not capable of signal amplification without introducing the background noise (e.g., signals at pH 7.4 due to their broad nature of pH response). In addition, the proton gradient across the tumor margins is expected to be diffusive due to the small size and high diffusivity of protons. Because of these reasons, we anticipate that the small molecular, extracellular pH sensors will not be able to achieve a binary delineation of tumor margins.

We hypothesized an irreversible "capture and integration" mechanism to explain the unique binary tumor margin delineation observation of UPS nanoprobes (**Figure 8.3.10**). At any specific time (t1, t2, or t3.), different regions of the tumor may be acidified below the pH threshold (e.g., 6.9) as indicated by the red spots in the front image. This acidic pH signal will first be captured by the transistor nanoprobe and then arrested in the on state due to albumin binding to ICG, unimer-cell surface interactions or other contributions that eventually lead to uptake in the cancer cells. Over time, the spatio-temporal fluctuations of acidic pH signals are 'integrated' to yield a binary fluorescence tumor map as a step function that can be approximated by 1 (tumor) and 0 (muscle). Such 'irreversible' activation and arrest mechanism of the nanotransistor

probes will convert spatio-temporal fluctuations of tumor acidic pH signals into stable binary output as illustrated.

To summarize, we performed biochemical mechanistic investigation of pH transistor nanoprobes to digitize tumor over normal muscle signals. Preliminary results suggested an 'irreversible' activation of pH nanoprobes following a 'capture and integration' mechanism to transduce acidic tumor pH signals into an emergent binary tumor digitization map for improved tumor diagnosis.
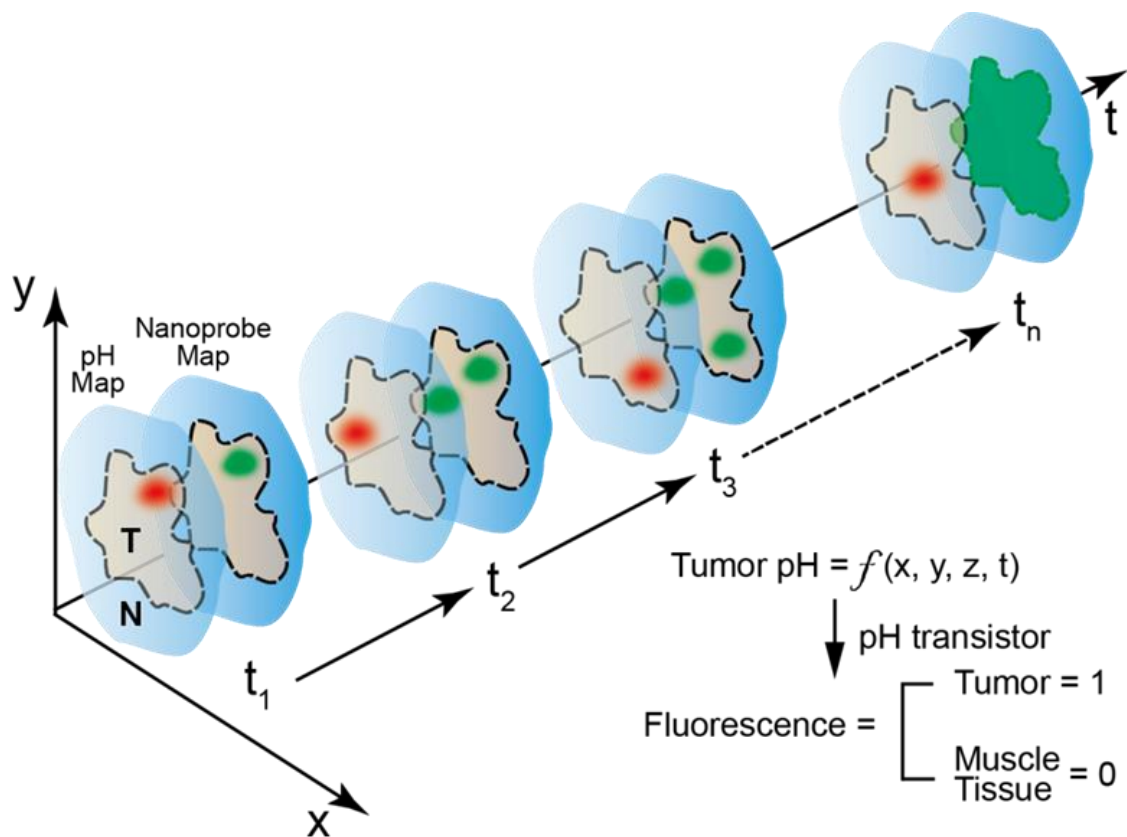
Figure 8.3.10. Schematic illustration of "capture and integration" of fluctuating tumor acidic pH signals to achieve binary delineation of tumor over surrounding muscle tissues.

8.4-Reference

1   Pelicano, H., Carney, D. & Huang, P. ROS stress in cancer cells and therapeutic implications. *Drug Resistance Updates* **7**, 97-110 (2004).

2   Trachootham, D., Alexandre, J. & Huang, P. Targeting cancer cells by ROS-mediated mechanisms: a radical therapeutic approach? *Nature reviews Drug discovery* **8**, 579-591 (2009).

3   Barar, J. & Omidi, Y. Dysregulated pH in tumor microenvironment checkmates cancer therapy. *Bioimpacts* **3**, 149-162 (2013).

4   Webb, B. A., Chimenti, M., Jacobson, M. P. & Barber, D. L. Dysregulated pH: a perfect storm for cancer progression. *Nature Reviews Cancer* **11**, 671-677 (2011).

5   Bardeen, J. Research leading to point-contact transistor. *Science* **126**, 105-112 (1957).

6   Andreev, O. A. *et al.* Mechanism and uses of a membrane peptide that targets tumors and other acidic tissues in vivo. *Proceedings of the National Academy of Sciences* **104**, 7893-7898 (2007).

7   Lei, J. & Ju, H. Signal amplification using functional nanomaterials for biosensing. *Chemical Society Reviews* **41**, 2122-2134 (2012).

8   Matsuyama, S., Llopis, J., Deveraux, Q. L., Tsien, R. Y. & Reed, J. C. Changes in intramitochondrial and cytosolic pH: early events that modulate caspase activation during apoptosis. *Nature cell biology* **2**, 318-325 (2000).

9   Miller-Chou, B. A. & Koenig, J. L. A review of polymer dissolution. *Progress in Polymer Science* **28**, 1223-1270 (2003).

10   Morimoto, N., Qiu, X.-P., Winnik, F. M. & Akiyoshi, K. Dual stimuli-responsive nanogels by self-assembly of polysaccharides lightly grafted with thiol-terminated poly (N-isopropylacrylamide) chains. *Macromolecules* **41**, 5985-5987 (2008).

11   Müller-Plathe, F. Coarse-graining in polymer simulation: from the atomistic to the mesoscopic scale and back. *ChemPhysChem* **3**, 754-769 (2002).

12   Neri, D. & Supuran, C. T. Interfering with pH regulation in tumours as a therapeutic strategy. *Nature reviews Drug discovery* **10**, 767-777 (2011).

13   Johnson, E. R. *et al.* Revealing noncovalent interactions. *Journal of the American Chemical Society* **132**, 6498-6506 (2010).

14   Tsumura, A., Koezuka, H. & Ando, T. Macromolecular electronic device: Field-effect transistor with a polythiophene thin film. *Applied Physics Letters* **49**, 1210-1212 (1986).

15   Sokal, N. O. & Sokal, A. D. Class EA new class of high-efficiency tuned single-ended switching power amplifiers. *IEEE Journal of solid-state circuits* **10**, 168-176 (1975).

16   Zhou, K. *et al.* Tunable, Ultrasensitive pH-Responsive Nanoparticles Targeting Specific Endocytic Organelles in Living Cells. *Angewandte Chemie* **123**, 6233-6238 (2011).

17   Li, Y. *et al.* Molecular basis of cooperativity in pH-triggered supramolecular self-assembly. *Nature communications* **7** (2016).

18   Zhao, T. *et al.* A transistor-like pH nanoprobe for tumour detection and image-guided surgery. *Nature Biomedical Engineering* **1**, 0006 (2016).

19   Nasongkla, N. *et al.* Multifunctional polymeric micelles as cancer-targeted, MRI-ultrasensitive drug delivery systems. *Nano letters* **6**, 2427-2430 (2006).

20   Hirche, C., Murawa, D., Mohr, Z., Kneif, S. & Hünerbein, M. ICG fluorescence-guided sentinel node biopsy for axillary nodal staging in breast cancer. *Breast cancer research and treatment* **121**, 373-378 (2010).

21   Gandorfer, A., Haritoglou, C., Gass, C. A., Ulbig, M. W. & Kampik, A. Indocyanine green-assisted peeling of the internal limiting membrane may cause retinal damage. *American journal of ophthalmology* **132**, 431-433 (2001).

22   Caesar, J., Shaldon, S., Chiandussi, L. e., Guevara, L. & Sherlock, S. The use of indocyanine green in the measurement of hepatic blood flow and as a test of hepatic function. *Clinical science* **21**, 43-57 (1961).

23   Cherrick, G. R., Stein, S. W., Leevy, C. M. & Davidson, C. S. Indocyanine green: observations on its physical properties, plasma decay, and hepatic extraction. *Journal of Clinical Investigation* **39**, 592 (1960).

24   Saxena, V., Sadoqi, M. & Shao, J. Degradation kinetics of indocyanine green in aqueous solution. *Journal of pharmaceutical sciences* **92**, 2090-2097 (2003).

25   Yoneya, S. *et al.* Binding properties of indocyanine green in human blood. *Investigative ophthalmology & visual science* **39**, 1286-1290 (1998).

26   Larsen, M. T., Kuhlmann, M., Hvam, M. L. & Howard, K. A. Albumin-based drug delivery: harnessing nature to cure disease. *Molecular and cellular therapies* **4**, 3 (2016).

27   Matsumoto, Y. *et al.* Vascular bursts enhance permeability of tumour blood vessels and improve nanoparticle delivery. *Nature nanotechnology* (2016).

CHAPTER NINE- Summary and Future Work

9.1-Summary of work

The primary research focus of my dissertation is on elucidating the molecular basis of the ultra-pH sensitivity in a series of PEO-b-PR block containing ionizable tertiary amines. Mechanistic understanding of observed binary on/off switch and signal amplification would help establish new paradigm in the development of nanomaterials-based sensors and drug delivery systems with significantly improved sensitivity and specificity.

Nanomaterials have received considerable attentions that allow for highly selective recognition, catalysis, and transfer operations in a wide range of photonic, electronic and biomedical applications[1,2]. Various nanoplatforms have been extensively investigated to address challenges in medicine and deficiencies of conventional small molecular sensors and drugs, resulting in the growing prosperity of nanomedicine[3].

In contrast to "top-down" methods such as lithography where the final structures are carved from a rigid mold, "bottom up" approach has become a major strategy to prepare functional nanomaterials where the formation of supramolecular architectures are driven by non-covalent interactions and self-assembly of molecular components[4,5]. Self-assembly, which bridges the structures of individual building blocks and the function of the obtained nanocomplex, is an essential part of nanotechnology. In contrast to covalent chemistry, supramolecular self-assembly engages a multitude of weak and reversible non-covalent interactions to achieve a thermodynamically stable nanostructure. A hallmark of self-assembled systems is positive cooperativity[6-8], which arises from the

interplay of two or more non-covalent interactions. As a result, the system as a whole behaves quite differently from the sum of individual parts acting in isolation.

In biological sensing, achieving high sensitivity and specificity of detection remains a great challenge due to the frequently small differences between pathological and normal physiological signals and the difficulty in signal amplification without introducing noise. Unimolecular sensors (e.g., Lysosensor) have a continuous response to the biological target concentration. Like all analog sensors, they are capable of distinguishing fine gradations in biological signals. However, analog sensors often suffer from low detection sensitivity and specificity due to lack of signal amplification without noise introduction.

Responsive nanomaterials have rapidly advanced in a variety of optical, electrical and mechanical systems for a wide range of applications such as biosensing, self-healing, and drug delivery[2,9,10]. Despite tremendous advances, there are still major scientific and technological barriers in the development of nanomedicine. There is a lack of mechanistic and molecular level understanding in the self-assembly process and accompanied cooperativity. Also, the thermodynamic and kinetic principles underlying cooperative responses are still not available, which hinders our capability in the rational design of more potent and sophisticated nanomedicine platforms. Another difficulty is that it is usually impractical to selectively change one parameter without affecting others to pin-point specific contributions from an individual interaction or component. To program, control and predict the performance of nanomaterials for the development of novel tools and therapies to address challenges in medicine, lots of efforts are still needed to unravel the supramolecular chemistry and cooperativity principles underlying the self-assembly

311

processes, which bridge the gap between individual molecular components and integrated functional nanostructures.

We elucidated the detailed molecular pathway of pH-induced supramolecular self-assembly of an ultra-pH sensitive block copolymer. We demonstrated that hydrophobic nanophase separation contributed to strong pH cooperativity as evidenced by the divergent proton distribution along the reversible protonation of UPS nanoparticles. pH cooperativity lead to significantly decreased pKa and sharpened pH response. Combining of theoretical modeling and experimental validation identified key structural parameters such as repeating unit hydrophobicity and polymer chain length that impact pKa and the sharpness of pH transition. Results from this study provide molecular insights to help establish the general principles in applying non-covalent self-assembly chemistry to achieve molecular cooperativity for the development of future nanomaterials-based sensors with binary stimuli response.

In another study, we systematically investigated a multitude of non-covalent bonds that affected the pH responsive behavior and resulting supramolecular self-assembly of amphiphilic UPS block copolymers. Increase of hydrophobic interactions and π-π stacking effect both stabilize the micelles and shifted the pKa to lower pH. Strengthening direct ionic bonding between protonated ammonium groups and anions will drive the protonation of tertiary amines and lead to increased pKa. Hydrogen bonding strength was also found to impact the pKa of UPS block copolymers. We identified and evaluated several key design parameters that affected the pKa and H transition sharpness of UPS nanoparticles, including hydrophobic chain length, hydrophobicity of substituents of tertiary amines and salt concentration. Alteration of

these structural parameters enabled fine tuning the pKa of UPS nanoparticles to cover the entire physiological pH ranges.

In addition to pH-triggered supramolecular self-assembly, we also observed a novel supramolecular self-assembled process triggered by specific anions. Unlike conventional micelles with neutral hydrophobic cores, the ionic micelles contain a large number of ion pairs in the core environment. The resulting micelles provide a good model system to study the fundamental process of supramolecular self-assembly through the interplay of non-covalent forces in the aqueous environment. From the application standpoint, results from this study may also open up new opportunities of using stabilized ion-pair interactions for the delivery of charged drug molecules and molecular imaging agents.

9.2- Future work

9.2.1-Dynamic polymer exchange between unimers and micelles

Based on a series of experiments including DLS and ultracentrifugation/pH we were able to clarify the thermodynamically stable intermediate states of copolymers at different protonation degree along the pH-triggered supramolecular self-assembly of UPS block copolymers. Hydrophobic micellization drove divergent proton distribution in either highly protonated unimer or neutral micelle states along the majority of the titration coordinate unlike conventional small molecular or polymeric bases. However, the kinetic process of how highly protonated unimers convert into mature micelles over time, may occur through two extreme scenarios. One possibility is the charged polymer chains first lose all of their protons in aqueous solution which is followed by the neutral unimers self-assembling into micelles. The other possibility is first the formation of loose aggregates from protonated unimers which then collapse into neutral mature micelles by sudden proton loss. It is also possible that the kinetic pathway follows somewhere between the two extremes. Generation of loose aggregates should not be ruled out as a possible mechanism for the formation of mature micelles. Future work is necessary to elucidate the kinetic pathway and transient intermediates during micelle formation,

9.2.2-PEO-b-PR polymers for anion sensing

Chemical sensors are molecular or macromolecular receptors that transduce chemical information into analytical signals upon binding to specific targets[11]. Although instrumental analysis such as atomic absorption or atomic emission spectroscopy are

currently used in chemical sensing applications such as the detection of toxic metal ions, inexpensive and easy methods for the detection and measurement of various chemical targets remain to be explored. Advances in nanomaterials and nanotechnology have inspired the development of different sensing platforms with drastically improved sensitivity and selectivity, compared to small molecular pH sensors.

Molecular recognition and supramolecular assembly offer a powerful strategy for the design of sensing systems based on controlling and analyzing host-guest interactions on the nanoscale. As demonstrated here, the hydrophobic phase separation dramatically changed the nanoscale host-guest interaction such as polycations/counter ions and protons/polyamines. The cooperative binding significantly enhanced the binding affinity compared to their unimolecular building blocks. The first step should be the identification of appropriate receptor-target pairs, in which the binding would result in change of solubility. The second step shall be the incorporation of the receptors into amphiphilic block copolymers, where the hydrophobic-hydrophilic balance is carefully design. Upon sensing targets, the receptor-conjugated block copolymers will undergo cooperative assembly and enable amplified signal output.

9.2.3-Next Generation UPS Nanoparticles

Nanomedicine research is heavily supported by public policy and investment, and is progressing rapidly[12]. Clinical benefits, including improved efficacy, bioavailability, dose–response, targeting ability, personalization, have been extensively investigated over past several decades. One major challenge in accelerating the translation of nanomaterials

315

in biomedicine is to minimize the side effect and potential toxicity. The use of biodegradable polymers for biomedical applications has increased in recent decades due to their biocompatibility, biodegradability, flexibility, and minimal side effects. Biocompatible and biodegradable nanomaterials not only improve drug safety, but also significantly shorten the timeline of drug development.

While we did not observe toxic effects in mice during our month long studies, we realize that the chemical composition of current UPS block copolymers, namely the non-degradable polymetharylate backbone,may cause concerns for their potential use in humans. Thus, the development of biodegradable pH-responsive nanoparticles with similar ultra-sensitivity and significantly improved safety profile will be the next challenge in order to bring our UPS technology into clinical settings. A multitude of hydrolysable polymers can serve as potential candidates for the design of next generation UPS block copolymers with degradable backbones, including polyesters, polycarbonate, and poly-anhydride. Our mechanistic investigation suggests that the biodegradable amphiphilic block copolymers should display similar or comparable sharp pH responsiveness and binary on/off fluorescent transition if the hydrophobicity of the monomers bearing tertiary amines was carefully tuned to meet the hydrophobic threshold for phase transition.
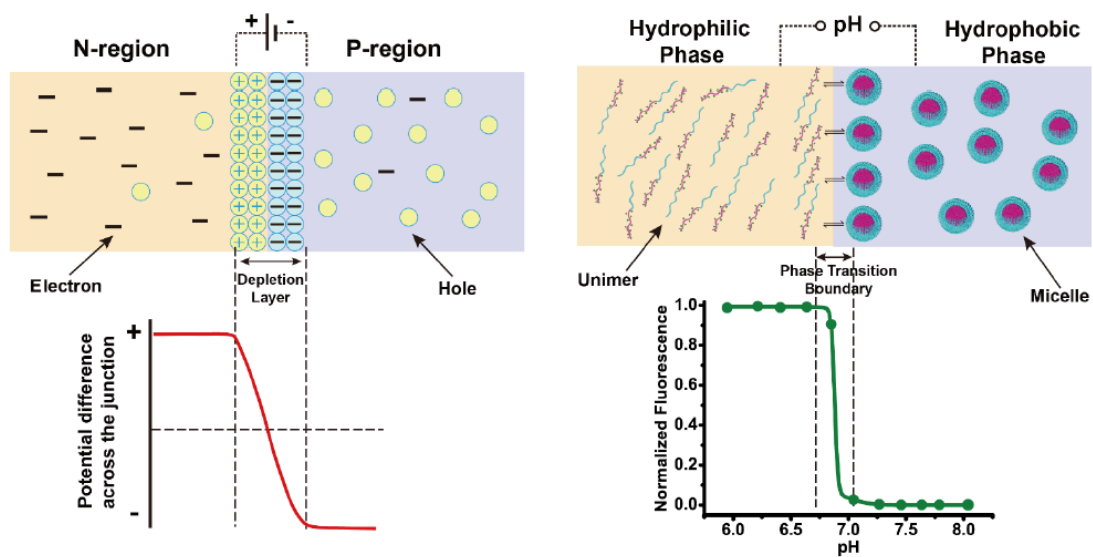
Figure 9.2.1. Analogy between an electronic transistor vs. pH nanotransistor

9.2.4-Development of nanomaterials-based chemical or biological sensors with binary on/off switch

We proposed a mechanism for the binary on/off switch and signal amplification of UPS nanoparticles, in analogy to electronic transistors (**Figure 9.2.1**). Both systems amplify/switch signals and arise from nanoscale phenomenon due to phase separation. Electronic transistors consist of P-doped and N-doped semiconductors that upon contact, form a depletion layer acting as a barrier for electron flow. For pH transistor nanoprobes, protonated unimer state and neutral micelle state are found across the transition pH to modulate the fluorescence signal. Threshold voltage and pHt values serve as gating signals for electronic transistor and pH nanotransistor, respectively. These nano-phase transition-inspired binary on/off switch and signal amplification strategy can potentially be applied for the development of a multitude of nanoplatforms for various biomedical applications.

Introduction of stimuli-responsive moieties has become a general strategy in the design of responsive functional nanomaterials. Temperature responsive materials usually contain amides surrounded by hydrophobic groups (e.g., PNIPAM[13], elastin-like peptides[14]). pH responsive materials consist of amines[15], carboxylic acids[16], or pH-sensitive labile bonds[17]. Disulfide bonds are used to synthesize redox-responsive systems[18]. Such stimuli-triggered supramolecular self-assembly arises from a multitude of non-covalent interactions that exist universally in various natural and synthetic macromolecular systems. Self-assembly based on selective and precise control of non-covalent interactions provides powerful and versatile tools for the development of complicated nanostructures at a molecular level. The development of functional

nanomaterials is characterized by a growing emphasis on identification and optimization of specific design parameters crucial to performance. The key parameters that affect the pH-triggered self-assembly elucidated here may also be applicable for tailoring the physical properties in other stimuli-responsive systems.

Our mechanistic investigation suggests that tuning the hydrophobicity may serve as a universal strategy for the design of binary on/off switchable nanomaterial-based chemical/biological sensors with improved sensitivity. Other than pH, reactive oxygen species are also recognized as biological parameters associated with many disease such as cancer[19,20]. The pathological abnormalities can also be targeted for the development of diagnostic and drug delivery systems.

9.3- Reference

1   De las Heras Alarcón, C., Pennadam, S. & Alexander, C. Stimuli responsive polymers for biomedical applications. *Chemical Society Reviews* **34**, 276-285 (2005).

2   Stuart, M. A. C. *et al.* Emerging applications of stimuli-responsive polymer materials. *Nature materials* **9**, 101-113 (2010).

3   Mura, S., Nicolas, J. & Couvreur, P. Stimuli-responsive nanocarriers for drug delivery. *Nature materials* **12**, 991-1003 (2013).

4   Chung, S. W. *et al.* Top-Down Meets Bottom-Up: Dip-Pen Nanolithography and DNA-Directed Assembly of Nanoscale Electrical Circuits. *small* **1**, 64-69 (2005).

5   Cheng, J. Y., Ross, C. A., Smith, H. I. & Thomas, E. L. Templated Self-Assembly of Block Copolymers: Top-Down Helps Bottom-Up. *Advanced Materials* **18**, 2505-2521 (2006).

6   Whitesides, G. M. & Boncheva, M. Beyond molecules: Self-assembly of mesoscopic and macroscopic components. *Proceedings of the National Academy of Sciences* **99**, 4769-4774 (2002).

7   Whitesides, G. M. & Grzybowski, B. Self-assembly at all scales. *Science* **295**, 2418-2421 (2002).

8   Hunter, C. A. & Anderson, H. L. What is cooperativity? *Angewandte Chemie International Edition* **48**, 7488-7499 (2009).

9   Webber, M. J., Appel, E. A., Meijer, E. W. & Langer, R. Supramolecular biomaterials. *Nat. Mater.* **15**, 13-26, doi:10.1038/nmat4474 (2016).

10   Webber, M. J., Appel, E. A., Meijer, E. & Langer, R. Supramolecular biomaterials. *Nature materials* **15**, 13-26 (2016).

11   Kolmakov, A. & Moskovits, M. Chemical sensing and catalysis by one-dimensional metal-oxide nanostructures. *Annu. Rev. Mater. Res.* **34**, 151-180 (2004).

12   Bawa, R. Regulating nanomedicine-can the FDA handle it? *Current drug delivery* **8**, 227-234 (2011).

13   Schild, H. G. Poly (N-isopropylacrylamide): experiment, theory and application. *Progress in polymer science* **17**, 163-249 (1992).

14   Quiroz, F. G. & Chilkoti, A. Sequence heuristics to encode phase behaviour in intrinsically disordered protein polymers. *Nature materials* (2015).

15   Bae, Y., Fukushima, S., Harada, A. & Kataoka, K. Design of environment-sensitive supramolecular assemblies for intracellular drug delivery: Polymeric micelles that are responsive to intracellular pH change. *Angewandte Chemie International Edition* **42**, 4640-4643 (2003).

16   Schmaljohann, D. Thermo-and pH-responsive polymers in drug delivery. *Advanced drug delivery reviews* **58**, 1655-1670 (2006).

17   Pang, X. *et al.* pH-responsive polymer–drug conjugates: Design and progress. *Journal of Controlled Release* **222**, 116-129 (2016).

18   Nakahata, M., Takashima, Y., Yamaguchi, H. & Harada, A. Redox-responsive self-healing materials formed from host–guest polymers. *Nature communications* **2**, 511 (2011).

19   Schumacker, P. T. Reactive oxygen species in cancer cells: live by the sword, die by the sword. *Cancer cell* **10**, 175-176 (2006).

20   Diehn, M. *et al.* Association of reactive oxygen species levels and radioresistance in cancer stem cells. *nature* **458**, 780-783 (2009).

BIBLIOGRAPHY

Al-Ahmady, Z. S., Al-Jamal, W. T., Bossche, J. V., Bui, T. T., Drake, A. F., Mason, A. J., & Kostarelos, K. (2012). Lipid–peptide vesicle nanoscale hybrids for triggered drug release by mild hyperthermia in vitro and in vivo. *ACS nano, 6*(10), 9335-9346.

Amiram, M., Luginbuhl, K. M., Li, X., Feinglos, M. N., & Chilkoti, A. (2013). Injectable protease-operated depots of glucagon-like peptide-1 provide extended and tunable glucose control. *Proceedings of the National Academy of Sciences, 110*(8), 2792-2797.

An, M., Wijesinghe, D., Andreev, O. A., Reshetnyak, Y. K., & Engelman, D. M. (2010). pH-(low)-insertion-peptide (pHLIP) translocation of membrane impermeable phalloidin toxin inhibits cancer cell proliferation. *Proceedings of the National Academy of Sciences, 107*(47), 20246-20250.

Andreev, O. A., Dupuy, A. D., Segala, M., Sandugu, S., Serra, D. A., Chichester, C. O., . . . Reshetnyak, Y. K. (2007). Mechanism and uses of a membrane peptide that targets tumors and other acidic tissues in vivo. *Proceedings of the National Academy of Sciences, 104*(19), 7893-7898.

Andreev, O. A., Karabadzhak, A. G., Weerakkody, D., Andreev, G. O., Engelman, D. M., & Reshetnyak, Y. K. (2010). pH (low) insertion peptide (pHLIP) inserts across a lipid bilayer as a helix and exits by a different path. *Proceedings of the National Academy of Sciences, 107*(9), 4081-4086.

Arakawa, T., & Timasheff, S. N. (1984). Mechanism of protein salting in and salting out by divalent cation salts: balance between hydration and salt binding. *Biochemistry, 23*(25), 5912-5923.

Bae, Y., Fukushima, S., Harada, A., & Kataoka, K. (2003). Design of environment-sensitive supramolecular assemblies for intracellular drug delivery: Polymeric micelles that are responsive to intracellular pH change. *Angewandte Chemie International Edition, 42*(38), 4640-4643.

Bae, Y. H., Okano, T., Hsu, R., & Kim, S. W. (1987). Thermo- sensitive polymers as on- off switches for drug release. *Die Makromolekulare Chemie, Rapid Communications, 8*(10), 481-485.

Barar, J., & Omidi, Y. (2013). Dysregulated pH in tumor microenvironment checkmates cancer therapy. *Bioimpacts, 3*(4), 149-162.

Bardeen, J. (1957). Research leading to point-contact transistor. *Science, 126*(3264), 105-112.

Barrera, F. N., Fendos, J., & Engelman, D. M. (2012). Membrane physical properties influence transmembrane helix formation. *Proceedings of the National Academy of Sciences, 109*(36), 14422-14427.

Barrera, F. N., Weerakkody, D., Anderson, M., Andreev, O. A., Reshetnyak, Y. K., & Engelman, D. M. (2011). Roles of carboxyl groups in the transmembrane insertion of peptides. *Journal of molecular biology, 413*(2), 359-371.

Bawa, R. (2011). Regulating nanomedicine-can the FDA handle it? *Current drug delivery, 8*(3), 227-234.

Betre, H., Liu, W., Zalutsky, M. R., Chilkoti, A., Kraus, V. B., & Setton, L. A. (2006). A thermally responsive biopolymer for intra-articular drug delivery. *Journal of controlled release, 115*(2), 175-182.

Bikram, M., & West, J. L. (2008). Thermo-responsive systems for controlled drug delivery. *Expert opinion on drug delivery, 5*(10), 1077-1091.

Blanco, E., Shen, H., & Ferrari, M. (2015). Principles of nanoparticle design for overcoming biological barriers to drug delivery. *Nature biotechnology, 33*(9), 941-951.

Blum, A. P., Kammeyer, J. K., Rush, A. M., Callmann, C. E., Hahn, M. E., & Gianneschi, N. C. (2015). Stimuli-Responsive Nanomaterials for Biomedical Applications. *Journal of the American Chemical Society, 137*(6), 2140-2154.

Boussif, O., Lezoualc'h, F., Zanta, M. A., Mergny, M. D., Scherman, D., Demeneix, B., & Behr, J.-P. (1995). A versatile vector for gene and oligonucleotide transfer into cells in culture and in vivo: polyethylenimine. *Proceedings of the National Academy of Sciences, 92*(16), 7297-7301.

Boyer, C., Whittaker, M. R., Luzon, M., & Davis, T. P. (2009). Design and synthesis of dual thermoresponsive and antifouling hybrid polymer/gold nanoparticles. *Macromolecules, 42*(18), 6917-6926.

Bradley, M., Alexander, L., Duncan, K., Chennaoui, M., Jones, A. C., & Sánchez-Martín, R. M. (2008). pH sensing in living cells using fluorescent microspheres. *Bioorganic & medicinal chemistry letters, 18*(1), 313-317.

Branden, C. I. (1999). *Introduction to protein structure*: Garland Science.

Brangwynne, C. P. (2013). Phase transitions and size scaling of membrane-less organelles. *J Cell Biol, 203*(6), 875-881.

Bryngelson, J. D., Onuchic, J. N., Socci, N. D., & Wolynes, P. G. (1995). Funnels, pathways, and the energy landscape of protein folding: a synthesis. *Proteins: Structure, Function, and Bioinformatics, 21*(3), 167-195.

Buchmueller, K. L., Webb, A. E., Richardson, D. A., & Weeks, K. M. (2000). A collapsed non-native RNA folding state. *Nature Structural & Molecular Biology, 7*(5), 362-366.

Burnett, J. C., & Rossi, J. J. (2012). RNA-based therapeutics: current progress and future prospects. *Chemistry & biology, 19*(1), 60-71.

Caesar, J., Shaldon, S., Chiandussi, L. e., Guevara, L., & Sherlock, S. (1961). The use of indocyanine green in the measurement of hepatic blood flow and as a test of hepatic function. *Clinical science, 21*, 43-57.

Camara-Campos, A., Hunter, C. A., & Tomas, S. (2006). Cooperativity in the self-assembly of porphyrin ladders. *Proceedings of the National Academy of Sciences of the United States of America, 103*(9), 3034-3038.

Cao, Y., Zhu, X., Luo, J., & Liu, H. (2007). Effects of substitution groups on the RAFT polymerization of N-alkylacrylamides in the preparation of thermosensitive block copolymers. *Macromolecules, 40*(18), 6481-6488.

Casey, J. R., Grinstein, S., & Orlowski, J. (2010). Sensors and regulators of intracellular pH. *Nature reviews Molecular cell biology, 11*(1), 50-61.

Chan, H. S., & Dill, K. A. (1998). Protein folding in the landscape perspective: Chevron plots and non- Arrhenius kinetics. *Proteins: Structure, Function, and Bioinformatics, 30*(1), 2-33.

Chandran, S. S., Dickson, K. A., & Raines, R. T. (2005). Latent fluorophore based on the trimethyl lock. *Journal of the American Chemical Society, 127*(6), 1652-1653.

Chang, R. (2000). *Physical chemistry for the chemical and biological sciences*: University Science Books.

Chen, J., Liu, Q., Xiao, J., & Du, J. (2015). EpCAM-antibody-labeled noncytotoxic polymer vesicles for cancer stem cells-targeted delivery of anticancer drug and siRNA. *Biomacromolecules, 16*(6), 1695-1705.

Chen, K.-J., Liang, H.-F., Chen, H.-L., Wang, Y., Cheng, P.-Y., Liu, H.-L., . . . Sung, H.-W. (2012). A thermoresponsive bubble-generating liposomal system for triggering localized extracellular drug delivery. *ACS nano, 7*(1), 438-446.

Chen, S., Zhang, Y., Wang, K., Zhou, H., & Zhang, W. (2016a). N-Ester-substituted polyacrylamides with a tunable lower critical solution temperature (LCST): the N-ester-substitute dependent thermoresponse. *Polymer Chemistry*.

Chen, S., Zhang, Y., Wang, K., Zhou, H., & Zhang, W. (2016b). N-Ester-substituted polyacrylamides with a tunable lower critical solution temperature (LCST): the N-ester-substitute dependent thermoresponse. *Polymer Chemistry, 7*(21), 3509-3519.

Chen, X., Li, C., Grätzel, M., Kostecki, R., & Mao, S. S. (2012). Nanomaterials for renewable energy production and storage. *Chemical Society Reviews, 41*(23), 7909-7937.

Cheng, J. Y., Ross, C. A., Smith, H. I., & Thomas, E. L. (2006). Templated Self- Assembly of Block Copolymers: Top- Down Helps Bottom- Up. *Advanced Materials, 18*(19), 2505-2521.

Cherrick, G. R., Stein, S. W., Leevy, C. M., & Davidson, C. S. (1960). Indocyanine green: observations on its physical properties, plasma decay, and hepatic extraction. *Journal of Clinical Investigation, 39*(4), 592.

Cheung, M. S., García, A. E., & Onuchic, J. N. (2002). Protein folding mediated by solvation: water expulsion and formation of the hydrophobic core occur after the structural collapse. *Proceedings of the National Academy of Sciences, 99*(2), 685-690.

Chiang, A. C., & Massagué, J. (2008). Molecular basis of metastasis. *New England Journal of Medicine, 359*(26), 2814-2823.

Cho, K., Wang, X., Nie, S., & Shin, D. M. (2008). Therapeutic nanoparticles for drug delivery in cancer. *Clinical Cancer Research, 14*(5), 1310-1316.

Choi, Y. H., Liu, F., Kim, J.-S., Choi, Y. K., Park, J. S., & Kim, S. W. (1998). Polyethylene glycol-grafted poly-L-lysine as polymeric gene carrier. *Journal of Controlled Release, 54*(1), 39-48.

Chung, S. W., Ginger, D. S., Morales, M. W., Zhang, Z., Chandrasekhar, V., Ratner, M. A., & Mirkin, C. A. (2005). Top- Down Meets Bottom- Up: Dip- Pen Nanolithography and DNA- Directed Assembly of Nanoscale Electrical Circuits. *small, 1*(1), 64-69.

Collins, K. D. (1997). Charge density-dependent strength of hydration and biological structure. *Biophysical Journal, 72*(1), 65-76. doi:10.1016/s0006-3495(97)78647-8

Collins, K. D., & Washabaugh, M. W. (1985). The Hofmeister effect and the behaviour of water at interfaces. *Quarterly Reviews of Biophysics, 18*(04), 323-422. doi:doi:10.1017/S0033583500005369

Compiani, M., & Capriotti, E. (2013). Computational and theoretical methods for protein folding. *Biochemistry, 52*(48), 8601-8624.

Conde, J., Oliva, N., & Artzi, N. (2016). Revisiting the 'One Material Fits All' Rule for Cancer Nanotherapy. *Trends in biotechnology, 34*(8), 618-626.

Connors, K. A., Paulson, A., & Toledo-Velasquez, D. (1988). Complexing of. alpha.-cyclodextrin with sym-4, 4'-disubstituted biphenyls. *The Journal of Organic Chemistry, 53*(9), 2023-2026.

Convertine, A. J., Diab, C., Prieve, M., Paschal, A., Hoffman, A., Johnson, P., & Stayton, P. (2010). pH-responsive polymeric micelle carriers for siRNA drugs. *Biomacromolecules, 11*(11), 2904-2911.

Cui, H., Chen, Z., Zhong, S., Wooley, K. L., & Pochan, D. J. (2007). Block copolymer assembly via kinetic control. *Science, 317*(5838), 647-650.

Cutler, J. I., Auyeung, E., & Mirkin, C. A. (2012). Spherical nucleic acids. *Journal of the American Chemical Society, 134*(3), 1376-1391.

Dai, S., Ravi, P., & Tam, K. C. (2009). Thermo-and photo-responsive polymeric systems. *Soft Matter, 5*(13), 2513-2533.

Daoud, M., Cotton, J., Farnoux, B., Jannink, G., Sarma, G., Benoit, H., . . . De Gennes, P. (1975). Solutions of flexible polymers. Neutron experiments and interpretation. *Macromolecules, 8*(6), 804-818.

Darling, S. (2007). Directing the self-assembly of block copolymers. *Progress in Polymer Science, 32*(10), 1152-1204.

Davis, M. E., & Shin, D. M. (2008). Nanoparticle therapeutics: an emerging treatment modality for cancer. *Nature reviews Drug discovery, 7*(9), 771-782.

De Greef, T. F., Smulders, M. M., Wolffs, M., Schenning, A. P., Sijbesma, R. P., & Meijer, E. (2009). Supramolecular polymerization. *Chemical Reviews, 109*(11), 5687-5754.

De las Heras Alarcón, C., Pennadam, S., & Alexander, C. (2005). Stimuli responsive polymers for biomedical applications. *Chemical Society Reviews, 34*(3), 276-285.

Deacon, J. C., Engelman, D. M., & Barrera, F. N. (2015). Targeting acidity in diseased tissues: mechanism and applications of the membrane-inserting peptide, pHLIP. *Archives of biochemistry and biophysics, 565*, 40-48.

Denker, S. P., & Barber, D. L. (2002). Cell migration requires both ion translocation and cytoskeletal anchoring by the Na-H exchanger NHE1. *Journal of Cell Biology, 159*(6), 1087-1096. doi:10.1083/jcb.200208050

Dickerson, R. E., & Geis, I. (1983). *Hemoglobin: structure, function, evolution, and pathology* (Vol. 1983): Benjamin-Cummings Publishing Company.

Diehn, M., Cho, R. W., Lobo, N. A., Kalisky, T., Dorie, M. J., Kulp, A. N., . . . Wong, M. (2009). Association of reactive oxygen species levels and radioresistance in cancer stem cells. *Nature, 458*(7239), 780-783.

Dill, K. A., & MacCallum, J. L. (2012). The protein-folding problem, 50 years on. *Science, 338*(6110), 1042-1046.

Dinner, A. R., Šali, A., Smith, L. J., Dobson, C. M., & Karplus, M. (2000). Understanding protein folding via free-energy surfaces from theory and experiment. *Trends in biochemical sciences, 25*(7), 331-339.

Discher, D. E., & Eisenberg, A. (2002). Polymer vesicles. *Science, 297*(5583), 967-973.

Doane, T. L., & Burda, C. (2012). The unique role of nanoparticles in nanomedicine: imaging, drug delivery and therapy. *Chemical Society Reviews, 41*(7), 2885-2911.

Dobson, C. M. (2003). Protein folding and misfolding. *Nature, 426*(6968), 884-890.

Dobson, C. M. (2004). *Principles of protein folding, misfolding and aggregation.* Paper presented at the Seminars in cell & developmental biology.

Dobson, C. M., Šali, A., & Karplus, M. (1998). Protein folding: a perspective from theory and experiment. *Angewandte Chemie International Edition, 37*(7), 868-893.

Doi, M., & Edwards, S. F. (1988). *The theory of polymer dynamics* (Vol. 73): oxford university press.

Domínguez, A., Fernández, A., González, N., Iglesias, E., & Montenegro, L. (1997). Determination of critical micelle concentration of some surfactants by three techniques. *J. Chem. Educ, 74*(10), 1227.

Doudna, J. A., & Doherty, E. A. (1997). Emerging themes in RNA folding. *Folding and Design, 2*(5), R65-R70.

Du, J.-Z., Du, X.-J., Mao, C.-Q., & Wang, J. (2011). Tailor-made dual pH-sensitive polymer–doxorubicin nanoparticles for efficient anticancer drug delivery. *Journal of the American Chemical Society, 133*(44), 17560-17563.

Du, J., Tang, Y., Lewis, A. L., & Armes, S. P. (2005). pH-sensitive vesicles based on a biocompatible zwitterionic diblock copolymer. *Journal of the American Chemical Society, 127*(51), 17982-17983.

Dvir, T., Timko, B. P., Kohane, D. S., & Langer, R. (2011). Nanotechnological strategies for engineering complex tissues. *Nature nanotechnology, 6*(1), 13-22.

Dyson, H. J., & Wright, P. E. (2002). Coupling of folding and binding for unstructured proteins. *Current opinion in structural biology, 12*(1), 54-60.

Eaton, W. A., Henry, E. R., Hofrichter, J., & Mozzarelli, A. (1999). Is cooperative oxygen binding by hemoglobin really understood? *Nature Structural & Molecular Biology, 6*(4), 351-358.

Edwards, E. W., Chanana, M., Wang, D., & Möhwald, H. (2008). Stimuli- Responsive Reversible Transport of Nanoparticles Across Water/Oil Interfaces. *Angewandte Chemie International Edition, 47*(2), 320-323.

Elghanian, R., Storhoff, J. J., Mucic, R. C., Letsinger, R. L., & Mirkin, C. A. (1997). Selective colorimetric detection of polynucleotides based on the distance-dependent optical properties of gold nanoparticles. *Science, 277*(5329), 1078-1081.

Ercolani, G., Piguet, C., Borkovec, M., & Hamacek, J. (2007). Symmetry numbers and statistical factors in self-assembly and multivalency. *The Journal of Physical Chemistry B, 111*(42), 12195-12203.

Eryazici, I., Prytkova, T. R., Schatz, G. C., & Nguyen, S. T. (2010). Cooperative melting in caged dimers with only two DNA duplexes. *Journal of the American Chemical Society, 132*(48), 17068-17070.

Etheridge, M. L., Campbell, S. A., Erdman, A. G., Haynes, C. L., Wolf, S. M., & McCullough, J. (2013). The big picture on nanomedicine: the state of investigational and approved nanomedicine products. *Nanomedicine: Nanotechnology, Biology and Medicine, 9*(1), 1-14.

Fang, J., Nakamura, H., & Maeda, H. (2011). The EPR effect: Unique features of tumor blood vessels for drug delivery, factors involved, and limitations and augmentation of the effect. *Advanced drug delivery reviews, 63*(3), 136-151. doi:http://dx.doi.org/10.1016/j.addr.2010.04.009

Favre, E., Nguyen, Q., Sacco, D., Moncuy, A., & Clement, R. (1995). Multicomponent polymer/solvents equilibria: an evaluation of Flory-Huggins theory for crosslinked PDMS networks swelled by binary mixtures. *Chemical Engineering Communications, 140*(1), 193-205.

Feil, H., Bae, Y. H., Feijen, J., & Kim, S. W. (1993). Effect of comonomer hydrophilicity and ionization on the lower critical solution temperature of N-isopropylacrylamide copolymers. *Macromolecules, 26*(10), 2496-2500.

Ferrari, M. (2005). Cancer nanotechnology: opportunities and challenges. *Nature Reviews Cancer, 5*(3), 161-171.

Flory, P. J. (1942). Thermodynamics of high polymer solutions. *The Journal of chemical physics, 10*(1), 51-61.

Flory, P. J., & Krigbaum, W. R. (1951). Thermodynamics of high polymer solutions. *Annual review of physical chemistry, 2*(1), 383-402.

Fredrickson, G. H., Liu, A. J., & Bates, F. S. (1994). Entropic corrections to the Flory-Huggins theory of polymer blends: Architectural and conformational effects. *Macromolecules, 27*(9), 2503-2511.

Freitas, R. A. (2005). What is nanomedicine? *Nanomedicine: Nanotechnology, Biology and Medicine, 1*(1), 2-9.

Frey, S., Richter, R. P., & Görlich, D. (2006). FG-rich repeats of nuclear pore proteins form a three-dimensional meshwork with hydrogel-like properties. *Science, 314*(5800), 815-817.

Frieden, E. (1975). Non-covalent interactions: key to biological flexibility and specificity. *J. Chem. Educ, 52*(12), 754.

Fujishige, S., Kubota, K., & Ando, I. (1989). Phase transition of aqueous solutions of poly (N-isopropylacrylamide) and poly (N-isopropylmethacrylamide). *Journal of Physical Chemistry, 93*(8), 3311-3313.

Fujita, N., Shinkai, S., & James, T. D. (2008). Boronic Acids in Molecular Self-Assembly. *Chemistry–An Asian Journal, 3*(7), 1076-1091.

Galande, A. K., Weissleder, R., & Tung, C.-H. (2006). Fluorescence probe with a pH-sensitive trigger. *Bioconjugate chemistry, 17*(2), 255-257.

Gandorfer, A., Haritoglou, C., Gass, C. A., Ulbig, M. W., & Kampik, A. (2001). Indocyanine green-assisted peeling of the internal limiting membrane may cause retinal damage. *American journal of ophthalmology, 132*(3), 431-433.

Gao, G. H., Park, M. J., Li, Y., Im, G. H., Kim, J.-H., Kim, H. N., . . . Lee, J. H. (2012). The use of pH-sensitive positively charged polymeric micelles for protein delivery. *Biomaterials, 33*(35), 9157-9164.

Gao, W., Chan, J. M., & Farokhzad, O. C. (2010). pH-responsive nanoparticles for drug delivery. *Molecular pharmaceutics, 7*(6), 1913-1920.

Gatenby, R. A., & Gillies, R. J. (2004a). Why do cancers have high aerobic glycolysis? *Nature Reviews Cancer, 4*(11), 891-899. doi:10.1038/nrc1478

Gatenby, R. A., & Gillies, R. J. (2004b). Why do cancers have high aerobic glycolysis? *Nature Reviews Cancer, 4*(11), 891-899. doi:10.1038/nrc1478

Gibbs-Davis, J. M., Schatz, G. C., & Nguyen, S. T. (2007). Sharp melting transitions in DNA hybrids without aggregate dissolution: Proof of neighboring-duplex cooperativity. *Journal of the American Chemical Society, 129*(50), 15535-15540.

Gibson, M. I., Paripovic, D., & Klok, H. A. (2010). Size‐ Dependent LCST Transitions of Polymer‐ Coated Gold Nanoparticles: Cooperative Aggregation and Surface Assembly. *Advanced Materials, 22*(42), 4721-4725.

Gillies, E. R., & Fréchet, J. M. (2003). A new approach towards acid sensitive copolymer micelles for drug delivery. *Chemical Communications*(14), 1640-1641.

Gillies, R. J., Liu, Z., & Bhujwalla, Z. (1994a). 31P-MRS measurements of extracellular pH of tumors using 3-aminopropylphosphonate. *American Journal of Physiology, 267*(1 Pt 1), C195-203.

Gillies, R. J., Liu, Z., & Bhujwalla, Z. (1994b). P-31-Mrs Measurements of Extracellular Ph of Tumors Using 3-Aminopropylphosphonate. *American Journal of Physiology, 267*(1), C195-C203.

Gillies, R. J., Raghunand, N., Garcia-Martin, M. L., & Gatenby, R. A. (2004a). PH imaging. *IEEE Engineering in Medicine and Biology Magazine, 23*(5), 57-64. doi:Doi 10.1109/Memb.2004.1360409

Gillies, R. J., Raghunand, N., Garcia-Martin, M. L., & Gatenby, R. A. (2004b). pH imaging. A review of pH measurement methods and applications in cancers. *IEEE Engineering in Medicine and Biology Magazine, 23*(5), 57-64.

Gottesman, M. M., Fojo, T., & Bates, S. E. (2002). Multidrug resistance in cancer: role of ATP–dependent transporters. *Nature Reviews Cancer, 2*(1), 48-58.

Grakoui, A., Bromley, S. K., Sumen, C., Davis, M. M., Shaw, A. S., Allen, P. M., & Dustin, M. L. (1999). The immunological synapse: a molecular machine controlling T cell activation. *Science, 285*(5425), 221-227.

Grillo-Hill, B. K., Choi, C., Jimenez-Vidal, M., & Barber, D. L. (2015). Increased H(+) efflux is sufficient to induce dysplasia and necessary for viability with oncogene expression. *Elife, 4*. doi:10.7554/eLife.03270

Grinberg, N. V., Dubovik, A. S., Grinberg, V. Y., Kuznetsov, D. V., Makhaeva, E. E., Grosberg, A. Y., & Tanaka, T. (1999). Studies of the thermal volume transition of poly (N-isopropylacrylamide) hydrogels by high-sensitivity differential scanning microcalorimetry. 1. Dynamic effects. *Macromolecules, 32*(5), 1471-1475.

Grunwell, J. R., Glass, J. L., Lacoste, T. D., Deniz, A. A., Chemla, D. S., & Schultz, P. G. (2001). Monitoring the Conformational Fluctuations of DNA Hairpins Using Single-Pair Fluorescence Resonance Energy Transfer. *Journal of the American Chemical Society, 123*(18), 4295-4303. doi:10.1021/ja0027620

Gumbiner, B. M. (1996). Cell adhesion: the molecular basis of tissue architecture and morphogenesis. *Cell, 84*(3), 345-357.

Gurau, M. C., Lim, S.-M., Castellana, E. T., Albertorio, F., Kataoka, S., & Cremer, P. S. (2004). On the mechanism of the Hofmeister effect. *Journal of the American Chemical Society, 126*(34), 10522-10523.

Ha, T., Ting, A. Y., Liang, J., Caldwell, W. B., Deniz, A. A., Chemla, D. S., . . . Weiss, S. (1999). Single-molecule fluorescence spectroscopy of enzyme conformational dynamics and cleavage mechanism. *Proceedings of the National Academy of Sciences of the United States of America, 96*(3), 893-898.

Habchi, J., Tompa, P., Longhi, S., & Uversky, V. N. (2014). Introducing protein intrinsic disorder. *Chemical reviews, 114*(13), 6561-6588.

Halo, T. L., McMahon, K. M., Angeloni, N. L., Xu, Y., Wang, W., Chinen, A. B., . . . Cheng, C. (2014). NanoFlares for the detection, isolation, and culture of live tumor cells from human blood. *Proceedings of the National Academy of Sciences, 111*(48), 17104-17109.

Han, J., & Burgess, K. (2009). Fluorescent indicators for intracellular pH. *Chemical reviews, 110*(5), 2709-2728.

Han, M. S., Lytton- Jean, A. K., Oh, B. K., Heo, J., & Mirkin, C. A. (2006). Colorimetric Screening of DNA- Binding Molecules with Gold Nanoparticle Probes. *Angewandte Chemie International Edition, 45*(11), 1807-1810.

Haraguchi, K., & Takehisa, T. (2002). Nanocomposite hydrogels: a unique organic-inorganic network structure with extraordinary mechanical, optical, and swelling/de-swelling properties. *Advanced Materials, 14*(16), 1120.

Haraguchi, K., Takehisa, T., & Fan, S. (2002). Effects of clay content on the properties of nanocomposite hydrogels composed of poly (N-isopropylacrylamide) and clay. *Macromolecules, 35*(27), 10162-10171.

Hayward, R. C., & Pochan, D. J. (2010). Tailored assemblies of block copolymers in solution: it is all about the process. *Macromolecules, 43*(8), 3577-3584.

Heller, J., Penhale, D., & Helwing, R. (1980). Preparation of polyacetals by the reaction of divinyl ethers and polyols. *Journal of Polymer Science: Polymer Letters Edition, 18*(4), 293-297.

Helmlinger, G., Sckell, A., Dellian, M., Forbes, N. S., & Jain, R. K. (2002). Acid production in glycolysis-impaired tumors provides new insights into tumor metabolism. *Clinical Cancer Research, 8*(4), 1284-1291.

Heskins, M., & Guillet, J. E. (1968). Solution properties of poly (N-isopropylacrylamide). *Journal of Macromolecular Science—Chemistry, 2*(8), 1441-1455.

Hirche, C., Murawa, D., Mohr, Z., Kneif, S., & Hünerbein, M. (2010). ICG fluorescence-guided sentinel node biopsy for axillary nodal staging in breast cancer. *Breast cancer research and treatment, 121*(2), 373-378.

Ho, K., Lapitsky, Y., Shi, M., & Shoichet, M. S. (2009). Tunable immunonanoparticle binding to cancer cells: thermodynamic analysis of targeted drug delivery vehicles. *Soft Matter, 5*(5), 1074-1080.

Hofmeister, F. (1888). Zur Lehre von der Wirkung der Salze. *Archiv für experimentelle Pathologie und Pharmakologie, 25*(1), 1-30. doi:10.1007/bf01838161

Holzinger, M., Le Goff, A., & Cosnier, S. (2014). Nanomaterials for biosensing applications: a review. *Frontiers in chemistry, 2*, 63.

Hong, S., Leroueil, P. R., Majoros, I. J., Orr, B. G., Baker, J. R., & Holl, M. M. B. (2007). The binding avidity of a nanoparticle-based multivalent targeted drug delivery platform. *Chemistry & biology, 14*(1), 107-115.

Hou, S., Zhang, A., & Su, M. (2016). Nanomaterials for Biosensing Applications: Multidisciplinary Digital Publishing Institute.

Huang, X., Huang, G., Zhang, S., Sagiyama, K., Togao, O., Ma, X., . . . Gao, J. (2013). Multi-chromatic pH-activatable 19F-MRI nanoprobes with binary ON/OFF pH transitions and chemical-shift barcodes. *Angewandte Chemie. International Edition in English, 52*(31), 8074-8078. doi:10.1002/anie.201301135

Huffman, A. S., Afrassiabi, A., & Dong, L. C. (1986). Thermally reversible hydrogels: II. Delivery and selective removal of substances from aqueous solutions. *Journal of controlled release, 4*(3), 213-222.

Huggins, M. L. (1941). Solutions of long chain compounds. *The Journal of chemical physics, 9*(5), 440-440.

Hunt, J. F., Rath, P., Rothschild, K. J., & Engelman, D. M. (1997). Spontaneous, pH-dependent membrane insertion of a transbilayer α-helix. *Biochemistry, 36*(49), 15177-15192.

Hunter, C. A., & Anderson, H. L. (2009). What is cooperativity? *Angewandte Chemie International Edition, 48*(41), 7488-7499.

Huppa, J. B., & Davis, M. M. (2003). T-cell-antigen recognition and the immunological synapse. *Nature Reviews Immunology, 3*(12), 973-983.

Hyman, A. A., & Simons, K. (2012). Beyond oil and water—phase transitions in cells. *Science, 337*(6098), 1047-1049.

Hyun, D. C., Levinson, N. S., Jeong, U., & Xia, Y. (2014). Emerging Applications of Phase- Change Materials (PCMs): Teaching an Old Dog New Tricks. *Angewandte Chemie International Edition, 53*(15), 3780-3795.

Idziak, I., Avoce, D., Lessard, D., Gravel, D., & Zhu, X. (1999). Thermosensitivity of aqueous solutions of poly (N, N-diethylacrylamide). *Macromolecules, 32*(4), 1260-1263.

Ieong, N. S., Hasan, M., Phillips, D. J., Saaka, Y., O'Reilly, R. K., & Gibson, M. I. (2012). Polymers with molecular weight dependent LCSTs are essential for cooperative behaviour. *Polymer Chemistry, 3*(3), 794-799.

Ieong, N. S., Redhead, M., Bosquillon, C., Alexander, C., Kelland, M., & O'Reilly, R. K. (2011). The missing lactam-thermoresponsive and biocompatible poly (N-vinylpiperidone) polymers by xanthate-mediated RAFT polymerization. *Macromolecules, 44*(4), 886-893.

Ito, D., & Kubota, K. (1997). Solution properties and thermal behavior of poly (N-n-propylacrylamide) in water. *Macromolecules, 30*(25), 7828-7834.

Jackson, S. E., & Fersht, A. R. (1991). Folding of chymotrypsin inhibitor 2. 1. Evidence for a two-state transition. *Biochemistry, 30*(43), 10428-10435.

Jacobs, T. W., Gown, A. M., Yaziji, H., Barnes, M. J., & Schnitt, S. J. (2000). HER-2/neu protein expression in breast cancer evaluated by immunohistochemistry. *American journal of clinical pathology, 113*(2), 251-258.

Jakes, K. S., & Cramer, W. A. (2012). Border crossings: colicins and transporters. *Annual review of genetics, 46*, 209-231.

James, M. L., & Gambhir, S. S. (2012). A molecular imaging primer: modalities, imaging agents, and applications. *Physiological reviews, 92*(2), 897-965.

Jares-Erijman, E. A., & Jovin, T. M. (2003). FRET imaging. *Nat Biotech, 21*(11), 1387-1395.

Jin, J., Iyoda, T., Cao, C., Song, Y., Jiang, L., Li, T. J., & Zhu, D. B. (2001). Self-Assembly of Uniform Spherical Aggregates of Magnetic Nanoparticles through π–π Interactions. *Angewandte Chemie International Edition, 40*(11), 2135-2138.

Jin, R., Wu, G., Li, Z., Mirkin, C. A., & Schatz, G. C. (2003). What controls the melting properties of DNA-linked gold nanoparticle assemblies? *Journal of the American Chemical Society, 125*(6), 1643-1654.

Johnson, E. R., Keinan, S., Mori-Sanchez, P., Contreras-Garcia, J., Cohen, A. J., & Yang, W. (2010). Revealing noncovalent interactions. *Journal of the American Chemical Society, 132*(18), 6498-6506.

Jonkheijm, P., van der Schoot, P., Schenning, A. P., & Meijer, E. (2006). Probing the solvent-assisted nucleation pathway in chemical self-assembly. *Science, 313*(5783), 80-83.

Jose, C., Bellance, N., & Rossignol, R. (2011). Choosing between glycolysis and oxidative phosphorylation: a tumor's dilemma? *Biochimica et Biophysica Acta, 1807*(6), 552-561. doi:10.1016/j.bbabio.2010.10.012

Jose, C., Bellance, N., & Rossignol, R. (2011). Choosing between glycolysis and oxidative phosphorylation: a tumor's dilemma? *Biochimica et Biophysica Acta (BBA)-Bioenergetics, 1807*(6), 552-561.

Jungwirth, P., & Cremer, P. S. (2014). Beyond hofmeister. *Nature chemistry, 6*(4), 261-263.

Kairdolf, B. A., & Nie, S. (2011). Multidentate-protected colloidal gold nanocrystals: pH control of cooperative precipitation and surface layer shedding. *Journal of the American Chemical Society, 133*(19), 7268-7271.

Kaizuka, Y., Douglass, A. D., Varma, R., Dustin, M. L., & Vale, R. D. (2007). Mechanisms for segregating T cell receptor and adhesion molecules during immunological synapse formation in Jurkat T cells. *Proceedings of the National Academy of Sciences, 104*(51), 20296-20301.

Karabadzhak, A. G., Weerakkody, D., Wijesinghe, D., Thakur, M. S., Engelman, D. M., Andreev, O. A., . . . Reshetnyak, Y. K. (2012). Modulation of the pHLIP transmembrane helix insertion pathway. *Biophysical journal, 102*(8), 1846-1855.

Karlström, G. (1985). A new model for upper and lower critical solution temperatures in poly (ethylene oxide) solutions. *The Journal of Physical Chemistry, 89*(23), 4962-4964.

Ke, S., Wen, X., Gurfinkel, M., Charnsangavej, C., Wallace, S., Sevick-Muraca, E. M., & Li, C. (2003). Near-infrared optical imaging of epidermal growth factor receptor in breast cancer xenografts. *Cancer research, 63*(22), 7870-7875.

Keeley, F. W., Bellingham, C. M., & Woodhouse, K. A. (2002). Elastin as a self–organizing biomaterial: use of recombinantly expressed human elastin

polypeptides as a model for investigations of structure and self–assembly of elastin. *Philosophical Transactions of the Royal Society of London B: Biological Sciences, 357*(1418), 185-189.

Keereweer, S., Kerrebijn, J. D., Van Driel, P. B., Xie, B., Kaijzel, E. L., Snoeks, T. J., . . . Mieog, J. S. D. (2011). Optical image-guided surgery—where do we stand? *Molecular Imaging and Biology, 13*(2), 199-207.

Keskin, O., Gursoy, A., Ma, B., & Nussinov, R. (2008). Principles of protein− protein interactions: What are the preferred ways for proteins to interact? *Chemical reviews, 108*(4), 1225-1244.

Kim, B., Rutka, J. T., & Chan, W. C. (2010). Nanomedicine. *N Engl J Med, 2010*(363), 2434-2443.

Kim, M. S., Hwang, S. J., Han, J. K., Choi, E. K., Park, H. J., Kim, J. S., & Lee, D. S. (2006). pH- Responsive PEG- Poly (β- amino ester) Block Copolymer Micelles with a Sharp Transition. *Macromolecular rapid communications, 27*(6), 447-451.

Kojima, C., & Irie, K. (2013). Synthesis of temperature- dependent elastin- like peptide- modified dendrimer for drug delivery. *Peptide Science, 100*(6), 714-721.

Kolmakov, A., & Moskovits, M. (2004). Chemical sensing and catalysis by one-dimensional metal-oxide nanostructures. *Annu. Rev. Mater. Res., 34*, 151-180.

Kono, K. (2001). Thermosensitive polymer-modified liposomes. *Advanced drug delivery reviews, 53*(3), 307-319.

Koo, H., Lee, S., Na, J. H., Kim, S. H., Hahn, S. K., Choi, K., . . . Kim, K. (2012). Bioorthogonal Copper- Free Click Chemistry In Vivo for Tumor- Targeted Delivery of Nanoparticles. *Angewandte Chemie International Edition, 51*(47), 11836-11840.

Koper, G. J., & Borkovec, M. (2010). Proton binding by linear, branched, and hyperbranched polyelectrolytes. *Polymer, 51*(24), 5649-5662.

Korevaar, P. A., George, S. J., Markvoort, A. J., Smulders, M. M., Hilbers, P. A., Schenning, A. P., . . . Meijer, E. (2012). Pathway complexity in supramolecular polymerization. *Nature, 481*(7382), 492-496.

Kozak, J. J., Knight, W. S., & Kauzmann, W. (1968). Solute- Solute Interactions in Aqueous Solutions. *The Journal of Chemical Physics, 48*(2), 675-690.

Kunz, W., Lo Nostro, P., & Ninham, B. W. (2004). The present state of affairs with Hofmeister effects. *Current Opinion in Colloid & Interface Science, 9*(1–2), 1-18. doi:http://dx.doi.org/10.1016/j.cocis.2004.05.004

Kurzbach, D., Hassouneh, W., McDaniel, J. R., Jaumann, E. A., Chilkoti, A., & Hinderberger, D. (2013). Hydration layer coupling and cooperativity in phase behavior of stimulus responsive peptide polymers. *Journal of the American Chemical Society, 135*(30), 11299-11308.

Ladokhin, A. S., Legmann, R., Collier, R. J., & White, S. H. (2004). Reversible refolding of the diphtheria toxin T-domain on lipid membranes. *Biochemistry, 43*(23), 7451-7458.

Lagadic-Gossmann, D., Huc, L., & Lecureur, V. (2004). Alterations of intracellular pH homeostasis in apoptosis: origins and roles. *Cell Death and Differentiation, 11*(9), 953-961. doi:10.1038/sj.cdd.4401466

Lammers, T., Aime, S., Hennink, W. E., Storm, G., & Kiessling, F. (2011). Theranostic nanomedicine. *Accounts of Chemical Research, 44*(10), 1029-1038.

Lane, L. A., Qian, X., Smith, A. M., & Nie, S. (2015). Physical chemistry of nanomedicine: Understanding the complex behaviors of nanoparticles in vivo. *Annual review of physical chemistry, 66*, 521-547.

Langer, R., & Tirrell, D. A. (2004). Designing materials for biology and medicine. *Nature, 428*(6982), 487-492.

Larsen, M. T., Kuhlmann, M., Hvam, M. L., & Howard, K. A. (2016). Albumin-based drug delivery: harnessing nature to cure disease. *Molecular and cellular therapies, 4*(1), 3.

Lee, E. S., Shin, H. J., Na, K., & Bae, Y. H. (2003). Poly (L-histidine)–PEG block copolymer micelles and pH-induced destabilization. *Journal of controlled release, 90*(3), 363-374.

Lee, H. i., Wu, W., Oh, J. K., Mueller, L., Sherwood, G., Peteanu, L., . . . Matyjaszewski, K. (2007). Light- induced reversible formation of polymeric micelles. *Angewandte Chemie, 119*(14), 2505-2509.

Lehn, J.-M. (1988). Supramolecular chemistry—Scope and perspectives: Molecules—Supermolecules—Molecular devices. *Journal of inclusion phenomena, 6*(4), 351-396.

Lehn, J.-M. (1993). Supramolecular chemistry. *Science, 260*(5115), 1762-1764.

Lehn, J.-M. (2002). Toward complex matter: supramolecular chemistry and self-organization. *Proceedings of the National Academy of Sciences, 99*(8), 4763-4768.

Lehn, J.-M. (2007). From supramolecular chemistry towards constitutional dynamic chemistry and adaptive chemistry. *Chemical Society Reviews, 36*(2), 151-160.

Lehn, J. M. (1988). Supramolecular chemistry—scope and perspectives molecules, supermolecules, and molecular devices (Nobel Lecture). *Angewandte Chemie International Edition in English, 27*(1), 89-112.

Lehn, J. M. (2013). Perspectives in chemistry—steps towards complex matter. *Angewandte Chemie International Edition, 52*(10), 2836-2850.

Lei, J., & Ju, H. (2012). Signal amplification using functional nanomaterials for biosensing. *Chemical Society Reviews, 41*(6), 2122-2134.

Leontidis, E. (2002). Hofmeister anion effects on surfactant self-assembly and the formation of mesoporous solids. *Current Opinion in Colloid & Interface Science, 7*(1–2), 81-91. doi:http://dx.doi.org/10.1016/S1359-0294(02)00010-9

Leopold, P. E., Montal, M., & Onuchic, J. N. (1992). Protein folding funnels: a kinetic approach to the sequence-structure relationship. *Proceedings of the National Academy of Sciences, 89*(18), 8721-8725.

Levy, Y., & Onuchic, J. N. (2006). Water mediation in protein folding and molecular recognition. *Annu. Rev. Biophys. Biomol. Struct., 35*, 389-415.

Li, N. K., Quiroz, F. G., Hall, C. K., Chilkoti, A., & Yingling, Y. G. (2014). Molecular description of the LCST behavior of an elastin-like polypeptide. *Biomacromolecules, 15*(10), 3522-3530.

Li, P., Banjade, S., Cheng, H.-C., Kim, S., Chen, B., Guo, L., . . . Banani, S. F. (2012). Phase transitions in the assembly of multivalent signalling proteins. *Nature, 483*(7389), 336-340.

Li, S., Su, Y., Dan, M., & Zhang, W. (2014). Thermo-responsive ABA triblock copolymer of PVEA-b-PNIPAM-b-PVEA showing solvent-tunable LCST in a methanol–water mixture. *Polymer Chemistry, 5*(4), 1219-1228.

Li, Y., Wang, Y., Huang, G., Ma, X., Zhou, K., & Gao, J. (2014). Chaotropic‐ Anion‐Induced Supramolecular Self‐ Assembly of Ionic Polymeric Micelles. *Angewandte Chemie International Edition, 53*(31), 8074-8078.

Li, Y., Zhao, T., Wang, C., Lin, Z., Huang, G., Sumer, B. D., & Gao, J. (2016). Molecular basis of cooperativity in pH-triggered supramolecular self-assembly. *Nature communications, 7*.

Ling, D., Park, W., Park, S.-j., Lu, Y., Kim, K. S., Hackett, M. J., . . . Na, K. (2014). Multifunctional tumor pH-sensitive self-assembled nanoparticles for bimodal imaging and treatment of resistant heterogeneous tumors. *Journal of the American Chemical Society, 136*(15), 5647-5655.

Liu, C.-W., Hsieh, Y.-T., Huang, C.-C., Lin, Z.-H., & Chang, H.-T. (2008). Detection of mercury (II) based on Hg 2+–DNA complexes inducing the aggregation of gold nanoparticles. *Chemical communications*(19), 2242-2244.

Liu, Q., Chen, S., Chen, J., & Du, J. (2015). An asymmetrical polymer vesicle strategy for significantly improving T 1 MRI sensitivity and cancer-targeted drug delivery. *Macromolecules, 48*(3), 739-749.

Liu, W., MacKay, J. A., Dreher, M. R., Chen, M., McDaniel, J. R., Simnick, A. J., . . . Chilkoti, A. (2010). Injectable intratumoral depot of thermally responsive polypeptide–radionuclide conjugates delays tumor progression in a mouse model. *Journal of controlled release, 144*(1), 2-9.

Liu, X., Yan, C.-H., & Capobianco, J. A. (2015). Photon upconversion nanomaterials. *Chemical Society Reviews, 44*(6), 1299-1301.

Lu, Y., Aimetti, A. A., Langer, R., & Gu, Z. (2016). Bioresponsive materials. *Nature Reviews Materials, 1*, 16075.

Lu, Y., Hu, Q., Lin, Y., Pacardo, D. B., Wang, C., Sun, W., . . . Gu, Z. (2015). Transformable liquid-metal nanomedicine. *Nature communications, 6*.

Luong, J. H., Male, K. B., & Glennon, J. D. (2008). Biosensor technology: technology push versus market pull. *Biotechnology advances, 26*(5), 492-500.

Ma, X., Wang, Y., Zhao, T., Li, Y., Su, L.-C., Wang, Z., . . . Gao, J. (2014). Ultra-pH-sensitive nanoprobe library with broad pH tunability and fluorescence emissions. *Journal of the American Chemical Society, 136*(31), 11085-11092.

Ma, Y., Tang, Y., Billingham, N. C., Armes, S. P., Lewis, A. L., Lloyd, A. W., & Salvage, J. P. (2003). Well-Defined Biocompatible Block Copolymers via Atom Transfer Radical Polymerization of 2-Methacryloyloxyethyl Phosphorylcholine in Protic Media. *Macromolecules, 36*(10), 3475-3484. doi:10.1021/ma021762c

Mai, Y., & Eisenberg, A. (2012). Self-assembly of block copolymers. *Chemical Society Reviews, 41*(18), 5969-5985.

Makhlof, A., Tozuka, Y., & Takeuchi, H. (2009). pH-Sensitive nanospheres for colon-specific drug delivery in experimentally induced colitis rat model. *European Journal of Pharmaceutics and Biopharmaceutics, 72*(1), 1-8.

Mammen, M., Choi, S.-K., & Whitesides, G. M. (1998). Polyvalent interactions in biological systems: implications for design and use of multivalent ligands and inhibitors. *Angewandte Chemie International Edition, 37*(20), 2754-2794.

Mammen, M., Simanek, E. E., & Whitesides, G. M. (1996). Predicting the relative stabilities of multiparticle hydrogen-bonded aggregates based on the number of hydrogen bonds and the number of particles and measuring these stabilities with titrations using dimethyl sulfoxide. *Journal of the American Chemical Society, 118*(50), 12614-12623.

Matsumoto, Y., Nichols, J. W., Toh, K., Nomoto, T., Cabral, H., Miura, Y., . . . Kano, M. R. (2016). Vascular bursts enhance permeability of tumour blood vessels and improve nanoparticle delivery. *Nature nanotechnology*.

Matsuyama, S., Llopis, J., Deveraux, Q. L., Tsien, R. Y., & Reed, J. C. (2000). Changes in intramitochondrial and cytosolic pH: early events that modulate caspase activation during apoptosis. *Nature cell biology, 2*(6), 318-325.

Matsuyama, S., Llopis, J., Deveraux, Q. L., Tsien, R. Y., & Reed, J. C. (2000). Changes in intramitochondrial and cytosolic pH: early events that modulate caspase activation during apoptosis. *Nature Cell Biology, 2*(6), 318-325. doi:10.1038/35014006

Mattia, E., & Otto, S. (2015). Supramolecular systems chemistry. *Nature nanotechnology, 10*(2), 111-119.

McDaniel, J. R., MacEwan, S. R., Li, X., Radford, D. C., Landon, C. D., Dewhirst, M., & Chilkoti, A. (2014). Rational design of "heat seeking" drug loaded polypeptide nanoparticles that thermally target solid tumors. *Nano letters, 14*(5), 2890-2895.

McDaniel, J. R., Radford, D. C., & Chilkoti, A. (2013). A unified model for de novo design of elastin-like polypeptides with tunable inverse transition temperatures. *Biomacromolecules, 14*(8), 2866-2872.

McNichols, R. J., & Cote, G. L. (2000). Optical glucose sensing in biological fluids: an overview. *Journal of biomedical optics, 5*(1), 5-16.

Mi, P., Kokuryo, D., Cabral, H., Wu, H., Terada, Y., Saga, T., . . . Kataoka, K. (2016). A pH-activatable nanoparticle with signal-amplification capabilities for non-invasive imaging of tumour malignancy. *Nature nanotechnology*.

Miller-Chou, B. A., & Koenig, J. L. (2003). A review of polymer dissolution. *Progress in Polymer Science, 28*(8), 1223-1270.

Min, K. H., Kim, J.-H., Bae, S. M., Shin, H., Kim, M. S., Park, S., . . . Kim, K. (2010). Tumoral acidic pH-responsive MPEG-poly (β-amino ester) polymeric micelles for cancer targeting therapy. *Journal of controlled release, 144*(2), 259-266.

Mirkin, C. A., Letsinger, R. L., Mucic, R. C., & Storhoff, J. J. (1996). A DNA-based method for rationally assembling nanoparticles into macroscopic materials. *Nature, 382*(6592), 607-609.

Moriki, T., Maruyama, H., & Maruyama, I. N. (2001). Activation of preformed EGF receptor dimers by ligand-induced rotation of the transmembrane domain. *Journal of molecular biology, 311*(5), 1011-1026.

Morimoto, N., Qiu, X.-P., Winnik, F. M., & Akiyoshi, K. (2008). Dual stimuli-responsive nanogels by self-assembly of polysaccharides lightly grafted with thiol-terminated poly (N-isopropylacrylamide) chains. *Macromolecules, 41*(16), 5985-5987.

Müller- Plathe, F. (2002). Coarse- graining in polymer simulation: from the atomistic to the mesoscopic scale and back. *ChemPhysChem, 3*(9), 754-769.

Mura, S., Nicolas, J., & Couvreur, P. (2013). Stimuli-responsive nanocarriers for drug delivery. *Nature materials, 12*(11), 991-1003.

Nakahata, M., Takashima, Y., Yamaguchi, H., & Harada, A. (2011). Redox-responsive self-healing materials formed from host–guest polymers. *Nature communications, 2*, 511.

Nakajima, T., Mitsunaga, M., Bander, N. H., Heston, W. D., Choyke, P. L., & Kobayashi, H. (2011). Targeted, activatable, in vivo fluorescence imaging of prostate-specific membrane antigen (PSMA) positive tumors using the quenched humanized J591 antibody–indocyanine green (ICG) conjugate. *Bioconjugate chemistry, 22*(8), 1700-1705.

Nam, J.-M., Thaxton, C. S., & Mirkin, C. A. (2003). Nanoparticle-based bio-bar codes for the ultrasensitive detection of proteins. *Science, 301*(5641), 1884-1886.

Napoli, A., Valentini, M., Tirelli, N., Müller, M., & Hubbell, J. A. (2004). Oxidation-responsive polymeric vesicles. *Nature materials, 3*(3), 183-189.

Nasongkla, N., Bey, E., Ren, J., Ai, H., Khemtong, C., Guthi, J. S., . . . Gao, J. (2006). Multifunctional polymeric micelles as cancer-targeted, MRI-ultrasensitive drug delivery systems. *Nano letters, 6*(11), 2427-2430.

Nasongkla, N., Bey, E., Ren, J., Ai, H., Khemtong, C., Guthi, J. S., . . . Gao, J. (2006). Multifunctional polymeric micelles as cancer-targeted, MRI-ultrasensitive drug delivery systems. *Nano Letters, 6*(11), 2427-2430. doi:10.1021/nl061412u

Nath, N., & Chilkoti, A. (2001). Interfacial phase transition of an environmentally responsive elastin biopolymer adsorbed on functionalized gold nanoparticles studied by colloidal surface plasmon resonance. *Journal of the American Chemical Society, 123*(34), 8197-8202.

Neri, D., & Supuran, C. T. (2011). Interfering with pH regulation in tumours as a therapeutic strategy. *Nature reviews Drug discovery, 10*(10), 767-777.

Neri, D., & Supuran, C. T. (2011). Interfering with pH regulation in tumours as a therapeutic strategy. *Nature Reviews. Drug Discovery, 10*(10), 767-777. doi:10.1038/nrd3554

Newell, K., Franchi, A., Pouyssegur, J., & Tannock, I. (1993). Studies with glycolysis-deficient cells suggest that production of lactic acid is not the only cause of tumor acidity. *Proceedings of the National Academy of Sciences of the United States of America, 90*(3), 1127-1131.

Nugent, S., Kumar, D., Rampton, D., & Evans, D. (2001). Intestinal luminal pH in inflammatory bowel disease: possible determinants and implications for therapy with aminosalicylates and other drugs. *Gut, 48*(4), 571-577.

Okada, Y., & Tanaka, F. (2005). Cooperative hydration, chain collapse, and flat LCST behavior in aqueous poly (N-isopropylacrylamide) solutions. *Macromolecules, 38*(10), 4465-4471.

Orellana, G. (2004). Luminescent optical sensors. *Analytical and bioanalytical chemistry, 379*(3), 344-346.

Otake, K., Inomata, H., Konno, M., & Saito, S. (1990). Thermal analysis of the volume phase transition with N-isopropylacrylamide gels. *Macromolecules, 23*(1), 283-289.

Paik, S., Bryant, J., Tan-Chiu, E., Yothers, G., Park, C., Wickerham, D. L., & Wolmark, N. (2000). HER2 and choice of adjuvant chemotherapy for invasive breast cancer: National Surgical Adjuvant Breast and Bowel Project Protocol B-15. *Journal of the National Cancer Institute, 92*(24), 1991-1998.

Panayiotou, C. G. (1987). Lattice-fluid theory of polymer solutions. *Macromolecules, 20*(4), 861-871.

Pang, X., Jiang, Y., Xiao, Q., Leung, A. W., Hua, H., & Xu, C. (2016). pH-responsive polymer–drug conjugates: Design and progress. *Journal of controlled release, 222*, 116-129.

Park, S. M., Kim, M. S., Park, S.-J., Park, E. S., Choi, K.-S., Kim, Y.-s., & Kim, H. R. (2013). Novel temperature-triggered liposome with high stability: Formulation, in vitro evaluation, and in vivo study combined with high-intensity focused ultrasound (HIFU). *Journal of controlled release, 170*(3), 373-379.

Parsegian, V. A. (1995). Hopes for Hofmeister. *Nature, 378*(6555), 335-336.

Parsons, D. F., Bostrom, M., Lo Nostro, P., & Ninham, B. W. (2011). Hofmeister effects: interplay of hydration, nonelectrostatic potentials, and ion size. *Physical Chemistry Chemical Physics, 13*(27), 12352-12367. doi:10.1039/c1cp20538b

Patel, N. R., Pattni, B. S., Abouzeid, A. H., & Torchilin, V. P. (2013). Nanopreparations to overcome multidrug resistance in cancer. *Advanced drug delivery reviews, 65*(13), 1748-1762.

Peer, D., Karp, J. M., Hong, S., Farokhzad, O. C., Margalit, R., & Langer, R. (2007). Nanocarriers as an emerging platform for cancer therapy. *Nature nanotechnology, 2*(12), 751-760.

Pelicano, H., Carney, D., & Huang, P. (2004). ROS stress in cancer cells and therapeutic implications. *Drug Resistance Updates, 7*(2), 97-110.

Peng, X., Song, F., Lu, E., Wang, Y., Zhou, W., Fan, J., & Gao, Y. (2005). Heptamethine cyanine dyes with a large stokes shift and strong fluorescence: a paradigm for excited-state intramolecular charge transfer. *Journal of the American Chemical Society, 127*(12), 4170-4171.

Perlmutter-Hayman, B. (1986). Cooperative binding to macromolecules. A formal approach. *Accounts of Chemical Research, 19*(3), 90-96.

Persidis, A. (1999). Cancer multidrug resistance. *Nature biotechnology, 17*(1), 94-95.

Perutz, M. F. (1989). Mechanisms of cooperativity and allosteric regulation in proteins. *Quarterly reviews of biophysics, 22*(02), 139-237.

Perutz, M. F., Rossmann, M. G., Cullis, A. F., Muirhead, H., Will, G., & North, A. (1960). Structure of haemoglobin: a three-dimensional Fourier synthesis at 5.5-A. resolution, obtained by X-ray analysis. *Nature, 185*(4711), 416-422.

Philipp, M., Kyriakos, K., Silvi, L., Lohstroh, W., Petry, W., Krüger, J. K., . . . Müller-Buschbaum, P. (2014). From molecular dehydration to excess volumes of

phase-separating PNIPAM solutions. *The Journal of Physical Chemistry B, 118*(15), 4253-4260.

Phillips, D. J., & Gibson, M. I. (2012). Degradable thermoresponsive polymers which display redox-responsive LCST Behaviour. *Chemical communications, 48*(7), 1054-1056.

Po, H. N., & Senozan, N. (2001). The Henderson-Hasselbalch equation: its history and limitations. *Journal of Chemical Education, 78*(11), 1499.

Pohl, F. M., & Jovin, T. M. (1972). Salt-induced co-operative conformational change of a synthetic DNA: equilibrium and kinetic studies with poly (dG-dC). *Journal of molecular biology, 67*(3), 375-396.

Popescu, M.-T., Korogiannaki, M., Marikou, K., & Tsitsilianis, C. (2014). CBABC terpolymer-based nanostructured vesicles with tunable membrane permeability as potential hydrophilic drug nanocarriers. *Polymer, 55*(13), 2943-2951.

Prescher, J. A., & Bertozzi, C. R. (2005). Chemistry in living systems. *Nature chemical biology, 1*(1), 13-21.

Pumera, M. (2010). Graphene-based nanomaterials and their electrochemistry. *Chemical Society Reviews, 39*(11), 4146-4157.

Qiu, X.-P., Tanaka, F., & Winnik, F. M. (2007). Temperature-induced phase transition of well-defined cyclic poly (N-isopropylacrylamide) s in aqueous solution. *Macromolecules, 40*(20), 7069-7071.

Quiroz, F. G., & Chilkoti, A. (2015). Sequence heuristics to encode phase behaviour in intrinsically disordered protein polymers. *Nature materials*.

Reshetnyak, Y. K., Andreev, O. A., Segala, M., Markin, V. S., & Engelman, D. M. (2008). Energetics of peptide (pHLIP) binding to and folding across a lipid bilayer membrane. *Proceedings of the National Academy of Sciences, 105*(40), 15340-15345.

Reshetnyak, Y. K., Segala, M., Andreev, O. A., & Engelman, D. M. (2007). A monomeric membrane peptide that lives in three worlds: in solution, attached to, and inserted across lipid bilayers. *Biophysical journal, 93*(7), 2363-2372.

Rim, H. P., Min, K. H., Lee, H. J., Jeong, S. Y., & Lee, S. C. (2011). pH- Tunable Calcium Phosphate Covered Mesoporous Silica Nanocontainers for Intracellular Controlled Release of Guest Drugs. *Angewandte Chemie International Edition, 50*(38), 8853-8857.

Robson, B., & Vaithilingam, A. (2008). Protein folding revisited. *Progress in molecular biology and translational science, 84*, 161-202.

Rodriguez-Hernandez, J., Chécot, F., Gnanou, Y., & Lecommandoux, S. (2005). Toward 'smart' nano-objects by self-assembly of block copolymers in solution. *Progress in Polymer Science, 30*(7), 691-724.

Rosi, N. L., & Mirkin, C. A. (2005). Nanostructures in biodiagnostics. *Chemical reviews, 105*(4), 1547-1562.

Roy, D., Brooks, W. L., & Sumerlin, B. S. (2013). New directions in thermoresponsive polymers. *Chemical Society Reviews, 42*(17), 7214-7243.

Roy, K., Mao, H.-Q., Huang, S.-K., & Leong, K. W. (1999). Oral gene delivery with chitosan–DNA nanoparticles generates immunologic protection in a murine model of peanut allergy. *Nature medicine, 5*(4), 387-391.

Russell, R., & Herschlag, D. (2001). Probing the folding landscape of the Tetrahymena ribozyme: commitment to form the native conformation is late in the folding pathway. *Journal of molecular biology, 308*(5), 839-851.

Rwei, A. Y., Wang, W., & Kohane, D. S. (2015). Photoresponsive nanoparticles for drug delivery. *Nano today, 10*(4), 451-467.

Saadoun, S., Papadopoulos, M. C., Hara-Chikuma, M., & Verkman, A. S. (2005). Impairment of angiogenesis and cell migration by targeted aquaporin-1 gene disruption. *Nature, 434*(7034), 786-792. doi:10.1038/nature03460

Sapsford, K. E., Berti, L., & Medintz, I. L. (2006). Materials for fluorescence resonance energy transfer analysis: beyond traditional donor-acceptor combinations. *Angewandte Chemie. International Edition in English, 45*(28), 4562-4589. doi:10.1002/anie.200503873

Sasaki, E., Kojima, H., Nishimatsu, H., Urano, Y., Kikuchi, K., Hirata, Y., & Nagano, T. (2005). Highly sensitive near-infrared fluorescent probes for nitric oxide and their application to isolated organs. *Journal of the American Chemical Society, 127*(11), 3684-3685.

Sasaki, S., Kawasaki, H., & Maeda, H. (1997). Volume phase transition behavior of N-isopropylacrylamide gels as a function of the chemical potential of water molecules. *Macromolecules, 30*(6), 1847-1848.

Sattin, B. D., Zhao, W., Travers, K., Chu, S., & Herschlag, D. (2008). Direct measurement of tertiary contact cooperativity in RNA folding. *Journal of the American Chemical Society, 130*(19), 6085-6087.

Saxena, V., Sadoqi, M., & Shao, J. (2003). Degradation kinetics of indocyanine green in aqueous solution. *Journal of pharmaceutical sciences, 92*(10), 2090-2097.

Scheutjens, J., & Fleer, G. (1979). Statistical theory of the adsorption of interacting chain molecules. 1. Partition function, segment density distribution, and adsorption isotherms. *Journal of Physical Chemistry, 83*(12), 1619-1635.

Schild, H. G. (1992). Poly (N-isopropylacrylamide): experiment, theory and application. *Progress in Polymer Science, 17*(2), 163-249.

Schilli, C. M., Zhang, M., Rizzardo, E., Thang, S. H., Chong, Y., Edwards, K., . . . Müller, A. H. (2004). A New Double-Responsive Block Copolymer Synthesized via RAFT Polymerization: Poly (N-isopropylacrylamide)-b lock-poly (acrylic acid). *Macromolecules, 37*(21), 7861-7866.

Schluep, T., Hwang, J., Cheng, J., Heidel, J. D., Bartlett, D. W., Hollister, B., & Davis, M. E. (2006). Preclinical efficacy of the camptothecin-polymer conjugate IT-101 in multiple cancer models. *Clinical Cancer Research, 12*(5), 1606-1614.

Schmaljohann, D. (2006). Thermo-and pH-responsive polymers in drug delivery. *Advanced drug delivery reviews, 58*(15), 1655-1670.

Scholtz, J. M., & Baldwin, R. L. (1992). The mechanism of alpha-helix formation by peptides. *Annual review of biophysics and biomolecular structure, 21*(1), 95-118.

Schumacker, P. T. (2006). Reactive oxygen species in cancer cells: live by the sword, die by the sword. *Cancer cell, 10*(3), 175-176.

Sclavi, B., Sullivan, M., Chance, M. R., Brenowitz, M., & Woodson, S. A. (1998). RNA folding at millisecond intervals by synchrotron hydroxyl radical footprinting. *Science, 279*(5358), 1940-1943.

Serres, A., Baudyš, M., & Kim, S. W. (1996). Temperature and pH-sensitive polymers for human calcitonin delivery. *Pharmaceutical research, 13*(2), 196-201.

Shamji, M. F., Betre, H., Kraus, V. B., Chen, J., Chilkoti, A., Pichika, R., . . . Setton, L. A. (2007). Development and characterization of a fusion protein between thermally responsive elastin- like polypeptide and interleukin- 1 receptor antagonist: Sustained release of a local antiinflammatory therapeutic. *Arthritis & Rheumatology, 56*(11), 3650-3661.

Shamji, M. F., Chen, J., Friedman, A. H., Richardson, W. J., Chilkoti, A., & Setton, L. A. (2008). Synthesis and characterization of a thermally-responsive tumor necrosis factor antagonist. *Journal of controlled release, 129*(3), 179-186.

Shan, J., Zhao, Y., Granqvist, N., & Tenhu, H. (2009). Thermoresponsive properties of N-isopropylacrylamide oligomer brushes grafted to gold nanoparticles: effects of molar mass and gold core size. *Macromolecules, 42*(7), 2696-2701.

Sharma, V., Kaila, V. R., & Annila, A. (2009). Protein folding as an evolutionary process. *Physica A: Statistical Mechanics and its Applications, 388*(6), 851-862.

Shen, H., & Eisenberg, A. (1999). Morphological phase diagram for a ternary system of block copolymer PS310-b-PAA52/dioxane/H2O. *The Journal of Physical Chemistry B, 103*(44), 9473-9487.

Sherrington, D. C., & Taskinen, K. A. (2001). Self-assembly in synthetic macromolecular systems via multiple hydrogen bonding interactions. *Chemical Society Reviews, 30*(2), 83-93.

Shibayama, M., Norisuye, T., & Nomura, S. (1996). Cross-link density dependence of spatial inhomogeneities and dynamic fluctuations of poly (N-isopropylacrylamide) gels. *Macromolecules, 29*(27), 8746-8750.

Sokal, N. O., & Sokal, A. D. (1975). Class EA new class of high-efficiency tuned single-ended switching power amplifiers. *IEEE Journal of solid-state circuits, 10*(3), 168-176.

Sosnick, T. R. (2008). Kinetic barriers and the role of topology in protein and RNA folding. *Protein Science, 17*(8), 1308-1318.

Stoffelen, C., & Huskens, J. (2016). Soft Supramolecular Nanoparticles by Noncovalent and Host–Guest Interactions. *Small, 12*(1), 96-119.

Storhoff, J. J., Lazarides, A. A., Mucic, R. C., Mirkin, C. A., Letsinger, R. L., & Schatz, G. C. (2000). What controls the optical properties of DNA-linked gold nanoparticle assemblies? *Journal of the American Chemical Society, 122*(19), 4640-4650.

Stuart, M. A. C., Huck, W. T., Genzer, J., Müller, M., Ober, C., Stamm, M., . . . Urban, M. (2010). Emerging applications of stimuli-responsive polymer materials. *Nature Materials, 9*(2), 101-113.

Stupp, S. I., & Palmer, L. C. (2013). Supramolecular chemistry and self-assembly in organic materials design. *Chemistry of Materials, 26*(1), 507-518.

Sumer, B., & Gao, J. (2008). Theranostic nanomedicine for cancer. *Nanomedicine, 3*(2), 137-140.

Sun, J.-Y., Zhao, X., Illeperuma, W. R., Chaudhuri, O., Oh, K. H., Mooney, D. J., . . . Suo, Z. (2012). Highly stretchable and tough hydrogels. *Nature, 489*(7414), 133-136.

Sun, T., Zhang, Y. S., Pang, B., Hyun, D. C., Yang, M., & Xia, Y. (2014). Engineered nanoparticles for drug delivery in cancer therapy. *Angewandte Chemie International Edition, 53*(46), 12320-12364.

Švastová, E., Hulíková, A., Rafajová, M., Zat'ovičová, M., Gibadulinová, A., Casini, A., . . . Pastorek, J. r. (2004). Hypoxia activates the capacity of tumor-associated carbonic anhydrase IX to acidify extracellular pH. *FEBS letters, 577*(3), 439-445.

Tanaka, F., Koga, T., Kaneda, I., & Winnik, F. M. (2011). Hydration, phase separation and nonlinear rheology of temperature-sensitive water-soluble polymers. *Journal of Physics: Condensed Matter, 23*(28), 284105.

Tanaka, F., Koga, T., Kojima, H., & Winnik, F. M. (2009). Temperature-and tension-induced coil− globule transition of Poly (N-isopropylacrylamide) chains in water and mixed solvent of water/methanol. *Macromolecules, 42*(4), 1321-1330.

Tanaka, F., Koga, T., & Winnik, F. M. (2008). Temperature-responsive polymers in mixed solvents: competitive hydrogen bonds cause cononsolvency. *Physical review letters, 101*(2), 028302.

Tanaka, N., Matsukawa, S., Kurosu, H., & Ando, I. (1998). A study on dynamics of water in crosslinked poly (N-isopropylacrylamide) gel by nmr spectroscopy. *Polymer, 39*(20), 4703-4706.

Tang, B., Yu, F., Li, P., Tong, L., Duan, X., Xie, T., & Wang, X. (2009). A near-infrared neutral pH fluorescent probe for monitoring minor pH changes: imaging in living HepG2 and HL-7702 cells. *Journal of the American Chemical Society, 131*(8), 3016-3023.

Taton, T. A., Mirkin, C. A., & Letsinger, R. L. (2000). Scanometric DNA array detection with nanoparticle probes. *Science, 289*(5485), 1757-1760.

Taton, T. A., Mucic, R. C., Mirkin, C. A., & Letsinger, R. L. (2000). The DNA-mediated formation of supramolecular mono-and multilayered nanoparticle structures. *Journal of the American Chemical Society, 122*(26), 6305-6306.

Taylor, P. N., & Anderson, H. L. (1999). Cooperative self-assembly of double-strand conjugated porphyrin ladders. *Journal of the American Chemical Society, 121*(49), 11538-11545.

Teramura, Y., Ichinose, J., Takagi, H., Nishida, K., Yanagida, T., & Sako, Y. (2006). Single- molecule analysis of epidermal growth factor binding on the surface of living cells. *The EMBO journal, 25*(18), 4215-4222.

Terzi, E., Hölzemann, G., & Seelig, J. (1995). Self-association of β-amyloid peptide (1–40) in solution and binding to lipid membranes. *Journal of molecular biology, 252*(5), 633-642.

Themistou, E., Battaglia, G., & Armes, S. P. (2014). Facile synthesis of thiol-functionalized amphiphilic polylactide–methacrylic diblock copolymers. *Polymer Chemistry, 5*(4), 1405-1417.

Thirumalai, D., & Woodson, S. (1996). Kinetics of folding of proteins and RNA. *Accounts of chemical research, 29*(9), 433-439.

Toretsky, J. A., & Wright, P. E. (2014). Assemblages: functional units formed by cellular phase separation. *J Cell Biol, 206*(5), 579-588.

Trachootham, D., Alexandre, J., & Huang, P. (2009). Targeting cancer cells by ROS-mediated mechanisms: a radical therapeutic approach? *Nature reviews Drug discovery, 8*(7), 579-591.

Treiber, D. K., & Williamson, J. R. (1999). Exposing the kinetic traps in RNA folding. *Current opinion in structural biology, 9*(3), 339-345.

Tsai, C. J., Lin, S. L., Wolfson, H. J., & Nussinov, R. (1997). Studies of protein- protein interfaces: A statistical analysis of the hydrophobic effect. *Protein Science, 6*(1), 53-64.

Tsarevsky, N. V., & Matyjaszewski, K. (2007). "Green" Atom Transfer Radical Polymerization: From Process Design to Preparation of Well-Defined Environmentally Friendly Polymeric Materials. *Chemical Reviews, 107*(6), 2270-2299. doi:10.1021/cr050947p

Tsumura, A., Koezuka, H., & Ando, T. (1986). Macromolecular electronic device: Field- effect transistor with a polythiophene thin film. *Applied Physics Letters, 49*(18), 1210-1212.

Underwood, A. L., & Anacker, E. W. (1987). Counterion lyotropy and micelle formation. *Journal of Colloid and Interface Science, 117*(1), 242-250. doi:http://dx.doi.org/10.1016/0021-9797(87)90188-3

Urry, D. W. (1992). Free energy transduction in polypeptides and proteins based on inverse temperature transitions. *Progress in biophysics and molecular biology, 57*(1), 23-57.

Van Dam, G. M., Themelis, G., Crane, L. M., Harlaar, N. J., Pleijhuis, R. G., Kelder, W., . . . Van Der Zee, A. G. (2011). Intraoperative tumor-specific fluorescence imaging in ovarian cancer by folate receptor-[alpha] targeting: first in-human results. *Nature medicine, 17*(10), 1315-1319.

van den Berg, B., Wain, R., Dobson, C. M., & Ellis, R. J. (2000). Macromolecular crowding perturbs protein refolding kinetics: implications for folding inside the cell. *The EMBO journal, 19*(15), 3870-3875.

van Sluis, R., Bhujwalla, Z. M., Raghunand, N., Ballesteros, P., Alvarez, J., Cerdan, S., . . . Gillies, R. J. (1999a). In vivo imaging of extracellular pH using 1H MRSI. *Magnetic Resonance in Medicine, 41*(4), 743-750.

van Sluis, R., Bhujwalla, Z. M., Raghunand, N., Ballesteros, P., Alvarez, J., Cerdan, S., . . . Gillies, R. J. (1999b). In vivo imaging of extracellular pH using (1)H MRSI. *Magnetic Resonance in Medicine, 41*(4), 743-750. doi:Doi 10.1002/(Sici)1522-2594(199904)41:4<743::Aid-Mrm13>3.0.Co;2-Z

Vargas-Uribe, M., Rodnin, M. V., & Ladokhin, A. S. (2013). Comparison of membrane insertion pathways of the apoptotic regulator Bcl-xL and the diphtheria toxin translocation domain. *Biochemistry, 52*(45), 7901-7909.

Veiseh, M., Gabikian, P., Bahrami, S.-B., Veiseh, O., Zhang, M., Hackman, R. C., . . . Hansen, S. J. (2007). Tumor paint: a chlorotoxin: Cy5. 5 bioconjugate for intraoperative visualization of cancer foci. *Cancer research, 67*(14), 6882-6888.

Vendruscolo, M., Paci, E., Dobson, C. M., & Karplus, M. (2001). Three key residues form a critical contact network in a protein folding transition state. *Nature, 409*(6820), 641-645.

Vendruscolo, M., Zurdo, J., MacPhee, C. E., & Dobson, C. M. (2003). Protein folding and misfolding: a paradigm of self–assembly and regulation in complex biological systems. *Philosophical Transactions of the Royal Society of London A: Mathematical, Physical and Engineering Sciences, 361*(1807), 1205-1222.

Veronese, F. M., & Pasut, G. (2005). PEGylation, successful approach to drug delivery. *Drug discovery today, 10*(21), 1451-1458.

Voets, I. K., Fokkink, R., Hellweg, T., King, S. M., de Waard, P., de Keizer, A., & Stuart, M. A. C. (2009). Spontaneous symmetry breaking: formation of Janus micelles. *Soft Matter, 5*(5), 999-1005.

Vogelstein, B., Papadopoulos, N., Velculescu, V. E., Zhou, S., Diaz, L. A., Jr., & Kinzler, K. W. (2013). Cancer genome landscapes. *Science, 339*(6127), 1546-1558. doi:10.1126/science.1235122

Vogelstein, B., Papadopoulos, N., Velculescu, V. E., Zhou, S., Diaz, L. A., & Kinzler, K. W. (2013). Cancer genome landscapes. *Science, 339*(6127), 1546-1558.

Volk, T., Jahde, E., Fortmeyer, H. P., Glusenkamp, K. H., & Rajewsky, M. F. (1993a). pH in human tumour xenografts: effect of intravenous administration of glucose. *British Journal of Cancer, 68*(3), 492-500.

Volk, T., Jahde, E., Fortmeyer, H. P., Glusenkamp, K. H., & Rajewsky, M. F. (1993b). pH in human tumour xenografts: effect of intravenous administration of glucose. *British Journal of Cancer, 68*(3), 492-500.

Wang, C., Wang, Y., Li, Y., Bodemann, B., Zhao, T., Ma, X., . . . White, M. A. (2015). A nanobuffer reporter library for fine-scale imaging and perturbation of endocytic organelles. *Nature communications, 6*.

Wang, C., Zhao, T., Li, Y., Huang, G., White, M. A., & Gao, J. (2016). Investigation of endosome and lysosome biology by ultra pH-sensitive nanoprobes. *Advanced drug delivery reviews*.

Wang, G., Tong, X., & Zhao, Y. (2004). Preparation of azobenzene-containing amphiphilic diblock copolymers for light-responsive micellar aggregates. *Macromolecules, 37*(24), 8911-8917.

Wang, J. (2005). Nanomaterial-based electrochemical biosensors. *Analyst, 130*(4), 421-426.

Wang, K., Song, Z., Liu, C., & Zhang, W. (2016). RAFT synthesis of triply responsive poly [N-[2-(dialkylamino) ethyl] acrylamide] s and their N-substitute determined response. *Polymer Chemistry*.

Wang, R., Yu, C., Yu, F., & Chen, L. (2010). Molecular fluorescent probes for monitoring pH changes in living cells. *TrAC Trends in Analytical Chemistry, 29*(9), 1004-1013.

Wang, Y., Zhou, K., Huang, G., Hensley, C., Huang, X., Ma, X., . . . Gao, J. (2013). A nanoparticle-based strategy for the imaging of a broad range of tumours by nonlinear amplification of microenvironment signals. *Nature Materials*. doi:10.1038/nmat3819

Wang, Y., Zhou, K., Huang, G., Hensley, C., Huang, X., Ma, X., . . . Gao, J. (2014). A nanoparticle-based strategy for the imaging of a broad range of tumours by nonlinear amplification of microenvironment signals. *Nature materials, 13*(2), 204-212.

Weaver, J., Bannister, I., Robinson, K., Bories-Azeau, X., Armes, S., Smallridge, M., & McKenna, P. (2004). Stimulus-responsive water-soluble polymers based on 2-hydroxyethyl methacrylate. *Macromolecules, 37*(7), 2395-2403.

Webb, B. A., Chimenti, M., Jacobson, M. P., & Barber, D. L. (2011). Dysregulated pH: a perfect storm for cancer progression. *Nature Reviews Cancer, 11*(9), 671-677. doi:10.1038/nrc3110

Webb, B. A., Chimenti, M., Jacobson, M. P., & Barber, D. L. (2011). Dysregulated pH: a perfect storm for cancer progression. *Nature Reviews Cancer, 11*(9), 671-677.

Webber, M. J., Appel, E. A., Meijer, E., & Langer, R. (2016). Supramolecular biomaterials. *Nature materials, 15*(1), 13-26.

Webber, M. J., Appel, E. A., Meijer, E. W., & Langer, R. (2016). Supramolecular biomaterials. *Nat Mater, 15*(1), 13-26. doi:10.1038/nmat4474

Weber, S. C., & Brangwynne, C. P. (2012). Getting RNA and protein in phase. *Cell, 149*(6), 1188-1191.

Weiss, J. N. (1997). The Hill equation revisited: uses and misuses. *The FASEB Journal, 11*(11), 835-841.

Wencel, D., Abel, T., & McDonagh, C. (2013). Optical chemical pH sensors. *Analytical chemistry, 86*(1), 15-29.

Whitesides, G., Mathias, J., & Seto, C. (1991). Molecular self-assembly and nanochemistry: a chemical strategy for the synthesis of nanostructures. *Science, 254*(5036), 1312-1319. doi:10.1126/science.1962191

Whitesides, G. M., & Boncheva, M. (2002). Beyond molecules: Self-assembly of mesoscopic and macroscopic components. *Proceedings of the National Academy of Sciences, 99*(8), 4769-4774.

Whitesides, G. M., & Grzybowski, B. (2002). Self-assembly at all scales. *Science, 295*(5564), 2418-2421.

Whitesides, G. M., Mathias, J. P., & Seto, C. T. (1991). *Molecular self-assembly and nanochemistry: a chemical strategy for the synthesis of nanostructures*. Retrieved from

Whitten, S. T., & Hilser, V. J. (2005). Local conformational fluctuations can modulate the coupling between proton binding and global structural transitions in proteins. *Proceedings of the National Academy of Sciences of the United States of America, 102*(12), 4282-4287.

Whitty, A. (2008). Cooperativity and biological complexity. *Nature Chemical Biology, 4*(8), 435-439.

Williamson, J. R. (2008). Cooperativity in macromolecular assembly. *Nature chemical biology, 4*(8), 458-465.

Wolynes, P. G., Onuchic, J. N., & Thirumalai, D. (1995). Navigating the folding routes. *SCIENCE-NEW YORK THEN WASHINGTON-*, 1619-1619.

Woodson, S. A. (2000). Compact but disordered states of RNA. *Nature Structural & Molecular Biology, 7*(5), 349-352.

Xia, L.-W., Xie, R., Ju, X.-J., Wang, W., Chen, Q., & Chu, L.-Y. (2013). Nano-structured smart hydrogels with rapid response and high elasticity. *Nature communications, 4*.

Yamada, K. M., & Even-Ram, S. (2002). Integrin regulation of growth factor receptors. *Nature cell biology, 4*(4), E75-E76.

Yamagata, M., Hasuda, K., Stamato, T., & Tannock, I. F. (1998a). The contribution of lactic acid to acidification of tumours: studies of variant cells lacking lactate dehydrogenase. *British Journal of Cancer, 77*(11), 1726-1731. doi:Doi 10.1038/Bjc.1998.289

Yamagata, M., Hasuda, K., Stamato, T., & Tannock, I. F. (1998b). The contribution of lactic acid to acidification of tumours: studies of variant cells lacking lactate dehydrogenase. *British Journal of Cancer, 77*(11), 1726-1731.

Yan, H., Fujiwara, H., Sasaki, K., & Tsujii, K. (2005). Rapid Swelling/Collapsing Behavior of Thermoresponsive Poly (N- isopropylacrylamide) Gel Containing Poly (2- (methacryloyloxy) decyl phosphate) Surfactant. *Angewandte Chemie International Edition, 44*(13), 1951-1954.

Yan, Q., & Hoffman, A. S. (1995). Synthesis of macroporous hydrogels with rapid swelling and deswelling properties for delivery of macromolecules. *Polymer, 36*(4), 887-889.

Yoneya, S., Saito, T., Komatsu, Y., Koyama, I., Takahashi, K., & Duvoll-Young, J. (1998). Binding properties of indocyanine green in human blood. *Investigative ophthalmology & visual science, 39*(7), 1286-1290.

Yong-Hee, K., Bae, Y. H., & Kim, S. W. (1994). pH/temperature-sensitive polymers for macromolecular drug loading and release. *Journal of controlled release, 28*(1), 143-152.

Yoshida, M., & Lahann, J. (2008). Smart nanomaterials. *ACS nano, 2*(6), 1101-1107.

Yoshida, R., Uchida, K., Kaneko, Y., & Sakai, K. (1995). Comb-type grafted hydrogels with rapid de-swelling response to temperature changes. *Nature, 374*(6519), 240.

Zakharov, S. D., Lindeberg, M., & Cramer, W. A. (1999). Kinetic description of structural changes linked to membrane import of the colicin E1 channel protein. *Biochemistry, 38*(35), 11325-11332.

Zang, L., Che, Y., & Moore, J. S. (2008). One-dimensional self-assembly of planar π-conjugated molecules: adaptable building blocks for organic nanodevices. *Accounts of chemical research, 41*(12), 1596-1608.

Zhan, H., Oh, K. J., Shin, Y.-K., Hubbell, W. L., & Collier, R. J. (1995). Interaction of the isolated transmembrane domain of diphtheria toxin with membranes. *Biochemistry, 34*(14), 4856-4863.

Zhang, B. (1993). Enthalpic domination of the chelate effect in cyclodextrin dimmers. *J. Am. Chem. Soc., 115*, 9353-9354.

Zhang, J., Chen, H., Xu, L., & Gu, Y. (2008). The targeted behavior of thermally responsive nanohydrogel evaluated by NIR system in mouse model. *Journal of controlled release, 131*(1), 34-40.

Zhang, S., Bellinger, A. M., Glettig, D. L., Barman, R., Lee, Y.-A. L., Zhu, J., . . . Nash, L. D. (2015). A pH-responsive supramolecular polymer gel as an enteric elastomer for use in gastric devices. *Nature materials, 14*(10), 1065-1071.

Zhang, W., Shi, L., Wu, K., & An, Y. (2005). Thermoresponsive micellization of poly (ethylene glycol)-b-poly (N-isopropylacrylamide) in water. *Macromolecules, 38*(13), 5743-5747.

Zhang, Y., & Cremer, P. S. (2006). Interactions between macromolecules and ions: The Hofmeister series. *Current Opinion in Chemical Biology, 10*(6), 658-663. doi:10.1016/j.cbpa.2006.09.020

Zhang, Y., & Cremer, P. S. (2009). The inverse and direct Hofmeister series for lysozyme. *Proceedings of the National Academy of Sciences of the United States of America, 106*(36), 15249-15253. doi:10.1073/pnas.0907616106

Zhang, Y., & Cremer, P. S. (2010). Chemistry of Hofmeister anions and osmolytes. *Annual review of physical chemistry, 61*, 63-83.

Zhang, Y., Furyk, S., Bergbreiter, D. E., & Cremer, P. S. (2005). Specific ion effects on the water solubility of macromolecules: PNIPAM and the Hofmeister series. *Journal of the American Chemical Society, 127*(41), 14505-14510.

Zhang, Y., Furyk, S., Sagle, L. B., Cho, Y., Bergbreiter, D. E., & Cremer, P. S. (2007). Effects of Hofmeister anions on the LCST of PNIPAM as a function of molecular weight. *The journal of physical chemistry. C, Nanomaterials and interfaces, 111*(25), 8916.

Zhao, D., & Moore, J. S. (2003). Nucleation–elongation: a mechanism for cooperative supramolecular polymerization. *Organic & Biomolecular Chemistry, 1*(20), 3471-3491.

Zhao, J., Fyles, T. M., & James, T. D. (2004). Chiral binol–bisboronic acid as fluorescence sensor for sugar acids. *Angewandte Chemie International Edition, 43*(26), 3461-3464.

Zhao, T., Huang, G., Li, Y., Yang, S., Ramezani, S., Lin, Z., . . . Luo, M. (2016). A transistor-like pH nanoprobe for tumour detection and image-guided surgery. *Nature Biomedical Engineering, 1*, 0006.

Zhou, K., Liu, H., Zhang, S., Huang, X., Wang, Y., Huang, G., . . . Gao, J. (2012). Multicolored pH-tunable and activatable fluorescence nanoplatform responsive to physiologic pH stimuli. *Journal of the American Chemical Society, 134*(18), 7803-7811. doi:10.1021/ja300176w

Zhou, K., Liu, H., Zhang, S., Huang, X., Wang, Y., Huang, G., . . . Gao, J. (2012). Multicolored pH-tunable and activatable fluorescence nanoplatform responsive to physiologic pH stimuli. *Journal of the American Chemical Society, 134*(18), 7803-7811.

Zhou, K., Wang, Y., Huang, X., Luby-Phelps, K., Sumer, B. D., & Gao, J. (2011). Tunable, ultrasensitive pH-responsive nanoparticles targeting specific endocytic organelles in living cells. *Angew Chem Int Ed Engl, 50*(27), 6109-6114. doi:10.1002/anie.201100884

Zhou, K., Wang, Y., Huang, X., Luby- Phelps, K., Sumer, B. D., & Gao, J. (2011a). Tunable, Ultrasensitive pH- Responsive Nanoparticles Targeting Specific Endocytic Organelles in Living Cells. *Angewandte Chemie, 123*(27), 6233-6238.

Zhou, K., Wang, Y., Huang, X., Luby- Phelps, K., Sumer, B. D., & Gao, J. (2011b). Tunable, Ultrasensitive pH- Responsive Nanoparticles Targeting Specific Endocytic Organelles in Living Cells. *Angewandte Chemie International Edition, 50*(27), 6109-6114.

Zhu, Y., Yang, B., Chen, S., & Du, J. (2016). Polymer vesicles: mechanism, preparation, application, and responsive behavior. *Progress in Polymer Science*.

Zhuang, J., Gordon, M. R., Ventura, J., Li, L., & Thayumanavan, S. (2013). Multi-stimuli responsive macromolecules and their assemblies. *Chemical Society Reviews, 42*(17), 7421-7435.

Zwicke, G. L., Ali Mansoori, G., & Jeffery, C. J. (2012). Utilizing the folate receptor for active targeting of cancer nanotherapeutics. *Nano reviews, 3*(1), 18496.